

https://dspace.org/

Generalisations of the Laplace-Runge-Lenz vector in classical mechanics

Gorringe, Vivian Mervyn

2015
http://hdl.handle.net/10539/18419

Downloaded from a DSpace repository. https://dspace.org/

Generalisations of the Laplace–Runge–Lenz Vector in Classical Mechanics

Vivian Mervyn Gorringe

CHAPTER 1 AND 2

A thesis submitted to the Faculty of Science, University of the Witwatersrand, Johannesburg, in fulfilment of the requirements for the degree of Doctor of Philosophy.

Johannesburg, June 1995

ABSTRACT

In this work new classes of vector equations of motion which possess Hamilton and Laplace–Runge–Lenz vector analogues are constructed by applying vector operations directly to the equations of motion. The velocity hodograph is easily derived from the Hamilton–like vector and the orbit equation using the Laplace–Runge–Lenz–like vector. The equations of motion are grouped according to the restrictions made on the nature of the angular momentum. Several solved problems which have already appeared in the literature are shown to be special cases of some of these equations of motion.

The special cases include the Kepler problem, the three–dimensional isotropic harmonic oscillator, an equation of motion describing the motion of low altitude satellites proposed by Danby [25], the McIntosh–Cisneros–Zwanziger monopole problem [94, 134] and the monopole–oscillator problem [94] amongst others. Kepler's laws are generalised to include some of these special cases and new insights into the geometry of the orbits of both the Kepler problem and the three–dimensional isotropic harmonic oscillator are obtained. One particular class of problems, having a velocity–dependent term in the equation of motion and focus–centred Keplerian orbits, has a period which is proportional to a half–integer power of the semi–major axis length. This generalisation of Kepler's third law is extended to include an analogue of the three–dimensional isotropic harmonic oscillator by means of a tensor analogue of the Jauch–Hill–Fradkin tensor of the three–dimensional isotropic harmonic oscillator. In the case of the MICZ monopole the planar conic section orbits are shown to be naturally associated with focus–centred Kepler orbits whereas in the case of the monopole–oscillator and related problems the orbit which is described by the intersection of a quadric surface and a right circular cone is shown to be naturally associated with geometrically centred conic sections.

The Lie method is applied to many of the systems mentioned above and the relationship between the existence of conserved vectors and the Lie symmetries is explored.

DECLARATION

I declare that the contents of this dissertation are original except where due references have been made. It has not been submitted before for any degree or examination to any other institution.



V. M. Gorringe
June 1995

Dedication

To my late grandparents Dorothea and Victor Henochsberg

ACKNOWLEDGEMENTS

I am deeply indebted to my supervisor Professor P G L Leach for having introduced me to the subject of classical mechanics and the Lie technique for studying differential equations. His enthusiasm for mathematics, his geometrical insights and resolve when solving seemingly intractible sets of coupled partial differential equations will hopefully serve as an inspiration in the years to come. His encouragement and guidance during the course of this research and hands–on approach to supervision is greatly appreciated. I am also very grateful for his critical appraisal of this manuscript during the process of revision.

I am also indebted to Professor D P Mason who took over from Professor Leach as my internal supervisor. He kindly assisted in providing both the computer hardware and software which were necessary to produce many of the results and figures in the thesis as well as for word processing the document. In addition, he supplied funds from his personal research finances to help purchase a printer for use after–hours by postgraduate students in the department. I am also very grateful for the technical assistance and encouragement he offered during the progress of my research.

I am also very grateful to Dr F M Mahomed for some very illuminating discussions on the intricacies of the Lie method and its application to classical mechanics. He also helped to classify some of the algebras mentioned in Chapter 4. In addition, he provided many relevant references during the course of this work and offered assistance with the finer points of the Latex software package.

Thanks is also due to Mrs F Goetze and Mrs S Bradu who provided assistance with typesetting many of the more intricate formulas as well as for offering advice on style and layout. Finally I thank the Foundation for Research and Development, the University of the Witwatersrand and the Centre for Nonlinear Studies for financial support.

Contents

Introduction 1

P Preliminaries 11

P1 Vector Identities 11

P2 The Geometry of Conic Sections 13

P2.1 Focus–Centred Conic Sections 13

P2.2 Geometric–Centred Conic Sections 15

P3 Lie Analysis and First Integrals 15

P3.1 The Lie Symmetries 15

P3.2 The First Integrals Associated with the Lie Symmetries 19

1 Motion with Conserved $\boldsymbol{L}$ 20

1.1 The Conserved Hamilton and Laplace–Runge–Lenz Vector Analogues for the Equation of Motion $\ddot{\boldsymbol{r}} + f\boldsymbol{r} = \boldsymbol{0}$ 20

1.2 The Velocity Hodograph and the Orbit Equation 23

1.3 The Motion in Time 24

1.4 Examples 25

1.5 The Geometry of the Kepler Problem 28

1.6 The Conserved Hamilton and Laplace–Runge–Lenz Vector Analogues and a Conserved Tensor for Central Force Problems using Fradkin's Method 50

1.7 The Geometry of the Three–Dimensional Isotropic Harmonic Oscillator 56

1.8 The First Integrals Associated with the Self–Similar Symmetry 70

1.9 The Connection with Hamilton–Jacobi Theory and with a Laplace–Runge–Lenz Vector Analogue 74

1.10 The Conserved Hamilton and Laplace–Runge–Lenz Vector Analogues for the Non–Autonomous Equation of Motion $\ddot{\boldsymbol{r}} + f(r,\theta,t)\boldsymbol{r} = \boldsymbol{0}$ . . . 77

1.11 The Orbit Equation . . . 79

1.12 Examples . . . 80

2 Motion with Conserved $\hat{L}$ **84**

2.1 The Conserved Hamilton and Laplace–Runge–Lenz Vector Analogues for the Equation of Motion $\ddot{\boldsymbol{r}} + g\hat{\boldsymbol{r}} + h\hat{\boldsymbol{\theta}} = \boldsymbol{0}$ . . . 84

2.2 The Velocity Hodograph and the Orbit Equation . . . 86

2.3 The Motion in Time . . . 87

2.4 Examples . . . 88

2.5 The Conserved Hamilton and Laplace–Runge–Lenz Vector Analogues for a Related Hamiltonian System . . . 90

2.6 The Lie Algebras of the First Integrals . . . 92

2.7 The Connection with Sen's Results . . . 95

2.8 The Extension of the Hamiltonian Treatment to Three Dimensions . 98

2.9 The First Integrals Associated with the Time Invariance Symmetry . 100

2.10 The Conserved Hamilton and Laplace–Runge–Lenz Vector Analogues for the Equation of Motion $\ddot{\boldsymbol{r}} + f\dot{\boldsymbol{r}} + g\boldsymbol{r} = \boldsymbol{0}$ . . . 103

2.11 The Velocity Hodograph and the Orbit Equation . . . 104

2.12 The Motion in Time . . . 107

2.13 Examples . . . 107

2.14 The Conserved Hamilton and Laplace–Runge–Lenz Vector Analogues for General Keplerian Orbits . . . 112

2.15 The Geometry of the Generalised Kepler Problem . . . 115

2.16 The Connection with Central Force Problems and the Conserved Hamilton and Laplace–Runge–Lenz Vector Analogues and a Conserved Jauch–Hill–Fradkin Tensor Analogue for General Oscillator Orbits . . 125

2.17 The Geometry of the Generalised Harmonic Oscillator 130

3 Motion with Conserved L **140**

3.1 The Conserved Laplace–Runge–Lenz Vector Analogue for the Equation of Motion $\ddot{\boldsymbol{r}} + f\boldsymbol{L} + g\hat{\boldsymbol{r}} = \boldsymbol{0}$ 140

3.2 The Orbit Equation 142

3.3 The Motion in Time 143

3.4 Examples 144

3.5 The Conserved Hamilton and Laplace–Runge–Lenz Vector Analogues and the Lie Algebras of the First Integrals of the Classical MICZ Problem 147

3.6 Geometric Preliminaries and the Connection with the Kepler Problem 150

3.7 The Geometry of the MICZ Problem with $\mu = 0$ 155

3.8 The Geometry of the MICZ Problem with $\mu = J$ 165

3.9 The Geometry of the MICZ Problem with $\mu > J$ 176

3.10 The Geometry of the MICZ Problem with $\mu < J$ 195

3.11 Discussion 206

3.12 The Lie Algebras of the Classical Monopole–Oscillator and Related Problems 207

3.13 The Lie Algebras of the First Integrals of the Monopole–Oscillator, Monopole–Free Particle and Monopole–Repulsor 209

3.14 The Geometry of the Monopole–Oscillator 213

3.15 The Geometry of the Monopole–Free Particle 234

3.16 The Geometry of the Monopole–Repulsor 237

3.17 The Stationary Solutions 252

3.17.1 The Monopole–Oscillator 252

3.17.2 The Monopole–Free Particle 252

3.17.3 The Monopole–Repulsor 253

3.18 Discussion 253

3.19 The First Integrals Associated with the Lie Symmetries of the Monopole–Oscillator 254

3.20 Discussion 260

4 Symmetries and the Existence of Conserved Vectors **262**

4.1 Preliminaries 262

4.2 The Lie Symmetries of the Equation of Motion $\ddot{\boldsymbol{r}} + f(r)\boldsymbol{L} + g(r)\boldsymbol{r} = \boldsymbol{0}$ 265

4.3 The Case $f = 0$ 269

4.4 The Case $f \neq 0$ 275

4.5 Discussion 279

Conclusions **282**

References **286**

INTRODUCTION

The Kepler problem and the three–dimensional isotropic harmonic oscillator are cornerstones of the theories of both classical and quantum mechanics. In fact the Kepler problem was responsible to a large extent for the development of Newtonian mechanics and the oscillator, and slightly later the Kepler problem, for the development of quantum mechanics. Since to date the major breakthroughs in physics are so closely connected with the study of these two central force problems, it would be fair to assume that any future fundamental revision of the theories of mechanics may well be linked to a study of the Kepler problem or the oscillator in some form or another. For this and other reasons both problems still attract considerable interest. As these two problems form the basis for many of the generalisations which are developed in subsequent chapters, it is worthwhile to study their development over the past four centuries. Due to the enormous interest which both problems have attracted over that time and the number of great scientists who have studied various aspects of these problems, it is possible only to look at that small subset of this material which is directly relevant to my research. The historical introduction which follows is therefore not an exhaustive study of the development of these two problems but a summary of some of the important milestones in the development of an analytic solution and the intermediate construction of conserved vectors or tensor quantities for these problems. It should also be mentioned that much of the surviving early original work can only be found in rare volumes, generally in protected collections, and often written in Latin.

The Kepler problem and the three–dimensional isotropic harmonic oscillator are both well–studied paradigms of classical mechanics. For many centuries the Kepler problem and the oscillator developed independently, although from the physical observations of Kepler and Galileo, the problems are in fact contemporaries. This independence continued well into the 20th century despite the emergence of the new quantum theory, thus reënacting the history of the previous three hundred years.

The first reference to the harmonic oscillator appears to be the recorded observation by Galileo in 1582 of the regular oscillations of the great hanging lamp in the cathedral at Pisa. Although the amplitude of the oscillations diminished, Galileo observed, using his pulse as a reference, that the oscillations were all completed in the same time. It is believed that he invented a *pulsilogium*, a ball and string pendulum, which he used for timing the pulses of patients.

The fascination of the motion of the planets goes back to time immemorial. While the imperial mathematician at the observatory in Prague, a title which was conferred on Kepler upon the death of Tycho Brahe in 1601, Kepler postulated laws to describe his own observations as well as those of his predecessor. Kepler believed he could unravel the 'whole scheme of the heavens in an all–embracing synthesis of geometry, music, astrology, astronomy and epistemology' [68, p214]. It seems a great pity that Kepler, lacking the mathematical sophistication of differential calculus or analytic geometry could never comprehend the importance of his three laws of planetary motion – in fact he was almost ashamed of the departure from the sacred circle – 'the ellipse had nothing to recommend it in the eyes of God and man' [68, p225]. He often referred to his second law as a mere calculating device, often to use a faulty approximation in its place. The third law was relegated to the position of a missing link in the concept of harmony.

In the books *Astronomia Nova* of 1609 and the *Harmonices Mundi* of 1619, Kepler proposed the following three laws :–

> *Itaque plane hoc est: orbita planetae non est circulus, sed ingrediens ad latera utraque paulatim, iterumque ad circuli amplitudinem in perigaeo exiens: cujusmodi figuram itineris ovalem appellitant. ... orbitam planetae non esse circulum, sed figurae ovalis.*
> [65, Pars Quarta, Cap. XLIV, pp336–7]

> Kepler's first law: 'Therefore this is obvious: the path of the planet is not a circle, but gradually curves inward on both sides and again departs to the width of the orbit at perigee: such a path is called an oval figure. ... the orbit of the planet is not a circle but an oval figure.'

> *Cumque scirem, infinita esse puncta eccentrici, et distantias earum infinitas, subiit, in plano eccentrici has distantias omnes inesse. Nam memineram, sic olim et Archimedem, cum circumferentiae proportionem ad diametrum quaereret, circulum in infinita triangula dissecuisse ...*
> [65, Pars Tertia, Cap. XL, p321]

> Kepler's second law: 'Since I was aware that there exists an infinite number of points on the orbit and accordingly an infinite number of distances [from the sun] it occurred to me that the sum of these distances is contained in the area of the orbit. For I remembered that in the same manner in times past, Archimedes too divided [the area] of a circle, for which he found the circumference proportional to the diameter, into an infinite number of triangles ...'
>
> *Sed res est certissima exactissimaque, quod proportio, quae est inter binorum quorumcunque planetarum tempora periodica, sit praecise sesquialtera proportionis mediarum distantiarum, id est orbium ipsorum ...*
> [66, Lib. V, Cap. III, Proposition No. 8, p279]
>
> Kepler's third law: 'But it is absolutely certain and exact that the ratio which exists between the periodic times of any two planets is precisely the ratio of the 3/2th power of the mean distances *i.e.* of the spheres themselves ...'

In 1670 the English physicist Robert Hooke discovered his law of elasticity which states that the stretching of a solid body is proportional to the applied force. This law would in time be rephrased mathematically as the harmonic oscillator and solved in a variety of ways over the centuries.

In August 1684, Edmund Halley visited Isaac Newton at Cambridge and informed him of Christopher Wren's challenge, which had a sizeable monetary reward attached, to derive the shape of the orbits of the planets around the sun. Inspired by his solution to Halley's problem, which he described in the tract *De Motu Corporum*, Newton hastily set about improving and expanding these ideas. During this revision he arrived at the law of universal gravitation as well as his three laws of motion, the first quantitative treatment explaining the motion of visible bodies. Using these laws, Newton showed that the centripetal force holding the planets in their given orbits around the sun must decrease with the square of the planets' distances from the sun and, in the process, confirm Kepler's observational laws. In two and a half years *De Motu Corporum* had grown into *Philosophiae Naturalis Principia Mathematica* [102], Newton's masterpiece and with it came the birth of modern science. Newton did a geometric investigation of the inverse square law force, because of its connection with the motion of the planets. He attempted to verify Kepler's first law by proving that if a particle moves in an elliptical orbit under the influence of a centripetal force directed

towards one focus then that force must must be inversely proportional to the square of the radius [102, prop XI p56], and obtained the same result for focus–centred parabolic [102, prop XIII p60] and hyperbolic motion [102, prop XII p57]. He further proved that equal areas were swept out by the radius vector in equal times [102, prop I–II p40ff] which was the content of Kepler's second law and also that the square of the periodic time of an inverse square law ellipse was proportional to the cube of the semi–major axis length and thus verified Kepler's third law [102, prop XV p62].

It should be noted, however, that Newton is also generally credited with having proved the converse of [102, prop XI-XIII p56ff] *i.e.* that all possible orbits of a particle moving under an inverse square law force are conic sections which is of more significance than [102, prop XI-XIII p56ff] themselves since this result verifies Newton's law of universal gravitation by showing that elliptical planetary orbits are a natural consequence of the gravitational interaction between the sun and the planets. Recently, however, the generally accepted view that Newton was responsible for this milestone achievement has been questioned by Weinstock [127, 128]. Proof that motion along a conic section orbit under the influence of a force directed towards one focus implies an inverse square law force does not demonstrate that a particle moving under the influence of an inverse square law force will move along a conic section orbit. The conic section orbit which was assumed initially is only a geometrical construction and not necessarily the actual path described by the particle. In fact the converse of [102, prop XI–XIII p56ff] is far more suited to an analytic proof rather than a geometric one as was favoured by Newton. Newton had been aware that his original proof of the converse [102, prop XIII cor 1 p61] was incomplete and unsuccessfully attempted to rectify this oversight. In 1709 he had instructed his editor to add two additional sentences to [102, prop XIII cor 1 p61] concerning the uniqueness of the orbit under a given force law when the initial position and velocity were known. This correction appeared in the second edition of the *Principia* of 1713. In 1710 Johann Bernoulli had also objected to Newton's underhand treatment of the proof of the converse of [102, prop XI-XIII p56ff] (see [127]). Newton's addition did not provide the necessary details to prove the converse and there is still much debate as to whether Newton deserves credit for what is today generally regarded as his finest achievement. Weinstock [128] also discovered that his misgivings about Newton's proof had previously been noted by Rosenberger in 1895 but these criticisms were not well–known among the current generation of Newton scholars who are very opposed to his position concerning several inconsistencies in the *Principia.*

The three–dimensional isotropic harmonic oscillator also featured prominently in *Principia* in the context of central force problems. Newton showed that if a particle moves in an elliptical orbit under the influence of a centripetal force directed towards the geometric centre of the ellipse then that force must be proportional to the radius [102, prop X p53]. He also proved that the periodic times of concentric elliptical orbits about the same centre were equal (isochronic) [102, prop XLVII p149ff].

In 1785, nearly a century after the publication of the *Principia*, Newton's law of gravitation was reaffirmed with the discovery by Charles Coulomb of the inverse square law to describe electrostatic forces. The mathematical similarity between these physically different forces was startling!

During Newton's time it was usual to determine the gravitational force law assuming that the planets moved along conic sections. The direct method of finding the orbits given an inverse square law force appears to have first been studied in 1710 by Jakob Hermann, a disciple of the Bernoullis [32]. (According to Aiton (see [127]), Johann Bernoulli's treatment predates that of Hermann). Using the new techniques of Leibniz's calculus, he obtained a constant of integration which was related to the eccentricity of the conic sections. Hermann summarised his results in a letter to Johan Bernoulli, who generalised Hermann's results to allow for an arbitrary orientation of the orbit in the plane, and in so doing arrived at the equivalent of a conserved vector which is today generally known as the Laplace–Runge–Lenz vector, although its historical lineage would suggest the more appropriate name Hermann–Bernoulli–Laplace vector.

Laplace's lucid derivation of the vector came somewhat later in 1799. In his *Traité de Mécanique Céleste* [69, 70] he obtained seven first integrals for the Kepler problem, three of which were the cartesian components of the angular momentum. A further three of the integrals were the cartesian components of the Laplace–Runge–Lenz vector. The remaining integral was given by the semi–major axis length for elliptical (bound state) orbits, which is of course inversely proportional to the total energy. Laplace further noted that there could only be five independent first integrals and went on to find two relationships between the seven integrals already mentioned. He further showed that the conserved components of the angular momentum were responsible for the planar motion and also demonstrated that the orbit equation could be expressed as a conic section [31].

Hamilton had long aspired to be to optics what Newton had been to celestial mechanics. In fact he often referred to MacCullagh (an early pioneer of optics who had described the phenomena of reflection and refraction using a system of mathematical laws) as the Kepler of optics, *i.e.* the person who had, 'without seeking yet to deduce these laws, as Newton did the laws of Kepler, from any higher and dynamic principle' undertaken 'the preparatory but important task of discovering from the phenomena themselves, the mathematical laws which connect and represent those phenomena, and are in a manner intermediate between facts and principles, between appearances and causes' [49, p160]. Hamilton started his working career as the Andrews Professor of Astronomy at the Dunsink Observatory in Dublin and this practical introduction to astronomy laid the groundwork for his ongoing interest in dynamics. In addition, having had success with his paper entitled 'On a General Method in Dynamics' on the problems of planetary perturbations twelve years earlier, it is not surprising that Hamilton from time to time would be drawn away from his ever more consuming interest in quaternions to return to his roots.

In July 1845 Hamilton delivered a paper to the Royal Irish Academy, entitled 'Applications of Quaternions to Some Dynamical Questions', in which he obtained a new constant of motion for the Kepler problem and subsequently named the 'eccentricity' vector. This vector, which is termed Hamilton's vector throughout this thesis, is perpendicular to the Laplace–Runge–Lenz vector and describes the velocity of the particle in a concise and useful way. Motivated by the discovery of Neptune which had been prompted by theoretical predictions, Hamilton chose this subject for his astronomical lectures of 1846. In the preparation of these lectures he discovered a new geometrical representation for planetary motion which he termed the 'hodograph' which means 'to describe the path'. He proved that the velocity hodograph arising from Newton's inverse square law force was circular, and also showed how the location of the origin depended on the type of conic section. Hamilton found that the velocity hodograph could be expressed rather elegantly in terms of the quaternion formulation of his eccentricity vector. Although Hamilton's consuming devotion to the subject of quaternions is often regarded as a tragedy, his quest to simplify many of the techniques used during those times was very commendable. Sir Edmund Whittaker in the 1940s suggested that Hamilton's work on quaternions be reëvaluated in an attempt to find the most 'natural expression of the new physics' [49, p325]. In fact many of the elegant quaternion techniques are equivalent to those described below which make use of modern vector operations. There is some dispute as to whether the velocity hodograph was in fact discovered by Hamilton or August Ferdinand Möbius. It would appear that Hamilton acknowledged Möbius' research in his *Lectures on*

Quaternions of 1853 [49, p333]. However, many of Hamilton's theorems relating to the velocity hodograph had not been suggested before. Gibbs is generally credited as being the first to express the classical Laplace–Runge–Lenz vector in terms of modern vector notation which antedates Runge's derivation by roughly twenty years [32].

The three–dimensional isotropic harmonic oscillator does not appear to have attracted the same amount of interest as the Kepler problem. However, after appearing in the *Principia* it would have gained considerable exposure. It is very difficult to trace its appearance in the literature subsequent to this, although between the years of 1700 to 1900 the only progress appears to have been in the mathematical formulation of the equation of motion and the solution in terms of the parametric equations which seems to have been well known in many of the late nineteenth and early twentieth century textbooks (see Tait [124, §363 p284ff] and Routh [113, §123 p64ff]). The construction of conserved vector and tensor quantities emerged only much later.

The next milestone in the development of the theory of the Kepler problem and the oscillator occurred in 1901 with the discovery by Planck of a law to explain the experimentally observed distribution of energy in the black–body radiation spectrum. This theory was based on a statistical distribution of energy amongst a set of simple linear harmonic oscillators. The radical departure from the classical theory was his assumption that the energy of the oscillators be allowed to take on a discrete linear set of values rather than vary continuously as had been previously demanded by classical physics. These ideas gave birth to the quantum theory.

Using the ideas of Planck, in 1913 Bohr was able to apply them to a Rutherford model of the hydrogen atom using a Kepler–Coulomb potential energy and succeeded in arriving at a theoretical formula for the wavelengths of the atomic spectrum which agreed with experimental observations.

The Laplace–Runge–Lenz vector came to prominence after a 1924 paper by Lenz [81] which referred to a popular text on vector analysis by Runge [114] in connection with the classical formulation of this vector. This paper by Lenz was widely referenced particularly as quantum mechanics was being reformulated as a mathematical theory during this period by Schrödinger, Born, Heisenberg, Pauli and Dirac amongst others. Pauli made good use of the vector in a pioneering paper on the new matrix mechanics published in 1926 [105], to derive an expression for the energy levels of the hydrogen atom. In a 1935 paper Fock [27] showed that the hydrogen atom pos-

sessed the 4–dimensional rotation group for the bound states and the symmetry of the Lorentz group for positive energy states. These results were confirmed by Bargmann in 1936 [5] by calculating the commutation relationships between the components of the angular momentum and the Laplace–Runge–Lenz vectors.

In a 1940 paper by Jauch and Hill [57] the n–dimensional quantum isotropic harmonic oscillator was shown to possess the $su(n)$ symmetry group. Fradkin [28] confirmed these results for the three–dimensional isotropic harmonic oscillator in 1964 and constructed a conserved symmetric tensor (the Jauch–Hill–Fradkin tensor) which, in the classical problem, could be used to specify the orientation of the orbit in an analogous fashion to the use of the Laplace–Runge–Lenz vector in the classical Kepler problem.

A large amount of research has been done on various aspects of the Kepler problem since 1960 and, where appropriate, this will be discussed in more detail in the following chapters.

This work is devoted to generalisations of the Hamilton and Laplace–Runge–Lenz vectors for a wide variety of Newtonian equations of motion. By making restrictions on the structure of the angular momentum and various other simplifying assumptions, it is possible to construct several new classes of equations of motion which possess Hamilton and Laplace–Runge–Lenz vector analogues. Various solved problems which are well documented in the literature are shown to be special cases of the ones mentioned above. By studying several of these more general problems, we gain new insights into both the Kepler problem and the three–dimensional isotropic harmonic oscillator.

In Chapter 1 we consider equations of motion arising from the conservation of both the magnitude and the direction of the angular momentum. Hamilton and Laplace–Runge–Lenz vector analogues are constructed together with the velocity and acceleration hodographs and the orbit equations. The Kepler problem is shown to be a special case. Two non–conserved orthogonal vectors which are closely related to the scalar Lagrangian and also the Hamilton and Laplace–Runge–Lenz vectors are introduced for the Kepler problem and their geometrical properties are investigated. Kepler's three laws of motion are derived. Fradkin's technique [29] for constructing Hamilton and Laplace–Runge–Lenz vector analogues for all central forces is also described together with a detailed application of this technique to the three–dimensional isotropic harmonic oscillator. A non–conserved tensor which is closely related to the

scalar Lagrangian and also the Jauch–Hill–Fradkin tensor is introduced for the three–dimensional isotropic harmonic oscillator and its geometrical properties are investigated. Analogues of Kepler's three laws of motion are derived for the oscillator and a connection between the periodic times for both the Kepler problem and the oscillator is established. The Lie method is then applied to the general central force problem and the existence of a Laplace–Runge–Lenz vector for the Kepler problem is shown to be unique. Finally we consider the existence of Hamilton and Laplace–Runge–Lenz vector analogues for a class of non–autonomous equations of motion.

Chapter 2 deals with the construction of Hamilton and Laplace–Runge–Lenz vector analogues for equations of motion subject to the restriction that the direction of the angular momentum is conserved. A class of problems which possesses a Hamiltonian is also studied and a further first integral is constructed using Poisson's theorem. These results are shown to be consistent with those derived by Sen [118]. The first integrals are then rederived using the Lie method. One further class of problems also having the direction of the angular momentum conserved is studied and shown to be a generalisation of the equation of motion for low altitude satellites proposed by Danby [25] for which a Laplace–Runge–Lenz–type vector has previously been discovered [58]. A further class of problems is also obtained for which orbit equations which are conic sections are constructed using the Laplace–Runge–Lenz–type vector. It is possible to generalise Kepler's laws, particularly the third one, for this class of problems and relate the period of the motion to a fractional power of the semi–major axis length. This generalisation is then shown to extend to the oscillator using a tensor analogue of the Jauch–Hill–Fradkin tensor for the three–dimensional isotropic harmonic oscillator.

Chapter 3 describes the construction of Laplace–Runge–Lenz–type vectors for equations of motion subject to the restriction that the magnitude of the angular momentum is conserved, but not its direction. These orbits are no longer confined to a plane. The MICZ monopole [94, 134] problem is shown to be a special case which is then studied in detail. The motion on the cone is shown to project onto a Keplerian orbit in the plane and provide a new insight into the location of the origin and the foci for the planar Kepler problem. Kepler's laws of motion are generalised to describe motion on the cone and the third law is shown to have a natural analogue on the cone. The monopole–oscillator [94] is also studied and its unique orbit on the cone is shown to project onto a three–dimensioanl isotropic harmonic oscillator ellipse in the plane. The question of the location of the origin in the planar problem

scalar Lagrangian and also the Jauch–Hill–Fradkin tensor is introduced for the three–dimensional isotropic harmonic oscillator and its geometrical properties are investigated. Analogues of Kepler's three laws of motion are derived for the oscillator and a connection between the periodic times for both the Kepler problem and the oscillator is established. The Lie method is then applied to the general central force problem and the existence of a Laplace–Runge–Lenz vector for the Kepler problem is shown to be unique. Finally we consider the existence of Hamilton and Laplace–Runge–Lenz vector analogues for a class of non–autonomous equations of motion.

Chapter 2 deals with the construction of Hamilton and Laplace–Runge–Lenz vector analogues for equations of motion subject to the restriction that the direction of the angular momentum is conserved. A class of problems which possesses a Hamiltonian is also studied and a further first integral is constructed using Poisson's theorem. These results are shown to be consistent with those derived by Sen [118]. The first integrals are then rederived using the Lie method. One further class of problems also having the direction of the angular momentum conserved is studied and shown to be a generalisation of the equation of motion for low altitude satellites proposed by Danby [25] for which a Laplace–Runge–Lenz–type vector has previously been discovered [58]. A further class of problems is also obtained for which orbit equations which are conic sections are constructed using the Laplace–Runge–Lenz–type vector. It is possible to generalise Kepler's laws, particularly the third one, for this class of problems and relate the period of the motion to a fractional power of the semi–major axis length. This generalisation is then shown to extend to the oscillator using a tensor analogue of the Jauch–Hill–Fradkin tensor for the three–dimensional isotropic harmonic oscillator.

Chapter 3 describes the construction of Laplace–Runge–Lenz–type vectors for equations of motion subject to the restriction that the magnitude of the angular momentum is conserved, but not its direction. These orbits are no longer confined to a plane. The MICZ monopole [94, 134] problem is shown to be a special case which is then studied in detail. The motion on the cone is shown to project onto a Keplerian orbit in the plane and provide a new insight into the location of the origin and the foci for the planar Kepler problem. Kepler's laws of motion are generalised to describe motion on the cone and the third law is shown to have a natural analogue on the cone. The monopole–oscillator [94] is also studied and its unique orbit on the cone is shown to project onto a three–dimensioanl isotropic harmonic oscillator ellipse in the plane. The question of the location of the origin in the planar problem

is also resolved. Kepler's laws of motion are also generalised in the same fashion as before. The Lie method is then applied to the construction of first integrals for the monopole–oscillator

Chapter 4 investigates the question of symmetries and the existence of conserved vectors for the general equation of motion described in Chapter 3. Various special cases are considered including combinations of power law central forces and the monopole–oscillator problem.

P1 Vector Identities

For $\boldsymbol{a} = a_1\boldsymbol{i} + a_2\boldsymbol{j} + a_3\boldsymbol{k}$ and $\boldsymbol{b} = b_1\boldsymbol{i} + b_2\boldsymbol{j} + b_3\boldsymbol{k}$ two vectors in three–space, where $\boldsymbol{i}$, $\boldsymbol{j}$ and $\boldsymbol{k}$ denote the orthonormal Cartesian basis vectors, with $\boldsymbol{i} \times \boldsymbol{j} = \boldsymbol{k}$, $\boldsymbol{j} \times \boldsymbol{k} = \boldsymbol{i}$, $\boldsymbol{k} \times \boldsymbol{i} = \boldsymbol{j}$, the scalar or dot product is given by

$$\boldsymbol{a} \cdot \boldsymbol{b} = a_1 b_1 + a_2 b_2 + a_3 b_3 \tag{P1.1}$$

and the vector or cross product by the determinant

$$\boldsymbol{a} \times \boldsymbol{b} = \begin{vmatrix} \boldsymbol{i} & \boldsymbol{j} & \boldsymbol{k} \\ a_1 & a_2 & a_3 \\ b_1 & b_2 & b_3 \end{vmatrix}. \tag{P1.2}$$

Given any non–null vector $\boldsymbol{a}$ it is possible to define a unit vector $\hat{\boldsymbol{a}}$ with unit magnitude in the direction of $\boldsymbol{a}$ such that

$$\boldsymbol{a} = |\boldsymbol{a}|\hat{\boldsymbol{a}} \equiv a\hat{\boldsymbol{a}}, \tag{P1.3}$$

where $|\boldsymbol{a}|$, also denoted a, is the magnitude of $\boldsymbol{a}$. It is then obvious that

$$\begin{aligned} &\hat{\boldsymbol{a}} \cdot \hat{\boldsymbol{a}} = |\hat{\boldsymbol{a}}|^2 = 1 \\ &\boldsymbol{a} \cdot \boldsymbol{a} = a\hat{\boldsymbol{a}} \cdot a\hat{\boldsymbol{a}} = a^2\hat{\boldsymbol{a}} \cdot \hat{\boldsymbol{a}} = a^2 \\ &\hat{\boldsymbol{a}} \times \hat{\boldsymbol{a}} = \boldsymbol{0} \\ &\boldsymbol{a} \times \boldsymbol{a} = a^2(\hat{\boldsymbol{a}} \times \hat{\boldsymbol{a}}) = \boldsymbol{0}. \end{aligned} \tag{P1.4}$$

Using the above definitions for the scalar and vector products (P1.1) and (P1.2) the following coordinate–free vector identities can be obtained.

The scalar product of two vectors $\boldsymbol{a}$ and $\boldsymbol{b}$ is commutative, *i.e.*,

$$\boldsymbol{a} \cdot \boldsymbol{b} = \boldsymbol{b} \cdot \boldsymbol{a}. \tag{P1.5}$$

The vector product of two vectors $\boldsymbol{a}$ and $\boldsymbol{b}$ is anticommutative

$$\boldsymbol{a} \times \boldsymbol{b} = -\boldsymbol{b} \times \boldsymbol{a}. \tag{P1.6}$$

The scalar triple product $\boldsymbol{a} \times \boldsymbol{b} \cdot \boldsymbol{c}$ also written $[\boldsymbol{a}, \boldsymbol{b}, \boldsymbol{c}]$ is cyclic, *i.e.*,

$$[\boldsymbol{a}, \boldsymbol{b}, \boldsymbol{c}] = [\boldsymbol{c}, \boldsymbol{a}, \boldsymbol{b}] = [\boldsymbol{b}, \boldsymbol{c}, \boldsymbol{a}] = -[\boldsymbol{a}, \boldsymbol{c}, \boldsymbol{b}] = -[\boldsymbol{c}, \boldsymbol{b}, \boldsymbol{a}] = -[\boldsymbol{b}, \boldsymbol{a}, \boldsymbol{c}]. \tag{P1.7}$$

The vector triple product of three arbitrary vectors $\boldsymbol{a}$, $\boldsymbol{b}$ and $\boldsymbol{c}$ is given by

$$\boldsymbol{a} \times (\boldsymbol{b} \times \boldsymbol{c}) = \boldsymbol{b}(\boldsymbol{a} \cdot \boldsymbol{c}) - \boldsymbol{c}(\boldsymbol{a} \cdot \boldsymbol{b}). \tag{P1.8}$$

The vector triple product obeys the Jacobi identity

$$\boldsymbol{a} \times (\boldsymbol{b} \times \boldsymbol{c}) + \boldsymbol{c} \times (\boldsymbol{a} \times \boldsymbol{b}) + \boldsymbol{b} \times (\boldsymbol{c} \times \boldsymbol{a}) = \boldsymbol{0}. \tag{P1.9}$$

For $\boldsymbol{a}$ and $\boldsymbol{b}$ arbitrary vectors in three–space, it is clear from (P1.4) and (P1.7) that

$$\begin{aligned} \boldsymbol{a} \cdot (\boldsymbol{a} \times \boldsymbol{b}) &= 0 \\ \boldsymbol{b} \cdot (\boldsymbol{a} \times \boldsymbol{b}) &= 0. \end{aligned} \tag{P1.10}$$

Use will also be made of the following results from vector calculus. For $\boldsymbol{a}$ and $\boldsymbol{b}$ differentiable vector functions of t, and $\phi(t)$ a differentiable scalar function

$$\begin{aligned} \frac{\mathrm{d}}{\mathrm{d}t}(\boldsymbol{a} + \boldsymbol{b}) &= \dot{\boldsymbol{a}} + \dot{\boldsymbol{b}} \\ \frac{\mathrm{d}}{\mathrm{d}t}(\phi \boldsymbol{a}) &= \dot{\phi}\boldsymbol{a} + \phi\dot{\boldsymbol{a}} \\ \frac{\mathrm{d}}{\mathrm{d}t}(\boldsymbol{a} \cdot \boldsymbol{b}) &= \dot{\boldsymbol{a}} \cdot \boldsymbol{b} + \boldsymbol{a} \cdot \dot{\boldsymbol{b}} \\ \frac{\mathrm{d}}{\mathrm{d}t}(\boldsymbol{a} \times \boldsymbol{b}) &= \dot{\boldsymbol{a}} \times \boldsymbol{b} + \boldsymbol{a} \times \dot{\boldsymbol{b}}, \end{aligned} \tag{P1.11}$$

where the superscript $\dot{}$ denotes differentiation with respect to t. It is then obvious from (P1.11) that

$$\begin{aligned} \hat{\boldsymbol{a}} \cdot \dot{\hat{\boldsymbol{a}}} &= \frac{1}{2}\frac{\mathrm{d}}{\mathrm{d}t}(\hat{\boldsymbol{a}} \cdot \hat{\boldsymbol{a}}) = 0 \\ \boldsymbol{a} \cdot \dot{\boldsymbol{a}} &= a\hat{\boldsymbol{a}} \cdot (\dot{a}\hat{\boldsymbol{a}} + a\dot{\hat{\boldsymbol{a}}}) = a\dot{a}. \end{aligned} \tag{P1.12}$$

P2 The Geometry of Conic Sections

P2.1 Focus–Centred Conic Sections

With reference to Figure P2.1 an ellipse is defined as the locus of a point such that the sum of the distances from two fixed points F and F' is constant. The points F and F' are called foci. From the diagram

$$r' + r = 2a, \tag{P2.1}$$

where a is the semi–major axis length or half of the largest diameter of the ellipse. Fixing the origin at the focus F and taking the scalar product of the vector $\boldsymbol{r}' = 2ae\boldsymbol{i} + \boldsymbol{r}$ with itself gives

$$r'^2 = r^2 + 4a^2e^2 + 4rae\cos\theta, \tag{P2.2}$$

where ae is the distance between each focus and the geometric centre of the ellipse. e is known as the eccentricity and varies between 0 (a circle) and 1 (a parabola). Replacing r' in (P2.2) using (P2.1) gives

$$r = \frac{a(1-e^2)}{1+e\cos\theta}, \tag{P2.3}$$

which is equivalent to the cartesian expression

$$\frac{(x+ae)^2}{a^2} + \frac{y^2}{a^2(1-e^2)} = 1. \tag{P2.4}$$

This is the equation of a focus–centred ellipse in plane polar coordinates. Referring to Figure P2.1 the semi–minor axis length or half of the smallest diameter is given by

$$b = a(1-e^2)^{\frac{1}{2}}. \tag{P2.5}$$

The area of the ellipse is easily shown by integration to be

$$S = \pi ab. \tag{P2.6}$$

A hyperbola is defined as the locus of a point such that the difference of its distances from two fixed points, the foci F and F' is constant. The two branches of the hyperbola are given by

$$\begin{aligned} r' - r &= 2a \quad (+ \text{ branch}) \\ r' - r &= -2a \quad (- \text{ branch}). \end{aligned} \tag{P2.7}$$

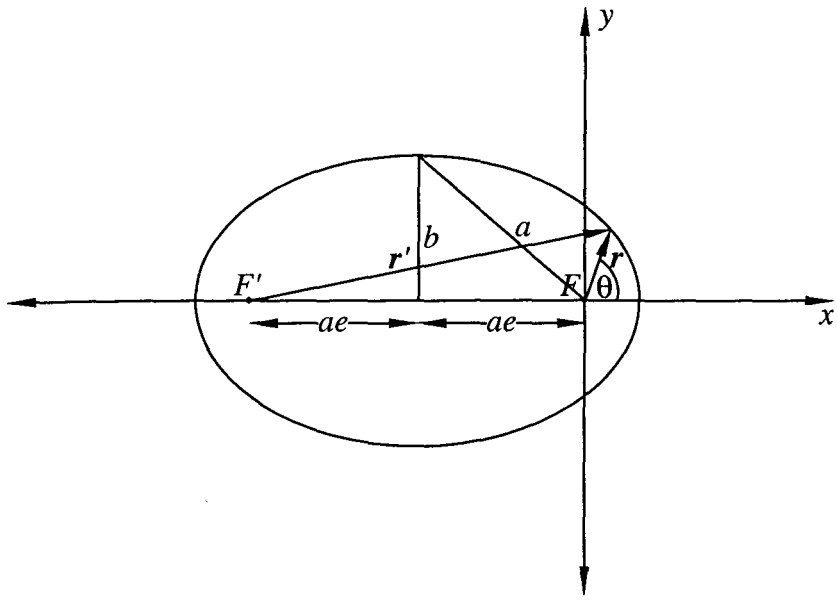


Figure P2.1. The geometry of the focus–centred ellipse.

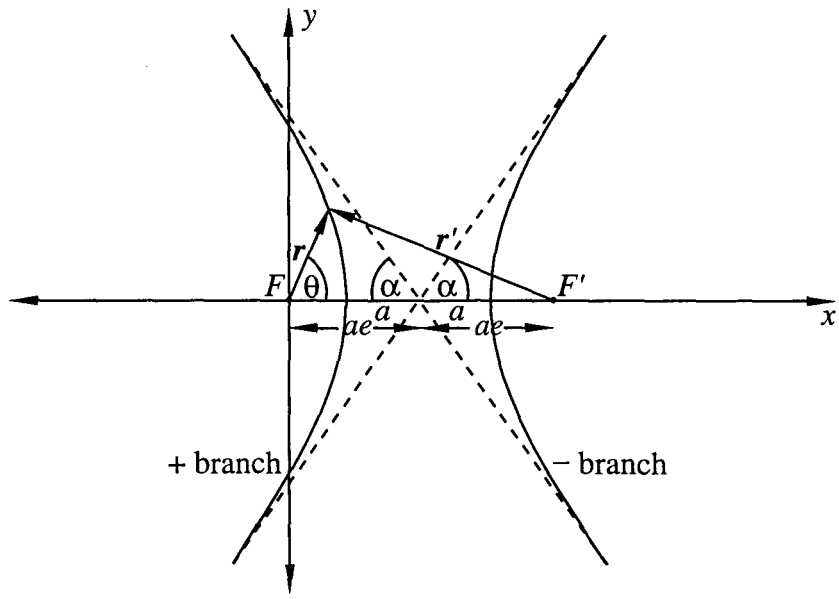


Figure P2.2. The geometry of the focus–centred hyperbola.

Referring to Figure P2.2 the branch which encircles F will be called the + branch and the other the − branch. The equation for the hyperbola in plane polar coordinates is easily seen to be

$$r = \frac{a(e^2 - 1)}{\pm 1 + e\cos\theta} \tag{P2.8}$$

in which the eccentricity is now larger than 1. The asymptotes of the hyperbola are given by

$$\cos\alpha = \mp\frac{1}{e}. \tag{P2.9}$$

The cartesian expression equivalent to equation (P2.8) is given by

$$\frac{(x - ae)^2}{a^2} - \frac{y^2}{a^2(e^2 - 1)} = 1, \tag{P2.10}$$

where e is now greater than 1.

The parabola is the locus of a point such that the distance from a fixed line D (the directrix) is equal to the distance from the fixed focus F. From Figure P2.3 we see that

$$r = \frac{2a}{1 + \cos\theta} \tag{P2.11}$$

where a is the distance from the focus F to the directrix D. The equivalent cartesian expression for (P2.11) is given by

$$y^2 = -4a(x - a). \tag{P2.12}$$

Subsuming all three polar expressions into the standard form

$$r = \frac{1}{A + B\cos\theta} \tag{P2.13}$$

it is easy to show that in all cases

$$e = \frac{B}{|A|} \tag{P2.14}$$

and also that

$$a = \left|\frac{A}{A^2 - B^2}\right| \tag{P2.15}$$

for the ellipse and the hyperbola.

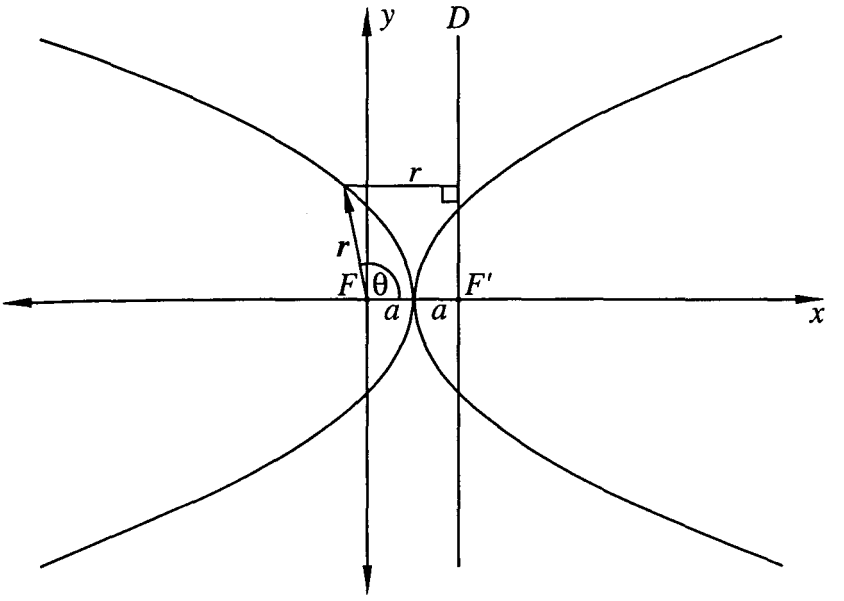


Figure P2.3. The geometry of the focus–centred parabola.

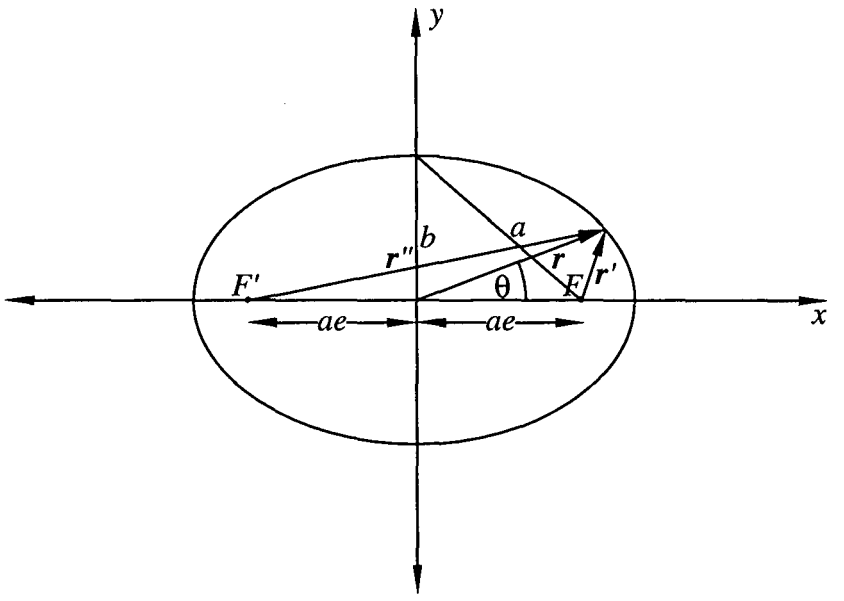


Figure P2.4. The geometry of the geometric–centred ellipse.

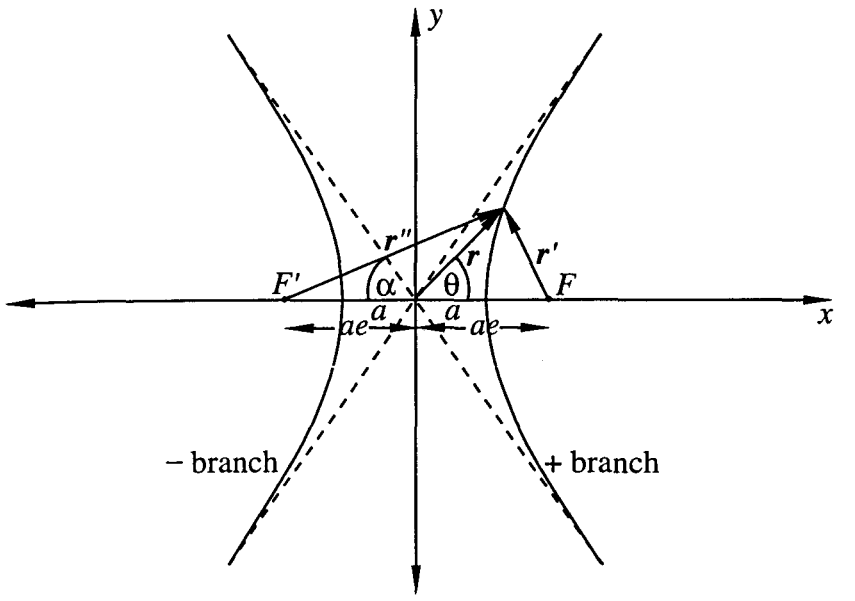


Figure P2.5. The geometry of the geometric–centred hyperbola.

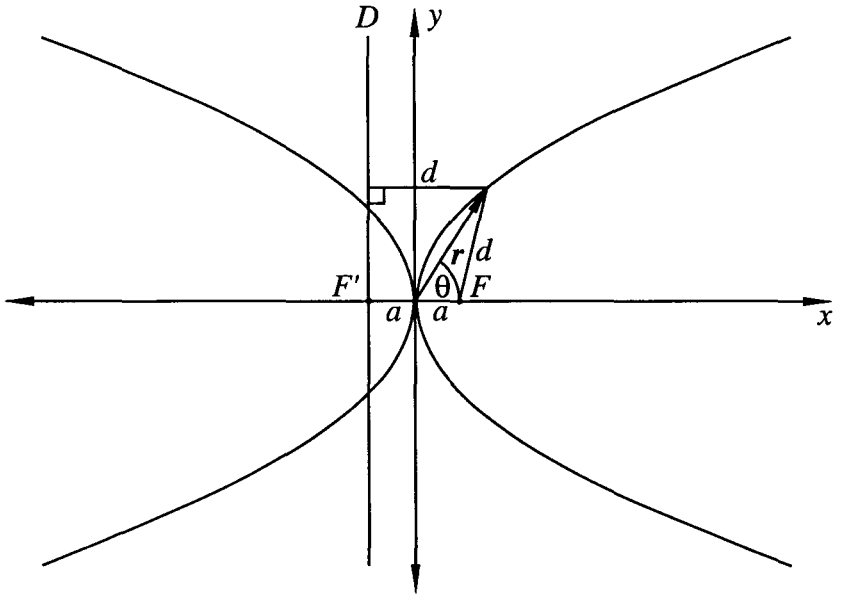


Figure P2.6. The geometry of the geometric–centred parabola.

P2.2 Geometric–Centred Conic Sections

Referring to Figure P2.4 and equation (P2.2) it is a straightforward calculation to show that the plane polar equation for a geometric–centred ellipse is given by

$$r^2 = \frac{2a^2(1-e^2)}{(2-e^2)-e^2\cos 2\theta} \tag{P2.16}$$

which is equivalent to the cartesian expression

$$\frac{x^2}{a^2} + \frac{y^2}{a^2(1-e^2)} = 1. \tag{P2.17}$$

The hyperbola shown in Figure P2.5 expressed in plane polar coordinates is also given by (P2.16) and the cartesian representation is given by (P2.17), realising of course that e is greater than 1. The plane polar representation for the parabola shown in Figure P2.6 is given by

$$r = -\frac{8a\cos\theta}{1-\cos 2\theta} \tag{P2.18}$$

with the equivalent cartesian representation

$$y^2 = -4ax. \tag{P2.19}$$

P3 Lie Analysis and First Integrals

P3.1 The Lie Symmetries

The following somewhat simplified discussion of Lie analysis is based on that given by Leach and Mahomed in [80]. More rigorous treatments of the Lie analysis are described in the textbooks of Bluman and Kumei [9], Sattinger and Weaver [117] and Ince [55] amongst a host of other books and papers dealing with this extensive subject. If we assume a general one–parameter group of transformations

$$\bar{x} = f(x,y;\varepsilon) \qquad \bar{y} = g(x,y;\varepsilon) \tag{P3.1}$$

with $x = f(x,y;0)$ and $y = g(x,y;0)$, then, expanding (P3.1) in a Taylor series around $\varepsilon = 0$ and retaining only linear terms in ε, we obtain

$$\bar{x} = x + \varepsilon\left.\frac{\mathrm{d}f}{\mathrm{d}\varepsilon}\right|_{\varepsilon=0} + O(\varepsilon^2) \qquad \bar{y} = y + \varepsilon\left.\frac{\mathrm{d}g}{\mathrm{d}\varepsilon}\right|_{\varepsilon=0} + O(\varepsilon^2). \tag{P3.2}$$

We define the functions ξ and η which describe the transformation (P3.2) around $\varepsilon = 0$ as

$$\xi(x,y) = \left.\frac{\mathrm{d}f}{\mathrm{d}\varepsilon}\right|_{\varepsilon=0} \qquad \eta(x,y) = \left.\frac{\mathrm{d}g}{\mathrm{d}\varepsilon}\right|_{\varepsilon=0}. \tag{P3.3}$$

Equation (P3.2) can be rewritten (ignoring powers of ε higher than 1) as

$$\bar{x} = (1 + \varepsilon G)x \quad \bar{y} = (1 + \varepsilon G)y, \tag{P3.4}$$

where

$$G = \xi(x, y)\frac{\partial}{\partial x} + \eta(x, y)\frac{\partial}{\partial y}. \tag{P3.5}$$

The infinitesimal transformation induced in a function $f(x, y)$ is (to the first order **in** ε)

$$\bar{f} := f(\bar{x}, \bar{y}) = (1 + \varepsilon G)f(x, y). \tag{P3.6}$$

Of particular interest are those transformations which leave a function invariant, *i.e.*, $\bar{f} = f$ which implies that

$$Gf = 0. \tag{P3.7}$$

If we consider the differential equation

$$E(x, y, y', \ldots, y^{(n)}) = 0, \tag{P3.8}$$

it is necessary to have transformation rules for the derivatives. We have

$$\begin{aligned} \frac{\mathrm{d}\bar{y}}{\mathrm{d}\bar{x}} &= \frac{\mathrm{d}(y + \varepsilon\eta)}{\mathrm{d}(x + \varepsilon\xi)} = \frac{\mathrm{d}y + \varepsilon\mathrm{d}\eta}{\mathrm{d}x + \varepsilon\mathrm{d}\xi} \\ &= \frac{\dfrac{\mathrm{d}y}{\mathrm{d}x} + \varepsilon\dfrac{\mathrm{d}\eta}{\mathrm{d}x}}{1 + \varepsilon\dfrac{\mathrm{d}\xi}{\mathrm{d}x}} = (y' + \varepsilon\eta')(1 + \varepsilon\xi')^{-1} \\ &= (y' + \varepsilon\eta')(1 - \varepsilon\xi' + \varepsilon^2\xi'^2 + \ldots) = y' + \varepsilon(\eta' - y'\xi') + O(\varepsilon^2) \end{aligned} \tag{P3.9}$$

neglecting powers of ε which are greater than one since ε is an infinitesimal. Equation (P3.9) can also be written as

$$\bar{y}' = y' + \varepsilon\eta^{[1]}(x, y, y'). \tag{P3.10}$$

Higher order derivatives transform according to

$$\frac{\mathrm{d}^k\bar{y}}{\mathrm{d}\bar{x}^k} = \frac{\mathrm{d}^k y}{\mathrm{d}x^k} + \varepsilon\eta^{[k]}(x, y, \ldots, y^{(k)}) + O(\varepsilon^2), \tag{P3.11}$$

where it can be proved that

$$\eta^{[k]} = \frac{\mathrm{d}}{\mathrm{d}x}\eta^{[k-1]} - y^{(k)}\frac{\mathrm{d}\xi}{\mathrm{d}x}, \quad k = 1, n \tag{P3.12}$$

with $y^{(k)} = \dfrac{\mathrm{d}^k y}{\mathrm{d}x^k}$ and $\eta^{[0]} \equiv \eta$. It should also be realised that $\dfrac{\mathrm{d}}{\mathrm{d}x} = \dfrac{\partial}{\partial x} + y'\dfrac{\partial}{\partial y} + \ldots + y^{(k)}\dfrac{\partial}{\partial y^{(k-1)}}$.

An nth order ordinary differential equation can be written implicitly as

$$E(x, y, y', \ldots, y^{(n)}) = 0. \tag{P3.13}$$

Invariance of (P3.13) under an infinitesimal transformation means that

$$E(\bar{x}, \bar{y}, \bar{y}', \ldots, \bar{y}^{(n)}) = 0. \tag{P3.14}$$

Now

$$\begin{aligned} E(\bar{x}, \bar{y}, \ldots, \bar{y}^{(n)}) &= E(x, y, \ldots, y^{(n)}) + \varepsilon \left.\frac{\mathrm{d}E}{\mathrm{d}\varepsilon}\right|_{\varepsilon=0} + O(\varepsilon^2) \\ &= E + \varepsilon \left(\frac{\partial E}{\partial \bar{x}} \frac{\mathrm{d}\bar{x}}{\mathrm{d}\varepsilon} + \frac{\partial E}{\partial \bar{y}} \frac{\mathrm{d}\bar{y}}{\mathrm{d}\varepsilon} + \ldots + \frac{\partial E}{\partial \bar{y}^{(n)}} \frac{\mathrm{d}\bar{y}^{(n)}}{\mathrm{d}\varepsilon} \right) \Bigg|_{\varepsilon=0} \\ &= E + \varepsilon \left(\xi(\bar{x}, \bar{y}) \frac{\partial E}{\partial \bar{x}} + \eta(\bar{x}, \bar{y}) \frac{\partial E}{\partial \bar{y}} + \ldots \right. \\ &\qquad \left. + \eta^{[n]}(\bar{x}, \bar{y}, \ldots, \bar{y}^{(n)}) \frac{\partial E}{\partial y^{(n)}} \right) \Bigg|_{\varepsilon=0} \\ &= E + \varepsilon G^{[n]} E + O(\varepsilon^2). \end{aligned} \tag{P3.15}$$

Since $E = 0$, the invariance requirement gives that

$$G^{[n]} E = 0, \tag{P3.16}$$

where

$$\begin{aligned} G^{[n]} &= \xi(x, y) \frac{\partial}{\partial x} + \eta(x, y) \frac{\partial}{\partial y} + \eta^{[1]}(x, y, y') \frac{\partial}{\partial y'} + \ldots \\ &\quad + \eta^{[n]}(x, y, \ldots, y^{[n]}) \frac{\partial}{\partial y^{(n)}} \\ &= G + \sum_{j=1}^{n} \eta^{[j]}(x, y, \ldots, y^{(j)}) \frac{\partial}{\partial y^{(j)}} \\ &\qquad \eta^{[0]} \equiv \eta, \quad y^{(0)} \equiv y \end{aligned} \tag{P3.17}$$

is referred to as the nth extension of G. The symmetries of an nth order ordinary differential equation are obtained by applying the nth extension of G to the differential equation, expanding all the derivatives and removing the nth derivative terms using the differential equation. Since the ξ and η terms of the resulting equation depend only on x and y, the resulting equation is separated according to powers of the derivatives of x and y and the resulting system of partial differential equations is solved to obtain ξ and η as functions of x and y containing a number of arbitrary parameters. The k–parameter symmetry is separated into k one parameter symmetries by setting each of the free parameters in turn to unity and the rest to zero (or some

equivalent procedure). The Lie algebra of the symmetries is obtained by calculating the commutators of the resulting symmetries and comparing the set to standard forms. From the symmetry algebra the differential equation can be transformed to a standard representative equation for that algebra, in which form it is hoped that the solution is more transparent.

It should be appreciated that this process is extremely tedious to apply by hand and prone to error. Many computer programs exist to automate this procedure. One very useful example is the public domain program LIE written by Allan Head [50]. It attempts to solve analytically the coupled sets of partial differential equations arising from application of the extended generator on either a single or coupled set of ordinary or partial differential equations. In the worst case, it can provide the full set of coupled partial differential equations, which is in itself a major task to implement by hand.

One can extend the treatment above to cater for systems of differential equations. By treating E as a vector differential equation, x and y as subscripted multivariables and ξ and η as the corresponding multifunctions, the technique described above can be implemented with no real changes. Chapter 4 demonstrates this procedure for a system of coupled second order equations.

Once the infinitesimal generators are known, it is possible to relate them to the finite equations of the invariance transformation. This is done using (P3.3), replacing ξ and η by the relevant quantities appearing in the generator *i.e.*

$$\frac{\mathrm{d}\bar{x}}{\mathrm{d}\varepsilon} = \xi(\bar{x},\bar{y}) \qquad \frac{\mathrm{d}\bar{y}}{\mathrm{d}\varepsilon} = \eta(\bar{x},\bar{y}) \tag{P3.18}$$

with $\bar{x}(\varepsilon = 0) = x$ and $\bar{y}(\varepsilon = 0) = y$.

To illustrate the procedure let us consider the self–similar symmetry

$$G_{SS} = x\frac{\partial}{\partial x} - \frac{2}{\alpha}y\frac{\partial}{\partial y}, \tag{P3.19}$$

where α is a constant, which is treated in some detail in §§2.15–2.17. Using (P3.18) and (P3.5) we find that

$$\frac{\mathrm{d}\bar{x}}{\mathrm{d}\varepsilon} = \bar{x} \quad \frac{\mathrm{d}\bar{y}}{\mathrm{d}\varepsilon} = -2\frac{\bar{y}}{\alpha}, \quad \bar{x}(\varepsilon = 0) = x \quad \bar{y}(\varepsilon = 0) = y. \tag{P3.20}$$

This set of equations can easily be solved to give

$$\bar{x} = e^{\varepsilon}x \qquad \bar{y} = e^{-\frac{2\varepsilon}{\alpha}}y, \tag{P3.21}$$

which can equivalently be rewritten as

$$\bar{x} = \gamma x \qquad \bar{y} = \gamma^{-\frac{2}{\alpha}} y, \tag{P3.22}$$

where γ is some constant.

Thus differential equations which possess the self–similar symmetry (P3.19) are invariant under the transformation (P3.22).

P3.2 The First Integrals Associated with the Lie Symmetries

A function $I(x, y, y', \ldots, y^{(j)})$, where j can take on any value from 0 to $n-1$ is an invariant of the extended group $G^{[j]}$ if $I(x, y, y', \ldots, y^{(j)}) = I(\bar{x}, \bar{y}, \bar{y}', \ldots, \bar{y}^{(j)})$, *i.e.*

$$G^{[j]} I = 0, \tag{P3.23}$$

which is equivalent to writing

$$\xi(x,y)\frac{\partial I}{\partial x} + \eta(x,y)\frac{\partial I}{\partial y} + \ldots + \eta^{[j]}(x, y, \ldots, y^{(j)})\frac{\partial I}{\partial y^{(j)}} = 0 \tag{P3.24}$$

which is a linear first–order partial differential equation. Associated with this partial differential equation we have $j+1$ equations which can in theory be solved for the j characteristics or differential invariants of the extended group. The equations are

$$\frac{\mathrm{d}x}{\xi(x,y)} = \frac{\mathrm{d}y}{\eta(x,y)} = \frac{\mathrm{d}y'}{\eta^{[1]}(x,y,y')} = \ldots = \frac{\mathrm{d}y^{(j)}}{\eta^{[j]}(x, y, \ldots, y^{(j)})}. \tag{P3.25}$$

The addition of the restriction that the invariant be a first integral also, *i.e.* that

$$\left.\frac{\mathrm{d}I}{\mathrm{d}x}\right|_{E=0} = 0, \tag{P3.26}$$

results in a system of j equations, which can be solved in terms of $j-1$ characteristics, each of which is a first integral of the differential equation E.

Although the solution of the characteristics in (P3.25) can be extremely involved, it does demonstrate one possible technique for constructing first integrals which does not require an *a priori* ansatz for the structure of the integral. It does, however, assume that the first integral is associated with a point transformation which is not always the case. For example

$$I = x^2 + y^2 + y'^2 \tag{P3.27}$$

is a first integral of the differential equation

$$y'y'' + yy' + x = 0 \tag{P3.28}$$

although (P3.28) does not possess any point symmetries.

CHAPTER 1

MOTION WITH CONSERVED L

1.1 The Conserved Hamilton and Laplace–Runge–Lenz Vector Analogues for the Equation of Motion $\ddot{\boldsymbol{r}} + f\boldsymbol{r} = \mathbf{0}$

The techniques in this and subsequent chapters which employ the use of scalar and vector products to obtain first integrals or constants of the motion, as well as the velocity hodograph and orbit equation, are natural extensions of those discussed by Runge [114, §5. p79ff] Bleuler and Kustaanheimo [8], Collas [20], Collinson [21, 22] and Pollard [108] which have been applied to the standard Kepler problem. By only requiring a constraint on the structure of the angular momentum it is possible to generalise many of the results for the standard Kepler problem and find analogues for Hamilton's vector [48] and the Laplace–Runge–Lenz vector [69, 114, 81].

We define the angular momentum of a particle as

$$\boldsymbol{L} = \boldsymbol{r} \times \dot{\boldsymbol{r}}. \tag{1.1.1}$$

It is immediately apparent from (P1.7) and (P1.10) that

$$\boldsymbol{L} \cdot \boldsymbol{r} = 0 \tag{1.1.2}$$

and

$$\boldsymbol{L} \cdot \dot{\boldsymbol{r}} = 0. \tag{1.1.3}$$

If we place the added restrictions on $\boldsymbol{L}$ that for any orbit both its magnitude and direction must be conserved, we have

$$\dot{\boldsymbol{L}} = \mathbf{0} \iff \begin{matrix} \dot{L} = 0 \\ \dot{\hat{\boldsymbol{L}}} = \mathbf{0}, \end{matrix} \tag{1.1.4}$$

i.e., L is a constant and $\hat{\boldsymbol{L}}$ is a constant vector, where $\boldsymbol{L}$ is assumed non–zero. Since $\hat{\boldsymbol{L}}$ is constant, the motion is *planar*. Equation (1.1.4) can be rewritten as

$$\boldsymbol{r} \times \ddot{\boldsymbol{r}} = \mathbf{0} = \boldsymbol{r} \times (\ddot{\boldsymbol{r}} + f\boldsymbol{r}) \tag{1.1.5}$$

where f is an unrestricted function of the equation's variables, and so the equation of motion

$$\ddot{\boldsymbol{r}} + f\boldsymbol{r} = \mathbf{0}, \tag{1.1.6}$$

describes motion in a plane with $\boldsymbol{L}$ conserved. When $f = \mu/r^3$, we obtain the Kepler problem which is one of the most widely studied paradigms of classical mechanics and, for $f = f(r)$, equation (1.1.6) describes the familiar central force problem with its characteristic planar orbit (see §1.6).

Many textbook treatments that deal with the Laplace–Runge–Lenz vector have been criticised as being too ad hoc [59] in obtaining the Laplace–Runge–Lenz vector. I have tried to provide a natural and systematic procedure for finding the first integrals and orbit equations using vector operations directly on the equation of motion. Using this technique it has been possible to generalise many of the systems for which first integrals have been previously obtained. Invariably previous techniques, which were based on guessing the structure of the integral, or applications of Noether's theorem or Lie analysis, were mathematically very technical and much of the elegant vector nature of the first integrals was obscured.

Equation (1.1.6) can be rewritten as

$$\frac{\mathrm{d}}{\mathrm{d}t}\left(\dot{\boldsymbol{r}}\right) + f\boldsymbol{r} = \boldsymbol{0} \tag{1.1.7}$$

which formally gives rise to the conserved Hamilton vector analogue

$$\boldsymbol{K} = \dot{\boldsymbol{r}} + \int f\boldsymbol{r}\ \mathrm{d}t. \tag{1.1.8}$$

Since $\hat{\boldsymbol{L}}$ is a constant vector, we can construct a further constant Laplace–Runge–Lenz vector analogue orthogonal to both $\boldsymbol{L}$ and $\boldsymbol{K}$ using the arguments of (P1.10) which gives

$$\boldsymbol{J} = \boldsymbol{K} \times \hat{\boldsymbol{L}} = \dot{\boldsymbol{r}} \times \hat{\boldsymbol{L}} - \hat{\boldsymbol{L}} \times \int f\boldsymbol{r}\ \mathrm{d}t. \tag{1.1.9}$$

Making use of the planar nature of the orbit allows us to express the vector constants of motion in terms of plane polar coordinates (r, θ), where θ is measured from $\boldsymbol{i}$. This allows us to write

$$\boldsymbol{r} = r\hat{\boldsymbol{r}}, \tag{1.1.10}$$

where

$$\hat{\boldsymbol{r}} = \boldsymbol{i}\cos\theta + \boldsymbol{j}\sin\theta. \tag{1.1.11}$$

The unit vector orthogonal to $\hat{\boldsymbol{r}}$ is given by

$$\hat{\boldsymbol{\theta}} = -\boldsymbol{i}\sin\theta + \boldsymbol{j}\cos\theta. \tag{1.1.12}$$

Now

$$\boldsymbol{L} = \boldsymbol{r}\times\dot{\boldsymbol{r}} = r^2\dot{\theta}\hat{\boldsymbol{L}} = r^2\dot{\theta}\boldsymbol{k}, \tag{1.1.13}$$

since $\hat{\boldsymbol{L}}$ is perpendicular to the plane of $\hat{\boldsymbol{r}}$ and $\hat{\boldsymbol{\theta}}$. It is easy to show by differentiating (1.1.11) and (1.1.12) that

$$\dot{\hat{\boldsymbol{r}}} = \dot{\theta}\hat{\boldsymbol{\theta}} \tag{1.1.14}$$

and

$$\dot{\hat{\boldsymbol{\theta}}} = -\dot{\theta}\hat{\boldsymbol{r}} \tag{1.1.15}$$

and also using (1.1.14) and (1.1.15) that

$$\dot{\boldsymbol{r}} = \dot{r}\hat{\boldsymbol{r}} + r\dot{\hat{\boldsymbol{r}}} = \dot{r}\hat{\boldsymbol{r}} + r\dot{\theta}\hat{\boldsymbol{\theta}}. \tag{1.1.16}$$

Returning to equation (1.1.8) and (1.1.9) and attempting to reduce $\int f\boldsymbol{r}\mathrm{d}t$ to a quadrature requires us to set

$$fr = v(\theta)\dot{\theta}. \tag{1.1.17}$$

This is, incidentally, a generalisation of the equation $\dot{\theta} = L/r^2$ which is used in conventional treatments of the power law central force problem in conjunction with the conserved energy to obtain the orbit equation [122, 33]. Using the substitution of (1.1.17)

$$\begin{aligned} \int f\boldsymbol{r}\ \mathrm{d}t &= \boldsymbol{i}\int_{\theta_0}^{\theta} v(\eta)\cos\eta\ \mathrm{d}\eta + \boldsymbol{j}\int_{\theta_0}^{\theta} v(\eta)\sin\eta\ \mathrm{d}\eta \\ &= \hat{\boldsymbol{r}}z'(\theta) - \hat{\boldsymbol{\theta}}z(\theta), \end{aligned} \tag{1.1.18}$$

where

$$z(\theta) = \int_{\theta_0}^{\theta} v(\eta)\sin(\theta-\eta)\ \mathrm{d}\eta \tag{1.1.19}$$

and

$$\begin{aligned} z'(\theta) &= v(\eta)\sin(\theta-\eta)\Big|_{\eta=\theta} + \int_{\theta_0}^{\theta} v(\eta)\cos(\theta-\eta)\ \mathrm{d}\eta \\ &= \int_{\theta_0}^{\theta} v(\eta)\cos(\theta-\eta)\ \mathrm{d}\eta. \end{aligned} \tag{1.1.20}$$

Alternatively we may write

$$z''(\theta) + z(\theta) = v(\theta), \tag{1.1.21}$$

where $z(\theta_0) = 0$ and $z'(\theta_0) = 0$. Hence

$$\boldsymbol{K} = \dot{\boldsymbol{r}} + z'(\theta)\hat{\boldsymbol{r}} - z(\theta)\hat{\boldsymbol{\theta}} \tag{1.1.22}$$

and

$$\boldsymbol{J} = \dot{\boldsymbol{r}}\times\hat{\boldsymbol{L}} - z(\theta)\hat{\boldsymbol{r}} - z'(\theta)\hat{\boldsymbol{\theta}}. \tag{1.1.23}$$

1.2 The Velocity Hodograph and the Orbit Equation

The procedure adopted here is to use the conserved Hamilton vector analogue $\boldsymbol{K}$ to construct the velocity hodograph and the conserved Laplace–Runge–Lenz vector analogue $\boldsymbol{J}$ to construct the the orbit equation using straightforward vector manipulations. It should also be mentioned that most references to the velocity hodograph appear to have focussed on the Kepler problem, no doubt as a result of its simplicity.

We use (1.1.22) to derive the velocity hodograph and (1.1.23) to obtain the orbit equation. Rewriting the expression for the Hamilton–like vector (1.1.22) as

$$\dot{\boldsymbol{r}} - \boldsymbol{K} = z(\theta)\hat{\boldsymbol{\theta}} - z'(\theta)\hat{\boldsymbol{r}} \tag{1.2.1}$$

and squaring gives the component form

$$(\dot{x} - K_x)^2 + (\dot{y} - K_y)^2 = z^2(\theta) + z'^2(\theta). \tag{1.2.2}$$

If we assume that the angle between $\boldsymbol{J}$ and $\boldsymbol{i}$ is θ_0,

$$K_x = -K\sin\theta_0, \quad K_y = K\cos\theta_0 \tag{1.2.3}$$

and we may rewrite (1.2.2) as

$$(\dot{x} + K\sin\theta_0)^2 + (\dot{y} - K\cos\theta_0)^2 = z^2 + z'^2. \tag{1.2.4}$$

In general (1.2.4) does not describe any recognisable curve since the right hand side of the expression depends on θ. For the particular choice $v(\theta) = A$, $z(\theta)$ and $z'(\theta)$ are given by

$$z = A\big(1 - \cos(\theta - \theta_0)\big), \quad z' = A\sin(\theta - \theta_0), \tag{1.2.5}$$

and the velocity hodograph can be expressed rather elegantly. If we compare the expression for $\boldsymbol{K}$ given in (1.1.22) written in terms of cartesian components, with the cartesian expression

$$\boldsymbol{K} = K_x\,\boldsymbol{i} + K_y\,\boldsymbol{j} = K(-\boldsymbol{i}\sin\theta_0 + \boldsymbol{j}\cos\theta_0), \tag{1.2.6}$$

it is possible to obtain expressions relating $\sin\theta$ and $\cos\theta$ in terms of $\sin\theta_0$ and $\cos\theta_0$, *i.e.*,

$$\begin{aligned} \sin\theta &= \frac{K_x - \dot{x}}{A} + \sin\theta_0 \\ \cos\theta &= \frac{\dot{y} - K_y}{A} + \cos\theta_0. \end{aligned} \tag{1.2.7}$$

Expanding the right hand side of (1.2.4) using (1.2.7) and rearranging gives the familiar form

$$(\dot{x} + (K - A)\sin\theta_0)^2 + (\dot{y} - (K - A)\cos\theta_0)^2 = A^2, \tag{1.2.8}$$

which describes a circle with centre $(-(K - A)\sin\theta_0,\ (K - A)\cos\theta_0)$ and radius A. Notice that both z and z' must satisfy the conditions $z(0) = z'(0) = 0$ which precludes the obvious choice z =constant, $z' = 0$. Equation (1.2.8) will be investigated further in §1.5.

The orbit equation is obtained by taking the scalar product of $\boldsymbol{r}$ with $\boldsymbol{J}$. As stated before, the angle between $\boldsymbol{J}$ and $\boldsymbol{i}$ is θ_0. Hence

$$r(\theta) = \frac{L}{z(\theta) + J\cos(\theta - \theta_0)}. \tag{1.2.9}$$

1.3 The Motion in Time

The motion in time can be evaluated by differentiating (1.2.9) to give t as a function of r or, alternatively, to use the conservation of angular momentum to yield t as a function of θ. Differentiation of (1.2.9) gives

$$\dot{r} = -z' + J\sin(\theta - \theta_0). \tag{1.3.1}$$

Using (1.1.20) to evaluate z' and providing the terms involving θ can be expressed in terms of r using (1.2.9), (1.3.1) can in principle be solved to yield

$$t = f_1(r), \tag{1.3.2}$$

where

$$f_1(r) = \int \frac{\mathrm{d}r}{(-z'(r) + J\sin(\theta(r) - \theta_0))}. \tag{1.3.3}$$

Using the expression for the angular momentum yields

$$\dot{\theta} = \frac{L}{r^2} \tag{1.3.4}$$

or alternatively

$$\mathrm{d}t = \frac{L\,\mathrm{d}\theta}{(z + J\cos(\theta - \theta_0))^2}. \tag{1.3.5}$$

Using (1.1.19) to express z in terms of θ, (1.3.5) can in principle be solved to yield

$$t = f_2(\theta). \tag{1.3.6}$$

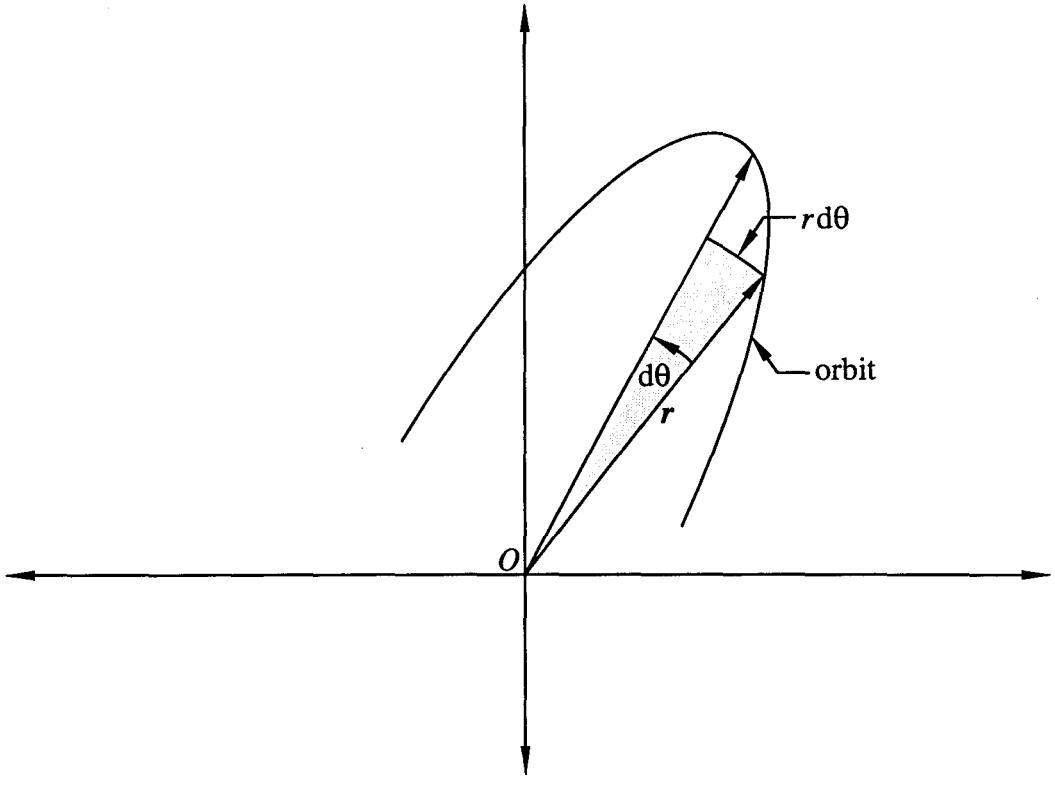


Figure 1.3.1. The area swept out by the radial vector $\boldsymbol{r}$ in a time $\mathrm{d}t$.

where

$$f_2(\theta) = \int \frac{L\mathrm{d}\theta}{(z(\theta) + J\cos(\theta - \theta_0))^2}. \tag{1.3.7}$$

In theory (1.3.2) and (1.3.6) can be inverted to give r and θ as functions of t. In practice, however, the equations are very complex (even for the classical Kepler problem) and inversion poses serious problems, as we shall see in some of the later examples.

The areal velocity or area swept out by the radius vector can be obtained as follows. With reference to Figure 1.3.1 which shows the area swept out by the radial vector $\boldsymbol{r}$ in a time $\mathrm{d}t$, the element of area $\mathrm{d}A$ is given by

$$\mathrm{d}A = \frac{1}{2}r(r\ \mathrm{d}\theta), \tag{1.3.8}$$

and dividing throughout by $\mathrm{d}t$ gives

$$\frac{\mathrm{d}A}{\mathrm{d}t} = \frac{1}{2}L. \tag{1.3.9}$$

Since the angular momentum is conserved for this class of problems, the areal velocity is constant or in other words equal areas are swept out in equal times. Since L is constant, (1.3.9) can be solved to give

$$A = \frac{1}{2}Lt. \tag{1.3.10}$$

If the orbit possesses a distinct shape such as an ellipse, by equating the area in terms of well-known geometric quantities such as the semi-major and semi-minor axis lengths, an expression relating the period and the geometric quantities can be obtained. A less geometric approach by evaluating the integral in (1.3.2) or (1.3.6) over a period will give the same result. See §§1.5 and 1.7.

1.4 Examples

The orbit equation (1.2.9) can give rise to a wide variety of orbits depending on the choice of the function f in (1.1.6). The treatment of the Kepler problem will be reserved for §1.5.

1.) Let us consider the equation of motion

$$\ddot{\boldsymbol{r}} + \frac{a\,(\theta - \theta_0) + b}{r^3}\boldsymbol{r} = \boldsymbol{0}. \tag{1.4.1}$$

In the notation of equation (1.1.6)

$$f = \frac{a\,(\theta - \theta_0) + b}{r^3}, \tag{1.4.2}$$

which describes a Kepler type force with an additional inverse square law term which depends on the polar angle θ. Equation (1.1.19) can be integrated to give

$$z(\theta) = \frac{a}{L}\big(\theta - \theta_0 - \sin(\theta - \theta_0)\big) + \frac{b}{L}\big(1 - \cos(\theta - \theta_0)\big) \tag{1.4.3}$$

and similarly, using (1.1.20), $z'(\theta)$ is given by

$$z'(\theta) = \frac{a}{L}\big(1 - \cos(\theta - \theta_0)\big) + \frac{b}{L}\sin(\theta - \theta_0). \tag{1.4.4}$$

The orbit is given by equation (1.2.9) with $z(\theta)$ replaced by (1.4.3). Similarly the velocity hodograph is given by (1.2.4) replacing $z(\theta)$ and $z'(\theta)$ by (1.4.3) and (1.4.4). The conserved vectors $\boldsymbol{K}$ and $\boldsymbol{J}$ are given by (1.1.22) and (1.1.23). The resultant expressions are lengthy but simple to construct and not reproduced for obvious reasons.

Figure 1.4.1 shows a spiralling orbit together with the conserved vectors $\boldsymbol{K}$ and $\boldsymbol{J}$ which are slightly displaced from the axes for the sake of clarity. Figure 1.4.2 shows the velocity hodograph associated with Figure 1.4.1. In many physical problems that display a spiralling behaviour such as the satellite drag problems of §2.13, the spiralling would not normally be as severe as that shown. Notice that the orbit spirals inward in a counter–clockwise fashion toward the origin, whilst the velocity hodograph spirals outward in a counter–clockwise fashion.

2.) On comparison of the equation of motion

$$\ddot{\boldsymbol{r}} + \frac{ae^{-(\theta-\theta_0)} + b}{r^3}\boldsymbol{r} = \boldsymbol{0} \tag{1.4.5}$$

with (1.1.6) we find that

$$f = \frac{ae^{-(\theta-\theta_0)} + b}{r^3} \tag{1.4.6}$$

which describes a Kepler type force with an additional inverse square law term which decays exponentially with the polar angle θ. Equations (1.1.19) and (1.1.20) can be integrated to give

$$\begin{aligned} z(\theta) \;=\; & \frac{a}{2L}\big(e^{-(\theta-\theta_0)} + \sin(\theta - \theta_0) - \cos(\theta - \theta_0)\big) + \\ & \frac{b}{L}\big(1 - \cos(\theta - \theta_0)\big) \end{aligned} \tag{1.4.7}$$

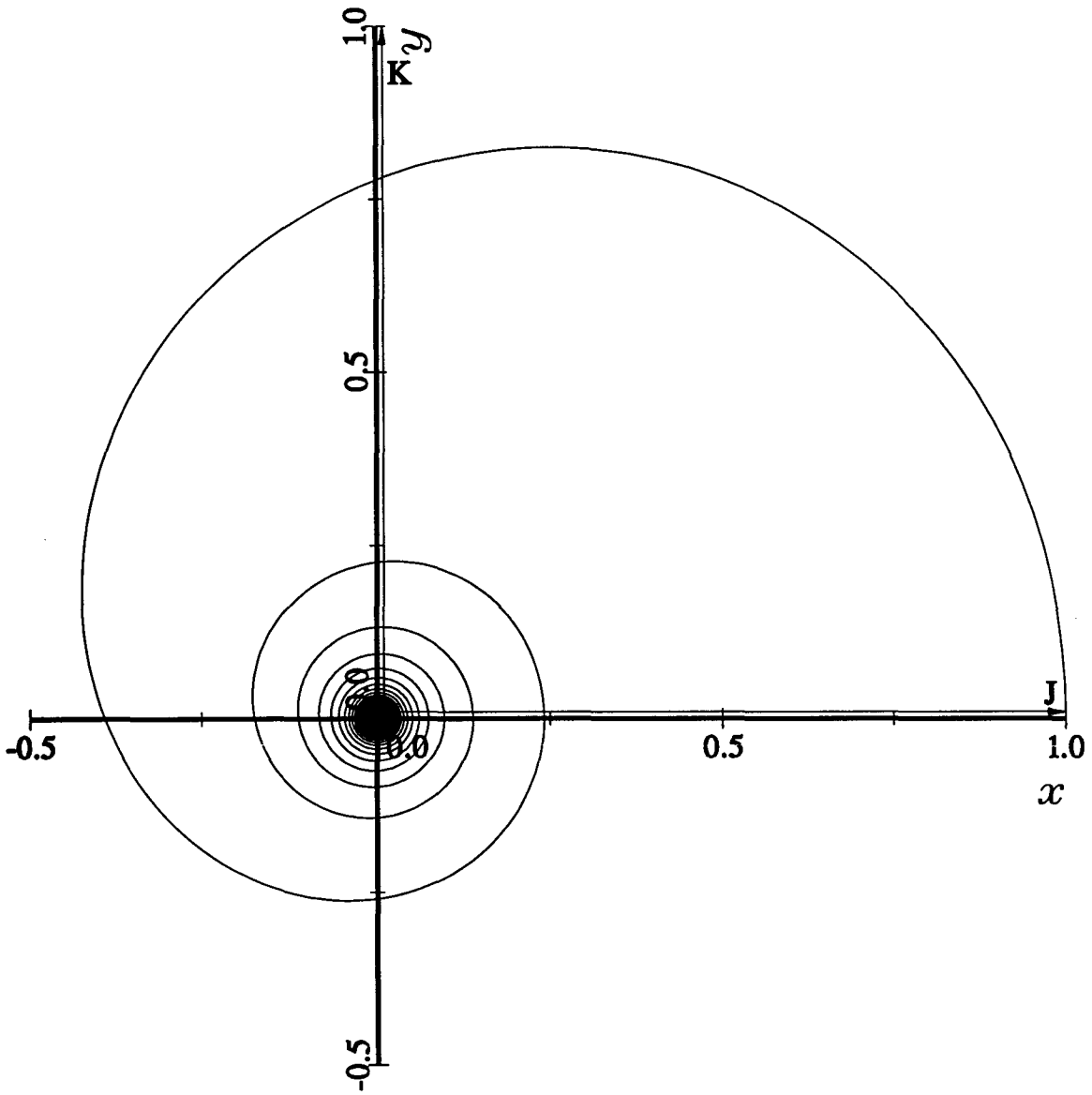


Figure 1.4.1. The spiralling orbit and the orientation of the conserved vectors $\boldsymbol{K}$ and $\boldsymbol{J}$. The constants have the values $a = 1/2$, $b = 1$, $\theta_0 = 0$, $K = J = 1$ and $L = 1$.

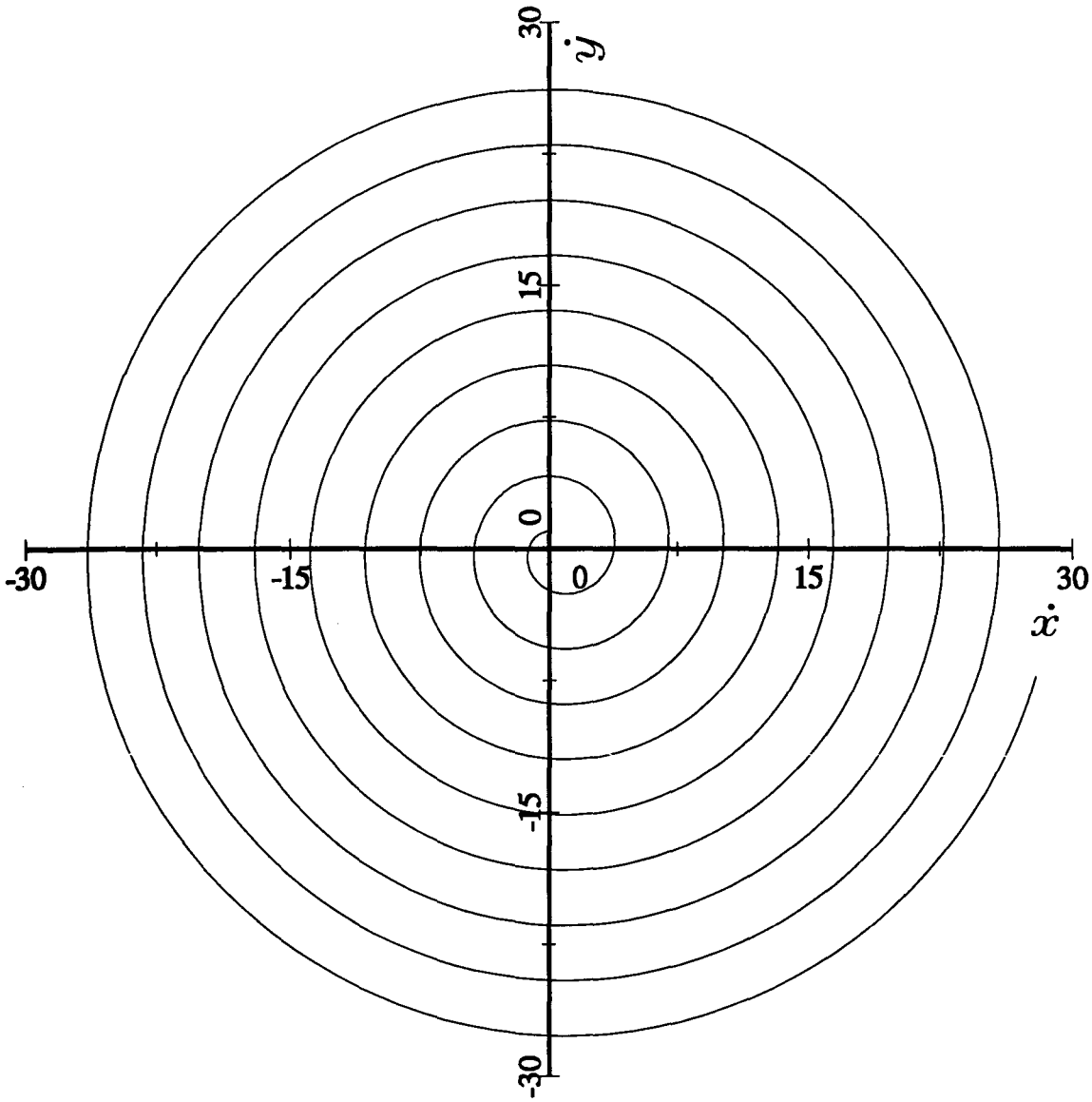


Figure 1.4.2. The velocity hodograph associated with Figure 1.4.1. Note that the orbit spirals inward in a counter–clockwise fashion toward the origin, whilst the velocity hodograph spirals outward in a counter–clockwise fashion.

and

$$z'(\theta) = \frac{a}{2L}\Big(-e^{-(\theta-\theta_0)} + \sin(\theta-\theta_0) + \cos(\theta-\theta_0)\Big) + \frac{b}{L}\sin(\theta-\theta_0). \tag{1.4.8}$$

The velocity hodograph and orbit equation are then given by (1.2.4) and (1.2.9) and $\boldsymbol{K}$ and $\boldsymbol{J}$ by (1.1.22) and (1.1.23) respectively.

Figure 1.4.3 shows the velocity hodograph (right) and the orbit (left) drawn on the same set of axes for convenience together with the conserved vectors $\boldsymbol{K}$ and $\boldsymbol{J}$ which are slightly displaced from the axes for the sake of clarity. The limit cycle behaviour is reminiscent of many physical systems such as the phase plot of the one–dimensional van der Pol oscillator. It should be noted that the velocity hodograph grows outward in a counter–clockwise fashion toward its limit cycle while the orbit grows inward in a counter–clockwise fashion towards its limit cycle.

3.) On comparison of the equation of motion

$$\ddot{\boldsymbol{r}} + \frac{a\sin 3(\theta-\theta_0)+b}{r^3}\boldsymbol{r} = \boldsymbol{0} \tag{1.4.9}$$

with (1.1.6) we find that

$$f = \frac{a\sin 3(\theta-\theta_0)+b}{r^3}, \tag{1.4.10}$$

which describes a Kepler type force with an additional inverse square law term which depends on the polar angle θ. Integration of (1.1.19) gives

$$z(\theta) = \frac{a}{L}\Big(-\frac{1}{8}\sin 3(\theta-\theta_0) + \frac{3}{8}\sin(\theta-\theta_0)\Big) + \frac{b}{L}\Big(1-\cos(\theta-\theta_0)\Big) \tag{1.4.11}$$

and similarly (1.1.20) gives

$$z'(\theta) = \frac{a}{L}\Big(-\frac{3}{8}\cos 3(\theta-\theta_0) + \frac{3}{8}\cos(\theta-\theta_0)\Big) + \frac{b}{L}\sin(\theta-\theta_0). \tag{1.4.12}$$

The velocity hodograph and orbit equation are then given by (1.2.4) and (1.2.9) and $\boldsymbol{K}$ and $\boldsymbol{J}$ by (1.1.22) and (1.1.23) respectively.

Figure 1.4.4 shows the velocity hodograph (left) and the orbit (right) drawn on the same set of axes for convenience together with the conserved vectors $\boldsymbol{K}$ and $\boldsymbol{J}$ which are slightly displaced from the axes for the sake of clarity. The three bulges in both the velocity hodograph and the orbit reflect the behaviour resulting from the compound angle in the force term.

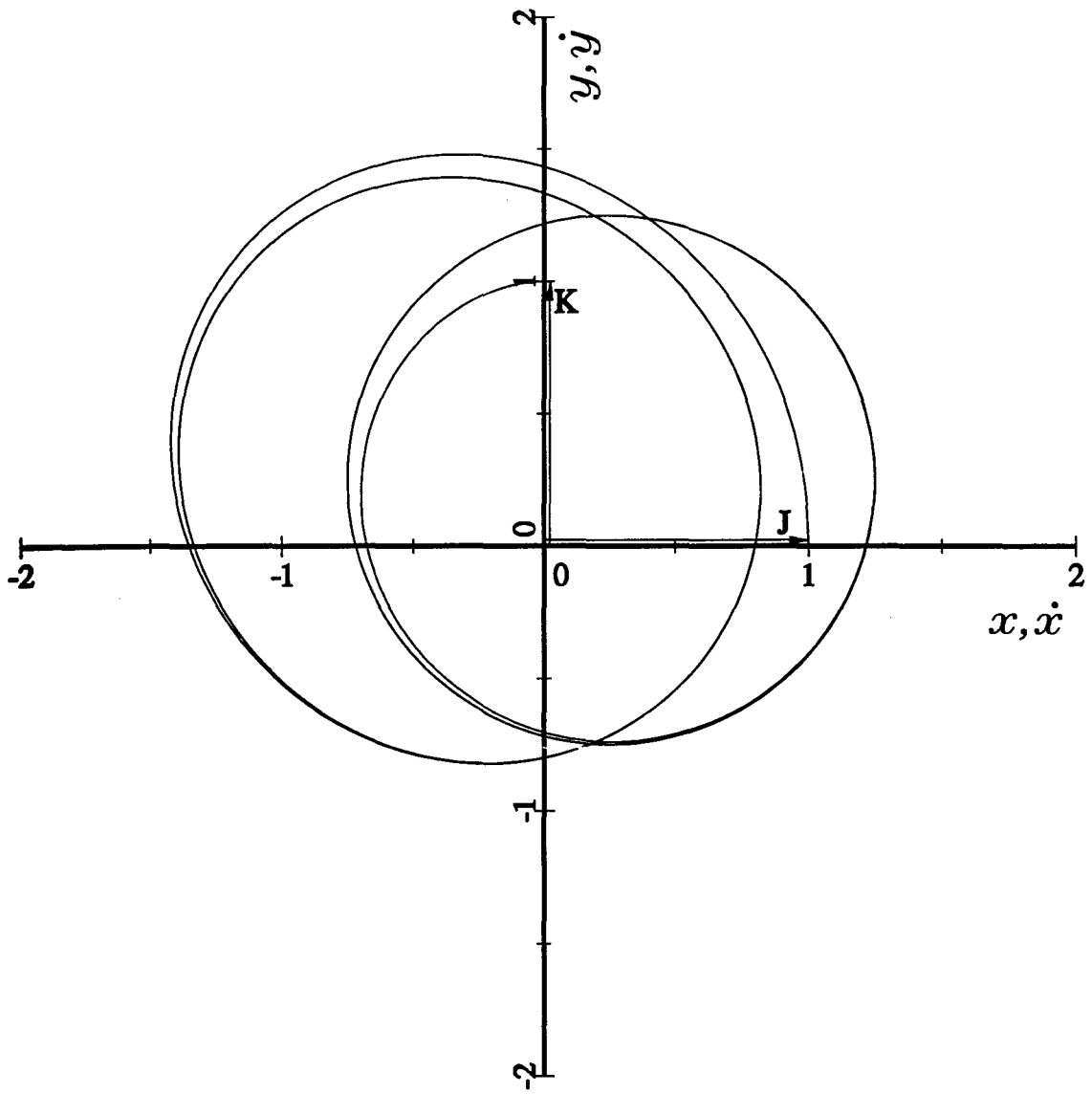


Figure 1.4.3. The velocity hodograph (right) and the orbit (left) drawn on the same set of axes for convenience together with the conserved vectors $\boldsymbol{K}$ and $\boldsymbol{J}$. The constants have the values $a = 1/2$, $b = 1$, $\theta_0 = 0$, $K = J = 1$ and $L = 1$. Note that the velocity hodograph grows outward in a counter–clockwise fashion toward its limit cycle whilst the orbit grows inward in a counter–clockwise fashion towards its limit cycle.

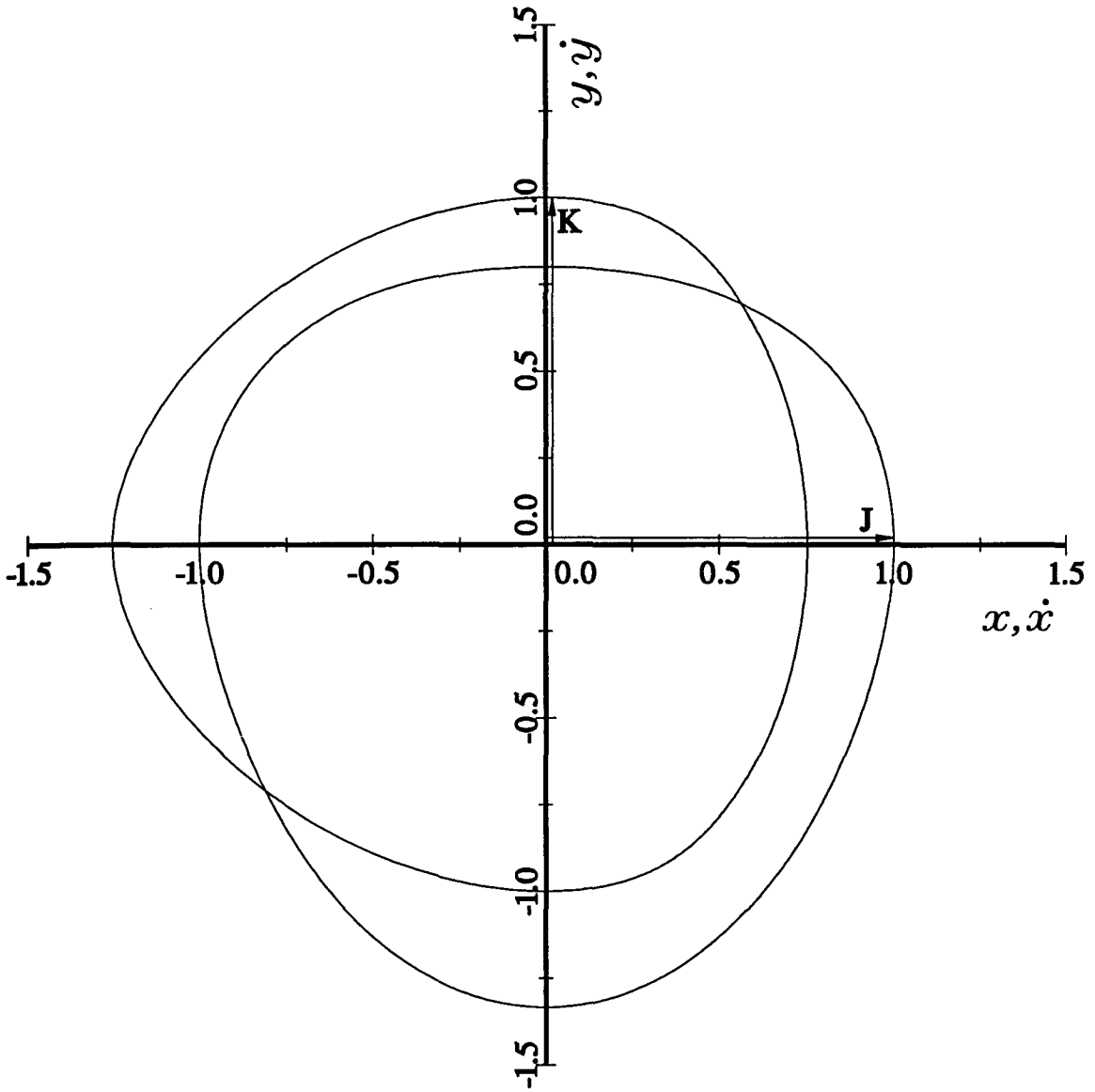


Figure 1.4.4. The velocity hodograph (left) and the orbit (right) drawn on the same set of axes for convenience together with the conserved vectors $\boldsymbol{K}$ and $\boldsymbol{J}$. The constants have the values $a = 1/2$, $b = 1$, $\theta_0 = 0$, $K = J = 1$ and $L = 1$. The three bulges in both the velocity hodograph and the orbit reflect the compound angle in the force term.

1.5 The Geometry of the Kepler Problem

The Kepler problem is named in honour of Johannes Kepler who formulated three phenomenological laws to describe the motion of the planets based on the empirical data of Tycho Brahe. Isaac Newton, the English physicist and mathematician verified the three laws of Kepler using a geometrical treatment, which is contained in his *Principia* [102]. The inverse square law and all its geometrical ramifications were the central focus of the *Principia.* Newton went on to prove that, for any central force, motion occurred in a plane and also that equal areas were swept out by the radius vector in equal times [102, prop I–II p40ff] (Kepler's second law). He proved that if a particle moves in an elliptical orbit under the influence of a centripetal force directed towards one focus then that force must be inversely proportional to the square of the radius [102, prop XI p56] (Kepler's first law), and obtained the same result for focus–centred parabolic [102, prop XIII p60] and hyperbolic motion [102, prop XII p57]. In [102, prop XV p62] Newton went on to verify Kepler's third law that the square of the periodic time of an inverse square law ellipse was proportional to the semi–major axis length cubed.

The number of papers related to various aspects of the Kepler problem (which must now number in the tens of thousands), some of which date back several centuries, precludes being able to attribute any particular result with any certainty to any individual. In fact even the origin of what is now termed the Laplace–Runge–Lenz vector has been questioned. Goldstein [31, 32] has researched the historical origins of the perihelion vector and cites several references dating back to about 1710, and proposes that the name be amended to Hermann–Bernoulli–Laplace vector to more accurately reflect its origins. As is so often the case in the scientific literature, the name Laplace–Runge–Lenz vector is undoubtedly the one that will survive, despite being credited unfairly. In fact this name is more suitable compared with the recent usages of Lenz or Runge–Lenz vector found in the Physics literature.

Jacob Hermann, a disciple of the Bernoullis, appears to have discovered the Laplace–Runge–Lenz vector in 1710 as a constant of integration in a direct integration of the equation of motion for the Kepler problem [32], although Aiton (see [127]) credits Johann Bernoulli with the discovery. He recognised the relationship between this constant and the eccentricity of the usual conic sections. Johan Bernoulli generalised Hermann's result and obtained the general result for an arbitrary orientation of the orbit in the plane and in the process discovered both the magnitude and direction of the Laplace–Runge–Lenz vector.

The Kepler problem had a prominent position in most of the early textbooks dealing with dynamics. After appearing in Newton's Principia [102] it became one of the standard central force problems which not only could be easily solved, but also had some rather interesting geometrical properties. In his monograph *Traité de Mécanique Céleste*, Laplace [69] discovered the usual seven first integrals for the Kepler problem, three of which were the cartesian components of the Laplace–Runge–Lenz vector. Hamilton's discovery of a conserved vector perpendicular to the Laplace–Runge–Lenz vector appeared in 1845 in the paper delivered to the Royal Irish Academy entitled 'Applications of Quaternions to Some Dynamical Questions'. He termed the vector an 'eccentricity' vector to reflect its origins [48, 124, §361ff p283ff, 49, p327].

The velocity hodograph appears to first have been discovered by August Ferdinand Möbius [49, p333]. It is generally attributed to Hamilton who independently discovered it in 1846 while working on the theory of planetary purturbations, a subject which had prompted many of his mechanical discoveries twelve years earlier. He coined the word 'hodograph' meaning 'to describe the path' and explained this invention in a paper delivered to the Royal Irish Academy on December 14, 1846. In his monograph *An Elementary Treatise on Quaternions* of 1867, Tait [124] first develops the velocity hodograph and then a few pages later derives the Laplace–Runge–Lenz vector as well as Hamilton's vector for the Kepler problem in terms of their elegant quaternion representations and then shows the natural association of Hamilton's vector with the velocity hodograph and the orbit equation [124, §353ff p279ff]. He acknowledges that the 'beautiful method of integration is due to Hamilton' and references Hamilton's *Elements of Quaternions* for a more detailed analysis of the circular velocity hodograph. William Thomson (later known as Lord Kelvin) made the velocity hodograph the subject of a prize essay for his students and together with Peter Guthrie Tait discovered a clever analytic proof of the circular velocity hodograph described in their famous *Treatise on Natural Philosophy* of 1879 [64, §37ff p26ff]. They rediscovered the conserved components of Hamilton's vector during the process. The velocity hodograph is also mentioned in their *Elements of Natural Philosophy* of 1872 [63, §49ff p14ff] where a purely geometric proof of the velocity hodograph is given. Kelland and Tait also discussed the velocity hodograph in their *Introduction to Quaternions* of 1873 [62, §72 p160] without applying it to any worked problems. Maxwell [93] discussed the velocity hodograph in *Matter and Motion* of 1877 although he found it preferable to rotate the velocity hodograph through $\pi/2$ radians [93, §132ff p107ff]. In his textbook *Dynamics of a Particle* of 1898, Routh [113] described the velocity hodograph in quite some detail and mentioned that the time derivative of the arc of the velocity hodograph was proportional

to the acceleration [113, §29ff p10, §394ff p252ff], but never appeared to calculate an acceleration hodograph. The first appearance of the Laplace–Runge–Lenz vector in modern vector notation is believed to be due to Gibbs and appeared in Gibbs' and Wilson's textbook *Vector Analysis* of 1901 which antedates Runge's derivation by roughly twenty years [32]. In the Preface of Levy's translation of Runge's textbook *Vector Analysis* of 1923, Runge [114, §5. p79ff] acknowledged that the notation he had used to represent scalar and vector products was that introduced by Gibbs and he applied vector operations directly to the equation of motion of the Kepler problem in much the same way as is done throughout this thesis. He proceeded to construct the orbit equation by taking the scalar product of the Laplace–Runge–Lenz vector with the vector $\boldsymbol{r}$ and immediately recognised the path of the velocity hodograph from the structure of the Laplace–Runge–Lenz vector and also arrived at Kepler's second law during the process. He found it preferable to scale both the orbit equation and the velocity hodograph in the subsequent discussion to illustrate some interesting features of the geometry.

A complete graphical study of the velocity hodograph for the different conic section orbits arising from the Kepler problem was done by Child [18] and is reproduced in [49, p326ff], however, there appear to be some inconsistencies regarding the velocity hodograph's location and also its closure in the case of the hyperbolic orbit no doubt as a result of the absence of suitable high–accuracy computing devices.

The connection between the classical Laplace–Runge–Lenz vector and quantum mechanics is a result of an early paper by Lenz [81] who made use of the vector to calculate the energy levels of the perturbed Kepler problem using the classical quantum theory. He referred to Runge's popular text *Vector Analysis* [114, §5. p79ff] as the source of the vector as used in classical mechanics. Pauli made use of the vector in his landmark paper of 1926 [105] to derive an expression for the energy levels of the quantised hydrogen atom. In a 1935 paper Fock [27] showed that the Schrödinger wave equation in momentum space for the quantum mechanical hydrogen atom could be transformed by stereographic projection into Laplace's equation for a hypersphere in the case of bound states, or a hyperboloid for positive energy states. These results were confirmed by Bargmann in 1936 [5] who calculated the commutation relationships between the components of the angular momentum and the Laplace–Runge–Lenz vectors and found the four–dimensional rotation group for bound energy states and the Lorentz group for positive energy states.

The Kepler problem still remains an important paradigm of classical mechanics and, as such, is dealt with in detail in most of the more prominent textbooks this century. As the number of books related to mechanics is so large, it is only worthwhile to look at a few good examples. Routh looked at Kepler's laws and several central force problems [113, §332ff p216ff] while Whittaker [129, §47ff p77ff] gave a reasonable overview of much of the early literature on the Kepler problem and other central forces in his *A Treatise on the Analytical Dynamics of Particles and Rigid Bodies* of 1904. In his textbook *Mechanics*, Symon [122, §3–13ff p120ff] looked at central forces in general from the point of view of an effective potential. He dealt with the Kepler problem in some detail without making use of any vector techniques. Goldstein [33, Chap 3] solved the Kepler problem both using the effective potential approach as well as by introducing the Laplace–Runge–Lenz vector as a vehicle for solving for the orbit.

Other approaches that employed vector techniques to solve the Kepler problem are described by Heintz [51] who assumed a structure for the Laplace–Runge–Lenz vector and solved component–wise to obtain the vector, and also Yoshida [133] who used a vector approach to obtain Kepler's equation.

The velocity hodograph, after disappearing from the literature for some time, reappeared in a book by Konopinski in one of the problem exercises [49, p447]. It appears that this problem was prompted by a lecture given by a Dr M Gutzwiller. More recently Goldstein [32, 33, p125 ex24] has rederived the velocity hodograph using the Laplace–Runge–Lenz vector and also gives a historical overview of its early development and its association with the Laplace–Runge–Lenz vector. The velocity hodograph for the Kepler problem has also been discussed more recently by Stickforth [121] who derived it after solving the Kepler problem in momentum space.

Most of the above treatments appear to me to be unnecessarily complicated, both by the choice of notation and the procedure adopted.

To demonstrate much of the preceding theory, it is instructive to consider the classical Kepler problem defined by the equation of motion

$$\ddot{\boldsymbol{r}} + \frac{\mu}{r^3}\boldsymbol{r} = \boldsymbol{0}. \tag{1.5.1}$$

From (1.1.17) we find

$$v(\theta) = \frac{\mu}{L}. \tag{1.5.2}$$

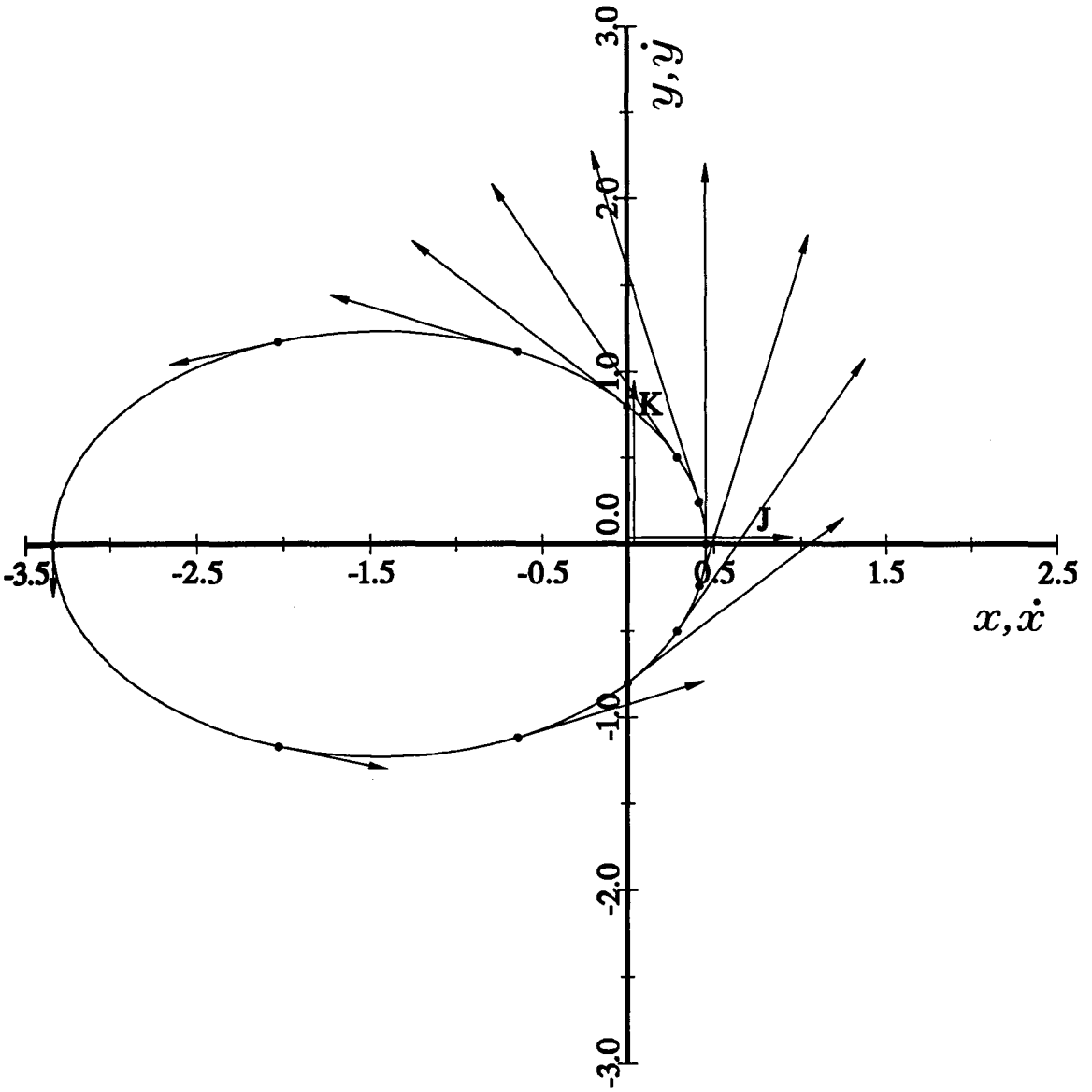


Figure 1.5.1. The elliptical Kepler orbit showing the velocity vectors at some points along the orbit and the orientation of the conserved vectors $\boldsymbol{K}$ and $\boldsymbol{J}$. The constants have the values $\mu = 1.25$, $\theta_0 = 0$, $K = J = 0.95$ and $L = 1$.

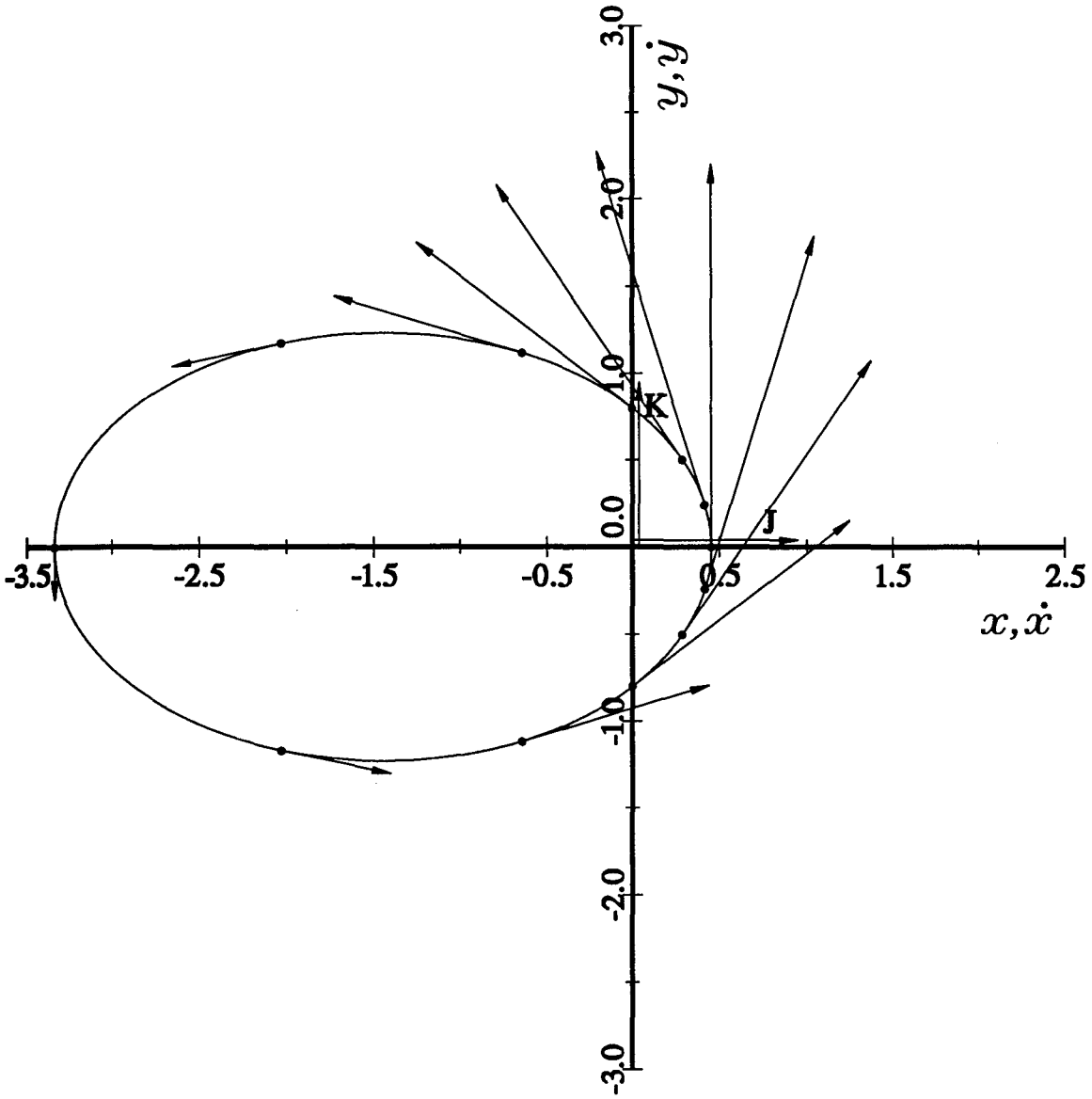


Figure 1.5.1. The elliptical Kepler orbit showing the velocity vectors at some points along the orbit and the orientation of the conserved vectors $\boldsymbol{K}$ and $\boldsymbol{J}$. The constants have the values $\mu = 1.25$, $\theta_0 = 0$, $K = J = 0.95$ and $L = 1$.

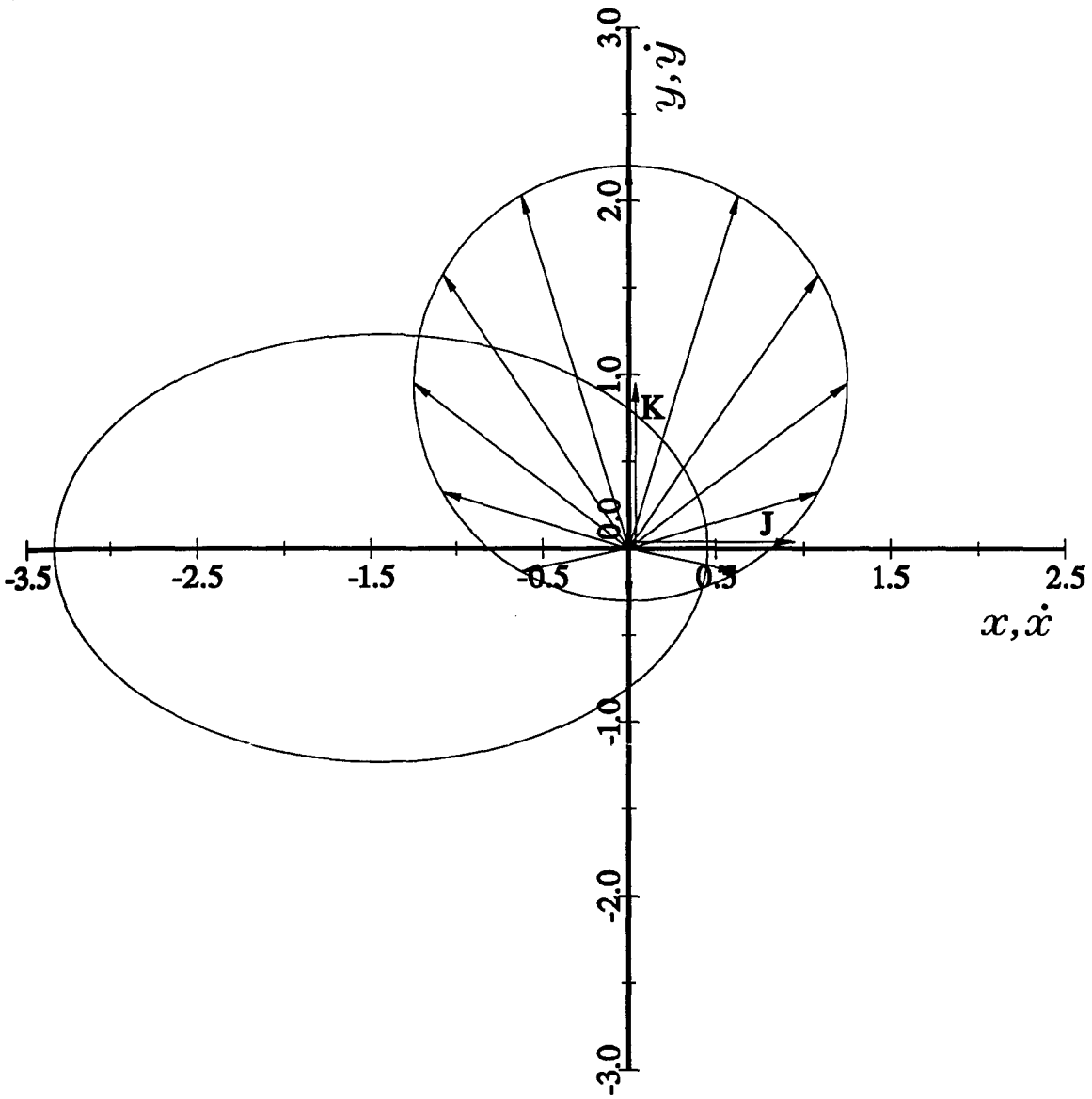


Figure 1.5.2. The elliptical Kepler orbit and the construction of the corresponding circular velocity hodograph with a selection of velocity vectors drawn from the origin on the same set of axes as the displacement. The origin lies inside the velocity hodograph. The constants are chosen as for Figure 1.5.1.

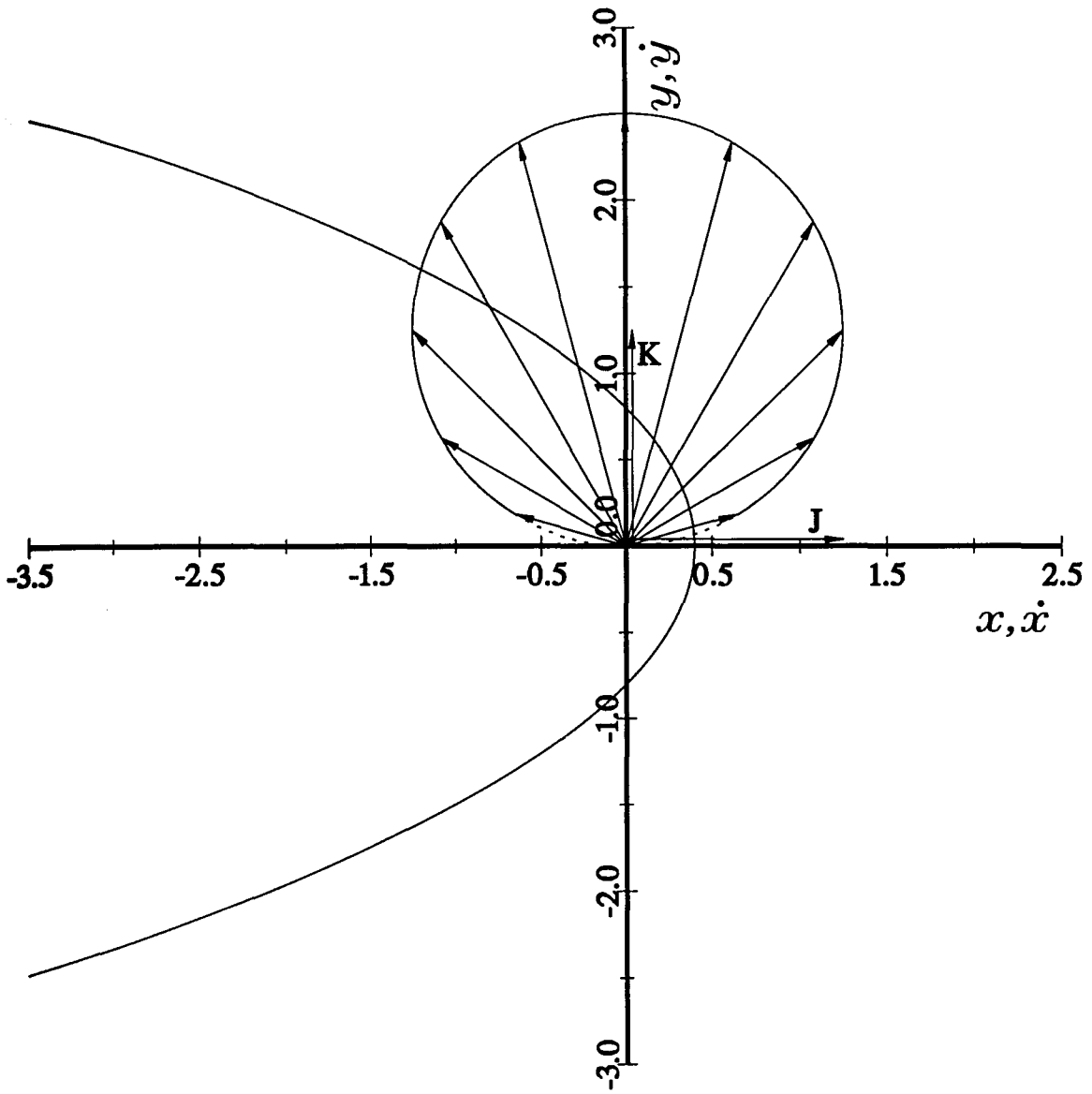


Figure 1.5.3. The parabolic Kepler orbit and the construction of the corresponding circular velocity hodograph with a selection of velocity vectors drawn from the origin on the same set of axes as the displacement. The constants have the values $\mu = 1.25$, $\theta_0 = 0$, $K = J = 1.25$ and $L = 1$. The origin lies on the circumference of the velocity hodograph. Note that the circle of the velocity hodograph is only completed as t ranges from negative through positive infinity.

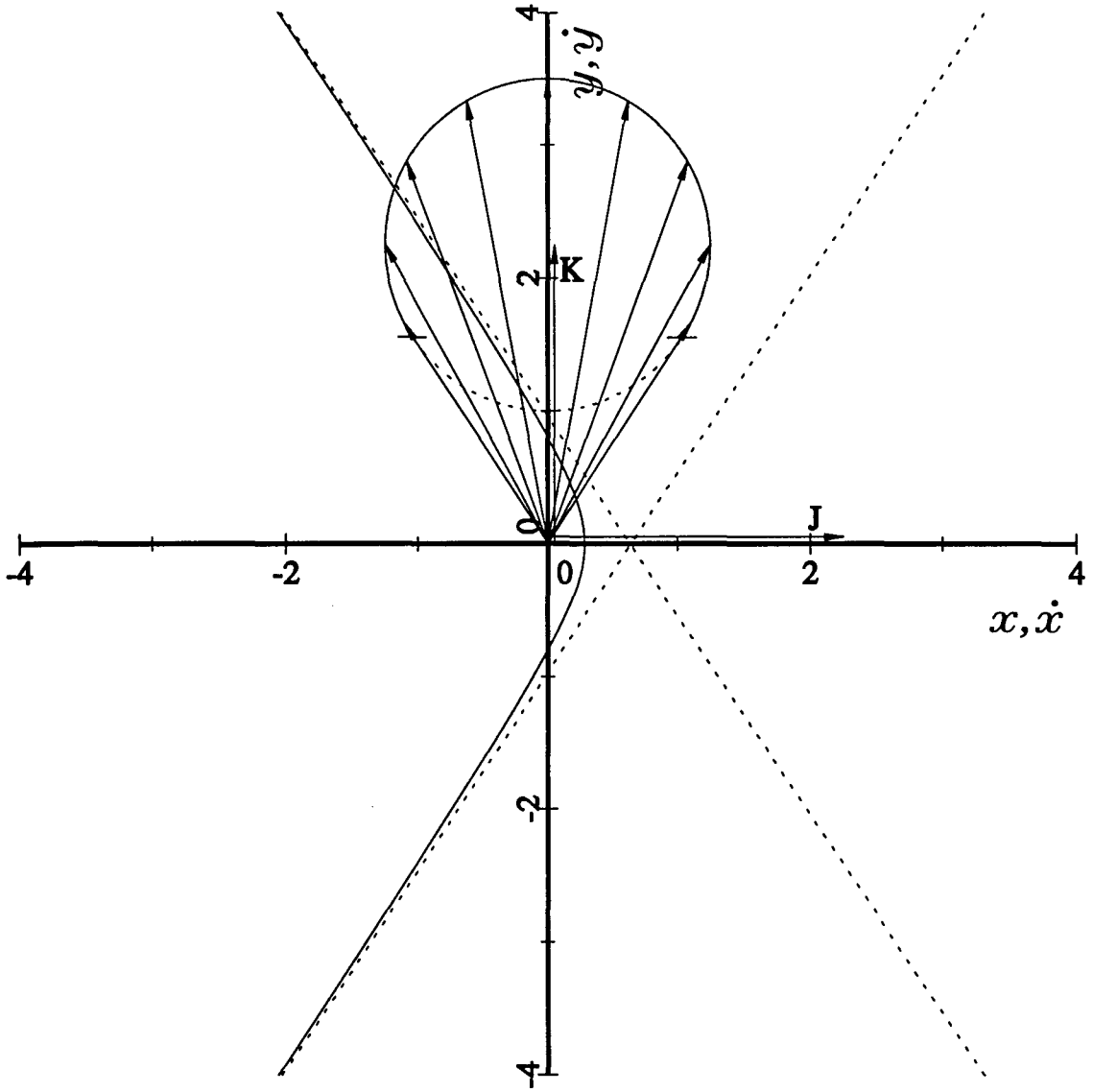


Figure 1.5.4. The hyperbolic Kepler orbit and the construction of the corresponding circular velocity hodograph with a selection of velocity vectors drawn from the origin on the same set of axes as the displacement. The constants have the values $\mu = 1.25$, $\theta_0 = 0$, $K = J = 2.25$ and $L = 1$. The origin lies below the velocity hodograph. Note that the circular velocity hodograph does not close as t ranges from negative through positive infinity.

$$\begin{aligned}
\dot{x}_e &= \frac{1}{JL}\left(\mp\mu L(2H)^{\frac{1}{2}}\cos\theta_0 - 2L^2H\sin\theta_0\right) \\
&= \frac{\mu^{\frac{1}{2}}}{a^{\frac{1}{2}}e(e^2-1)^{\frac{1}{2}}}\left(\mp(e^2-1)^{\frac{1}{2}}\cos\theta_0 - (e^2-1)\sin\theta_0\right) \\
\dot{y}_e &= \frac{1}{JL}\left(2L^2H\cos\theta_0 \pm \mu L(2H)^{\frac{1}{2}}\sin\theta_0\right) \\
&= \frac{\mu^{\frac{1}{2}}}{a^{\frac{1}{2}}e(e^2-1)^{\frac{1}{2}}}\left((e^2-1)\cos\theta_0 \pm (e^2-1)^{\frac{1}{2}}\sin\theta_0\right) \qquad (1.5.12)
\end{aligned}$$

making the substitutions

$$\begin{aligned}
\cos\theta &= \frac{1}{e}\left(-\cos\theta_0 \pm (e^2-1)^{\frac{1}{2}}\sin\theta_0\right) \\
\sin\theta &= \frac{1}{e}\left(\pm(e^2-1)^{\frac{1}{2}}\cos\theta_0 - \sin\theta_0\right) \qquad (1.5.13)
\end{aligned}$$

which are solutions to the equations of the asymptotes of the hyperbola $\cos(\theta-\theta_0) = -1/e$.

Denoting the angle between $\dot{\boldsymbol{r}}$ and $\boldsymbol{i}$ as ψ and using (1.5.11) gives

$$\tan\psi = \frac{\dot{y}}{\dot{x}} = -\frac{(\cos\theta + e\cos\theta_0)}{\sin\theta + e\sin\theta_0}. \qquad (1.5.14)$$

Note that when $\theta = \theta_0$, $\psi = \arctan(-\cos\theta_0/\sin\theta_0) = \pi/2 + \theta_0$ as expected.

Figure 1.5.5 geometrically demonstrates the construction of $\boldsymbol{L}$ corresponding with Figures 1.5.1 and 1.5.2. The shaded parallelograms which represent the magnitude of $\boldsymbol{L} = \boldsymbol{r} \times \dot{\boldsymbol{r}}$ have equal areas. Figure 1.5.6 shows both the displacements and corresponding velocities at regular time intervals for the Kepler problem. The shaded regions confirm Kepler's second law that equal areas are swept out in equal times. It should be obvious that the initial phase difference between the displacement and velocity vectors is $\pi/2$ radians as the displacement lies along the $+x-$axis at $t = 0$ while the velocity is purely along the $+\dot{y}-$axis. The phase difference in general between the displacement and velocity vectors is not constant since $\boldsymbol{r}\cdot\dot{\boldsymbol{r}} = r\dot{r}$ which is nonzero except when $\dot{r} = 0$, *i.e.* at the extremities of the motion. This is also evident by comparing the angle between the corresponding displacement and velocity vectors for a range of time intervals using the solid round time markers on the orbit and the corresponding solid square time markers on the velocity hodograph and counting the number of round markers from the rightmost vertex of the ellipse in a

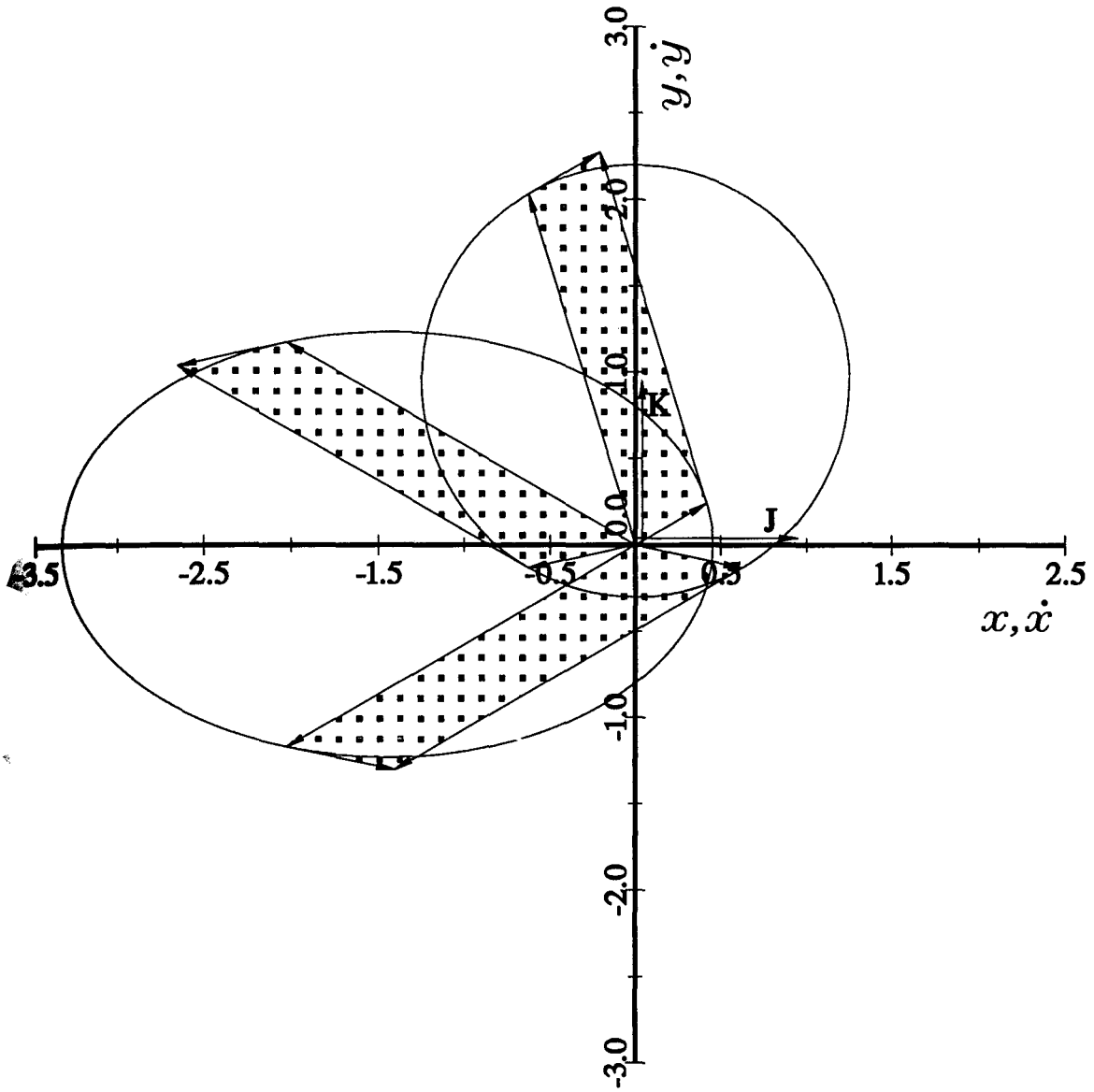


Figure 1.5.5. The elliptical Kepler orbit with its corresponding circular velocity hodograph demonstrating the constancy of $\boldsymbol{L}$. The shaded parallelograms have equal areas as a consequence of $\boldsymbol{L}$ being conserved. The constants are chosen as for Figure 1.5.1.

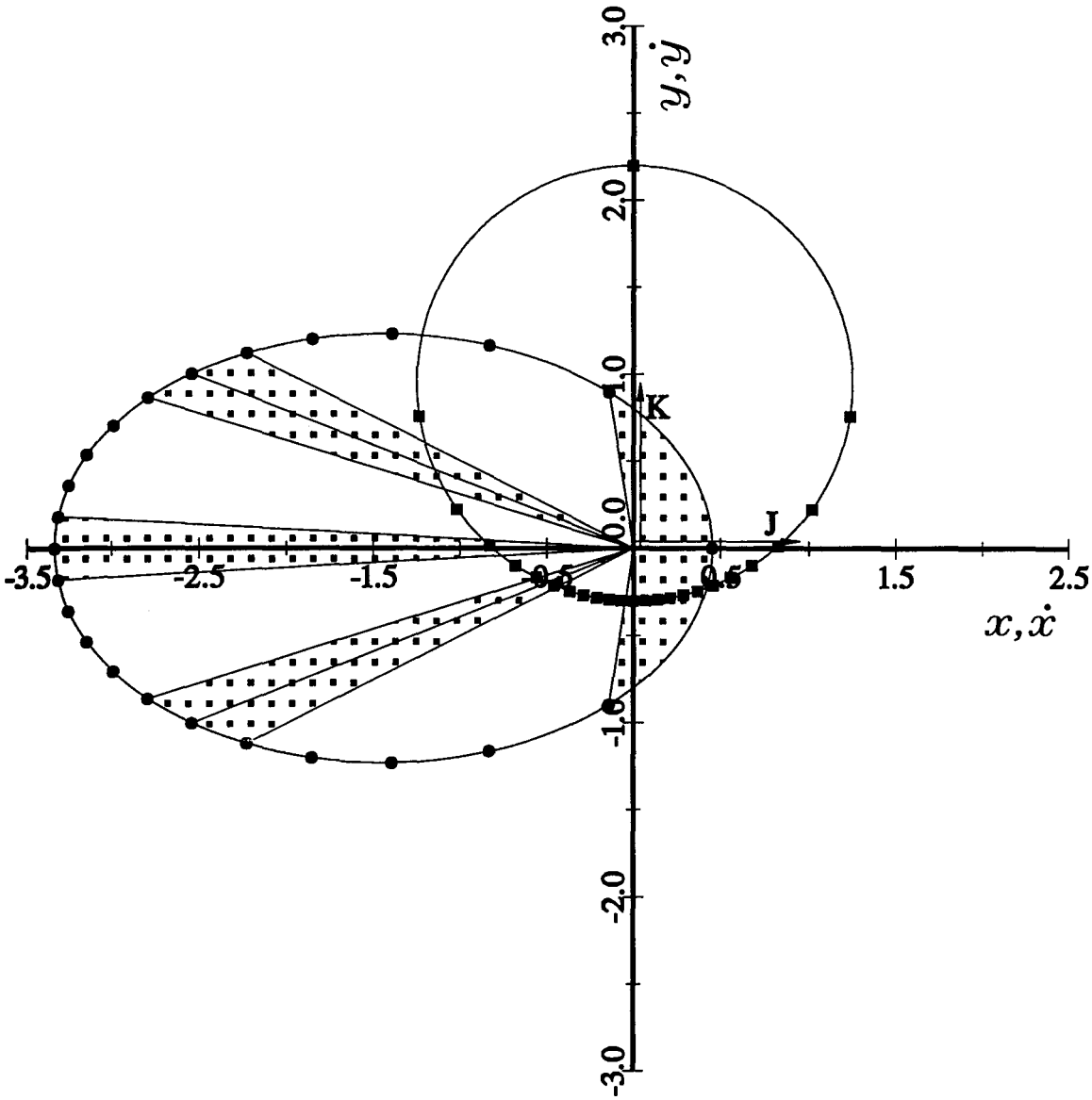


Figure 1.5.6. The elliptical Kepler orbit with its corresponding circular velocity hodograph. The circles (–•–•–•–) show the displacements of the particle at the time intervals $iT/24$, $i = 0, \ldots, 24$ and the squares (–■–■–■–) give the corresponding velocities. The shaded regions confirm Kepler's second law that equal areas are swept out in equal times. The phase difference between the velocity and displacement vectors is not constant although it is a constant $\pi/2$ radians between the displacement vector and the vector directed from the centre of the velocity hodograph to the head of the corresponding velocity vector. The constants are chosen as for Figure 1.5.1.

counter–clockwise direction to the displacement of interest and then counting off the same number of square markers on the velocity hodograph starting from the square marker at the top of the velocity hodograph (since at $t = 0$ the velocity is purely along the $+\dot{y}$–axis) in a counter–clockwise direction to obtain the corresponding velocity or *vice versa*. Note, however, that the phase difference between the radial vector $\boldsymbol{r}$ and the vector directed from the head of the Hamilton vector $\boldsymbol{K}$ (the centre of the circular velocity hodograph) to the head of the vector $\dot{\boldsymbol{r}}$, *i.e.* $\dot{\boldsymbol{r}} - \boldsymbol{K}$ is a constant $\pi/2$ radians since $\boldsymbol{r} \cdot (\dot{\boldsymbol{r}} - \boldsymbol{K}) = 0$. This behaviour is also evident on translating the velocity hodograph so that the centre of the circle coincides with the origin of the orbit. Alternatively, if in addition to the translation described above, the velocity hodograph is rotated clockwise through $\pi/2$ radians about the centre of the circle, it is apparent that the corresponding displacements, velocities and the origin are collinear which demonstrates the constant $\pi/2$ phase difference. In summary, the phase difference between $\boldsymbol{r}$ and $\dot{\boldsymbol{r}}$ is not constant in the Kepler problem but the phase difference between $\boldsymbol{r}$ and $\dot{\boldsymbol{r}} - \boldsymbol{K}$ is constant at $\pi/2$ radians or, in other words, the radial vector directed from the origin which is also a focus of the ellipse in the plane moves in phase with an offset velocity vector directed from the head of the Hamilton vector (the centre of the circular velocity hodograph).

It would now seem natural to consider the curve described by $\ddot{\boldsymbol{r}}$. Splitting the two terms of (1.5.1) across the equal sign, taking the dot product of each term with itself followed by square roots on both sides gives the plane polar equation for the magnitude of $\ddot{\boldsymbol{r}}$, *i.e.*,

$$|\ddot{\boldsymbol{r}}| = -\frac{\mu}{r^2} = -\frac{\mu}{L^4}\big(\mu + J\cos(\theta - \theta_0)\big)^2 \tag{1.5.15}$$

using (1.5.10) to substitute for r and realising that the angle between $|\ddot{\boldsymbol{r}}|$ and $\boldsymbol{r}$ is π radians since $\boldsymbol{r} \times \ddot{\boldsymbol{r}} = \boldsymbol{0}$ using (1.5.1) which accounts for the negative sign in the second and third terms of (1.5.15). The angle $\theta - \theta_0$ in the hyperbolic case is restricted to the open interval $(\arccos(1/e) - \pi, \pi - \arccos(1/e))$ and at both endpoints of the interval $|\ddot{\boldsymbol{r}}| \to 0$. The angle between $\ddot{\boldsymbol{r}}$ and $\boldsymbol{r}$ will in fact be π radians for any central force and so the acceleration hodograph is easily constructed provided the orbit can be solved. For more complicated forces such as those described in Chapters 2 and 3, the phase difference between $\ddot{\boldsymbol{r}}$ and $\boldsymbol{r}$ will no longer be constant, and consequently the acceleration hodograph cannot be easily constructed. Equation (1.5.15) is a variant of *Pascal's limaçon* $r = a + b\cos\theta$ of which the cardioid is a special case. Assuming $\theta_0 = 0$, for $\mu > J$ equation (1.5.15) describes a curve consisting of a single loop surrounding the origin which tends to a circle as μ increases in size. For this case there is no cusp. When $\mu = J$, the loops merge into one which meets the origin in a cusp. For $\mu < J$ the single loop splits into two interlocking loops, the larger

extending in the $-x$ direction, and the other, smaller and pear–shaped extending in the $+x$ direction, meeting the origin in a cusp. Note that the bounds on θ prevent the limaçon from being completed in the hyperbolic case, however, the curve does close.

Figure 1.5.7 shows the tangential acceleration vectors drawn at some points along the velocity hodograph. Figure 1.5.8 shows the construction of the acceleration hodograph for the elliptical case when the tangential acceleration vectors are shifted to the same origin. Figure 1.5.9 shows the construction of the acceleration hodograph for the parabolic case. Figure 1.5.10 shows the construction of the acceleration hodograph for the hyperbolic case. The two short line segments intersecting the velocity hodograph indicate the limits of extent of the velocity hodograph as t ranges from negative through positive infinity or equivalently when $\theta - \theta_0$ ranges from $\arccos(1/e) - \pi$ through $\pi - \arccos(1/e)$ radians. Figure 1.5.11 shows the graph of equation (1.5.15) plotted over the interval $[-\pi, \pi]$. Equation (1.5.15) behaves in some ways like the velocity hodograph. For $\mu > J$ the acceleration hodograph encloses the origin (for the elliptical case see Figures 1.5.7 and 1.5.8) while for $\mu \leq J$ it circles the origin and finally touches it as t ranges from negative through positive infinity or equivalently when $\theta - \theta_0$ ranges from $-\pi$ through π radians in the parabolic case or when $\theta - \theta_0$ ranges from $\arccos(1/e) - \pi$ through $\pi - \arccos(1/e)$ radians in the hyperbolic case (see Figure 1.5.9 for the parabolic case and Figure 1.5.10 for the hyperbolic case). In both the parabolic and hyperbolic cases, the acceleration hodograph closes since $|\ddot{\mathbf{r}}| = -\mu/r^2 \to 0$ as $r \to \infty$.

In summary the Kepler problem gives rise to three plane polar curves, the ellipse, the circle and the variant of the limaçon. It is rather interesting that the latter curve has such profound physical origins.

The radial motion in time can be found by differentiating (1.5.10)

$$\mathrm{d}t = \frac{L\,\mathrm{d}r}{J\sin(\theta - \theta_0)}. \tag{1.5.16}$$

Using the orbit equation (1.5.10)

$$\sin(\theta - \theta_0) = \frac{1}{Jr}\left((J^2 - \mu^2)r^2 + 2L^2\mu r - L^4\right)^{\frac{1}{2}}. \tag{1.5.17}$$

Substituting (1.5.17) into (1.5.16) gives

$$\mathrm{d}t = \frac{r\,\mathrm{d}r}{\left((J^2 - \mu^2)r^2/L^2 + 2\mu r - L^2\right)^{\frac{1}{2}}}. \tag{1.5.18}$$

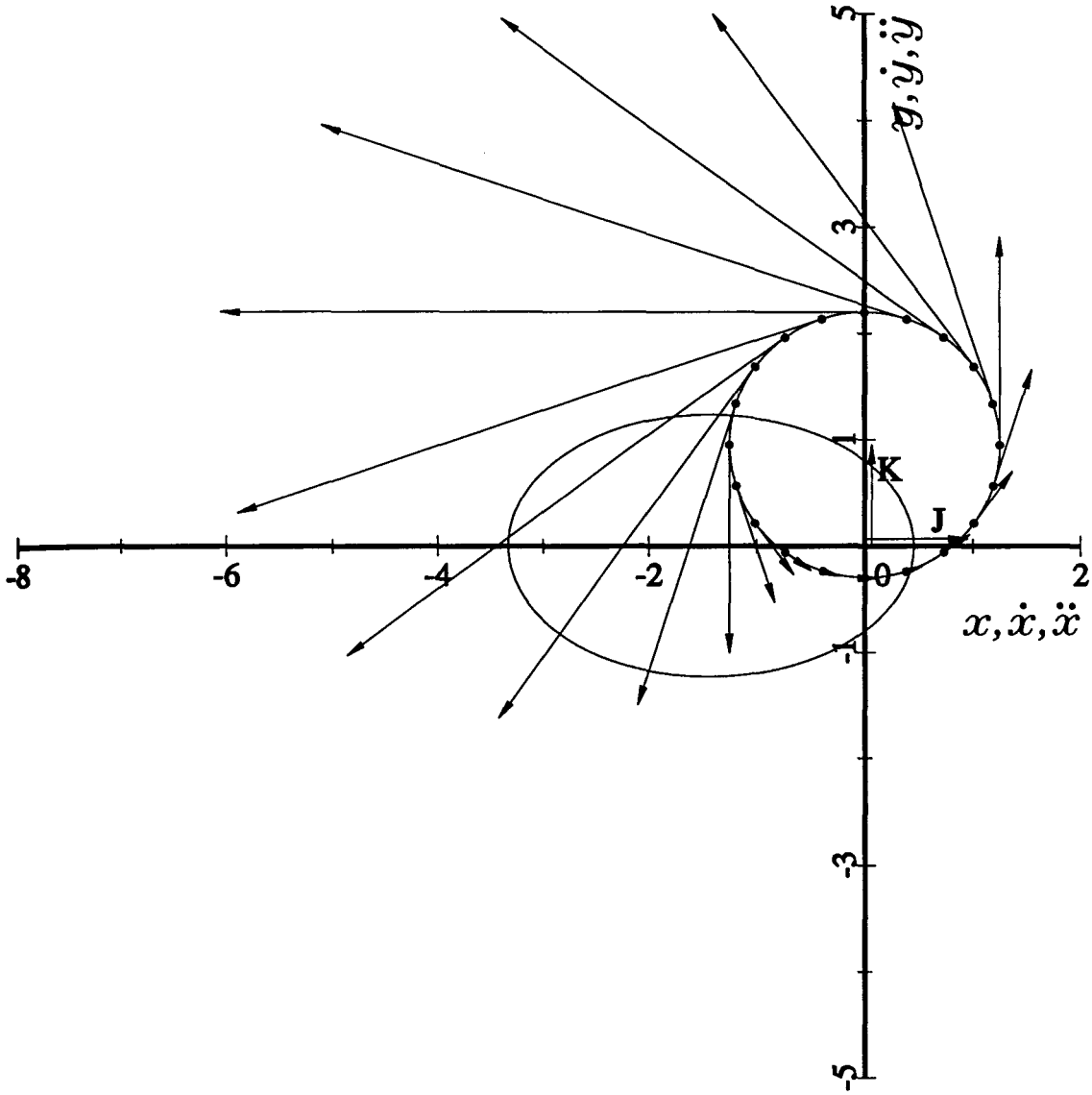


Figure 1.5.7. The elliptical Kepler orbit and the circular velocity hodograph showing the acceleration vectors at some points along the velocity hodograph and the orientation of the conserved vectors $\boldsymbol{K}$ and $\boldsymbol{J}$. The constants are chosen as for Figure 1.5.1.

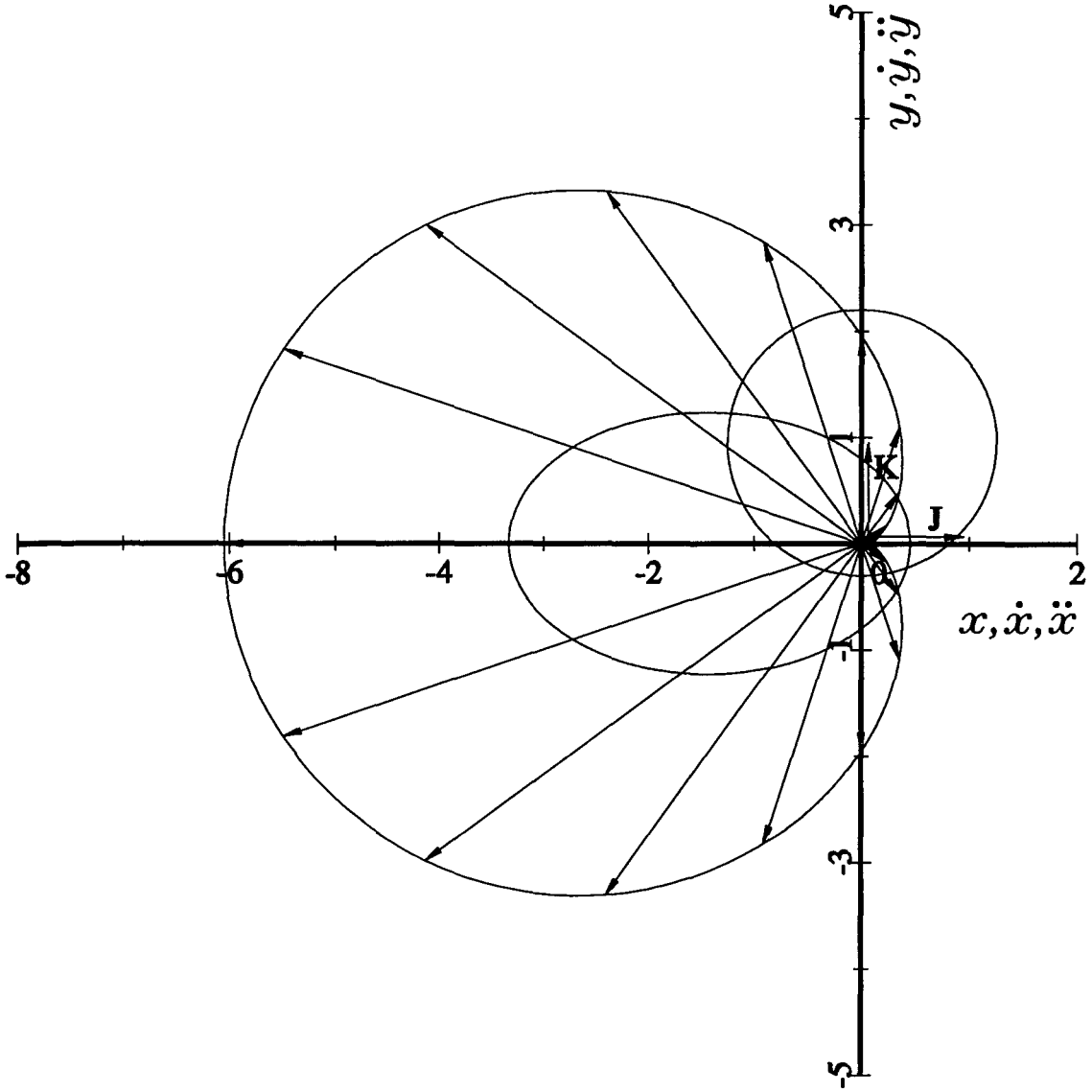


Figure 1.5.8. The elliptical Kepler orbit, circular velocity hodograph and the construction of the corresponding acceleration hodograph with a selection of acceleration vectors drawn from the origin on the same set of axes. The origin lies inside the acceleration hodograph. The phase difference between the acceleration and displacement vectors is a constant π radians but varies between the acceleration and velocity vectors although it is a constant $\pi/2$ radians between the acceleration vector and the vector directed from the centre of the velocity hodograph to the head of the corresponding velocity vector. The constants are chosen as for Figure 1.5.1.

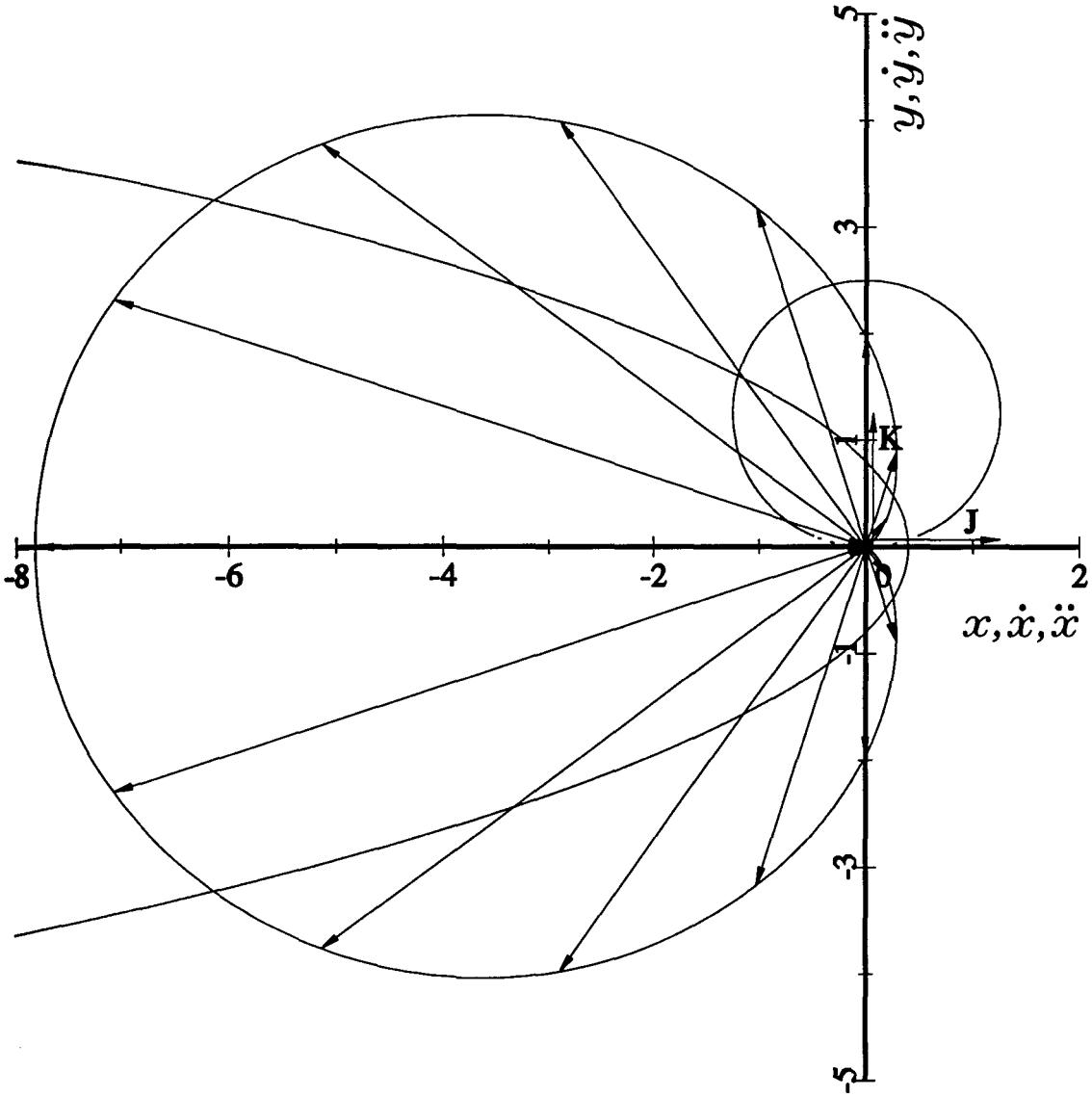


Figure 1.5.9. The parabolic Kepler orbit, circular velocity hodograph and the construction of the corresponding acceleration hodograph with a selection of acceleration vectors drawn from the origin on the same set of axes. The origin lies at a cusp on the acceleration hodograph. The phase difference between the acceleration and displacement vectors is a constant π radians but varies between the acceleration and velocity vectors although it is a constant $\pi/2$ radians between the acceleration vector and the vector directed from the centre of the velocity hodograph to the head of the corresponding velocity vector. The constants are chosen as for Figure 1.5.3.

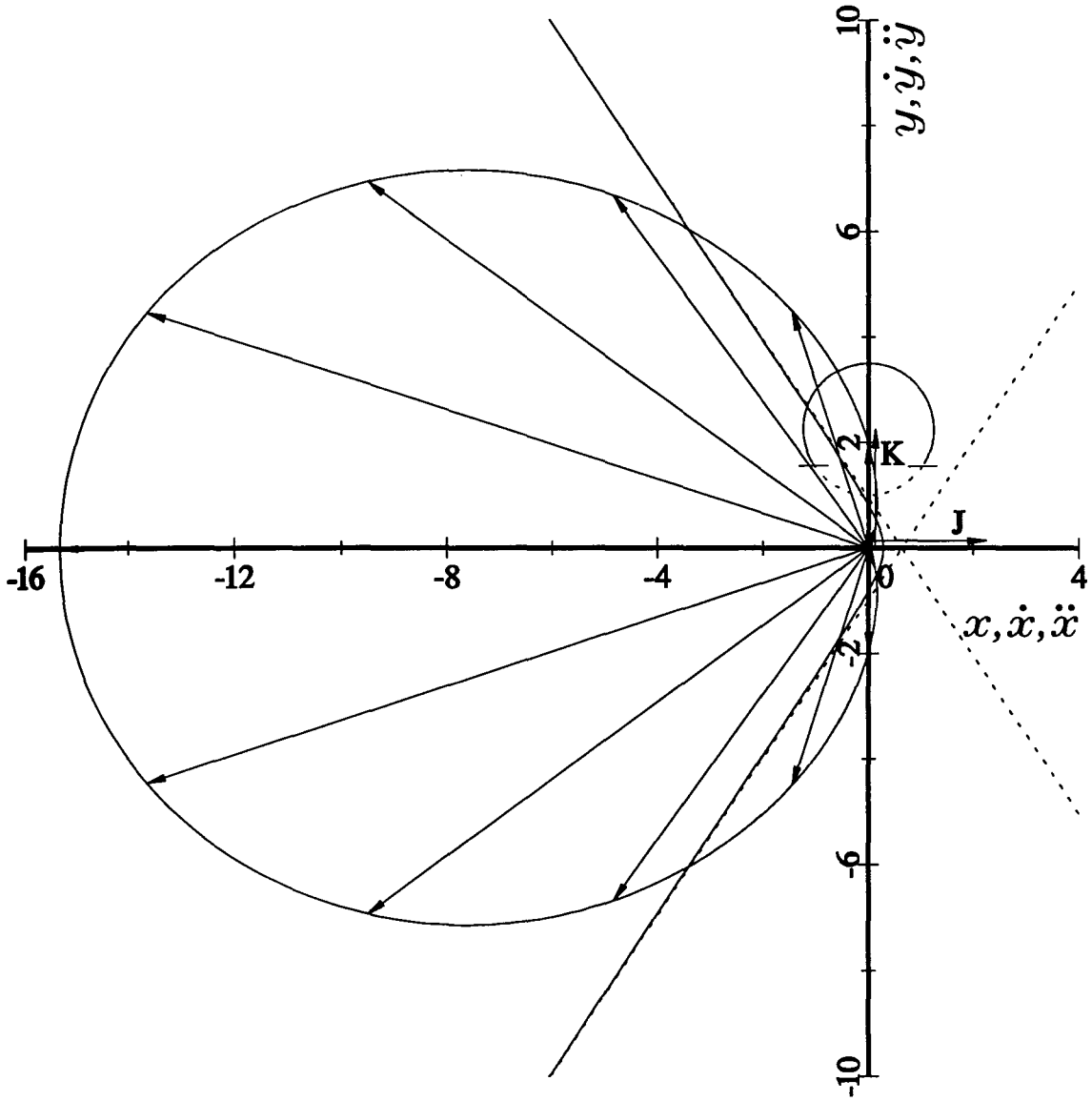


Figure 1.5.10. The hyperbolic Kepler orbit, circular velocity hodograph and the construction of the corresponding acceleration hodograph with a selection of acceleration vectors drawn from the origin on the same set of axes. The origin is not enclosed by the acceleration hodograph. The phase difference between the acceleration and displacement vectors is a constant π radians but varies between the acceleration and velocity vectors although it is a constant $\pi/2$ radians between the acceleration vector and the vector directed from the centre of the velocity hodograph to the head of the corresponding velocity vector. The constants are chosen as for Figure 1.5.4.

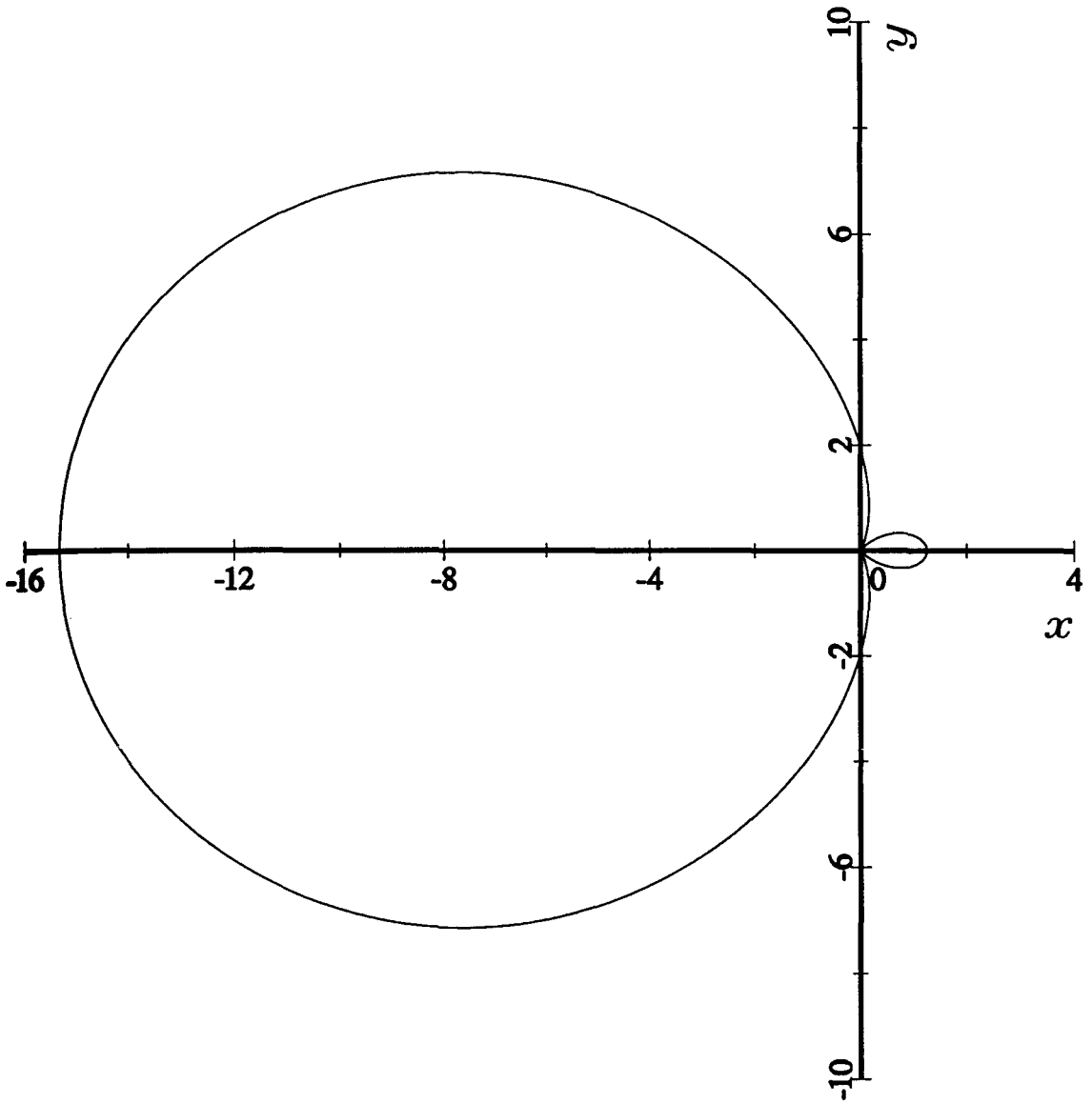


Figure 1.5.11. The polar equation $r = -\mu\big(\mu + J\cos(\theta - \theta_0)\big)^2/L^4$ for $\mu = 1.25$, $\theta_0 = 0$, $J = 2.25$ and $L = 1$.

From (1.5.8) we find that

$$J^2 = 2L^2E + \mu^2 \tag{1.5.19}$$

and so

$$\frac{J^2 - \mu^2}{L^2} = 2E. \tag{1.5.20}$$

Replacement of the coefficient of r^2 in (1.5.18) using (1.5.20) gives the more usual form for the radial velocity which is usually derived by rearranging the equation describing the conservation of energy (which is also the Hamiltonian in this case)

$$E = \frac{1}{2}\dot{r}^2 + \frac{1}{2}\frac{L^2}{r^2} - \frac{\mu}{r}. \tag{1.5.21}$$

Equation (1.5.19) illustrates a rather important point concerning the functional dependence of the first integrals. A system with n degrees of freedom can at most possess $2n - 1$ independent autonomous first integrals (see [59]). For the Kepler problem the representative set of first integrals are the three components of the angular momentum, the three components of the Laplace–Runge–Lenz vector and the scalar energy (1.5.21). Since Hamilton's vector $\boldsymbol{K}$ is essentially a rotation of $\boldsymbol{J}$, *i.e.*, $\boldsymbol{J} = \boldsymbol{K} \times \boldsymbol{L}$, it does not provide any other new independent integrals to the set. As the system possesses three degrees of freedom, we would only expect 5 independent autonomous first integrals, or alternatively two relations between members of the set. The two relations are (1.5.19) and

$$\boldsymbol{J}\cdot\boldsymbol{L} = 0. \tag{1.5.22}$$

The Lagrangian for this conservative system is given by

$$\mathcal{L} = \frac{1}{2}\dot{r}^2 + \frac{1}{2}\frac{L^2}{r^2} + \frac{\mu}{r}. \tag{1.5.23}$$

One further aspect arising from the functional dependence of the first integrals is the construction of an associated vector quantity which is related in the same way to the Lagrangian as the conserved Laplace–Runge–Lenz vector is related to the Hamiltonian, *i.e.*

$$M^2 = 2L^2\mathcal{L} + \mu^2 \tag{1.5.24}$$

where $\boldsymbol{M}$ will be called a Lagrangian vector due to its close connection with the scalar Lagrangian $\mathcal{L}$. In this instance, the Euler–Lagrange equations applied to the square of the magnitude of $\boldsymbol{M}$ do not give rise to the equations of motion of the particle since the factor L^2 would be expressed in terms of generalised coordinates mixed in with other terms of the vector $\boldsymbol{M}$ and disrupt the normal function of the Lagrangian. This would appear to prevent using the Euler–Lagrange equations to determine constraints

on a trial Lagrangian vector assumed to have a particular structure. At this stage the connection between the vector $\boldsymbol{M}$ and Hamilton's action integral is not clear. One possible structure for $\boldsymbol{M}$ which meets the requirement (1.5.24) is

$$\boldsymbol{M} = \dot{\boldsymbol{r}} \times \boldsymbol{L} + \mu \hat{\boldsymbol{r}} \tag{1.5.25}$$

and similarly the Hamilton vector equivalent is given by

$$\boldsymbol{N} = \dot{\boldsymbol{r}} + \frac{\mu}{L} \hat{\boldsymbol{\theta}}. \tag{1.5.26}$$

It is also worth noting that in this conservative system H (1.5.21) and $\mathcal{L}$ (1.5.23) are conjugate to each other and this structure also extends to the vector pairs $\boldsymbol{M}$ and $\boldsymbol{J}$ and $\boldsymbol{N}$ and $\boldsymbol{K}$ respectively.

Due to the close resemblance of the pair of Lagrangian vectors with their conserved counterparts it would seem worthwhile to investigate the equivalent Poisson bracket relationships in the same way as has been done for the conserved vectors of the Kepler problem [57, 29, 33, p421]. The Poisson bracket relations between the components of $\boldsymbol{L}$ and the conserved Laplace–Runge–Lenz vector $\boldsymbol{J}$ and the scalar energy or Hamiltonian H for the Kepler problem are

$$\begin{aligned}
[L_i, L_j] &= \varepsilon_{ijk} L_k \\
[J_i, L_j] &= \varepsilon_{ijk} J_k \\
[J_i, J_j] &= -2H \varepsilon_{ijk} L_k \\
[L_i, H] &= 0 \\
[J_i, H] &= 0.
\end{aligned} \tag{1.5.27}$$

For $H \neq 0$ it is usual to rescale $\boldsymbol{J}$ by the factor $(\mp 2H)^{\frac{1}{2}}$ depending on whether H is negative or positive respectively, to obtain the standard forms

$$\begin{aligned}
\left[\frac{J_i}{(\mp 2H)^{\frac{1}{2}}}, L_j \right] &= \varepsilon_{ijk} \frac{J_k}{(\mp 2H)^{\frac{1}{2}}} \\
\left[\frac{J_i}{(\mp 2H)^{\frac{1}{2}}}, \frac{J_j}{(\mp 2H)^{\frac{1}{2}}} \right] &= \pm \varepsilon_{ijk} L_k \\
\left[\frac{J_i}{(\mp 2H)^{\frac{1}{2}}}, H \right] &= 0,
\end{aligned} \tag{1.5.28}$$

d thus the components of $\boldsymbol{L}$ and $\boldsymbol{J}$ together form the symmetry groups $so(4)$ $H < 0$ (elliptic orbits), $e(3)$ for $H = 0$ (parabolic orbits) and $so(3,1)$ for > 0 (hyperbolic orbits). The following Poisson bracket relations were found be- ween the components of $\boldsymbol{L}$ and the non–conserved Lagrangian vector $\boldsymbol{M}$ and the calar Lagrangian $\mathcal{L}$

$$\begin{aligned}
&[L_i, L_j] = \varepsilon_{ijk} L_k \\
&[M_i, L_j] = \varepsilon_{ijk} M_k \\
&[M_i, M_j] = -2\mathcal{L}\varepsilon_{ijk} L_k \\
&[L_i, \mathcal{L}] = 0 \\
&[M_i, \mathcal{L}] = 0.
\end{aligned} \tag{1.5.29}$$

Notice that the Poisson bracket expressions have the same structure as those between the components of the conserved quantities as shown in equations (1.5.27) except that the multiplier appearing in (1.5.29.3) involves the Lagrangian which is not conserved. It is even possible to rescale $\boldsymbol{M}$ by the factor $(2\mathcal{L})^{\frac{1}{2}}$ to obtain the standard forms

$$\begin{aligned}
&\left[\frac{M_i}{(2\mathcal{L})^{\frac{1}{2}}}, L_j\right] = \varepsilon_{ijk} \frac{M_k}{(2\mathcal{L})^{\frac{1}{2}}} \\
&\left[\frac{M_i}{(2\mathcal{L})^{\frac{1}{2}}}, \frac{M_j}{(2\mathcal{L})^{\frac{1}{2}}}\right] = -\varepsilon_{ijk} L_k \\
&\left[\frac{M_i}{(2\mathcal{L})^{\frac{1}{2}}}, \mathcal{L}\right] = 0
\end{aligned} \tag{1.5.30}$$

which have the same structure as the Poisson bracket expressions between the components of the conserved quantities in the Kepler problem for $H > 0$ since $\mathcal{L}$ is always positive. Thus the non–conserved Lagrangian vector $\boldsymbol{M}$ behaves in the same fashion as the conserved vector $\boldsymbol{J}$ for positive energy states under the operation of taking the Poisson bracket which is curious.

One possible method for verifying whether an autonomous vector is conserved is to determine whether the Poisson brackets of the separate components of the vector taken with H vanish simultaneously. The procedure for determining a Lagrangian vector would by analogy seem to suggest that the components of the Lagrangian vector commute with the Lagrangian under the operation of the Poisson bracket. It must of course be remembered, however, that the Lagrangian must be recast into the Hamiltonian structure as a function of the generalised coordinates and momenta, $L(q_i, p_i)$ rather than the more usual $L(q_i, \dot{q}_i)$. Thus it would seem that a suitable definition for a Lagrangian vector would be that the Poisson bracket of the components

taken separately with the Lagrangian vanish and further that the Poisson bracket between pairs of different components of $\boldsymbol{M}$ generates the relevant components of the conserved vector $\boldsymbol{L}$. In expanded form, the useful Poisson bracket expressions are given by

$$\frac{\partial M_i}{\partial q_j}\dot{q}_j - \frac{\partial M_i}{\partial p_j}\frac{\partial \mathcal{L}(q_l, p_l)}{\partial q_j} = 0$$

$$\frac{\partial M_i}{\partial q_k}\frac{\partial M_j}{\partial p_k} - \frac{\partial M_i}{\partial p_k}\frac{\partial M_j}{\partial q_k} = -2\mathcal{L}\varepsilon_{ijk}L_k. \tag{1.5.31}$$

The top expression of (1.5.31) can also be written as

$$\frac{\partial M_i}{\partial p_j}\dot{p}_j - \frac{\partial M_i}{\partial q_j}\dot{q}_j = \frac{\partial M_i}{\partial p_j}p_k\frac{\partial \dot{p}_j}{\partial p_k} \tag{1.5.32}$$

writing the Lagrangian as $p_k\dot{q}_k - H$ and using Hamilton's equations and the result that $\partial\dot{q}_k/\partial q_j = -\partial\dot{p}_j/\partial p_k$. Equation (1.5.32) can also be expressed in terms of the total time derivative of M_i as

$$\dot{M}_i = \frac{\partial M_i}{\partial p_j}\left(2\dot{p}_j - p_k\frac{\partial \dot{p}_j}{\partial p_k}\right). \tag{1.5.33}$$

It would appear that the approach to adopt when constructing such a vector is to assume a structure for the Lagrangian vector such as $\boldsymbol{M} = A(q_l, p_l)\boldsymbol{p} \times \boldsymbol{L} + B(q_l, p_l)\hat{\boldsymbol{r}}$ and then to use the Poisson bracket with $\mathcal{L}$ to obtain restrictions on the unknown functions A and B. This would be followed by applying the other Poisson bracket constraints (1.5.31.2) on $\boldsymbol{M}$. A similar procedure for constructing conserved vectors and tensors for a general central force problem also based on Poisson brackets due to Fradkin [29] will be outlined in §§1.6–1.7. Note that the technique described above needs a Lagrangian and also that $\partial\mathcal{L}(q_l, p_l)/\partial q_j$ is not equal to $\dot{p}_j$ since $\mathcal{L}$ is now recast in the Hamiltonian representation. If this were the case, however, then (1.5.31.1) would be the conjugate of the expanded exact derivative of $\boldsymbol{M}$ which is very appealing and this apparent lack of symmetry may suggest further complications during the construction process.

Despite the shortcomings and apparent lack of applications for the Lagrangian vector it is an interesting tool which can be used to describe the geometry of the Kepler problem, especially with regard to its connection with Hamilton's velocity hodograph which it appears to mimic and in addition it also gives a geometric interpretation to the scalar Lagrangian.

The path of $\boldsymbol{N}$ is easily calculated by expressing $\boldsymbol{N}$ in terms of $\boldsymbol{K}$ which gives

$$\boldsymbol{N} = \boldsymbol{K} + \frac{2\mu}{L}\hat{\boldsymbol{\theta}}, \tag{1.5.34}$$

which can be rearranged and squared to give the cartesian equation

$$(N_x + K\sin\theta_0)^2 + (N_y - K\cos\theta_0)^2 = \left(\frac{2\mu}{L}\right)^2 \tag{1.5.35}$$

which describes a circle in the N_x, N_y plane with centre $(-K\sin\theta_0, K\cos\theta_0)$ and radius $2\mu/L$, *i.e.* Hamilton's vector gives the centre of the circle traced out by the Lagrange vector $\boldsymbol{N}$. Since $\boldsymbol{N}\times\boldsymbol{L} = \boldsymbol{M}$ the vector $\boldsymbol{M}$ also traces out a circle which is rotated clockwise by $\pi/2$ radians about the origin and scaled by L.

Figures 1.5.12–1.5.14 show the displacements, velocities and the path of the Lagrangian vector $\boldsymbol{N}$ at regular increments in θ for the Kepler problem. It should be obvious that the initial phase difference between the displacement and Lagrangian vectors is $\pi/2$ radians as the displacement lies along the $+x-$axis when $\theta = 0$ while the Lagrangian vector lies along the $+y, \dot{y}-$axis. The phase difference in general between the displacement and Lagrangian vectors is not constant since $\boldsymbol{r}\cdot\boldsymbol{N} = r\dot{r}$ which is nonzero except when $\dot{r} = 0$, *i.e.* at the extremities of the motion. This is also evident by comparing the angle between the corresponding displacement and Lagrangian vectors for a range of increments in θ using the solid round time markers on the orbit and the corresponding arrowheads on the path of the Lagrangian vector and counting the number of round markers from the rightmost vertex of the ellipse in a counter–clockwise direction to the displacement of interest and then counting off the same number of arrowheads on the path of the Lagrangian vector starting from the arrowhead at the top of the path of the Lagrangian vector (since when $\theta = 0$ the Lagrangian vector lies along the $+y, \dot{y}-$axis) in a counter–clockwise direction to obtain the corresponding Lagrangian vector or *vice versa.* Note, however, that the phase difference between the radial vector $\boldsymbol{r}$ and the vector directed from the head of the Hamilton vector $\boldsymbol{K}$ (the centre of the circular velocity hodograph) to the head of the vector $\boldsymbol{N}$, *i.e.* $\boldsymbol{N} - \boldsymbol{K}$ is a constant $\pi/2$ radians since $\boldsymbol{r}\cdot(\boldsymbol{N} - \boldsymbol{K}) = 0$ and it follows that $\dot{\boldsymbol{r}} - \boldsymbol{K}$ is collinear with $\boldsymbol{N} - \boldsymbol{K}$. This behaviour is also evident on translating the velocity hodograph and the path of the Lagrangian vector so that the common centre of the two concentric circles coincides with the origin of the orbit. Alternatively, if in addition to the translation described above, the velocity hodograph and the path of the Lagrangian vector are rotated clockwise through $\pi/2$ radians about the common centre of the two concentric circles, it is apparent that the corresponding displacements, velocities, Lagrangian vectors and the origin are collinear which demonstrates the constant $\pi/2$ phase difference. In summary, the phase difference between $\boldsymbol{r}$ and $\boldsymbol{N}$ is not constant in the Kepler problem but the phase difference between $\boldsymbol{r}$ and $\boldsymbol{N} - \boldsymbol{K}$ is constant at $\pi/2$ radians or, in other words, the radial vector directed from the origin which is also a focus of the ellipse in the

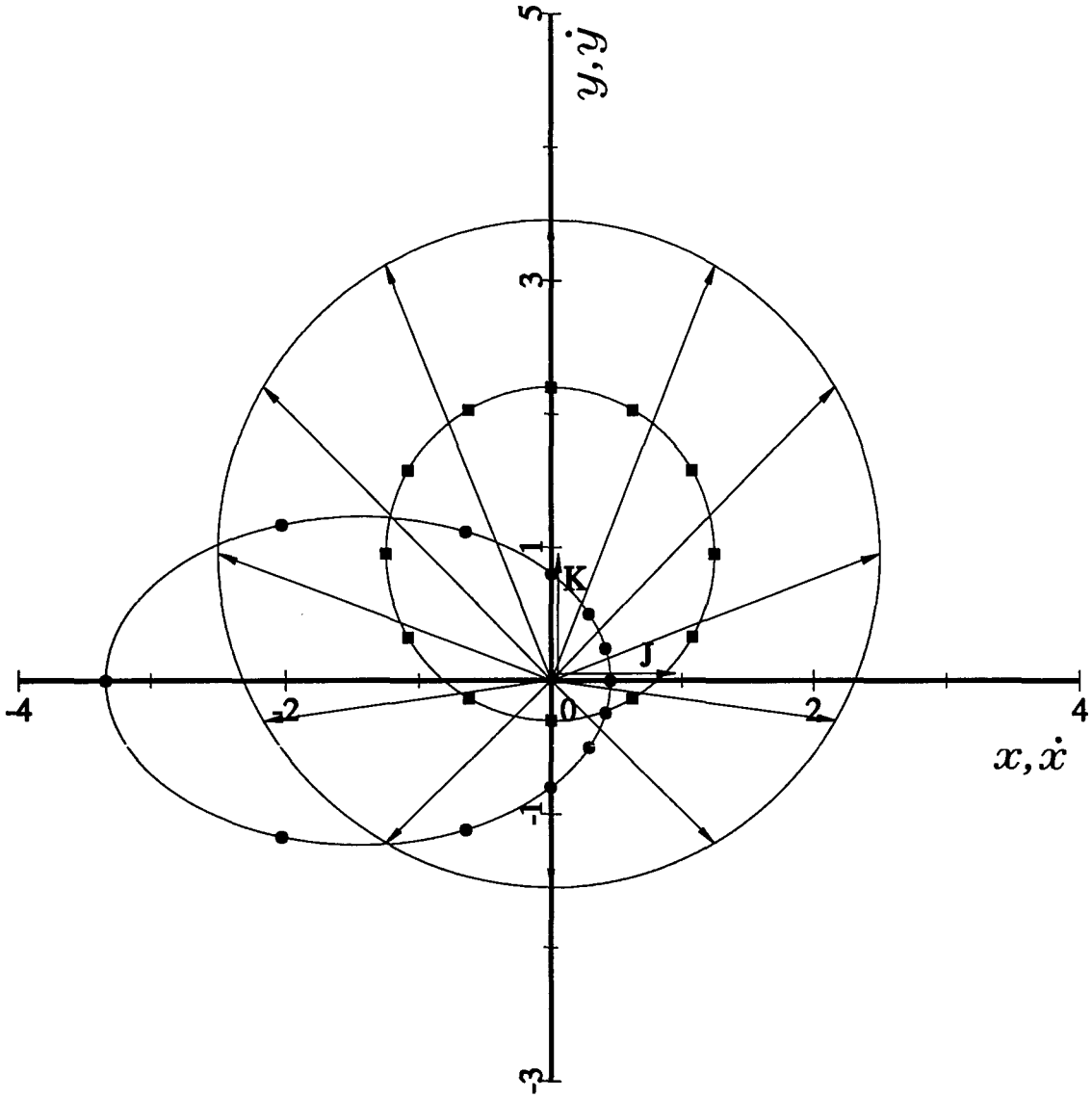


Figure 1.5.12. The elliptical Kepler orbit, the circular velocity hodograph and the construction of the circular path of the Lagrangian vector with a selection of Lagrangian vectors drawn from the origin on the same set of axes as the displacement. The circles (-●-●-●-) show the displacements of the particle at the angular increments $\theta = i\ \pi/6$, $i = 0, \ldots, 12$ and the squares (-■-■-■-) give the corresponding velocities. The phase difference between the velocity or Lagrangian vectors and the displacement vector is not constant. The constants are chosen as for Figure 1.5.1.

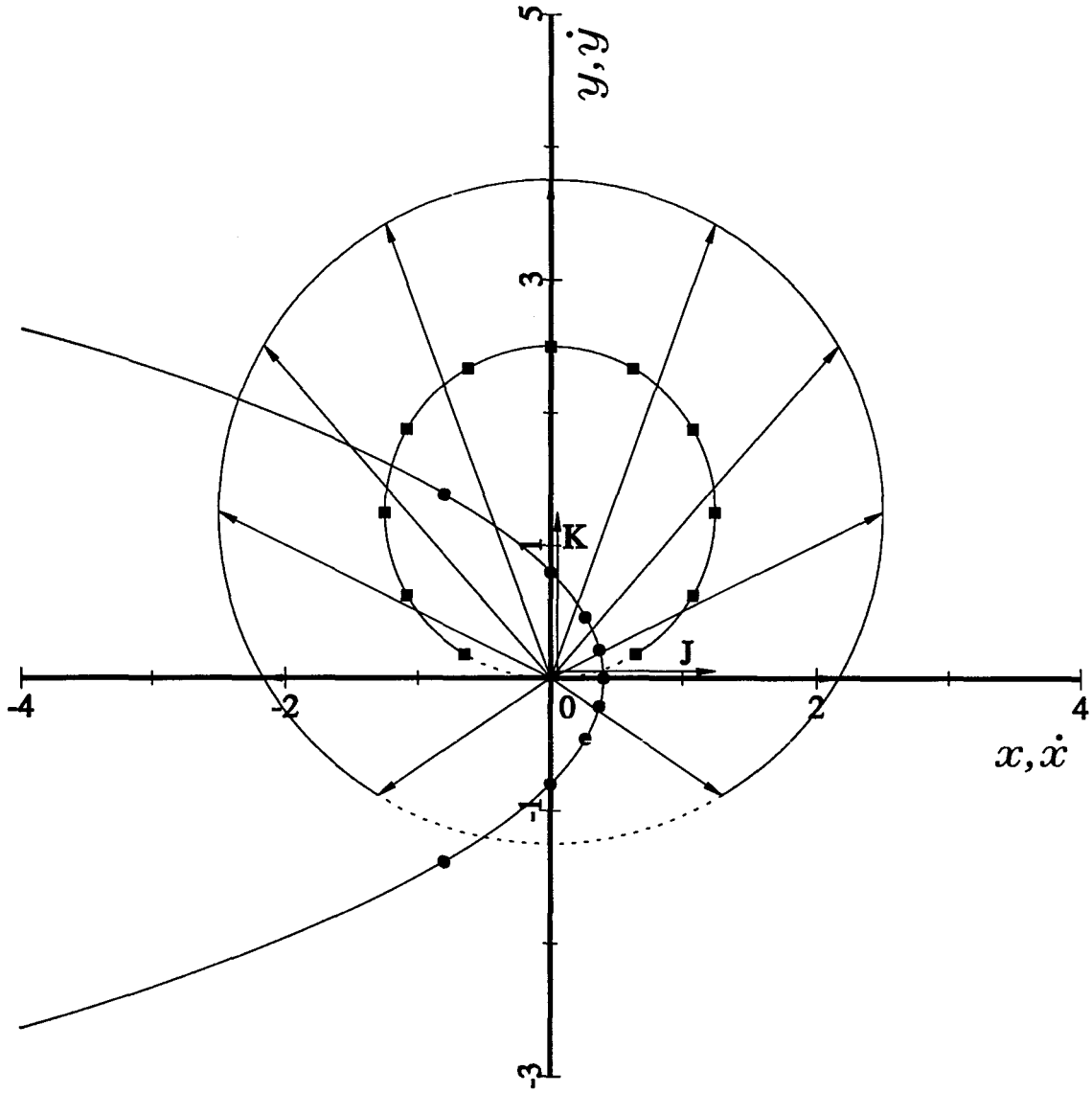


Figure 1.5.13. The parabolic Kepler orbit, the circular velocity hodograph and the construction of the circular path of the Lagrangian vector with a selection of Lagrangian vectors drawn from the origin on the same set of axes as the displacement. The circles (-●-●-●-) show the displacements of the particle at the angular increments $\theta = i\ \pi/6$, $i = 0, \ldots, 12$ and the squares (-■-■-■-) give the corresponding velocities. The phase difference between the velocity or Lagrangian vectors and the displacement vector is not constant. The constants are chosen as for Figure 1.5.3.

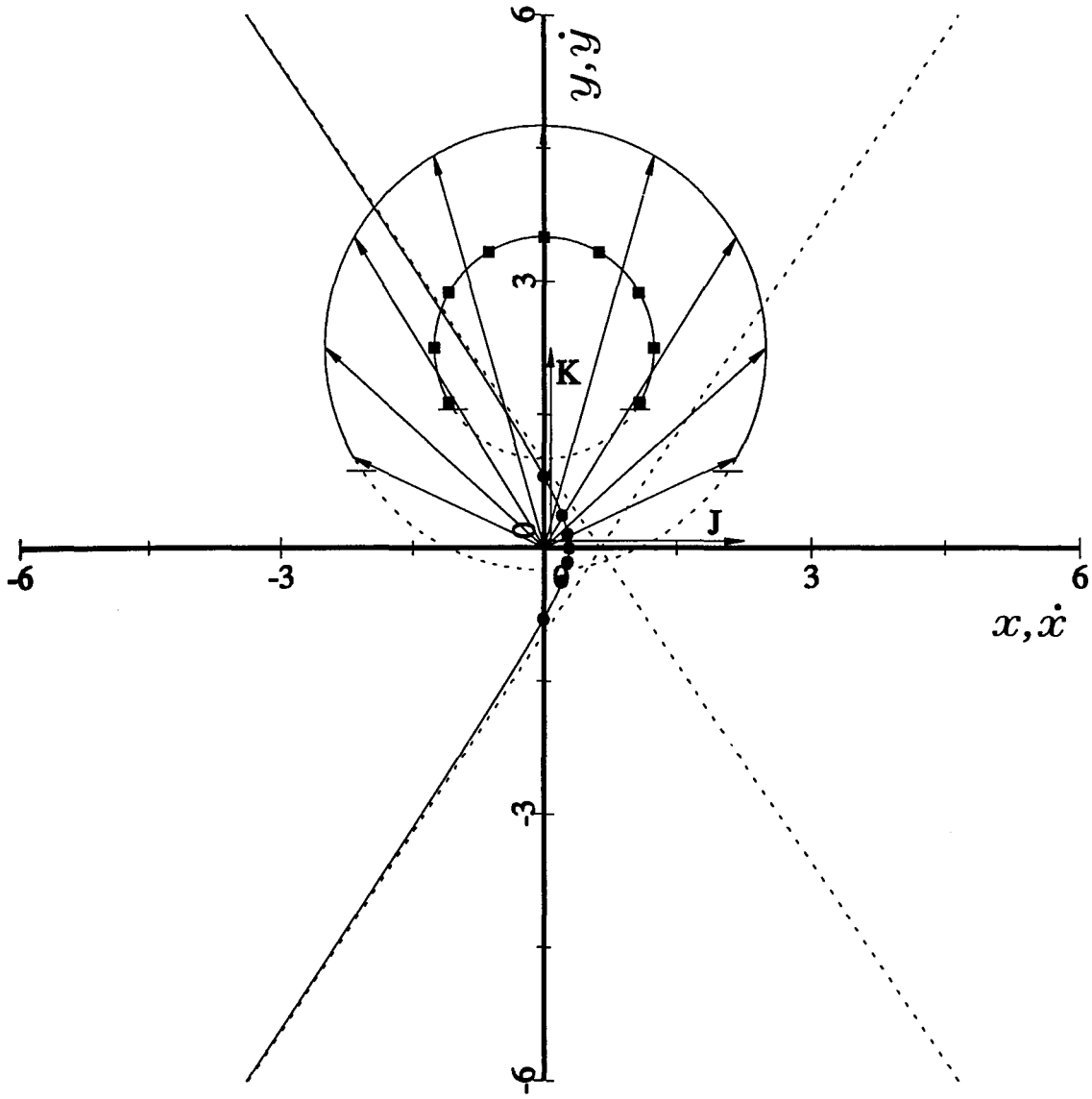


Figure 1.5.14. The hyperbolic Kepler orbit, the circular velocity hodograph and the construction of the circular path of the Lagrangian vector with a selection of Lagrangian vectors drawn from the origin on the same set of axes as the displacement. The circles (–•–•–•–) show the displacements of the particle at the angular increments $\theta = i\ \pi/6$, $i = 0, \ldots, 12$ and the squares (–■–■–■–) give the corresponding velocities. The phase difference between the velocity or Lagrangian vectors and the displacement vector is not constant. The constants are chosen as for Figure 1.5.4.

plane moves in phase with an offset Lagrangian vector directed from the head of the Hamilton vector (the centre of the circular velocity hodograph). Figure 1.5.12 shows the construction of the circular path of the Lagrangian vector $\boldsymbol{N}$ for the elliptical case. Figure 1.5.13 shows the construction of the circular path of the Lagrangian vector $\boldsymbol{N}$ for the parabolic case. Figure 1.5.14 shows the construction of the circular path of the Lagrangian vector $\boldsymbol{N}$ for the hyperbolic case. It should be noted that as in the case of the velocity hodograph the path of the Lagrangian vector closes in the elliptical case, only closes as t ranges from negative through positive infinity or equivalently when $\theta - \theta_0$ ranges from $-\pi$ through π radians in the parabolic case and never closes in the hyperbolic case since it is bounded by the asymptotes. The two short line segments intersecting the path of the Lagrangian vector $\boldsymbol{N}$ indicate the limits of extent of the path as t ranges from negative through positive infinity or equivalently when $\theta - \theta_0$ ranges from $\arccos(1/e) - \pi$ through $\pi - \arccos(1/e)$ radians and are calculated as follows. The parametric equations for the path of the Lagrangian vector $\boldsymbol{N}$ can be shown to have the form

$$\begin{aligned} N_x &= -\frac{1}{L}\big(2\mu\sin\theta + J\sin\theta_0\big) = -\frac{\mu^{\frac{1}{2}}}{a^{\frac{1}{2}}(e^2-1)^{\frac{1}{2}}}\big(2\sin\theta + e\sin\theta_0\big) \\ N_y &= \frac{1}{L}\big(2\mu\cos\theta + J\cos\theta_0\big) = \frac{\mu^{\frac{1}{2}}}{a^{\frac{1}{2}}(e^2-1)^{\frac{1}{2}}}\big(2\cos\theta + e\cos\theta_0\big) \end{aligned} \tag{1.5.36}$$

using the orbit equation (1.5.10) to substitute for r and $\dot{r}$ in terms of θ and in the hyperbolic case the limits of extent are given by

$$\begin{aligned} N_{xe} &= \frac{1}{JL}\left(\mp 2\mu L(2H)^{\frac{1}{2}}\cos\theta_0 - (2L^2H - \mu^2)\sin\theta_0\right) \\ &= \frac{\mu^{\frac{1}{2}}}{a^{\frac{1}{2}}e(e^2-1)^{\frac{1}{2}}}\left(\mp 2(e^2-1)^{\frac{1}{2}}\cos\theta_0 - (e^2-2)\sin\theta_0\right) \\ N_{ye} &= \frac{1}{JL}\left((2L^2H - \mu^2)\cos\theta_0 \pm 2\mu L(2H)^{\frac{1}{2}}\sin\theta_0\right) \\ &= \frac{\mu^{\frac{1}{2}}}{a^{\frac{1}{2}}e(e^2-1)^{\frac{1}{2}}}\left((e^2-2)\cos\theta_0 \pm 2(e^2-1)^{\frac{1}{2}}\sin\theta_0\right) \end{aligned} \tag{1.5.37}$$

using the solutions (1.5.13) to the equations of the asymptotes of the hyperbola as before.

Denoting the angle between the Lagrangian vector $\boldsymbol{N}$ and $\boldsymbol{i}$ as ρ and using (1.5.36) gives

$$\tan\rho = \frac{N_y}{N_x} = -\frac{(2\cos\theta + e\cos\theta_0)}{2\sin\theta + e\sin\theta_0}. \tag{1.5.38}$$

Note that when $\theta = \theta_0$, $\rho = \arctan(-\cos\theta_0/\sin\theta_0) = \pi/2 + \theta_0$ as expected.

As is to be expected, the orbit equation can be found by either taking the scalar product of $\boldsymbol{r}$ with $\boldsymbol{M}$ or from the vector product of $\boldsymbol{r}$ with $\boldsymbol{N}$ and rearranging the scalar part of the expression. The second approach is more convenient in this case as an expression for ρ (the angle between $\boldsymbol{N}$ and $\boldsymbol{i}$) in terms of θ has already been obtained in (1.5.38). The orbit equation in terms of the magnitude of the non-conserved Lagrangian vector $\boldsymbol{N}$ is then given by

$$r = \frac{L^2}{NL\sin\big(\rho - (\theta - \theta_0)\big) - \mu}, \tag{1.5.39}$$

where the angle between $\boldsymbol{N}$ and $\boldsymbol{r}$ is $\rho - (\theta - \theta_0)$. The magnitude of $\boldsymbol{N}$ can be expressed in terms of θ using $N = (2\mathcal{L} + \mu^2/L^2)^{\frac{1}{2}}$ where

$$\mathcal{L} = \frac{J^2 + 4\mu J\cos(\theta - \theta_0) + 3\mu^2}{2L^2} = \frac{\mu^2(e^2 + 4e\cos(\theta - \theta_0) + 3)}{2L^2}. \tag{1.5.40}$$

Using a standard trigonometric identity to expand the term $\sin(\rho - (\theta - \theta_0))$ and (1.5.38) to find expressions for $\sin\rho$ and $\cos\rho$, (1.5.39) reduces to the more familiar form for the orbit equation (1.5.10). Notice that the orbit equation expressed in terms of $\boldsymbol{N}$ closely resembles (1.5.10) and, although the path is not immediately apparent, a better understanding of Lagrangian type vectors could help to identify orbits without having to convert to expressions involving only conserved vectors.

Figures 1.5.15–1.5.17 show the displacements, velocities, accelerations, the path of the Lagrangian vector and the path of the magnitude of the scalar Lagrangian in the direction of $\hat{\boldsymbol{r}}$ at regular increments in θ for the Kepler problem. Figure 1.5.15 shows the construction of the path of the magnitude of the scalar Lagrangian in the direction of $\hat{\boldsymbol{r}}$ for the elliptical case. Figure 1.5.16 shows the construction of the path of the magnitude of the scalar Lagrangian in the direction of $\hat{\boldsymbol{r}}$ for the parabolic case. Figure 1.5.17 shows the construction of the path of the magnitude of the scalar Lagrangian in the direction of $\hat{\boldsymbol{r}}$ for the hyperbolic case. It should be noted that the path is closed in the elliptical case, only closes as t ranges from negative through positive infinity or equivalently when $\theta - \theta_0$ ranges from $-\pi$ through π radians in the parabolic case and never closes in the hyperbolic case since it is bounded by the asymptotes. The two short line segments intersecting the path of the magnitude of the scalar Lagrangian in the direction of $\hat{\boldsymbol{r}}$ indicate the limits of extent of the curve as t ranges from negative through positive infinity or equivalently when $\theta - \theta_0$ ranges from $\arccos(1/e) - \pi$ through $\pi - \arccos(1/e)$ radians and are given by

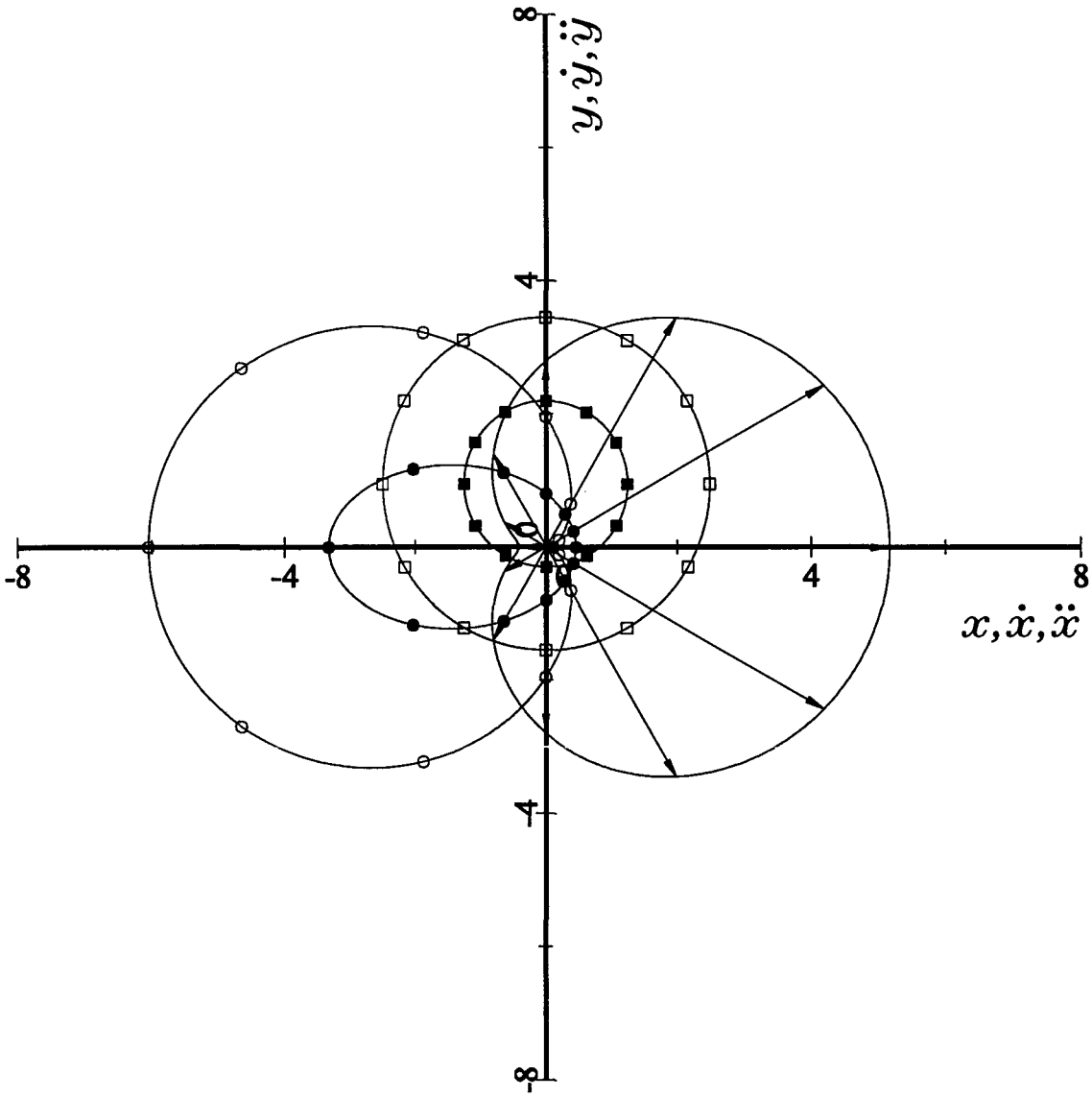


Figure 1.5.15. The elliptical Kepler orbit, the circular velocity hodograph, the acceleration hodograph, the circular path of the Lagrangian vector and the construction of the path of the magnitude of the scalar Lagrangian in the direction of $\hat{r}$ with a selection of vectors drawn from the origin on the same set of axes. The circles (–●–●–●–) show the displacements of the particle at the angular increments $\theta = i\ \pi/6$, $i = 0, \ldots, 12$ and the squares (–■–■–■–) give the corresponding velocities. The unfilled circles (–o–o–o–) and the unfilled squares (–□–□–□–) show the corresponding points along the acceleration hodograph and the path of the Lagrangian vector respectively. The constants are chosen as for Figure 1.5.1.

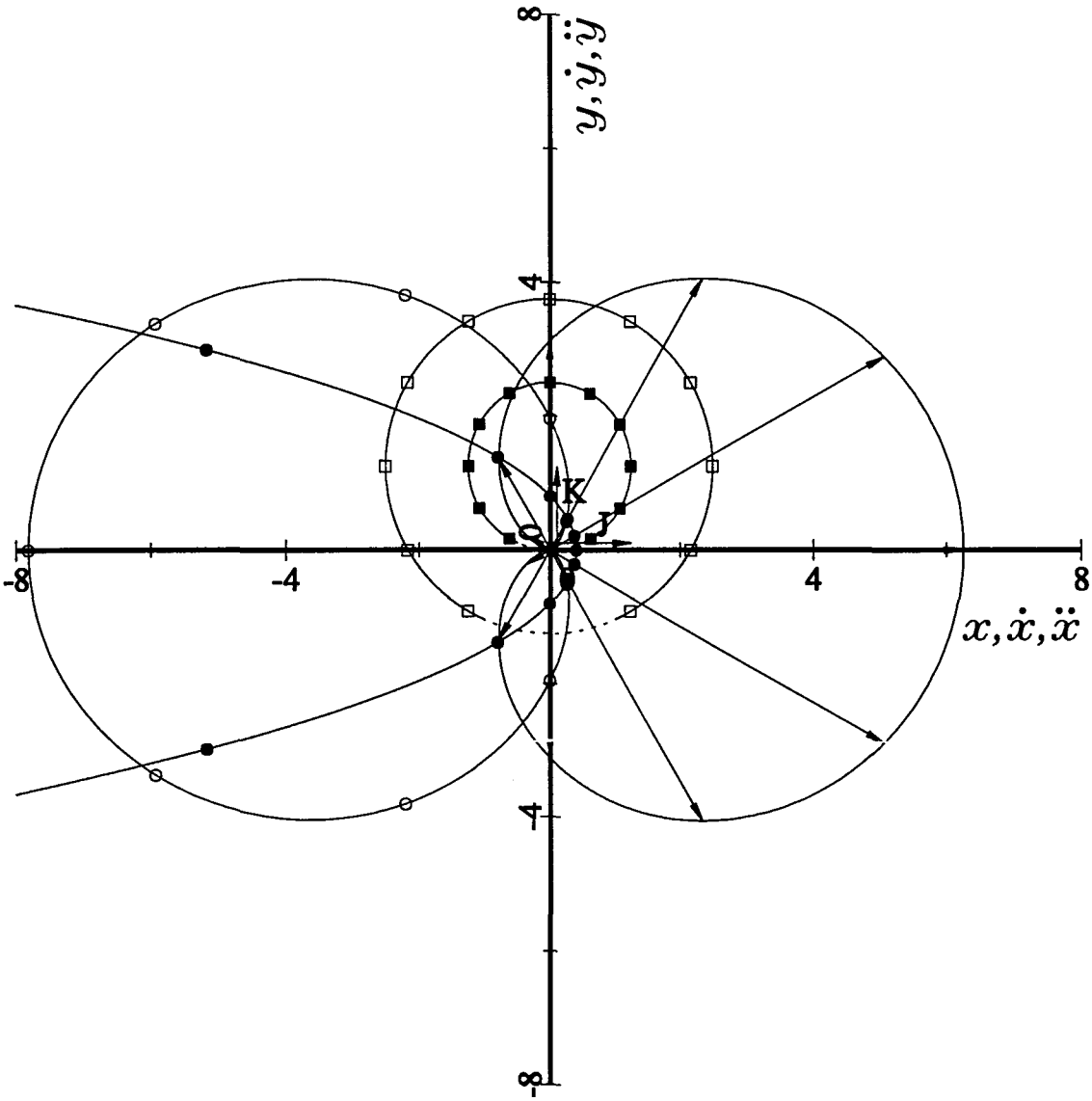


Figure 1.5.16. The parabolic Kepler orbit, the circular velocity hodograph, the acceleration hodograph, the circular path of the Lagrangian vector and the construction of the path of the magnitude of the scalar Lagrangian in the direction of $\hat{\boldsymbol{r}}$ with a selection of vectors drawn from the origin on the same set of axes. The circles (–•–•–•–) show the displacements of the particle at the angular increments $\theta = i\ \pi/6$, $i = 0, \ldots, 12$ and the squares (–■–■–■–) give the corresponding velocities. The unfilled circles (–o–o–o–) and the unfilled squares (–□–□–□–) show the corresponding points along the acceleration hodograph and the path of the Lagrangian vector respectively. The constants are chosen as for Figure 1.5.3.

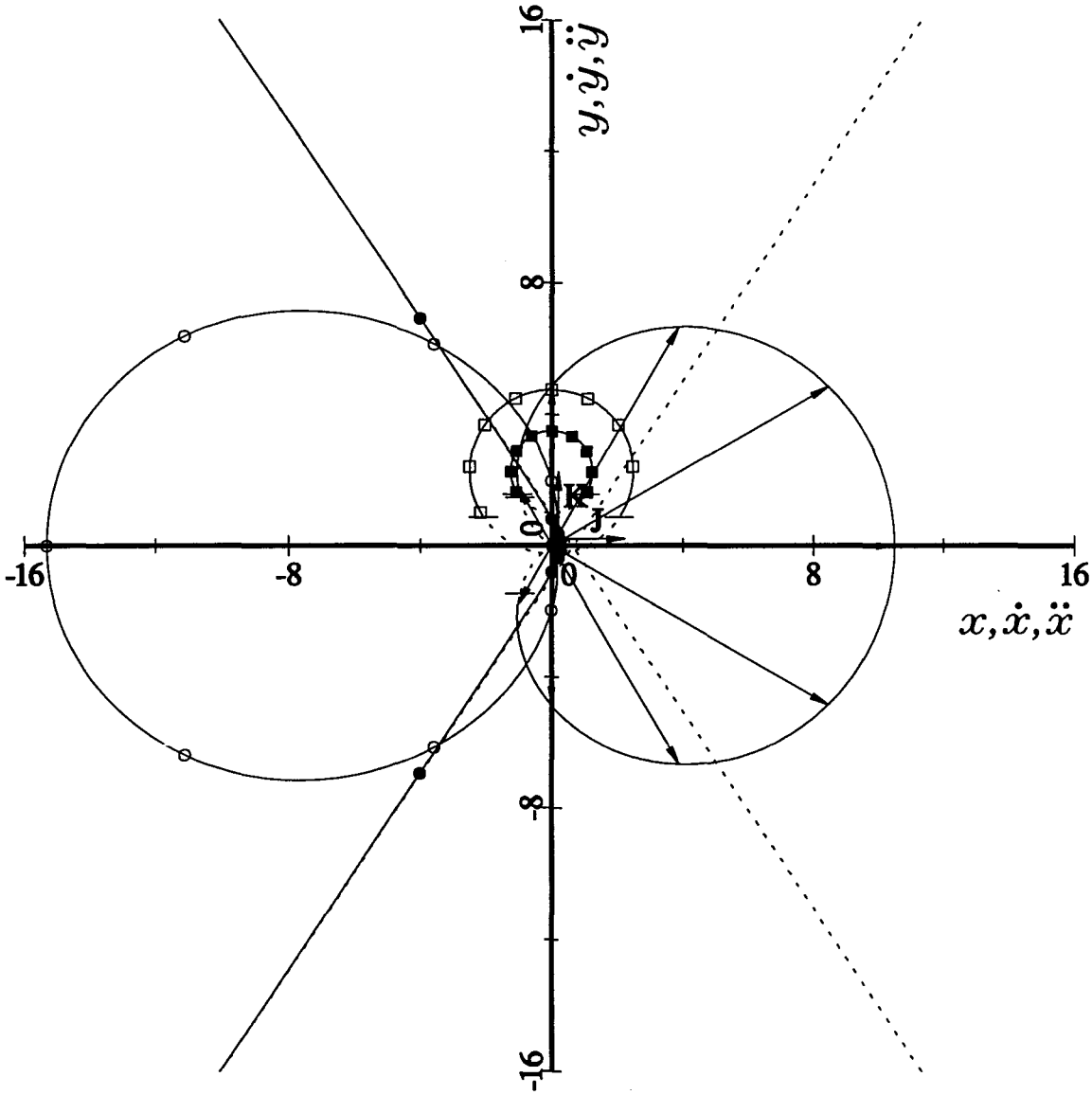


Figure 1.5.17. The hyperbolic Kepler orbit, the circular velocity hodograph, the acceleration hodograph, the circular path of the Lagrangian vector and the construction of the path of the magnitude of the scalar Lagrangian in the direction of $\hat{\boldsymbol{r}}$ with a selection of vectors drawn from the origin on the same set of axes. The circles (–●–●–●–) show the displacements of the particle at the angular increments $\theta = i\,\pi/6$, $i = 0, \ldots, 12$ and the squares (–■–■–■–) give the corresponding velocities. The unfilled circles (–o–o–o–) and the unfilled squares (–□–□–□–) show the corresponding points along the acceleration hodograph and the path of the Lagrangian vector respectively. The constants are chosen as for Figure 1.5.4.

$$\begin{aligned}
\mathcal{L}_{xe} &= \mathcal{L}\cos\theta = \frac{H}{J}\left(-\mu\cos\theta_0 \pm L(2H)^{\frac{1}{2}}\sin\theta_0\right) \\
&= \frac{\mu}{2a}\left(-\cos\theta_0 \pm (e^2-1)^{\frac{1}{2}}\sin\theta_0\right) \\
\mathcal{L}_{ye} &= \mathcal{L}\sin\theta = \frac{H}{J}\left(\pm L(2H)^{\frac{1}{2}}\cos\theta_0 - \mu\sin\theta_0\right) \\
&= \frac{\mu}{2a}\left(\pm(e^2-1)^{\frac{1}{2}}\cos\theta_0 - \sin\theta_0\right) \qquad (1.5.41)
\end{aligned}$$

using the solutions (1.5.13) to the equations of the asymptotes of the hyperbola as before. Note that $\mathcal{L} = H$ as $t \to \pm\infty$.

Figures 1.5.18–1.5.20 show the unscaled displacements and both the velocities and the path of the Lagrangian vector $\boldsymbol{N}$ scaled by the factor $(2\mathcal{L})^{\frac{1}{2}}$ at regular increments in θ for the Kepler problem. By using the same analysis as that used to describe Figures 1.5.12–1.5.14 it should be obvious that the phase difference in general between the displacement and the scaled velocity or Lagrangian vectors is not constant, however, the phase difference between the radial vector $\boldsymbol{r}$ and the vector directed from the head of the scaled Hamilton vector $\boldsymbol{K}/(2\mathcal{L})^{\frac{1}{2}}$ to either the head of the scaled velocity vector $\dot{\boldsymbol{r}}/(2\mathcal{L})^{\frac{1}{2}}$ or the head of the scaled Lagrangian vector $\boldsymbol{N}/(2\mathcal{L})^{\frac{1}{2}}$ *i.e.*, $\dot{\boldsymbol{r}}/(2\mathcal{L})^{\frac{1}{2}} - \boldsymbol{K}/(2\mathcal{L})^{\frac{1}{2}}$ or $\boldsymbol{N}/(2\mathcal{L})^{\frac{1}{2}} - \boldsymbol{K}/(2\mathcal{L})^{\frac{1}{2}}$ is a constant $\pi/2$ radians since both $\boldsymbol{r}\cdot(\dot{\boldsymbol{r}}/(2\mathcal{L})^{\frac{1}{2}} - \boldsymbol{K}/(2\mathcal{L})^{\frac{1}{2}}) = 0$ and $\boldsymbol{r}\cdot(\boldsymbol{N}/(2\mathcal{L})^{\frac{1}{2}} - \boldsymbol{K}/(2\mathcal{L})^{\frac{1}{2}}) = 0$ and it follows that $\dot{\boldsymbol{r}}/(2\mathcal{L})^{\frac{1}{2}} - \boldsymbol{K}/(2\mathcal{L})^{\frac{1}{2}}$ is collinear with $\boldsymbol{N}/(2\mathcal{L})^{\frac{1}{2}} - \boldsymbol{K}/(2\mathcal{L})^{\frac{1}{2}}$. In other words since both the vectors $\dot{\boldsymbol{r}}/(2\mathcal{L})^{\frac{1}{2}}$ and $\boldsymbol{N}/(2\mathcal{L})^{\frac{1}{2}}$ are scaled by equal amounts along both axes they are still collinear with $\dot{\boldsymbol{r}}$ and $\boldsymbol{N}$ respectively but reduced in length and consequently $\dot{\boldsymbol{r}}/(2\mathcal{L})^{\frac{1}{2}} - \boldsymbol{K}$ and $\boldsymbol{N}/(2\mathcal{L})^{\frac{1}{2}} - \boldsymbol{K}$ are not parallel to $\dot{\boldsymbol{r}} - \boldsymbol{K}$ and $\boldsymbol{N} - \boldsymbol{K}$ respectively unless $\boldsymbol{K}$ is also scaled by $(2\mathcal{L})^{\frac{1}{2}}$. In summary, the phase differences between $\boldsymbol{r}$ and both $\dot{\boldsymbol{r}}/(2\mathcal{L})^{\frac{1}{2}}$ and $\boldsymbol{N}/(2\mathcal{L})^{\frac{1}{2}}$ are not constant in the Kepler problem but the phase differences between $\boldsymbol{r}$ and both $\dot{\boldsymbol{r}}/(2\mathcal{L})^{\frac{1}{2}} - \boldsymbol{K}/(2\mathcal{L})^{\frac{1}{2}}$ and $\boldsymbol{N}/(2\mathcal{L})^{\frac{1}{2}} - \boldsymbol{K}/(2\mathcal{L})^{\frac{1}{2}}$ are constant at $\pi/2$ radians or, in other words, the radial vector directed from the origin which is also a focus of the ellipse in the plane moves in phase with both an offset scaled velocity vector and an offset scaled Lagrangian vector both of which are directed from the head of the scaled Hamilton vector $\boldsymbol{K}/(2\mathcal{L})^{\frac{1}{2}}$, *i.e.* the scaling changes with time. In the diagrams to follow, the magnitude of $\boldsymbol{K}/(2\mathcal{L})^{\frac{1}{2}}$ at a particular value of θ can be obtained graphically by finding the intersection of the line connecting the relevant solid square time marker on the scaled velocity hodograph with its corresponding arrowhead on the scaled Lagrangian vector with the $y, \dot{y}$–axis. Figure 1.5.18 shows the scaled velocity hodograph and also the construction of the path of the scaled

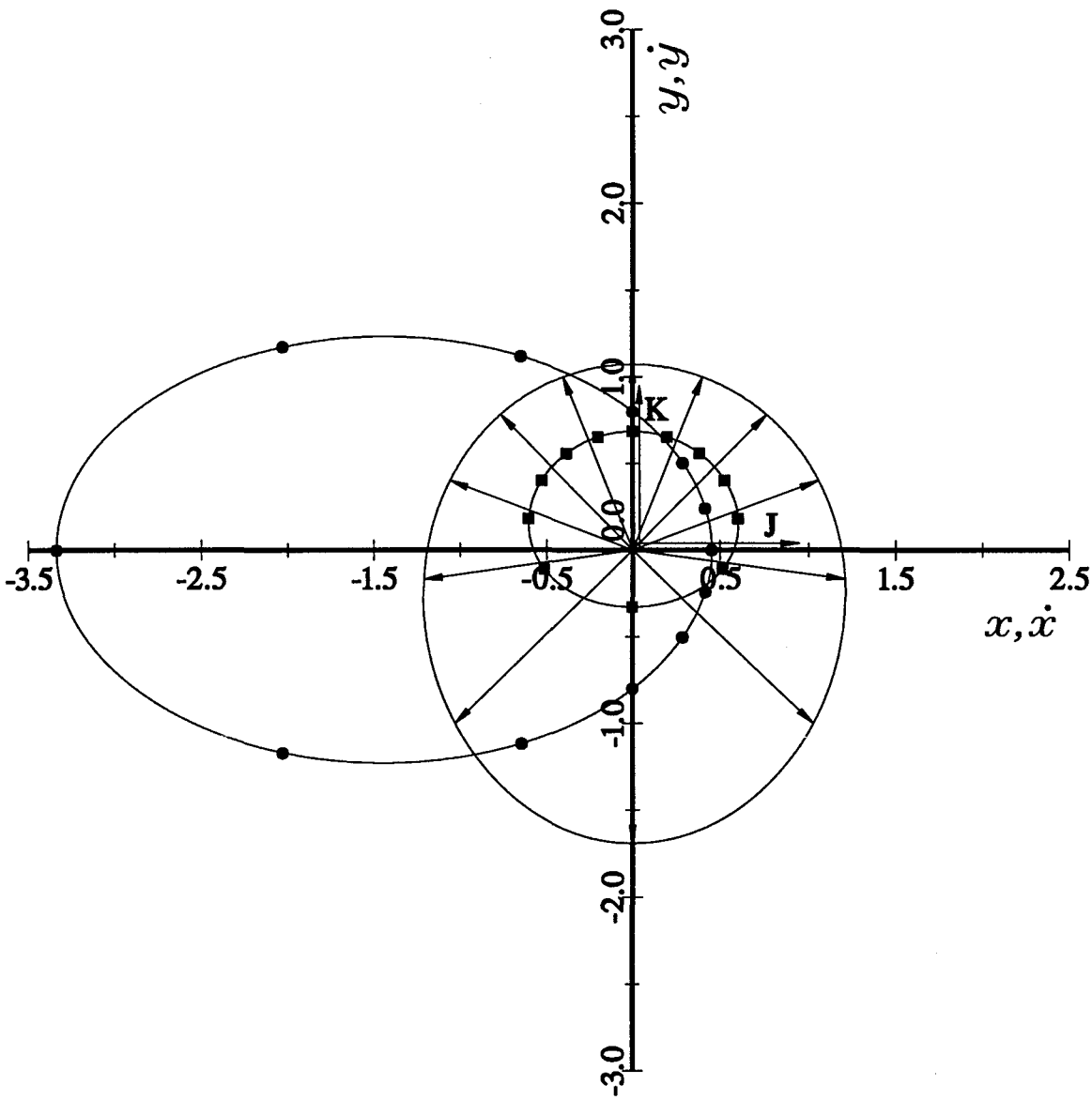


Figure 1.5.18. The elliptical Kepler orbit, the scaled velocity hodograph and the construction of the path of the scaled Lagrangian vector with a selection of vectors drawn from the origin on the same set of axes. The circles (–●–●–●–) show the displacements of the particle at the angular increments $\theta = i\ \pi/6$, $i = 0, \ldots, 12$ and the squares (–■–■–■–) give the corresponding velocities. The phase difference between the scaled velocity or Lagrangian vectors and the displacement vector is not constant although it is a constant $\pi/2$ radians between the displacement vector and the vector directed from the head of the scaled Hamilton vector to the head of the corresponding scaled velocity or Lagrangian vector. The constants are chosen as for Figure 1.5.1.

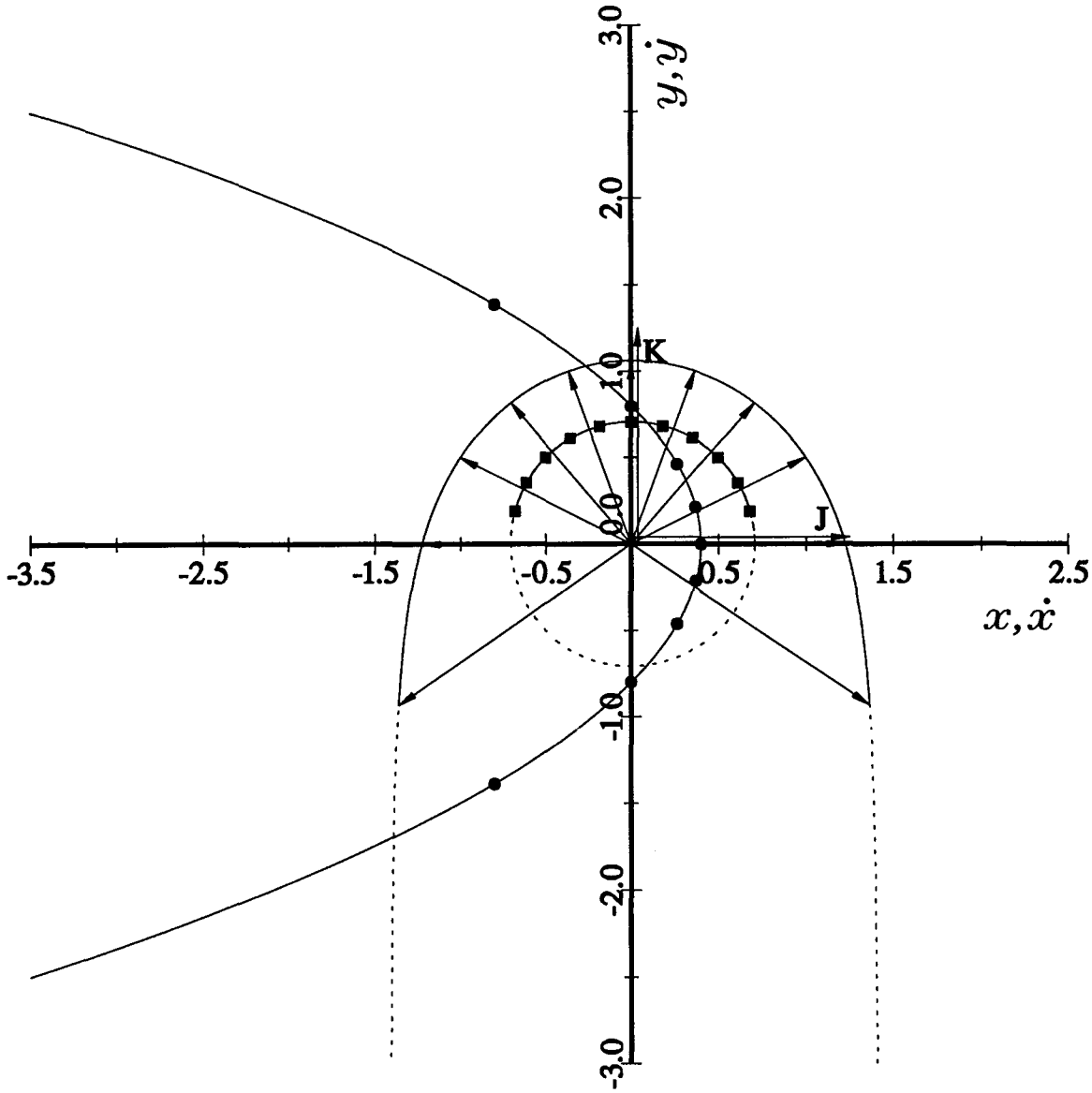


Figure 1.5.19. The parabolic Kepler orbit, the scaled velocity hodograph and the construction of the path of the scaled Lagrangian vector with a selection of vectors drawn from the origin on the same set of axes. The circles (–•–•–•–) show the displacements of the particle at the angular increments $\theta = i\,\pi/6$, $i = 0, \ldots, 12$ and the squares (–■–■–■–) give the corresponding velocities. The phase difference between the scaled velocity or Lagrangian vectors and the displacement vector is not constant although it is a constant $\pi/2$ radians between the displacement vector and the vector directed from the head of the scaled Hamilton vector to the head of the corresponding scaled velocity or Lagrangian vector. The constants are chosen as for Figure 1.5.3.

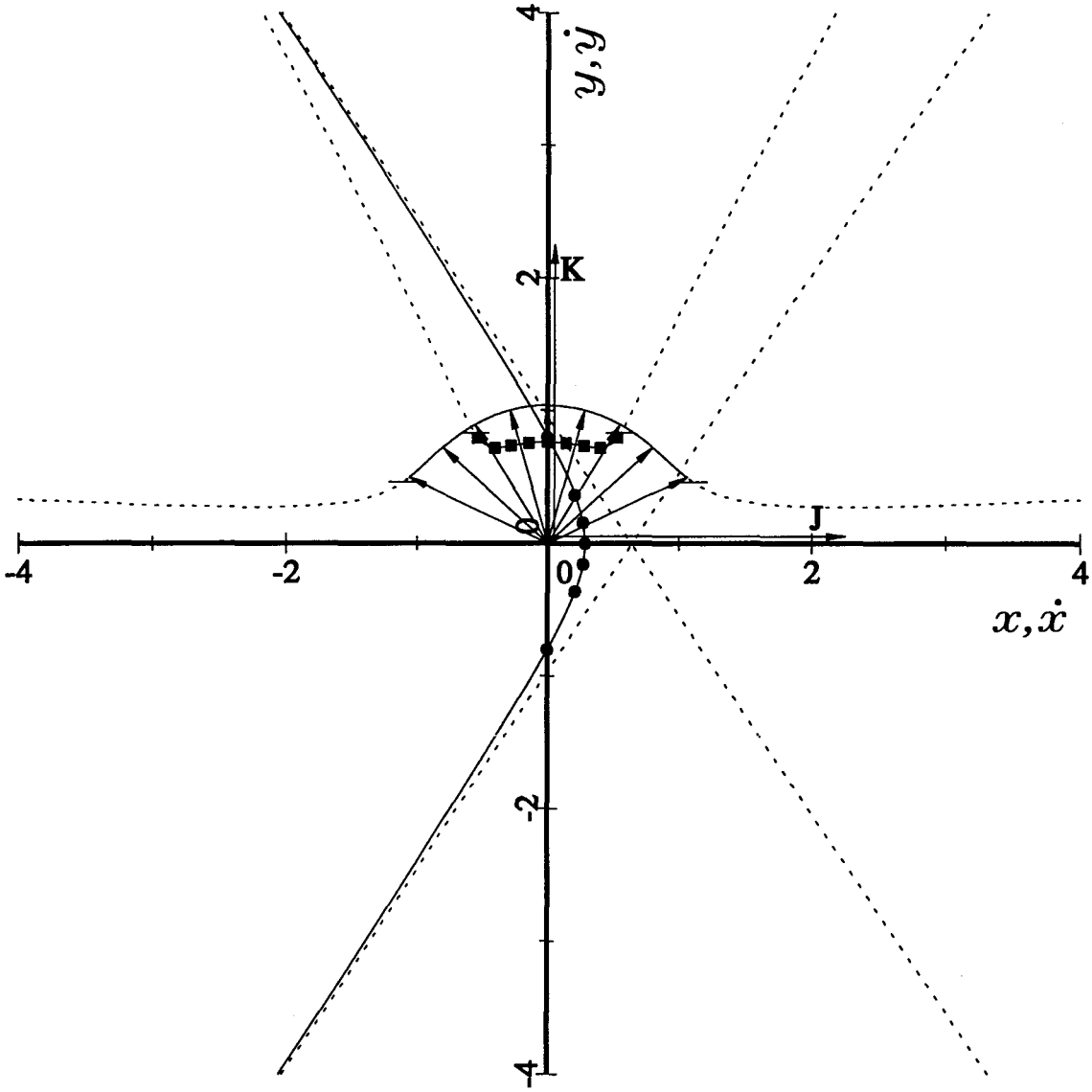


Figure 1.5.20. The hyperbolic Kepler orbit, the scaled velocity hodograph and the construction of the path of the scaled Lagrangian vector with a selection of vectors drawn from the origin on the same set of axes. The circles (-•-•-•-) show the displacements of the particle at the angular increments $\theta = i\,\pi/6$, $i = 0, \ldots, 12$ and the squares (-■-■-■-) give the corresponding velocities. The phase difference between the scaled velocity or Lagrangian vectors and the displacement vector is not constant although it is a constant $\pi/2$ radians between the displacement vector and the vector directed from the head of the scaled Hamilton vector to the head of the corresponding scaled velocity or Lagrangian vector. The constants are chosen as for Figure 1.5.4.

Lagrangian vector for the elliptical case. The path of the scaled Lagrangian vector appears to be elliptical, however, this is not the case. Both the scaled velocity hodograph and the scaled path of the Lagrangian vector are closed. Figure 1.5.19 shows the scaled velocity hodograph and also the construction of the path of the scaled Lagrangian vector for the parabolic case. In this case the scaled velocity hodograph can be shown to follow a semi–circle of radius $2^{-1/2}$ with centre at the origin. Neither the scaled velocity hodograph nor the path of the scaled Lagrangian vector closes as t ranges from negative through positive infinity or equivalently when $\theta - \theta_0$ ranges from $-\pi$ through π radians. Figure 1.5.20 shows the scaled velocity hodograph and also the construction of the path of the scaled Lagrangian vector for the hyperbolic case. Neither the scaled velocity hodograph nor the path of the scaled Lagrangian vector closes but are bounded by the asymptotes. The two short line segments intersecting both the scaled velocity hodograph and the path of the scaled Lagrangian vector indicate the limits of extent of the path as t ranges from negative through positive infinity or equivalently when $\theta - \theta_0$ ranges from $\arccos(1/e) - \pi$ through $\pi - \arccos(1/e)$ radians and are calculated as follows. The parametric equations for the scaled velocity hodograph can be shown to have the form

$$\begin{aligned}
\frac{\dot{x}}{(2\mathcal{L})^{\frac{1}{2}}} &= -\frac{\mu \sin\theta + J \sin\theta_0}{(J^2 + 4\mu J \cos(\theta - \theta_0) + 3\mu^2)^{\frac{1}{2}}} = -\frac{\sin\theta + e\sin\theta_0}{(e^2 + 4e\cos(\theta - \theta_0) + 3)^{\frac{1}{2}}} \\
\frac{\dot{y}}{(2\mathcal{L})^{\frac{1}{2}}} &= \frac{\mu \cos\theta + J \cos\theta_0}{(J^2 + 4\mu J \cos(\theta - \theta_0) + 3\mu^2)^{\frac{1}{2}}} = \frac{\cos\theta + e\cos\theta_0}{(e^2 + 4e\cos(\theta - \theta_0) + 3)^{\frac{1}{2}}}
\end{aligned} \tag{1.5.42}$$

using the orbit equation (1.5.10) to substitute for r and $\dot{r}$ in terms of θ and in the hyperbolic case the limits of extent are given by

$$\begin{aligned}
\frac{\dot{x}_e}{(2\mathcal{L})^{\frac{1}{2}}} &= \frac{1}{JL}\left(\mp\mu L\cos\theta_0 - L^2(2H)^{\frac{1}{2}}\sin\theta_0\right) \\
&= \frac{1}{e(e^2-1)^{\frac{1}{2}}}\left(\mp(e^2-1)^{\frac{1}{2}}\cos\theta_0 - (e^2-1)\sin\theta_0\right) \\
\frac{\dot{y}_e}{(2\mathcal{L})^{\frac{1}{2}}} &= \frac{1}{JL}\left(L^2(2H)^{\frac{1}{2}}\cos\theta_0 \pm \mu L\sin\theta_0\right) \\
&= \frac{1}{e(e^2-1)^{\frac{1}{2}}}\left((e^2-1)\cos\theta_0 \pm (e^2-1)^{\frac{1}{2}}\sin\theta_0\right),
\end{aligned} \tag{1.5.43}$$

making the substitution $\cos(\theta - \theta_0) = -1/e$ in (1.5.42). Similarly, the two short line segments intersecting the path of the Lagrangian vector scaled by $(2\mathcal{L})^{\frac{1}{2}}$ indicate the limits of extent of the path as t ranges from negative through positive infinity or equivalently when $\theta - \theta_0$ ranges from $\arccos(1/e) - \pi$ through $\pi - \arccos(1/e)$ radians and are given by

$$\begin{aligned}
\frac{N_{xe}}{(2\mathcal{L})^{\frac{1}{2}}} &= \frac{1}{JL(2H)^{\frac{1}{2}}}\left(\mp 2\mu L(2H)^{\frac{1}{2}}\cos\theta_0 - (2L^2H - \mu^2)\sin\theta_0\right) \\
&= \frac{1}{e(e^2-1)^{\frac{1}{2}}}\left(\mp 2(e^2-1)^{\frac{1}{2}}\cos\theta_0 - (e^2-2)\sin\theta_0\right) \\
\frac{N_{ye}}{(2\mathcal{L})^{\frac{1}{2}}} &= \frac{1}{JL(2H)^{\frac{1}{2}}}\left((2L^2H - \mu^2)\cos\theta_0 \pm 2\mu L(2H)^{\frac{1}{2}}\sin\theta_0\right) \\
&= \frac{1}{e(e^2-1)^{\frac{1}{2}}}\left((e^2-2)\cos\theta_0 \pm 2(e^2-1)^{\frac{1}{2}}\sin\theta_0\right) \qquad (1.5.44)
\end{aligned}$$

by scaling (1.5.37) by $\mu^{\frac{1}{2}}/a^{\frac{1}{2}} = (2H)^{\frac{1}{2}}$. The angle θ can be eliminated from the parametric equations scaled by $(2\mathcal{L})^{\frac{1}{2}}$ (1.5.44). However, the resulting expression involving the components of $\boldsymbol{N}$ does not have an easily recognisable structure.

Returning to equation (1.5.18) and using Gradshteyn and Rhyzhik [43, 2.264.2 and 2.261.3] (hereafter referred to as G&R) we obtain

$$t - t_0 = \frac{(2Er^2 + 2\mu r - L^2)^{\frac{1}{2}}}{2E} + \frac{\mu}{2E(-2E)^{\frac{1}{2}}}\arcsin\left(\frac{2Er + \mu}{(2EL^2 + \mu^2)^{\frac{1}{2}}}\right)\Bigg|_{r_0}^{r}, \qquad (1.5.45)$$

where $2E = (J^2 - \mu^2)/L^2$. If we consider the time taken for the orbit to progress from $\theta = \theta_0 = 0$ to $\theta = \pi$, *i.e.*, $r_0 = L^2/(\mu + J)$ to $r = r_1 = L^2/(\mu - J)$ using (1.5.10), we then obtain

$$\frac{T}{2} = \frac{\mu\pi}{-2E(-2E)^{\frac{1}{2}}}, \qquad (1.5.46)$$

where T is the period of the orbit. Equation (1.5.46) can be written in terms of the semi–major axis length

$$\begin{aligned}
2a &= r_1 + r_0 = -\frac{\mu}{E} \\
\Longrightarrow \qquad a &= \frac{\mu}{-2E}. \qquad (1.5.47)
\end{aligned}$$

Thus the period of revolution is given by

$$T = 2\pi\left(\frac{a^3}{\mu}\right)^{\frac{1}{2}}. \qquad (1.5.48)$$

Figure 1.5.21 shows a family of focus–centred Keplerian ellipses with differing semi–major axis lengths and eccentricities. Figure 1.5.22 shows the relationship between the periodic time of the orbit and the semi–major axis lengths for the family of ellipses shown in Figure 1.5.21. Notice that the period is independent of the eccentricity as suggested by Kepler's third law. In §2.15 other families of ellipses will be considered where the period of revolution depends on both the eccentricity and the length of the semi–major axis.

The dependence of t on θ can be found using the expression for the angular momentum, *i.e.*,

$$\dot{\theta} = \frac{L}{r^2} = \frac{1}{L^3}\big(\mu + J\cos(\theta - \theta_0)\big)^2 \tag{1.5.49}$$

using the expression (1.5.10) to substitute for r in terms of θ. Equation (1.5.49) can be integrated using G&R [43, 2.554.3 and 2.553.3 (case $a^2 > b^2$)] to yield

$$t - t_0 = \frac{L}{2E}\left(\frac{J\sin(\theta - \theta_0)}{\mu + J\cos(\theta - \theta_0)} - \frac{2\mu}{L(-2E)^{\frac{1}{2}}}\arctan\frac{L(-2E)^{\frac{1}{2}}\tan\frac{1}{2}(\theta - \theta_0)}{\mu + J}\right). \tag{1.5.50}$$

Equation (1.5.50) like (1.5.45) poses serious problems for inversion. The advent of cheap fast computers has eliminated this problem to a certain extent since a numerical inversion will, for all practical purposes, be sufficient.

The mathematical basis for Kepler's three laws of motion has now been established. The three laws are :–

(i) Planets move in ellipses around the sun which is at one of the foci. This is obvious from equation (1.5.10).

(ii) Equal areas are swept out by the radius vector in equal times. This is a consequence of equation (1.3.10) since L is constant.

(iii) The cube of the length of the semi–major axis is proportional to the square of the period of a revolution. This is described by equation (1.5.48).

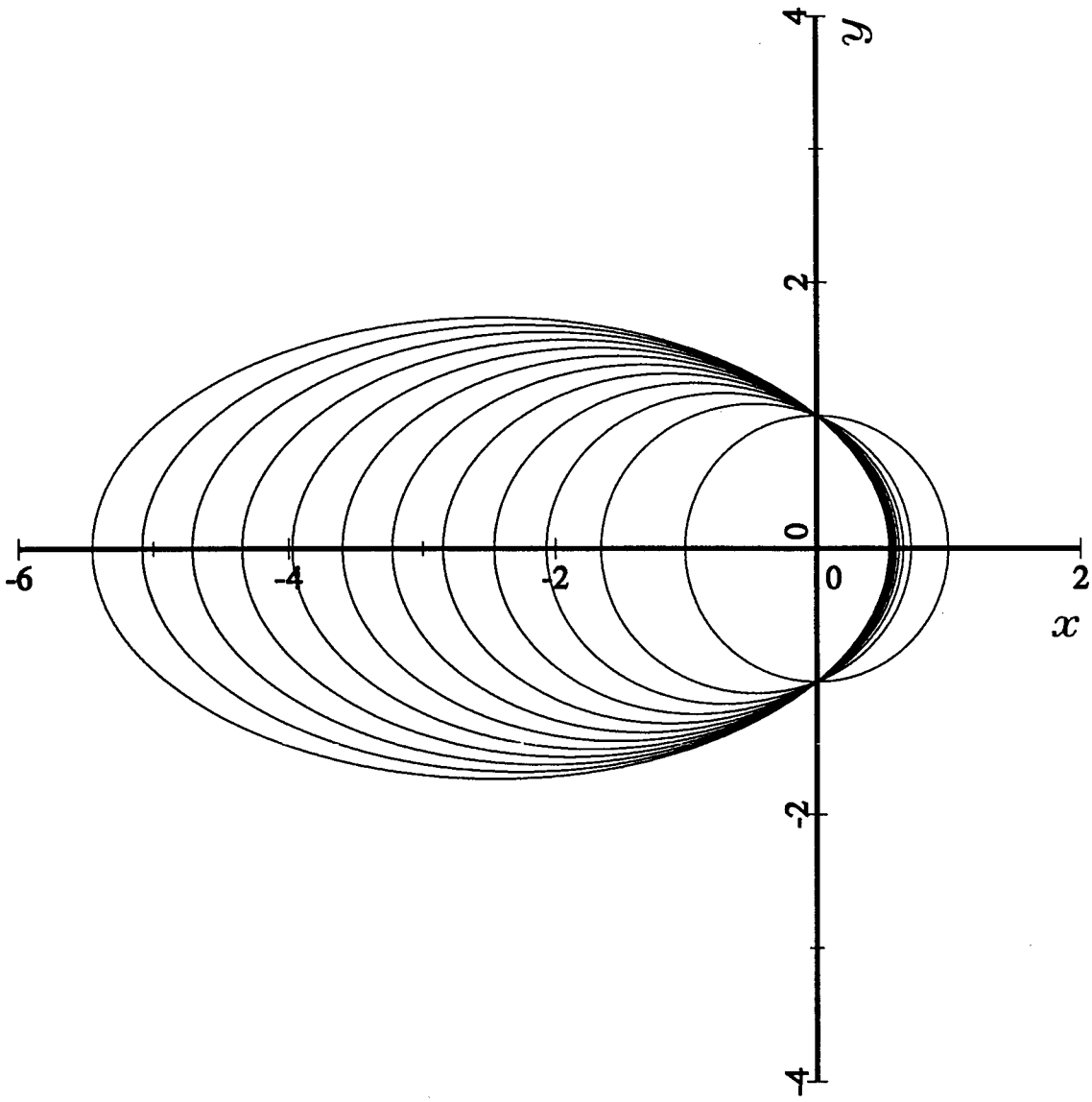


Figure 1.5.21. A family of Keplerian orbital ellipses with differing semi-major axis lengths and eccentricities. The constants have the values $\mu = 1$, $\theta_0 = 0$, $a = 2i/11+1$, $i = 0, \ldots, 11$, $e = \left((\mu a - L^2)/(\mu a)\right)^{1/2}$, $K = J = \mu e$ and $L = 1$.

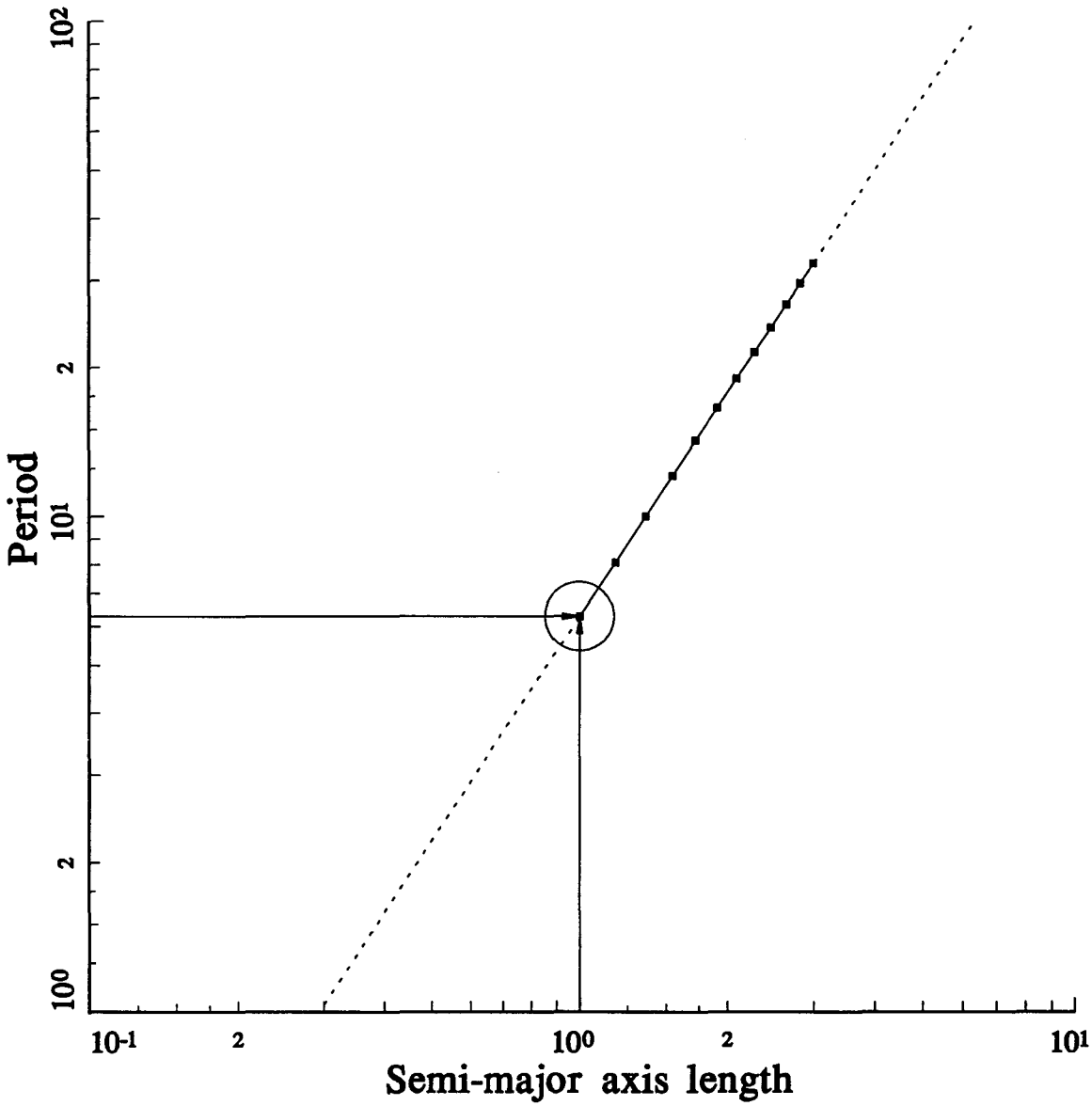


Figure 1.5.22. The periodic time versus the semi-major axis length for the family of Keplerian orbital ellipses shown in Figure 1.5.21. The slope of the curve is 3/2 and the $y-$intercept is 2π, *i.e.* the period is given by $2\pi a^{3/2}$. The period is independent of the eccentricity.

It should be noted that in his description of Kepler's three laws of motion, Maxwell [93, §128ff p105ff] renumbers the first two laws mentioned above, *i.e.* he refers to the equal areas in equal times law as Kepler's first law whilst the elliptical motion about the sun which is at one focus is termed Kepler's second law. In fact Kepler obtained his three empirical laws in this chronological order and Newton's geometrical treatment also followed this natural order [19, p163]. It is therefore puzzling as to why the modern convention does not follow the natural order of calculation.

One additional result worth mentioning is that of the derivation of Kepler's equation which is of historical interest. By comparing the orbit equation (1.5.10) with the standard equation for a conic section in polar coordinates

$$r = \frac{1}{c\left(1 + e\cos(\theta - \theta_0)\right)} \tag{1.5.51}$$

where c and e, the eccentricity, are constants, it is clear that e in (1.5.51) is given in terms of (1.5.10) as

$$e = \frac{J}{\mu}. \tag{1.5.52}$$

Use of (1.5.52), (1.5.47) and (1.5.20) allows us to find an expression for L^2,

$$L^2 = \mu a(1 - e^2). \tag{1.5.53}$$

Equation (1.5.18) becomes, using (1.5.47) and (1.5.53),

$$\mathrm{d}t = \frac{r\,\mathrm{d}r}{\left(-\mu r^2/a + 2\mu r - \mu a(1 - e^2)\right)^{\frac{1}{2}}}. \tag{1.5.54}$$

Equation (1.5.54) can be further simplified by making the substitution

$$r = a(1 - e\cos\psi), \tag{1.5.55}$$

where ψ is known as the eccentric anomaly as distinct from θ which was known as the true anomaly in mediæval astronomy (see Goldstein [33, p99]). Equation (1.5.54) becomes

$$\mathrm{d}t = \left(\frac{a^3}{\mu}\right)^{\frac{1}{2}}(1 - e\cos\psi)\,\mathrm{d}\psi \tag{1.5.56}$$

which can be integrated to yield

$$t = \left(\frac{a^3}{\mu}\right)^{\frac{1}{2}}(\psi - e\sin\psi), \tag{1.5.57}$$

where the lower bound of integration in assumed to be zero in both cases. Integration of (1.5.57) between 0 and 2π is an alternative route to Kepler's third law. Using the expression for the period of revolution (1.5.48) we obtain Kepler's equation

$$\omega t = \frac{2\pi}{\tau} t = \psi - e\sin\psi. \tag{1.5.58}$$

The quantity ωt varies through the range 0 to 2π as do ψ and θ and is known as the mean anomaly. Equation (1.5.58) is useful in the procedure for calculating r and θ for a particular time. It is solved to give ψ for a particular value of t. Equation (1.5.55) gives the corresponding value of r. The polar angle θ is obtained by rewriting (1.5.10) as

$$r = \frac{L^2}{\mu\big(1 + J/\mu\,\cos(\theta - \theta_0)\big)} \tag{1.5.59}$$

using (1.5.53) to substitute for L^2 and (1.5.52) to replace the coefficient of the cosine term in (1.5.59). Equating (1.5.59) with (1.5.55) gives

$$1 + e\cos(\theta - \theta_0) = \frac{1 - e^2}{1 - e\cos\psi}, \tag{1.5.60}$$

which simplifies to

$$\cos(\theta - \theta_0) = \frac{\cos\psi - e}{1 - e\cos\psi}. \tag{1.5.61}$$

Equation (1.5.61) reduces to the useful form

$$\tan\left(\frac{\theta - \theta_0}{2}\right) = \left(\frac{1 - \cos(\theta - \theta_0)}{1 + \cos(\theta - \theta_0)}\right)^{\frac{1}{2}} = \left(\frac{1 + e}{1 - e}\right)^{\frac{1}{2}} \tan\frac{\psi}{2}. \tag{1.5.62}$$

Using either (1.5.61) or (1.5.62), θ can be obtained once ψ has been calculated from t using (1.5.58). In pre–computer times, the solution of (1.5.58) attracted much attention for accurate astronomical calculations (see the exercises of Chapter 3 of Goldstein [33] for a sample of the more than one hundred methods developed).

1.6 The Conserved Hamilton and Laplace–Runge–Lenz Vector Analogues and a Conserved Tensor for Central Force Problems using Fradkin's Method

The central force problem was the cornerstone of Newton's *Principia* [102]. In fact most of the *Principia* is devoted to the geometry connected with central force and other related problems. Newton studied the linear, inverse square and inverse cube central force problems amongst others, all of which have rather interesting geometrical properties. He proved that any motion in a central force occurred in a plane and that equal areas were swept out by the radius vector in equal times (Kepler's second law) [102, prop I–II p40ff]. He also showed that for any central force problem with periodic time proportional to r^n that the centripetal force would be proportional to r^{1-2n} [102, prop IV cor VII p46]. Later he demonstrated that if a particle moves in an elliptical orbit under the influence of a centripetal force directed towards the geometric centre of the ellipse then that force must be proportional to the radius and also that concentric geometric–centred elliptical orbits for the three–dimensional isotropic harmonic oscillator were isochronic [102, prop XLVII p149ff].

It has been shown that the only central force orbits which result in closed orbits for all bounded motions (for arbitrary choices of E and L) are the Kepler problem and the three–dimensional isotropic harmonic oscillator. This result was first proved by J. Bertrand [7] and is often termed Bertrand's Theorem. Also see Goldstein [33, p93] for a proof. It can also be shown that, provided the central force is attractive, it is possible to find initial conditions that depend on E and L which give rise to circular orbits. If the force law is of the form

$$f(r) = -\frac{k}{r^{3-\beta^2}} \tag{1.6.1}$$

and β is a non–zero rational number, the closed orbits can be shown to be stable for a set of initial conditions that differ only slightly from those defining a circle. However, it is only in the case of the Kepler problem ($E < 0$) and the three–dimensional isotropic harmonic oscillator where all orbits are closed and stable.

The three–dimensional isotropic harmonic oscillator appears less prominently than the Kepler problem in most textbooks despite its exposure in Newton's *Principia.* After this auspicious introduction, very little progress appears to have been made with regard to the construction of conserved vector and tensor quantities. Between 1700 and 1900 the only progress of note was the mathematical formulation of the equation of motion and the solution in terms of the parametric equations which appeared in most of the well–known late nineteenth and early twentieth century textbooks. In Tait's 1867 *An Elementary Treatise on Quaternions* [124, §363 p284ff] the three–dimensional isotropic harmonic oscillator and linear repulsor problems are solved component–wise to obtain the parametric equations for the orbit which are then differentiated to obtain the components of the velocity hodograph. However, there is no indication that any conserved quantities apart from the angular momentum and the energy were known at this stage. He also looks briefly at the inverse cube force [124, §364 p285ff]. In Kelvin and Tait's *Elements of Natural Philosophy* of 1872 [63, §80ff p26] and also *Treatise on Natural Philosophy* of 1879 [64, §65 p48] they do mention the fact that equal areas are swept out by the radius vector in equal times and also that concentric orbits are isochronic. Maxwell considered both the inverse square law force [93, §127ff p105ff] and also simple harmonic motion [93, §116ff p94ff] in *Matter and Motion* of 1877 but not the three–dimensional isotropic harmonic oscillator as such. In [93, §118 p95] he discussed isochronicity with regard to simple harmonic motion. Routh [113, §332ff p216ff] discussed the central force problem in *A Treatise on Dynamics of a Particle* of 1898 in quite some detail and looked at the inverse square, cube, fourth and fifth powers in particular as well as the three–dimensional isotropic harmonic oscillator [113, §119ff p61ff].

Whittaker [129, §47ff p77ff] described exact solutions for a variety of central force problems in his textbook *A Treatise on the Analytical Dynamics of Particles and Rigid Bodies* of 1904. For the power law central force r^n, with $n = -7, -5, -4, -3, -\frac{5}{2}, -\frac{7}{3}, -2, -\frac{5}{3}, -\frac{3}{2}, -\frac{1}{3}, 0,\ 1,\ 3$ and 5, the orbit is obtainable in terms of either circular or elliptic functions. There are further results pertaining to various geometric constructions of significance. Much of this work dates back to Newton and Lagrange. Broucke [13] has extended the results of Whittaker to include six more central force laws which are a combination of up to four independent powers of r, which can be solved in terms of elliptic functions. He also considers stability of the circular solutions by considering the characteristic exponents of the variational equations of the canonical equations of motion. A detailed investigation of the inverse cube force is also made and a connection with both the three–dimensional isotropic harmonic oscillator and the eccentric anomaly of the Kepler problem is established. A stability

analysis of singular solutions for the central force problem is shown to generalise to stable elliptic solutions in the two–fixed centres problem. In his textbook *Mechanics*, Symon [122, §3–10 p106ff] discusses the three–dimensional isotropic harmonic oscillator and solves component–wise to obtain the parametric equations. He also touches on the concept of isochronicity.

The three–dimensional isotropic harmonic oscillator has been studied by Jauch and Hill [57] in a quantum mechanical context. In addition to the energy and the angular momentum they discovered the six conserved components of the Jauch–Hill–Fradkin tensor for the two–dimensional isotropic harmonic oscillator and generalised these results to the n–dimensional isotropic harmonic oscillator. Fradkin [28] extended the results by showing that the symmetric tensor found by Jauch and Hill could be used to specify the orientation of the elliptical orbit in a similar fashion to that of the Laplace–Runge–Lenz vector for the classical Kepler problem. Fradkin [29] also developed a general technique for constructing Laplace–Runge–Lenz vectors and Jauch–Hill–Fradkin tensor analogues for any central force problem. His approach is described in more detail below. Bacry *et al.* [4] have made a study of the group theoretic aspects of general central force problems. They described the differences between the local Lie algebras of $so(4)$ and $su(3)$ which are incidentally symmetry algebras for any problem with three degrees of freedom, *i.e.*, not necessarily a central force problem (which Fradkin uses to construct his conserved quantities) and the global dynamic symmetries of $SO(4)$ and $SU(3)$ which are specific to only two central forces, the Kepler problem ($E < 0$) and the three–dimensional isotropic harmonic oscillator respectively. This aspect was not made clear by Fradkin or Leach and Gorringe [79] and further explanation is given in the comment on [79] by Bacry [3]. Greenberg [45] studied the rôle of accidental degeneracy and the existence of conserved vectors in the context of Newtonian, relativistic and quantum mechanics.

Buch and Denman [15] studied the implications of the piecewise–conserved Laplace–Runge–Lenz vector for the three–dimensional isotropic harmonic oscillator, as obtained by Fradkin [29]. They concluded that the symmetry of the orbit favoured a piecewise–conserved vector and attempted to remedy the situation through the addition of a sign. In a separate paper [16] they constructed a Laplace–Runge–Lenz analogue for the forced damped three–dimensional isotropic harmonic oscillator, through the use of a finite canonical transformation to the time–independent three–dimensional isotropic harmonic oscillator. Peres [106] independently generalised the Laplace–Runge–Lenz vector for any central force and obtained a set of differential equations to describe the solutions of the unknown functions in the gen-

eralised Laplace–Runge–Lenz analogue. He also realised that in general the vector he had constructed was not conserved at the turning points of the motion. Yoshida [132] managed to show equivalence between the techniques of Peres [106] and Fradkin [29]. In a separate paper [131] he replicated the results of Fradkin for the Laplace–Runge–Lenz vector of the Kepler problem and the three–dimensional isotropic harmonic oscillator and obtained a more elegant representation for the latter problem using a canonical treatment. Yan [130] proposed a similar technique for central force problems to that of Peres [106] and also obtained a set of differential equations to describe the unknown functions that he introduced in the ansatz for the structure of the Laplace–Runge–Lenz analogue. Sivardière [120] used the Jauch–Hill–Fradkin tensor to obtain both the Hamilton and Laplace–Runge–Lenz analogues for the three–dimensional isotropic harmonic oscillator and also obtained a neater representation than Fradkin. In a separate paper [119] he considered the rate of precession of various perturbations of the Kepler and three–dimensional isotropic harmonic oscillator problems using the Laplace–Runge–Lenz vector. Chen [17] used a Kustaanheimo–Stiefel transformation of coordinates and velocities to transform the Kepler–Coulomb problem into a pair of coupled two–dimensional harmonic oscillators with both oscillators having the same angular momentum. The Laplace–Runge–Lenz vector appeared as a natural constraint condition of the transformation. Martínez–y–Romero *et al.* [91] considered the implications of the existence of closed and bounded plane orbits and the existence of hidden symmetries. Holas and March [54] considered the generalised Laplace–Runge–Lenz vector construction of Fradkin and attempted to resolve the problems associated with the Laplace–Runge–Lenz vector being only piecewise conserved or, alternatively, a multivalued constant of the motion. In the case of a closed orbit with n pairs of turning points they proposed an $n-$arm star of n different perihelion vectors as a true invariant of the motion, which can also be related to an $n-$rank tensor expression.

Although all central force orbits do belong to the class of problems discussed in §§1.1–1.5, it is worthwhile to study the technique of Fradkin [29] as it demonstrates a different approach to finding Laplace–Runge–Lenz vectors and Jauch–Hill–Fradkin tensor analogues for all central force problems using Poisson brackets. It does suffer from the complication, however, that the orbit equation must be solved as well as inverted during the process. In practice the orbit equation may not be solvable in a useful form and, as has been seen before, global inversion is fraught with problems. The technique does show, however, how to construct conserved vectors starting from an expression in terms of Cartesian basis vectors and then expressing them in the more useful form of the dynamic system variables.

Since all central force problems are two dimensional, we need only consider our Laplace–Runge–Lenz analogue to lie in the plane of the orbit. This is consistent with the treatment of §1.1. If we assume that the angle between the unit Laplace–Runge–Lenz vector and the unit vector $\boldsymbol{i}$ is given by θ_0 then

$$\hat{\boldsymbol{J}} = \cos\theta_0\, \boldsymbol{i} + \sin\theta_0\, \boldsymbol{j} = \cos(\theta - \theta_0)\, \hat{\boldsymbol{r}} - \sin(\theta - \theta_0)\, \hat{\boldsymbol{\theta}} \tag{1.6.2}$$

in terms of the polar coordinate unit vectors. Provided the sine and cosine terms can be expressed in terms of the variables of the dynamic system the unit vector $\hat{\boldsymbol{J}}$ can be constructed.

The Newtonian equation of motion for a general central force is given by

$$\ddot{\boldsymbol{r}} = \left(\ddot{r} - \frac{L^2}{r^3}\right) \hat{\boldsymbol{r}} = g(r)\hat{\boldsymbol{r}}. \tag{1.6.3}$$

Taking the scalar product of (1.6.3) with $\dot{\boldsymbol{r}}$ and integrating with respect to time give

$$E = \frac{1}{2}\left(\dot{r}^2 + \frac{L^2}{r^2}\right) + V(r), \tag{1.6.4}$$

where E is the energy or Hamiltonian of the system and $V(r)$ is the potential energy $V = -\int g(r)\, \mathrm{d}r$.

Equation (1.6.4) can be rewritten as

$$t - t_0 = \int_{r_0}^{r} \frac{\mathrm{d}r}{\left(2(E - V - \frac{1}{2}L^2/r^2)\right)^{\frac{1}{2}}}. \tag{1.6.5}$$

The expression for the angular momentum

$$L\, \mathrm{d}t = r^2\, \mathrm{d}\theta \tag{1.6.6}$$

allows us to write

$$\theta - \theta_0 = \int_{r_0}^{r} \frac{\mathrm{d}r}{r^2\left(2(E - V)/L^2 - 1/r^2\right)^{\frac{1}{2}}}. \tag{1.6.7}$$

Changing the variable to $u = 1/r$ gives

$$\theta - \theta_0 = \int_{u_0}^{u} \frac{-\mathrm{d}u}{\left(2(E - V)/L^2 - u^2\right)^{\frac{1}{2}}}. \tag{1.6.8}$$

Provided (1.6.8) can be integrated to give expressions for $\cos(\theta - \theta_0)$ and $\sin(\theta - \theta_0)$ we will have constructed a suitable $\hat{\boldsymbol{J}}$. Assuming that we may write

$$\cos(\theta - \theta_0) = f(u, L^2, E), \tag{1.6.9}$$

differentiation of both sides of (1.6.9) with respect to t gives

$$-\sin(\theta-\theta_0)\dot{\theta} = \frac{\partial f}{\partial u}\dot{u} = \frac{\partial f}{\partial u}\frac{\mathrm{d}u}{\mathrm{d}r}\dot{r} \tag{1.6.10}$$

$$\Longrightarrow \quad \sin(\theta-\theta_0) = \frac{\dot{r}}{L}\frac{\partial f}{\partial u}. \tag{1.6.11}$$

The motivation for obtaining $\sin(\theta-\theta_0)$ in this way is that it simplifies the final expression for $\hat{\boldsymbol{J}}$ as will soon become apparent. Thus

$$\hat{\boldsymbol{J}} = f\hat{\boldsymbol{r}} - \frac{\dot{r}}{L}\frac{\partial f}{\partial u}\hat{\boldsymbol{\theta}}. \tag{1.6.12}$$

Equation (1.6.12) is the Laplace–Runge–Lenz vector although somewhat disguised. The scalar product of (1.6.12) with $\boldsymbol{r}$ returns (1.6.9) which is of course the orbit equation. To make the structure of (1.6.12) more apparent it is worthwhile to manipulate it into the Kepler–like structure

$$\hat{\boldsymbol{J}} = A\hat{\boldsymbol{r}} + B\,\dot{\boldsymbol{r}}\times\boldsymbol{L} = (A+BLr\dot{\theta})\hat{\boldsymbol{r}} - BL\dot{r}\hat{\boldsymbol{\theta}}, \tag{1.6.13}$$

where A and B are unrestricted functions at this point. Comparison of (1.6.12) with (1.6.13) gives

$$\hat{\boldsymbol{J}} = \left(f - u\frac{\partial f}{\partial u}\right)\hat{\boldsymbol{r}} + \frac{1}{L^2}\frac{\partial f}{\partial u}\dot{\boldsymbol{r}}\times\boldsymbol{L}. \tag{1.6.14}$$

Equation (1.6.14) describes the unit Laplace–Runge–Lenz vector for any central force problem. Fradkin then supposes that a planar orbit requires that the Lie algebra arising from the Poisson bracket relations between the components of $\boldsymbol{L}$ and $\boldsymbol{J}$ must be isomorphic to $so(4)$, *i.e.*

$$\begin{aligned}
&[L_i, L_j] = \varepsilon_{ijk}L_k \\
&[J_i, L_j] = \varepsilon_{ijk}J_k \\
&[J_i, J_j] = \varepsilon_{ijk}L_k \\
&[L_i, H] = 0 \\
&[J_i, H] = 0
\end{aligned} \tag{1.6.15}$$

and further that the Lie algebra arising from the Poisson bracket relations between the components of $\boldsymbol{L}$ and a conserved tensor A_{ij} should be isomorphic to $su(3)$, *i.e.*

$$\begin{aligned}
&[L_i, L_j] = \varepsilon_{ijk}L_k \\
&[L_i, A_{jk}] = \varepsilon_{ijn}A_{nk} + \varepsilon_{ikn}A_{jn} \\
&[A_{ij}, A_{kl}] = \left(\varepsilon_{ikn}\delta_{jl} + \varepsilon_{jln}\delta_{ik} + \varepsilon_{iln}\delta_{jk} + \varepsilon_{jkn}\delta_{il}\right)L_n \\
&[L_i, H] = 0 \\
&[A_{ij}, H] = 0.
\end{aligned} \tag{1.6.16}$$

He then constructs conserved vectors and tensors for any central force problem by using these algebras to force constraints on unknown functions which are introduced into the conserved vectors and tensors. The conserved vectors and tensors are assumed to have the form

$$\begin{aligned} \boldsymbol{J} &= J\hat{\boldsymbol{J}} \\ \boldsymbol{K} &= K\hat{\boldsymbol{L}}\times\hat{\boldsymbol{J}} \\ A_{ij} &= F\hat{\boldsymbol{J}}_i\hat{\boldsymbol{J}}_j + G(\hat{\boldsymbol{L}}\times\hat{\boldsymbol{J}})_i(\hat{\boldsymbol{L}}\times\hat{\boldsymbol{J}})_j, \end{aligned} \tag{1.6.17}$$

where J, K, F and G are undetermined functions of E and L. By evaluating the Poisson brackets $\{J_i, J_j\}$ $\{K_i, K_j\}$ $\{A_{ij}, A_{kl}\}$ and comparing them with the standard forms for $so(4)$ and $su(3)$ it is possible to show that the undetermined functions take the form

$$\begin{aligned} \boldsymbol{J} &= [P^2(E) - L^2]^{\frac{1}{2}}\hat{\boldsymbol{J}} \\ \boldsymbol{K} &= [P^2(E) - L^2]^{\frac{1}{2}}\hat{\boldsymbol{L}}\times\hat{\boldsymbol{J}} \\ A_{ij} &= \left[P(E)\pm[P^2(E) - L^2]^{\frac{1}{2}}\right]\hat{\boldsymbol{J}}_i\hat{\boldsymbol{J}}_j \\ &+ \left[P(E)\mp[P^2(E) - L^2]^{\frac{1}{2}}\right](\hat{\boldsymbol{L}}\times\hat{\boldsymbol{J}})_i(\hat{\boldsymbol{L}}\times\hat{\boldsymbol{J}})_j, \end{aligned} \tag{1.6.18}$$

where $P(E)$ is an arbitrary function of E.

1.7 The Geometry of the Three–Dimensional Isotropic Harmonic Oscillator

This technique can be successfully applied to the three–dimensional isotropic harmonic oscillator giving rise to a Laplace–Runge–Lenz analogue as well as the Jauch–Hill–Fradkin tensor. The equation of motion for the three–dimensional isotropic harmonic oscillator is given by

$$\ddot{\boldsymbol{r}} = -\lambda^2 r\hat{\boldsymbol{r}}. \tag{1.7.1}$$

Using (1.7.1) the orbit equation (1.6.8) becomes

$$\theta - \theta_0 = \int_{u_0}^{u} \frac{-\mathrm{d}u}{\left(\frac{2}{L^2}(E - \frac{\lambda^2}{2u^2}) - u^2\right)^{\frac{1}{2}}}, \tag{1.7.2}$$

where u_0 is the inverse of the semi–major axis length of the ellipse or the largest root of (1.6.4) with $\dot{r}$ set equal to zero. By making the substitution $u^2 = \rho$ (1.7.2) can be integrated using G&R [43, 2.261] and rearranged to obtain

$$\cos(\theta - \theta_0) = \left(\frac{E + (E^2 - \lambda^2 L^2)^{\frac{1}{2}} - L^2 u^2}{2\,(E^2 - \lambda^2 L^2)^{\frac{1}{2}}} \right)^{\frac{1}{2}}. \tag{1.7.3}$$

Using equation (1.6.14) and the magnitude of the vector from (1.6.18), where

$$P(E) = \frac{E}{\lambda}, \tag{1.7.4}$$

$$\boldsymbol{J} = \pm \left(\frac{J}{2\lambda} \right)^{\frac{1}{2}} \left[E + \lambda J - L^2 u^2 \right]^{-\frac{1}{2}} \left((E + \lambda J)\, \hat{\boldsymbol{r}} - u(\dot{\boldsymbol{r}} \times \boldsymbol{L}) \right), \tag{1.7.5}$$

where

$$J = \left(\frac{E^2}{\lambda^2} - L^2 \right)^{\frac{1}{2}}. \tag{1.7.6}$$

The choice for $P(E)$ is motivated by the structure of the Jauch–Hill–Fradkin tensor. This result (1.7.5) is equivalent to that obtained by Fradkin [29]. However, he assumed that the semi–minor axis lay along the $x-$axis which accounts for some discrepancies in signs. Equation (1.7.5) is only piecewise conserved and is discontinuous at $\pi/2 + \theta_0$ and $3\pi/2 + \theta_0$, where the discontinuity signals a change in sign. The unwieldy expression (1.7.5) has been simplified somewhat, both by Yoshida [131] and also by Sivardière [120] using more specialised methods. The same simplification can be achieved by making use of the energy expression (1.6.4) to replace $\dot{r}$, expressions for the semi–major and semi–minor axis lengths (1.7.20) to replace terms involving $E + \lambda J$ and the results that $L = \lambda ab$ and $E = \lambda^2(a^2 + b^2)/2$ to give

$$\boldsymbol{J} = \pm J \frac{1}{e\,(r^2 - b^2)^{\frac{1}{2}}} \left(\boldsymbol{r} - \frac{b^2}{L^2} \dot{\boldsymbol{r}} \times \boldsymbol{L} \right) \tag{1.7.7}$$

where the positive sign is used over the interval $(-\pi/2 + \theta_0, \pi/2 + \theta_0)$ and the negative one over $(\pi/2 + \theta_0, 3\pi/2 + \theta_0)$. Expression (1.7.7) is discontinuous at $\pi/2 + \theta_0$ and $3\pi/2 + \theta_0$. Similarly the vector $\boldsymbol{K}$ can be constructed using

$$\begin{aligned} \boldsymbol{K} &= \hat{\boldsymbol{L}} \times \boldsymbol{J} \\ &= \pm J \frac{(1 - e^2)^{\frac{1}{2}}}{e\,(a^2 - r^2)^{\frac{1}{2}}} \left(\frac{a^2}{L^2} \dot{\boldsymbol{r}} \times \boldsymbol{L} - \boldsymbol{r} \right), \end{aligned} \tag{1.7.8}$$

where the positive sign is used over the interval $(\theta_0, \pi + \theta_0)$ and the negative one over $(\pi + \theta_0, 2\pi + \theta_0)$. Equation (1.7.8) is discontinuous at θ_0 and $\pi + \theta_0$. a and b are the semi–major and semi–minor axis lengths respectively and e denotes the eccentricity.

The choice of (1.7.4) gives the familiar form for A_{ij} in (1.6.18)

$$A_{ij} = \frac{1}{\lambda}(p_i p_j + \lambda^2 r_i r_j). \tag{1.7.9}$$

A_{ij} is usually obtained directly from the differential equation for the three–dimensional isotropic harmonic oscillator by integrating the sum of $(1.7.1)_i \dot{x}_j + (1.7.1)_j \dot{x}_i$ and this result is a factor of λ larger than that given by (1.7.9). For consistency we will scale (1.7.9) by λ in the calculations to follow.

It does not seem possible to construct the velocity hodograph easily from the Hamilton–like vector $\boldsymbol{K}$. However, the Jauch–Hill–Fradkin tensor can be used to obtain the equation of the velocity hodograph as

$$\dot{\boldsymbol{r}}^T(2EI - A)\dot{\boldsymbol{r}} = \lambda^2 L^2. \tag{1.7.10}$$

Since $\hat{\boldsymbol{L}}$ is constant, the motion is planar and for convenience we assign x_3 to be the variable in the direction of $\hat{\boldsymbol{L}}$. The eigenvalues of the 2x2 matrix in (1.7.10), which determine the velocity hodograph in the plane, are

$$\lambda = E \mp \left(E^2 - \lambda^2 L^2\right)^{\frac{1}{2}} \tag{1.7.11}$$

and, if we rotate the velocity hodograph (1.7.10) so that the cartesian unit vectors $\boldsymbol{i}$ and $\boldsymbol{j}$ become the principal axes,

$$\frac{\dot{x}^2}{\left(E + (E^2 - \lambda^2 L^2)^{\frac{1}{2}}\right)/\lambda^2} + \frac{\dot{y}^2}{\left(E - (E^2 - \lambda^2 L^2)^{\frac{1}{2}}\right)/\lambda^2} = \lambda^2 \tag{1.7.12}$$

which is more compactly written as

$$\frac{\dot{x}^2}{a^2} + \frac{\dot{y}^2}{b^2} = \lambda^2. \tag{1.7.13}$$

Equation (1.7.13) is the equation of an ellipse in the velocity coordinates where a and b are the semi–major and semi–minor axis lengths respectively.

The equation of the orbit is then given by

$$\boldsymbol{r}^T[2EI - A]\boldsymbol{r} = L^2. \tag{1.7.14}$$

If we also rotate the orbit (1.7.14) so that the cartesian unit vectors $\boldsymbol{i}$ and $\boldsymbol{j}$ become the principal axes,

$$\frac{x^2}{a^2} + \frac{y^2}{b^2} = 1 \tag{1.7.15}$$

which is the equation for an ellipse with geometric centre at the origin. It should be noted that (1.7.13) describes an ellipse scaled by the factor λ concentric to (1.7.15). Expressing (1.7.15) in terms of plane polar coordinates where the angle between $\boldsymbol{J}$ and $\boldsymbol{i}$ is θ_0 gives

$$\begin{aligned} r^2 &= \frac{L^2}{E - (E^2 - \lambda^2 L^2)^{\frac{1}{2}} \cos 2(\theta - \theta_0)} \\ &= \frac{L^2}{E - \lambda J \cos 2(\theta - \theta_0)} \end{aligned} \tag{1.7.16}$$

and consequently r is a function of the double angle $2(\theta - \theta_0)$ rather than $\theta - \theta_0$ as was the case for the Kepler problem. It should be appreciated that (1.7.16) is distinct from (1.5.10) where the origin is at the focus of the ellipse and not at the geometric centre. The parametric equations describing the orbit are obtained by solving (1.7.1) directly which gives

$$\begin{aligned} x &= a \cos(\lambda t + \phi_1) \\ y &= b \sin(\lambda t + \phi_2). \end{aligned} \tag{1.7.17}$$

By differentiating (1.7.17) we obtain

$$\begin{aligned} \dot{x} &= -a\lambda \sin(\lambda t + \phi_1) \\ \dot{y} &= b\lambda \cos(\lambda t + \phi_2). \end{aligned} \tag{1.7.18}$$

Using (1.7.17) and (1.7.18) to calculate the angular momentum constant $x\dot{y} - y\dot{x} = \lambda ab$, (or using (1.7.15) or (1.7.13)) it can be shown that

$$\phi_1 = \phi_2 = -\lambda t_0. \tag{1.7.19}$$

The constant a is obtained by comparing (1.7.17) with $y = 0$ with (1.7.16) $\theta - \theta_0 = 0$. b is obtained in a similar fashion with $x = 0$ and $\theta - \theta_0 = \pi/2$. The parametric equations (1.7.17) become

$$\begin{aligned} x &= \frac{(E + \lambda J)^{\frac{1}{2}}}{\lambda} \cos\big(\lambda(t - t_0)\big) \\ y &= \frac{(E - \lambda J)^{\frac{1}{2}}}{\lambda} \sin\big(\lambda(t - t_0)\big). \end{aligned} \tag{1.7.20}$$

Denoting the angle between $\boldsymbol{r}$ and $\boldsymbol{i}$ as θ and using (1.7.17) gives

$$\tan\theta = \frac{y}{x} = \frac{b}{a}\tan\lambda(t - t_0) \tag{1.7.21}$$

and similarly denoting the angle between $\dot{\boldsymbol{r}}$ and $\boldsymbol{i}$ as ψ and using (1.7.18) gives

$$\tan\psi = \frac{\dot{y}}{\dot{x}} = -\frac{b}{a}\cot\lambda(t - t_0). \tag{1.7.22}$$

Clearly $\boldsymbol{r}(\pi/2 + t)$ moves in phase with the vector $\dot{\boldsymbol{r}}(t)$.

The equation for the acceleration hodograph is given by

$$\ddot{\boldsymbol{r}}^T(2EI - A)\ddot{\boldsymbol{r}} = \lambda^4 L^2 \tag{1.7.23}$$

which can be rotated onto principal axes to give

$$\left(\frac{\ddot{x}}{a}\right)^2 + \left(\frac{\ddot{y}}{b}\right)^2 = \lambda^4 \tag{1.7.24}$$

which again describes an ellipse which is concentric to (1.7.15). Notice also that the phase difference between the acceleration and displacement vectors is again π radians since $\boldsymbol{r} \times \ddot{\boldsymbol{r}} = \boldsymbol{0}$, but it is not constant between the velocity and displacement vectors.

Figure 1.7.1 shows the tangential velocity vectors drawn at some points along the orbit of the three–dimensional isotropic harmonic oscillator. Figure 1.7.2 shows the construction of the velocity hodograph when the tangential velocity vectors are shifted to the same origin. Notice that the velocity hodograph encloses the origin which is at the geometric centre of both of the ellipses.

Figure 1.7.3 geometrically demonstrates the construction of $\boldsymbol{L}$ corresponding with Figures 1.7.1 and 1.7.2. The shaded parallelograms which represent the magnitude of $\boldsymbol{L} = \boldsymbol{r} \times \dot{\boldsymbol{r}}$ have equal areas. Figure 1.7.4 shows both the displacements and corresponding velocities at regular time intervals for the three–dimensional isotropic harmonic oscillator problem. The shaded regions confirm Kepler's second law that equal areas are swept out in equal times. It should be obvious that the initial phase difference between the displacement and velocity vectors is $\pi/2$ radians as the displacement lies along the $+x-$axis at $t = 0$ while the velocity is purely along the $+\dot{y}-$axis. The phase difference in general between the displacement and velocity vectors is not constant since $\boldsymbol{r} \cdot \dot{\boldsymbol{r}} = r\dot{r}$ which is nonzero except when $\dot{r} = 0$, *i.e.* at the extremities of the motion. This is also evident by comparing the angle between the corresponding displacement and velocity vectors for a range of time intervals using the solid round time markers on the orbit and the corresponding solid square

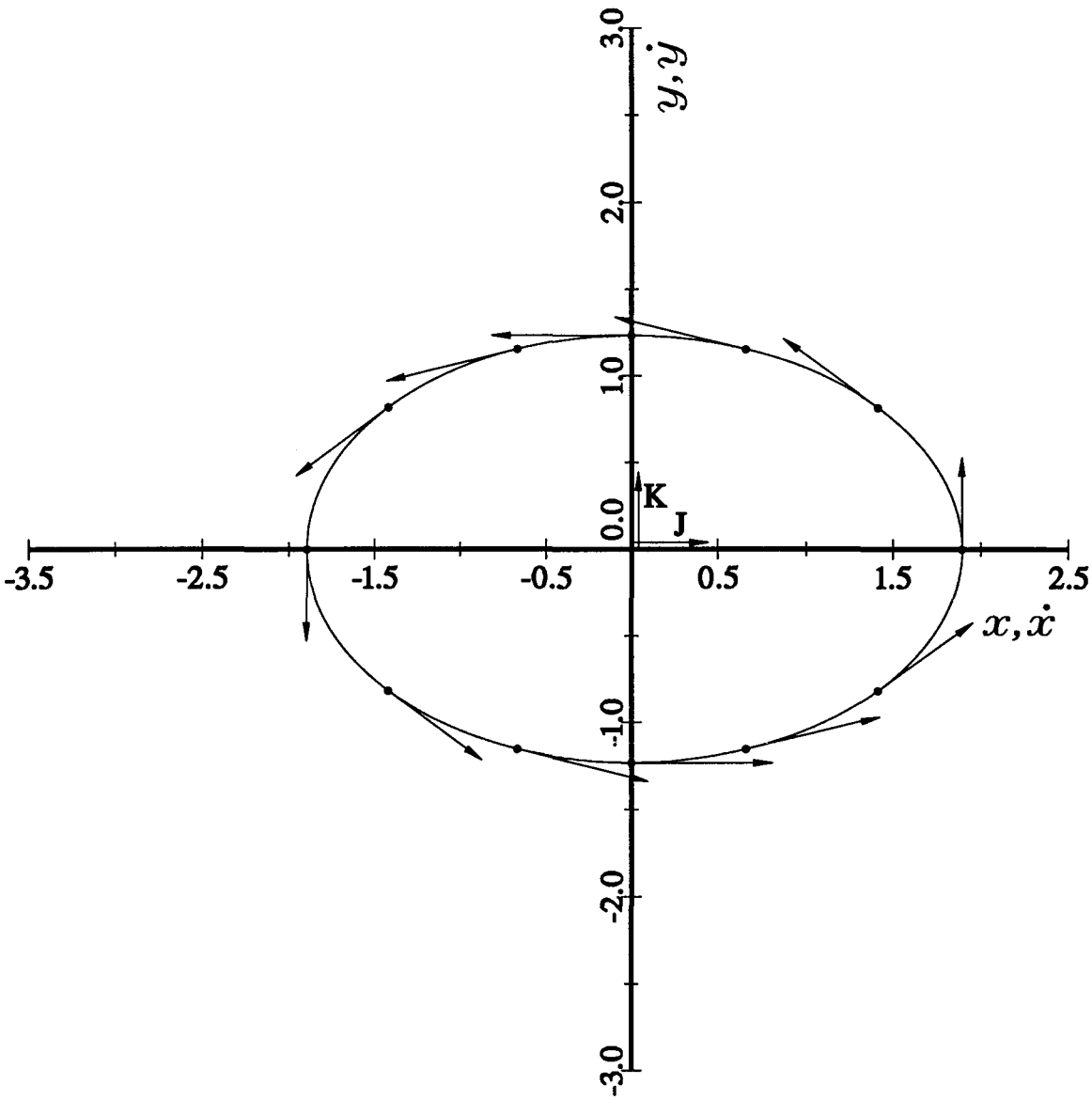


Figure 1.7.1. The elliptical oscillator orbit showing the velocity vectors at some points along the orbit and the orientation of the conserved vectors $\boldsymbol{K}$ and $\boldsymbol{J}$. The constants have the values $\mu_k = 1.25$, $\theta_0 = 0$, $a_k = 1.893\dot{9}$, $\lambda = (\mu_k/a_k^3)^{1/2}$, $K = J = 0.4444$, $L = 1$ and $E = 0.4694$. The subscript k refers to the constants which were used to plot the elliptical Kepler orbit shown in Figure 1.5.1 which has the same dimensions as the oscillator orbit shown above. The axes have been kept the same as those in the Kepler plots for purposes of comparison. Note that $\boldsymbol{K}$ is discontinuous when $\theta = 0$ or π and $\boldsymbol{J}$ is discontinuous when $\theta = \pi/2$ or $3\pi/2$.

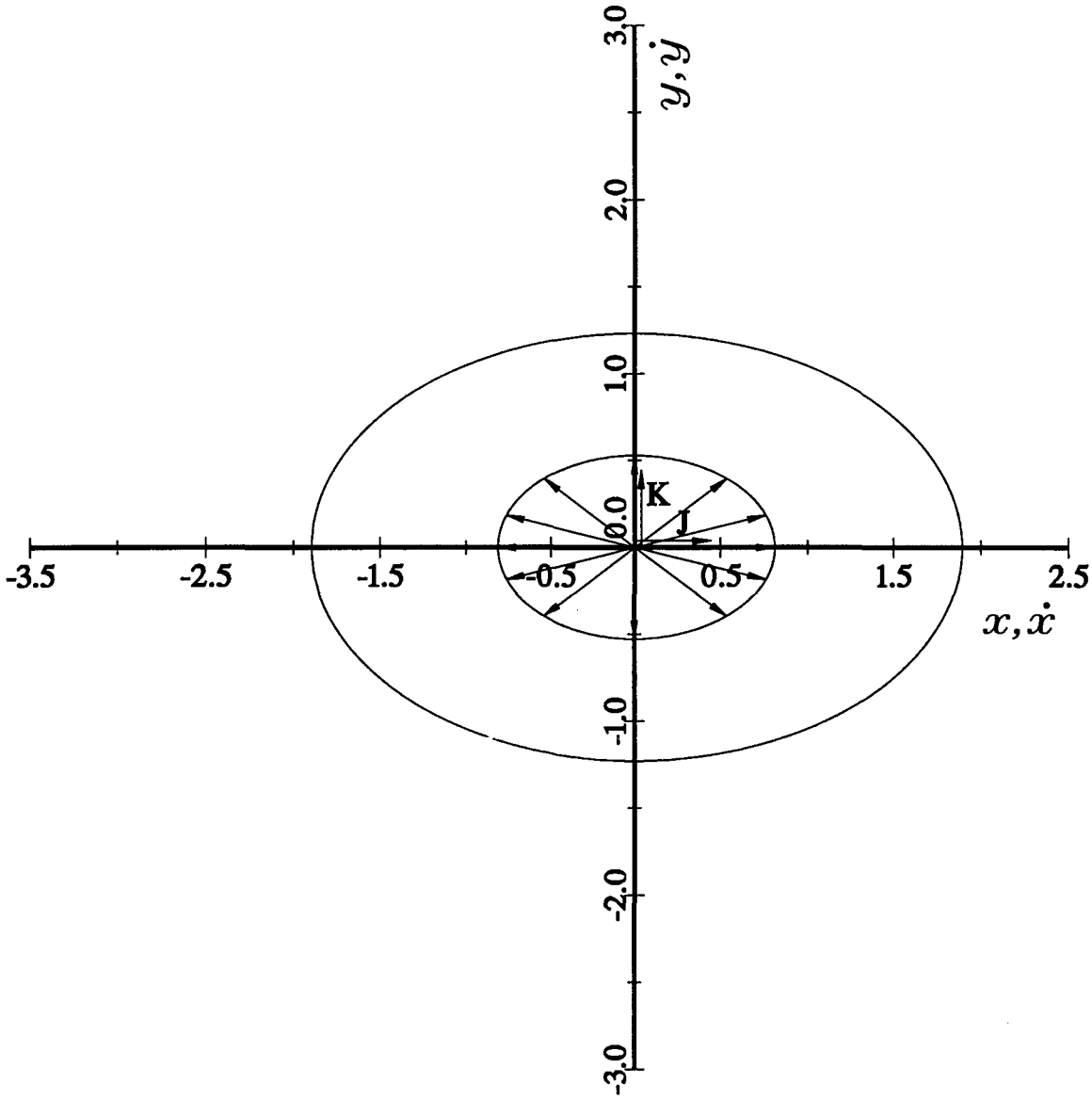


Figure 1.7.2. The elliptical oscillator orbit and the construction of the corresponding elliptical velocity hodograph with a selection of velocity vectors drawn from the origin on the same set of axes as the displacement. The origin lies inside the velocity hodograph. The constants are chosen as for Figure 1.7.1.

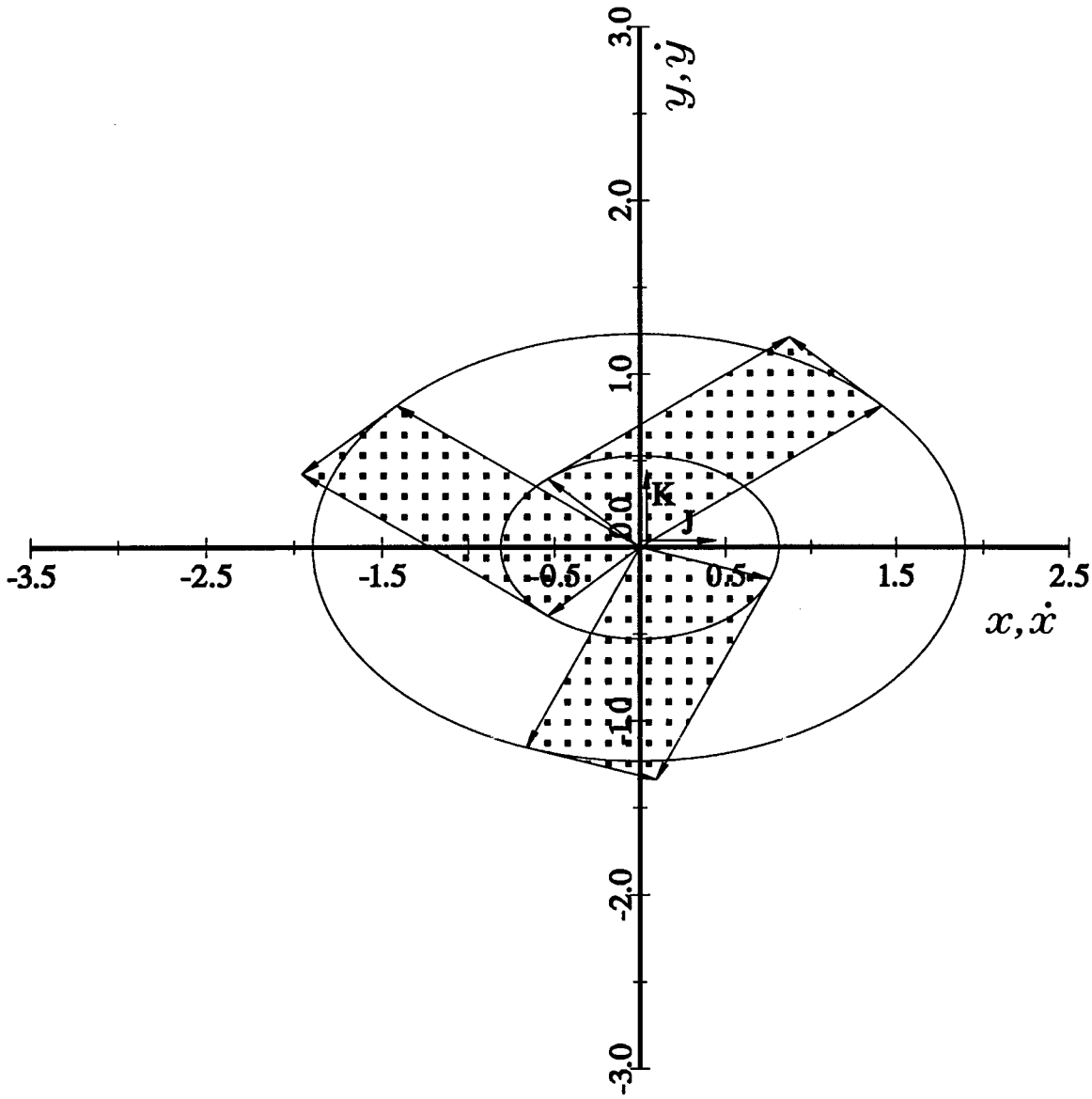


Figure 1.7.3. The elliptical oscillator orbit with its corresponding elliptical velocity hodograph demonstrating the constancy of $\boldsymbol{L}$. The shaded parallelograms have equal areas as a consequence of $\boldsymbol{L}$ being conserved. The constants are chosen as for Figure 1.7.1.

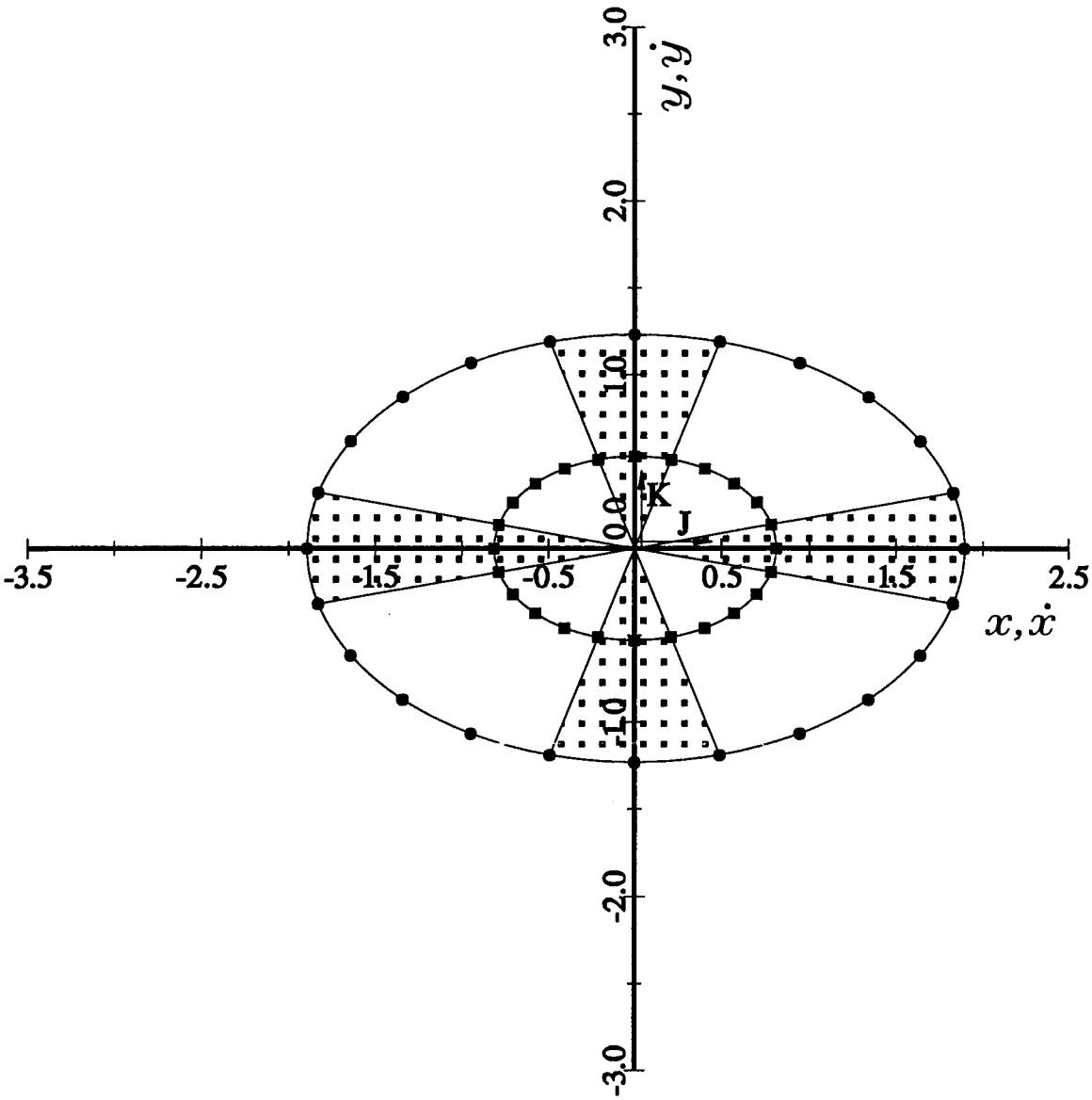


Figure 1.7.4. The elliptical oscillator orbit with its corresponding elliptical velocity hodograph. The circles (-•-•-•-) show the displacements of the particle at the time intervals $iT/24$, $i = 0, \ldots, 24$ and the squares (-■-■-■-) give the corresponding velocities. The shaded regions confirm Kepler's second law that equal areas are swept out in equal times. The phase difference between the velocity and displacement vectors is not constant although the displacement vector shifted in time by $\pi/2$ radians moves in phase with the corresponding velocity vector. The constants are chosen as for Figure 1.7.1.

time markers on the velocity hodograph and counting the number of round markers from the rightmost vertex of the ellipse in a counter–clockwise direction to the displacement of interest and then counting off the same number of square markers on the velocity hodograph starting from the square marker at the top of the velocity hodograph (since at $t = 0$ the velocity is purely along the $+\dot{y}-$axis) in a counter–clockwise direction to obtain the corresponding velocity or *vice versa*. Alternatively, if the velocity hodograph plot is rotated clockwise through $\pi/2$ radians about the geometric centre of the ellipse, it is apparent that the corresponding displacements, velocities and the origin are not collinear except at the vertices of the ellipses. Note, however, that the radial vector $\boldsymbol{r}(t)$ with the addition of $\pi/2$ radians to its argument, *i.e.*, $\boldsymbol{r}(\pi/2 + t)$ moves in phase with the vector $\dot{\boldsymbol{r}}(t)$ since radii drawn from the origin to the solid round time markers on the orbit also pass through the solid square time markers on the velocity hodograph. This behaviour is also apparent from equation (1.7.21) which gives the plane polar angle θ in terms of the tangent of a function of t which can be converted into an equation of the same form as that for the plane polar angle ψ (1.7.22) which involves a cotangent of the same function of t through the addition of $\pi/2$ radians to the argument of the tangent function in (1.7.21) and *vice versa*. Further, with reference to both (1.7.21) and (1.7.22) and Figure 1.7.4, the sum of the plane polar angles $\theta(\pi/2 - t) + \psi(t) = \pi$ radians realising that the solid round and solid square time markers on the orbit and velocity hodograph respectively represent the displacement and velocity of the particle at the regular time intervals $iT/24 = i\pi/(12\lambda), i = 0, \ldots, 24$ and so an addition of $\pi/2$ radians to the argument of time represents a shift of 6 consecutive time markers along either the orbit or the velocity hodograph which does not necessarily correspond with a plane polar angular shift of $\pi/2$ radians. In other words the regular time intervals do not correspond with regular increments of the plane polar angles θ and ψ respectively and as a result the collinearity between the origin, the displacements shifted in time by $\pi/2$ radians and the velocities is no longer present when the markers are drawn at regular increments in θ as is evident from Figures 1.7.7–1.7.9. In summary, the phase difference between $\boldsymbol{r}$ and $\dot{\boldsymbol{r}}$ is not constant in the three–dimensional isotropic harmonic oscillator although the origin, the displacements shifted in time by $\pi/2$ radians and the velocities are collinear.

Figure 1.7.5 shows the tangential acceleration vectors drawn at some points along the velocity hodograph. Figure 1.7.6 shows the construction of the acceleration hodograph when the tangential acceleration vectors are shifted to the same origin.

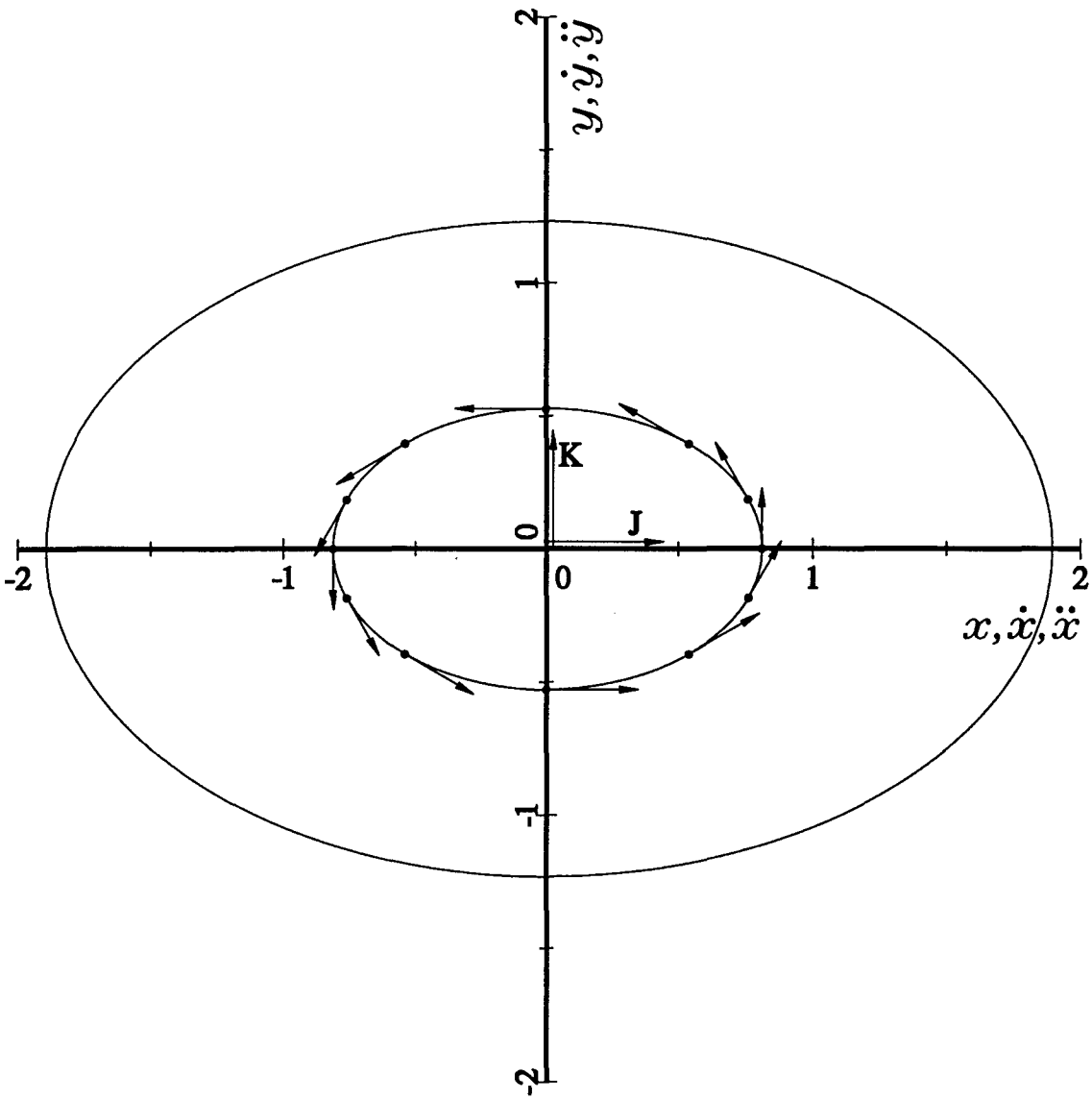


Figure 1.7.5. The elliptical oscillator orbit and the elliptical velocity hodograph showing the acceleration vectors at some points along the velocity hodograph and the orientation of the conserved vectors $\boldsymbol{K}$ and $\boldsymbol{J}$. The constants are chosen as for Figure 1.7.1.

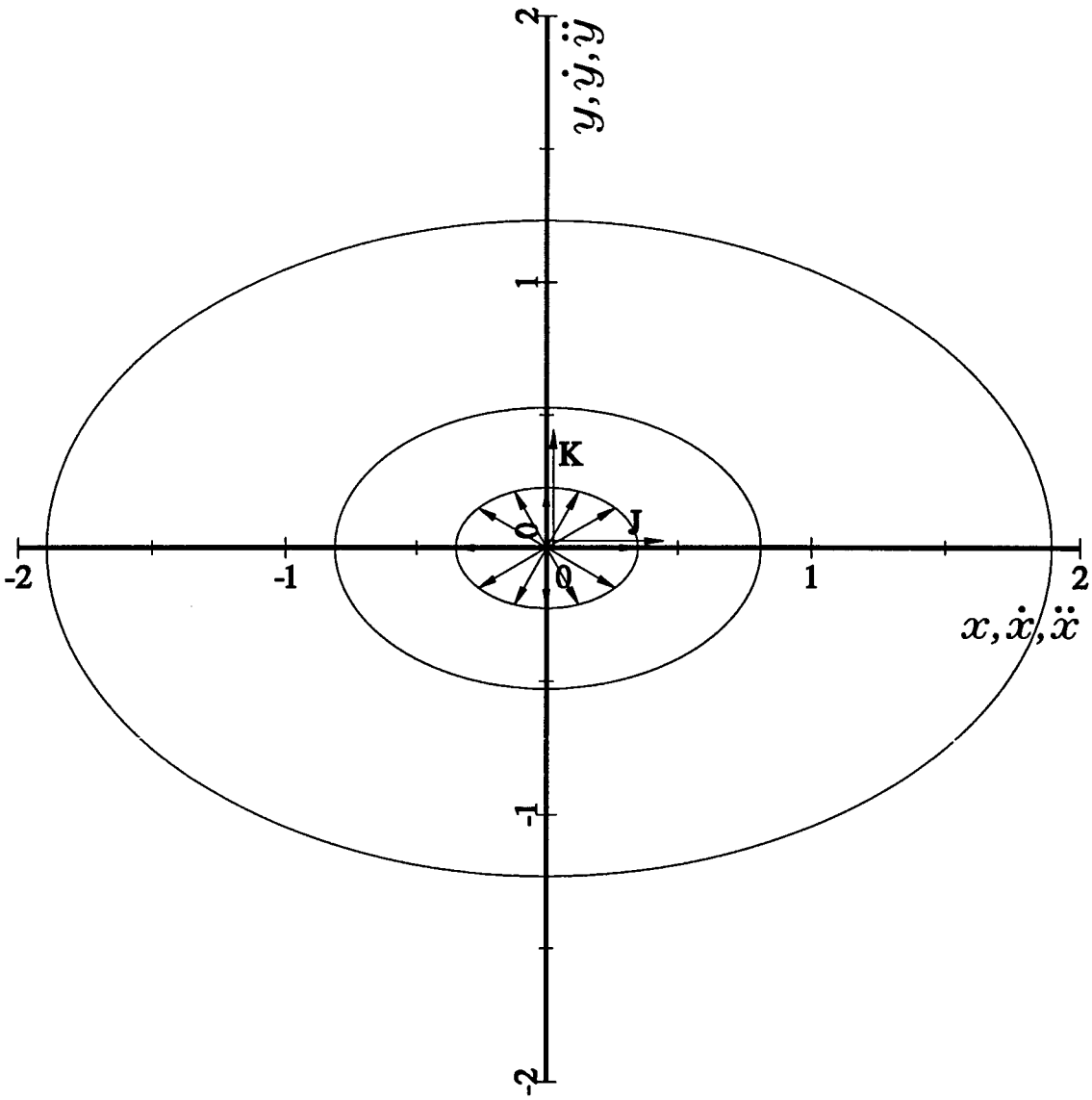


Figure 1.7.6. The elliptical oscillator orbit, elliptical velocity hodograph and the construction of the corresponding elliptical acceleration hodograph with a selection of acceleration vectors drawn from the origin on the same set of axes as the displacement. The origin lies inside the acceleration hodograph. The phase difference between the acceleration and displacement vectors is a constant π radians but varies between the acceleration and velocity vectors although the velocity vector shifted in time by $\pi/2$ radians moves in phase with the acceleration vector. The constants are chosen as for Figure 1.7.1.

In summary the three–dimensional isotropic harmonic oscillator gives rise to an ellipse in the orbit, velocity hodograph and also the acceleration hodograph. The only distinguishing feature between the ellipses is the successive scalings by λ from the orbit to the acceleration hodograph (see Figure 1.7.6).

It is also possible to extend the idea of a conserved Lagrangian vector which was proposed in §1.5 to encompass tensor quantities as well. As in the Kepler problem this sytem is conservative and the Lagrangian is given by

$$\mathcal{L} = \frac{1}{2}\left(\dot{r}^2 + \frac{L^2}{r^2}\right) - \frac{1}{2}\lambda^2 r^2. \tag{1.7.25}$$

As before we assume that the Lagrangian tensor is related to the Lagrangian in the same way as the Jauch–Hill–Fradkin tensor is related to the Hamiltonian, *i.e.*

$$\mathrm{tr}\,(B_{ij}) = B_{ii} = 2\mathcal{L}. \tag{1.7.26}$$

One possible structure for B_{ij} which meets this requirement is the tensor

$$B_{ij} = \dot{x}_i\dot{x}_j - \lambda^2 x_i x_j. \tag{1.7.27}$$

It is also worth noting that in this conservative system the Hamiltonian (which is also the energy (1.6.4) in this case) and the Lagrangian (1.7.25) are conjugate to each other and this structure also extends to the tensor pairs A_{ij} and B_{ij}.

As was done in the case of the Lagrangian vectors, the Poisson bracket relations between the components of $\boldsymbol{L}$ and the non–conserved Lagrangian tensor B_{ij} and the scalar Lagrangian $\mathcal{L}$ were calculated and found to have the form

$$\begin{aligned}
&[L_i, L_j] = \varepsilon_{ijk}L_k \\
&[L_i, B_{jk}] = \varepsilon_{ijn}B_{nk} + \varepsilon_{ikn}B_{jn} \\
&[B_{ij}, B_{kl}] = -\left(\varepsilon_{ikn}\delta_{jl} + \varepsilon_{jln}\delta_{ik} + \varepsilon_{iln}\delta_{jk} + \varepsilon_{jkn}\delta_{il}\right)L_n \\
&[L_i, \mathcal{L}] = 0 \\
&[B_{ij}, \mathcal{L}] = 0.
\end{aligned} \tag{1.7.28}$$

Notice that the Poisson bracket expressions have the same structure as those between the components of the conserved quantities as shown in equation (1.6.16) except that the relation between components of B_{ij} has the opposite sign to that for the components of the conserved tensor. The same is true in the Kepler problem for the Poisson bracket relations between components of the Lagrangian vector for bound state energies which have the opposite sign to the relations between components of the Laplace–Runge–Lenz vector.

Thus it would seem that a suitable definition for a Lagrangian tensor would be that the Poisson bracket of the components taken separately with the Lagrangian vanish and further that the Poisson bracket between pairs of different components of B_{ij} generates the relevant components of the conserved vector $\boldsymbol{L}$. It should be realised that components of the vector $\boldsymbol{L}$ automatically bring about a rotation when applied to the separate components of any vector or tensor of a suitable form and so this Poisson bracket relationship is not unique to either a Lagrangian or a conserved vector or tensor.

In expanded form, the useful Poisson bracket expressions are given by

$$\frac{\partial B_{ij}}{\partial q_k}\dot{q}_k - \frac{\partial B_{ij}}{\partial p_k}\frac{\partial \mathcal{L}(q_l,p_l)}{\partial q_k} = 0$$

$$\frac{\partial B_{ij}}{\partial q_m}\frac{\partial B_{kl}}{\partial p_m} - \frac{\partial B_{ij}}{\partial p_m}\frac{\partial B_{kl}}{\partial q_m} =$$

$$-\left(\varepsilon_{ikn}\delta_{jl} + \varepsilon_{jln}\delta_{ik} + \varepsilon_{iln}\delta_{jk} + \varepsilon_{jkn}\delta_{il}\right) L_n. \tag{1.7.29}$$

The top expression of (1.7.29) can also be written as

$$\frac{\partial B_{ij}}{\partial p_k}\dot{p}_k - \frac{\partial B_{ij}}{\partial q_k}\dot{q}_k = \frac{\partial B_{ij}}{\partial p_k}p_l\frac{\partial \dot{p}_k}{\partial p_l} \tag{1.7.30}$$

writing the Lagrangian as $p_k\dot{q}_k - H$ and using Hamilton's equations and the result that $\partial\dot{q}_k/\partial q_j = -\partial\dot{p}_j/\partial p_k$. Equation (1.7.30) can also be expressed in terms of the total time derivative of B_{ij} as

$$\dot{B}_{ij} = \frac{\partial B_{ij}}{\partial p_k}\left(2\dot{p}_k - p_l\frac{\partial \dot{p}_k}{\partial p_l}\right). \tag{1.7.31}$$

It would appear that the approach to adopt when constructing such a tensor is to assume a structure for the Lagrangian vector such as $\boldsymbol{M} = A(q_l,p_l)\boldsymbol{p}\times\boldsymbol{L} + B(q_l,p_l)\hat{\boldsymbol{r}}$ and then to form a tensor $B_{ij} = F\hat{\boldsymbol{M}}_i\hat{\boldsymbol{M}}_j + G(\hat{\boldsymbol{L}}\times\boldsymbol{M})_i(\hat{\boldsymbol{L}}\times\boldsymbol{M})_j$ and use the Poisson bracket with $\mathcal{L}$ to obtain restrictions on the unknown functions F and G. This would be followed by applying the other Poisson bracket constraints (1.7.29.2) on B_{ij}. Note that the technique described above needs a Lagrangian and also that $\partial\mathcal{L}(q_k,p_k)/\partial q_j$ is not equal to $\dot{p}_j$ since $\mathcal{L}$ is now recast in the Hamiltonian representation. If this were the case, however, then (1.7.29.1) would be the conjugate of the expanded exact derivative of $\boldsymbol{M}$ which is very appealing and this apparent lack of symmetry may suggest further complications during the construction process.

The construction of a Lagrangian vector for the three–dimensional isotropic harmonic oscillator as well as a Lagrangian tensor for the Kepler problem will be investigated in the future as the process described above appears to be more complicated to apply than that of Fradkin for the conserved quantities as it does not seem possible to use the orbit equation to find the unit vector initially as is done in the conserved case.

The Lagrangian tensor equivalent of the velocity hodograph is given by

$$\dot{\boldsymbol{r}}^T(2\mathcal{L}I - B)\dot{\boldsymbol{r}} = -\lambda^2 L^2. \tag{1.7.32}$$

Since $\hat{\boldsymbol{L}}$ is constant, the motion is planar and for convenience we assign x_3 to be the variable in the direction of $\hat{\boldsymbol{L}}$. The eigenvalues of the 2x2 matrix in (1.7.32), which determine the velocity hodograph in the plane, are

$$\lambda = \mathcal{L} \mp \left(\mathcal{L}^2 + \lambda^2 L^2\right)^{\frac{1}{2}} \tag{1.7.33}$$

and, if we rotate the velocity hodograph (1.7.32) so that the cartesian unit vectors $\boldsymbol{i}$ and $\boldsymbol{j}$ become the principal axes,

$$\frac{\dot{x}^2}{\left(\mathcal{L} + (\mathcal{L}^2 + \lambda^2 L^2)^{\frac{1}{2}}\right)/\lambda^2} + \frac{\dot{y}^2}{\left(\mathcal{L} - (\mathcal{L}^2 + \lambda^2 L^2)^{\frac{1}{2}}\right)/\lambda^2} = \lambda^2 \tag{1.7.34}$$

which is more compactly written as

$$\frac{\dot{x}^2}{a^{*2}} + \frac{\dot{y}^2}{b^{*2}} = \lambda^2. \tag{1.7.35}$$

Equation (1.7.35) describes an ellipse although this is not immediately apparent since $\mathcal{L}$ is not constant.

The Lagrangian tensor equivalent of the equation of the orbit is given by

$$\boldsymbol{r}^T[2\mathcal{L}I - B]\boldsymbol{r} = L^2. \tag{1.7.36}$$

If we also rotate the orbit (1.7.36) so that the cartesian unit vectors $\boldsymbol{i}$ and $\boldsymbol{j}$ become the principal axes,

$$\frac{x^2}{a^{*2}} + \frac{y^2}{b^{*2}} = 1 \tag{1.7.37}$$

which again describes an ellipse although this is not immediately apparent since $\mathcal{L}$ is not constant. Expressing (1.7.37) in terms of plane polar coordinates where the angle between $\boldsymbol{J}$ and $\boldsymbol{i}$ is θ_0 gives

$$r^2 = \frac{L^2}{\mathcal{L} - (\mathcal{L}^2 + \lambda^2 L^2)^{\frac{1}{2}} \cos 2(\gamma - \gamma_0)}, \tag{1.7.38}$$

which has the same structure as that of the orbit equation of the three–dimensional isotropic harmonic oscillator (see (1.7.16)). It does not seem possible to easily obtain an expression relating the angle $\gamma - \gamma_0$ to $\theta - \theta_0$ so that (1.7.38) can be reduced to (1.7.16) as was done for the Lagrange vector in the Kepler problem. The equation for the acceleration hodograph is given by

$$\ddot{\boldsymbol{r}}^T(2\mathcal{L}I - B)\ddot{\boldsymbol{r}} = \lambda^4 L^2 \tag{1.7.39}$$

which can be rotated onto principal axes to give

$$\left(\frac{\ddot{x}}{a^*}\right)^2 + \left(\frac{\ddot{y}}{b^*}\right)^2 = \lambda^4 \tag{1.7.40}$$

which again describes an ellipse although this is not immediately apparent since $\mathcal{L}$ is not constant.

The Lagrangian can be expressed in terms of θ as

$$\mathcal{L} = \frac{\lambda J\big(\lambda J - E\cos 2(\theta - \theta_0)\big)}{E - \lambda J \cos 2(\theta - \theta_0)}. \tag{1.7.41}$$

The parametric equations for the path of the vector $\dot{\boldsymbol{r}}$ can be shown to have the form

$$\begin{aligned} \dot{x} &= -\frac{E\sin\theta + \lambda J \sin(\theta - 2\theta_0)}{\big(E - \lambda J\cos 2(\theta - \theta_0)\big)^{\frac{1}{2}}} \\ \dot{y} &= \frac{E\cos\theta - \lambda J\cos(\theta - 2\theta_0)}{\big(E - \lambda J\cos 2(\theta - \theta_0)\big)^{\frac{1}{2}}} \end{aligned} \tag{1.7.42}$$

using the orbit equation (1.7.16) to substitute for r and $\dot{r}$ in terms of θ. Denoting the angle between $\dot{\boldsymbol{r}}$ and $\boldsymbol{i}$ as ψ and setting $\theta_0 = 0$ in (1.7.42) for convenience gives

$$\tan\psi = \frac{\dot{y}}{\dot{x}} = -\frac{(E - \lambda J)}{(E + \lambda J)}\cot\theta = -\frac{b^2}{a^2}\cot\theta. \tag{1.7.43}$$

Note that when $\theta = \theta_0 = 0$, $\psi = \lim_{\theta\uparrow 0} \arctan(-b^2\cot\theta/a^2) = \pi/2$ as expected.

The components of the Jauch–Hill–Fradkin and Lagrangian tensors A_{ij} and B_{ij} can be shown to have the form

$$
\begin{aligned}
A_{11} &= E + \lambda J \cos 2\theta_0 \\
A_{12} &= \lambda J \sin 2\theta_0 \\
A_{22} &= E - \lambda J \cos 2\theta_0 \\
B_{11} &= \frac{-E^2 \cos 2\theta - E\lambda J\big(\cos 2(\theta - \theta_0) - \cos 2\theta_0\big)}{E - \lambda J \cos 2(\theta - \theta_0)} \\
&+ \frac{\lambda^2 J^2\big(\sin^2(\theta - 2\theta_0) + \cos^2\theta\big)}{E - \lambda J \cos 2(\theta - \theta_0)} \\
B_{12} &= \frac{-E^2 \sin 2\theta + E\lambda J \sin 2\theta_0 + \lambda^2 J^2 \sin 2(\theta - \theta_0)\cos 2\theta_0}{E - \lambda J \cos 2(\theta - \theta_0)} \\
B_{22} &= \frac{E^2 \cos 2\theta - E\lambda J\big(\cos 2(\theta - \theta_0) + \cos 2\theta_0\big)}{E - \lambda J \cos 2(\theta - \theta_0)} \\
&+ \frac{\lambda^2 J^2\big(\cos^2(\theta - 2\theta_0) + \sin^2\theta\big)}{E - \lambda J \cos 2(\theta - \theta_0)}
\end{aligned}
\tag{1.7.44}
$$

using the orbit equation (1.7.16) to substitute for r and $\dot{r}$ in terms of θ. In order to better understand the geometry of the Lagrangian tensor it is convenient to represent the tensor as a parametric curve with two separate components of the tensor taken as the two parametric equations of the curve. Denoting the angle between B_{12} and B_{11} as α and setting $\theta_0 = 0$ in (1.7.44) for convenience gives

$$\tan\alpha = \frac{B_{12}}{B_{11}} = -\frac{(E - \lambda J)\sin 2\theta}{\lambda J - E\cos 2\theta}. \tag{1.7.45}$$

Note that when $\theta = \theta_0 = 0$, $\alpha = \lim_{\theta \uparrow 0} \arctan(B_{12}/B_{11}) = \pi$ as expected. Similarly denoting the angle between B_{22} and B_{12} as β and setting $\theta_0 = 0$ in (1.7.44) for convenience gives

$$\tan\beta = \frac{B_{22}}{B_{12}} = -\frac{(E\cos 2\theta - \lambda J)}{(E + \lambda J)\sin 2\theta}. \tag{1.7.46}$$

Note that when $\theta = \theta_0 = 0$, $\beta = \lim_{\theta \uparrow 0} \arctan(B_{22}/B_{12}) = \pi/2$ as expected.

Figure 1.7.7 shows the displacements, velocities and the path described by the B_{11} and B_{12} components of the Lagrangian tensor. It should be obvious that the initial phase difference between the displacement and the vector drawn to the point with components (B_{11}, B_{12}) is π radians as the displacement lies along the $+x-$axis at $t = 0$ while the vector touching the point with components (B_{11}, B_{12}) lies along the $-x-$axis. The phase difference in general between the displacement and the corresponding vector touching the path described by the components of the Lagrangian tensor is not constant. Figure 1.7.8 shows the displacements, velocities and the path described by the B_{12} and B_{22} components of the Lagrangian tensor. It should be obvious that the initial phase difference between the displacement and the vector drawn to the point with components (B_{12}, B_{22}) is $\pi/2$ radians as the displacement lies along the $+x-$axis at $t = 0$ while the vector touching the point with components (B_{12}, B_{22}) lies along the $+y-$axis. The phase difference in general between the displacement and the corresponding vector touching the path described by the components of the Lagrangian tensor is not constant. Figure 1.7.9 shows the displacements, velocities, accelerations, the path described by the B_{11} and B_{12} components of the Lagrangian tensor, the path described by the B_{12} and B_{22} components of the Lagrangian tensor and the path of the magnitude of the scalar Lagrangian in the direction of $\hat{\boldsymbol{r}}$.

The radial motion in time can be found by integrating (1.6.5) which can be inverted to yield

$$r = \frac{1}{\lambda}\Big(E + \lambda J \cos\Big(2\lambda(t - t_1)\Big)\Big)^{\frac{1}{2}}. \tag{1.7.47}$$

By squaring the components of (1.7.17) and adding it is possible to show that $t_1 = t_0$ by comparing the result with (1.7.47).

The period of the motion is easily seen to be

$$T = \frac{2\pi}{\lambda} \tag{1.7.48}$$

by integrating (1.6.5) over one quarter of a period, *i.e.* from the semi–major axis to the semi–minor axis, and multiplying by four to get the full period. Equation (1.7.48) is the equivalent of Kepler's third law for the three–dimensional isotropic harmonic oscillator. Notice that the period is now independent of the size of the elliptical orbit and depends only upon the force constant λ.

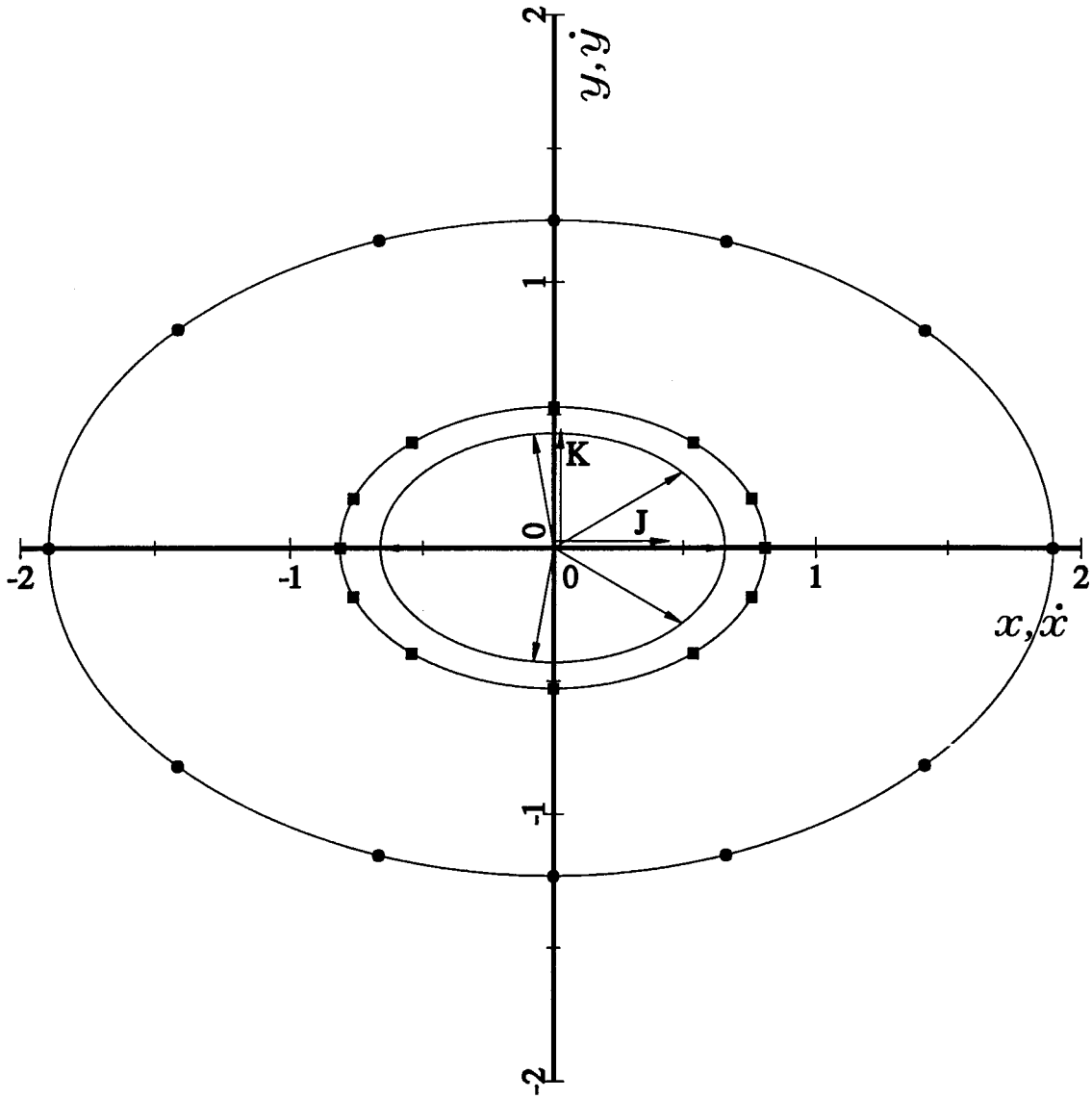


Figure 1.7.7. The elliptical oscillator orbit, elliptical velocity hodograph and the construction of the elliptical path described by the B_{11} and B_{12} components of the Lagrangian tensor with a selection of vectors drawn from the origin on the same set of axes as the displacement. The circles (-•-•-•-) show the displacements of the particle at the angular increments $\theta = i\ \pi/6$, $i = 0, \ldots, 12$ and the squares (-■-■-■-) give the corresponding velocities. The phase difference between the vector drawn to the point with components (B_{11}, B_{12}) and the displacement vector is not constant. The constants are chosen as for Figure 1.7.1.

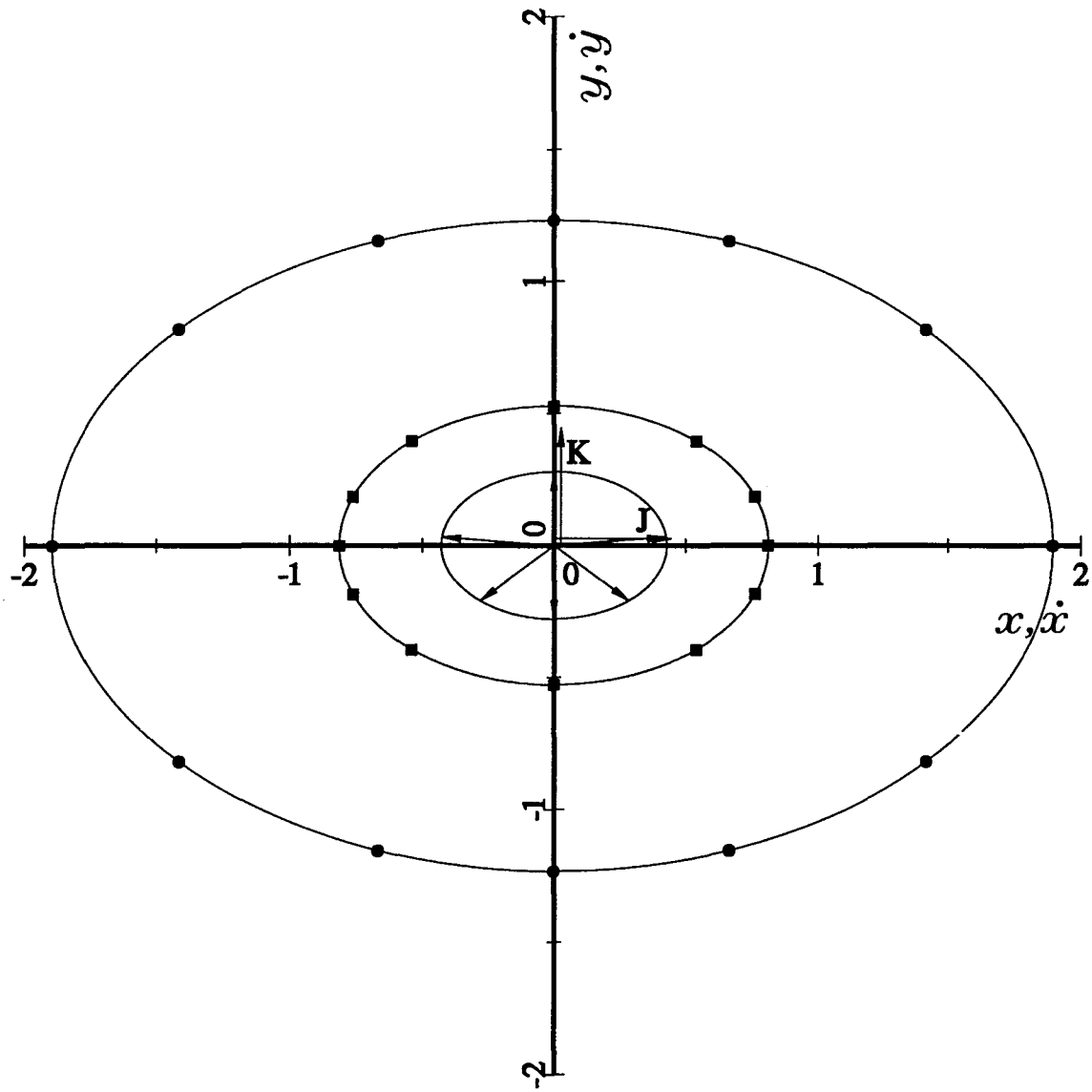


Figure 1.7.8. The elliptical oscillator orbit, elliptical velocity hodograph and the construction of the elliptical path described by the B_{12} and B_{22} components of the Lagrangian tensor with a selection of vectors drawn from the origin on the same set of axes as the displacement. The circles (-•-•-•-) show the displacements of the particle at the angular increments $\theta = i\ \pi/6$, $i = 0, \ldots, 12$ and the squares (-■-■-■-) give the corresponding velocities. The phase difference between the vector drawn to the point with components (B_{12}, B_{22}) and the displacement vector is not constant. The constants are chosen as for Figure 1.7.1.

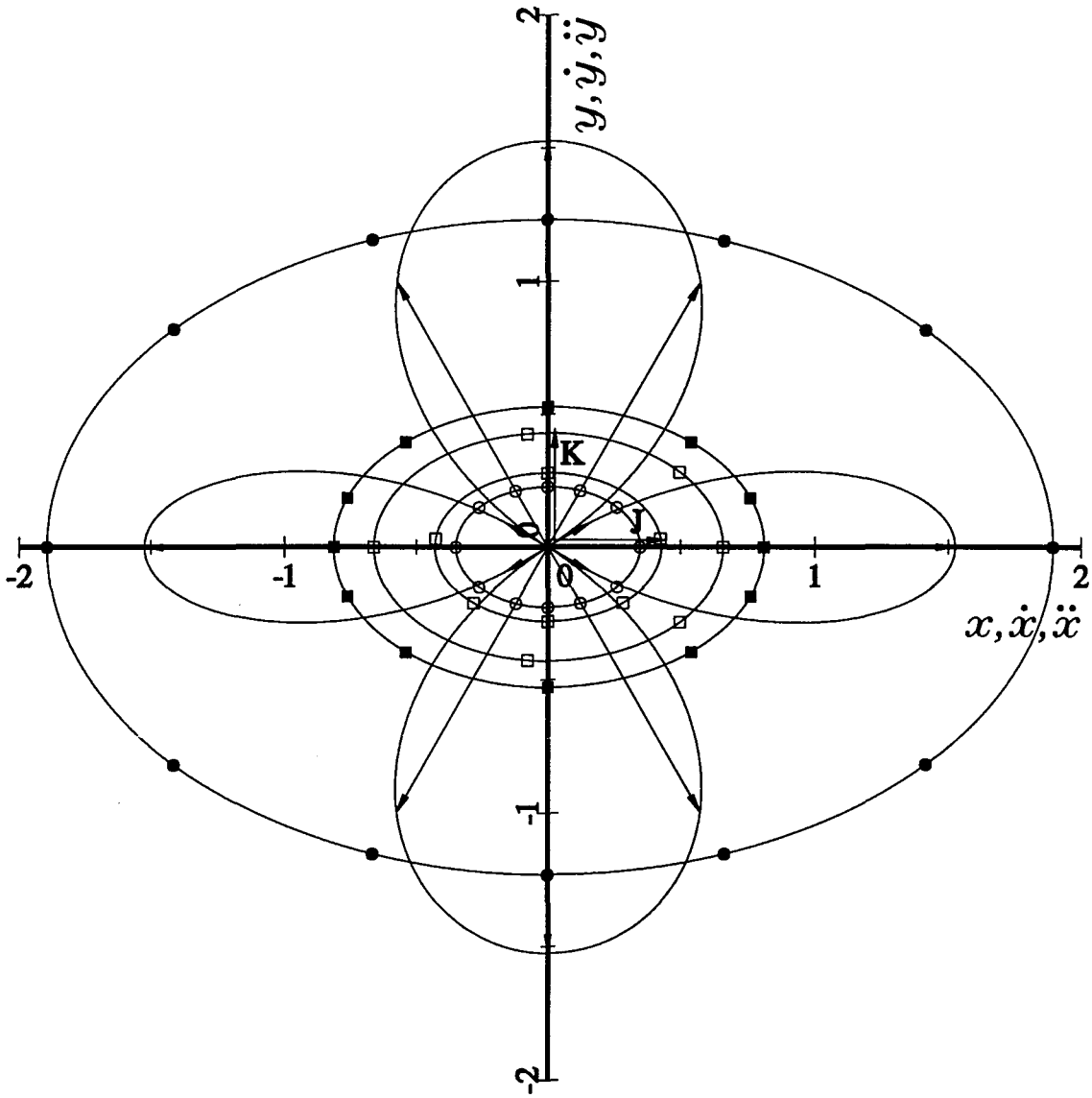


Figure 1.7.9. The elliptical oscillator orbit, velocity hodograph, acceleration hodograph, paths of the B_{11}, B_{12} and B_{12}, B_{22} components of the Lagrangian tensor and the construction of the path of the magnitude of the scalar Lagrangian in the direction of $\hat{\boldsymbol{r}}$ with a selection of vectors drawn from the origin on the same set of axes as the displacement. The circles (–●–●–●–) show the displacements of the particle at the angular increments $\theta = i\ \pi/6$, $i = 0, \ldots, 12$ and the squares (–■–■–■–) give the corresponding velocities. The unfilled circles (–o–o–o–) and the unfilled squares (–□–□–□–) show the corresponding points along the acceleration hodograph and the paths described by the components of the Lagrangian tensor respectively.

Figure 1.7.10 shows a family of geometric–centred oscillator ellipses with differing semi–major axis lengths and eccentricities. Figure 1.7.11 shows the relationship between the periodic time of the orbit and the semi–major axis length for the family of ellipses shown in Figure 1.7.10. Notice that the period is independent of the eccentricity as suggested by (1.7.48). In §2.17 other families of ellipses will be considered where the period of revolution depends on both the eccentricity and the length of the semi–major axis.

The angular motion in time is found by solving

$$\dot{\theta} = \frac{L}{r^2} = \frac{1}{L}\big(E - \lambda J \cos 2(\theta - \theta_0)\big). \tag{1.7.49}$$

For all cases of physical interest $E > \lambda J$ from (1.7.6) and, using G&R [43, 2.562.1],

$$\theta = \arctan\left(\frac{E - \lambda J}{E + \lambda J}\right)^{\frac{1}{2}} \tan\big(\lambda(t - t_0)\big) + \theta_0. \tag{1.7.50}$$

The analogues of Kepler's laws for the three–dimensional isotropic harmonic oscillator are :–

(i) The motion around the origin, which is the geometric centre, is elliptical. This is obvious from equation (1.7.16).

(ii) Equal areas are swept out by the radius vector in equal times. This is a consequence of equation (1.3.10) since $\boldsymbol{L}$ is constant.

(iii) The period of revolution is independent of the length of the semi–major axis and inversely proportional to the force constant λ. This is described by equation (1.7.48).

Since both the Kepler problem and the three–dimensional isotropic harmonic oscillator have elliptical orbits it is possible to make a comparison between the two. If we ignore the difference in location between the two ellipses and make the semi–major axis length and semi–minor axis length of both ellipses the same, we find that

$$\begin{aligned} a_k &= \frac{\mu}{-2E_k} = a_o = \frac{L_o}{\Big(E_o - \big(E_o{}^2 - \lambda^2 L_o{}^2\big)^{\frac{1}{2}}\Big)^{\frac{1}{2}}} \\ b_k &= \frac{L_k}{(-2E_k)^{\frac{1}{2}}} = b_o = \frac{L_o}{\Big(E_o + \big(E_o{}^2 - \lambda^2 L_o{}^2\big)^{\frac{1}{2}}\Big)^{\frac{1}{2}}}, \end{aligned} \tag{1.7.51}$$

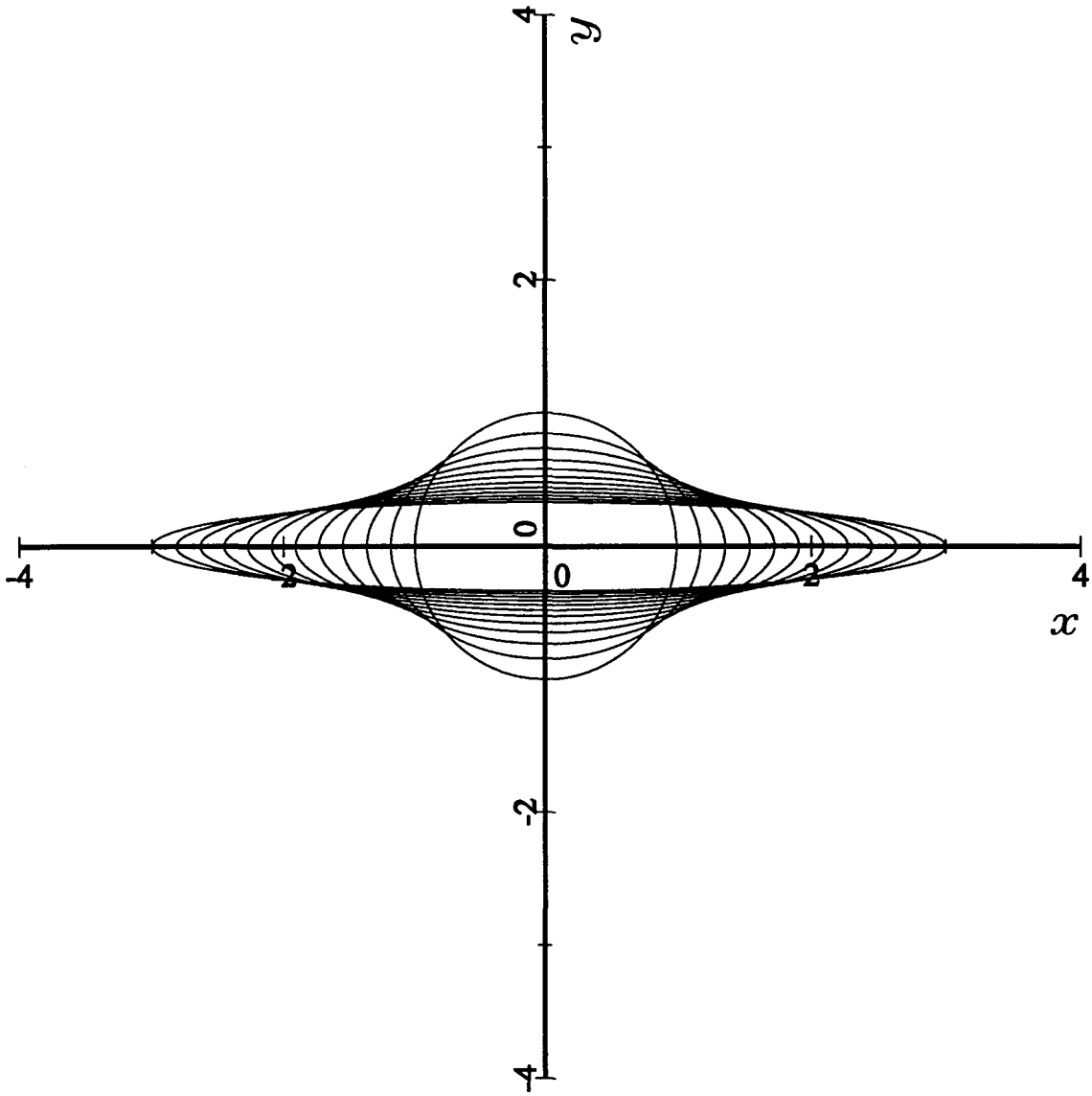


Figure 1.7.10. A family of oscillator orbital ellipses with differing semi–major axis lengths and eccentricities. The constants have the values $\lambda = 1$, $\theta_0 = 0$, $a = 2i/11+1$, $i = 0, \ldots, 11$, $L = 1$ and $E = \left(L^2/a^2 + \lambda^2 a^2\right)/2$.

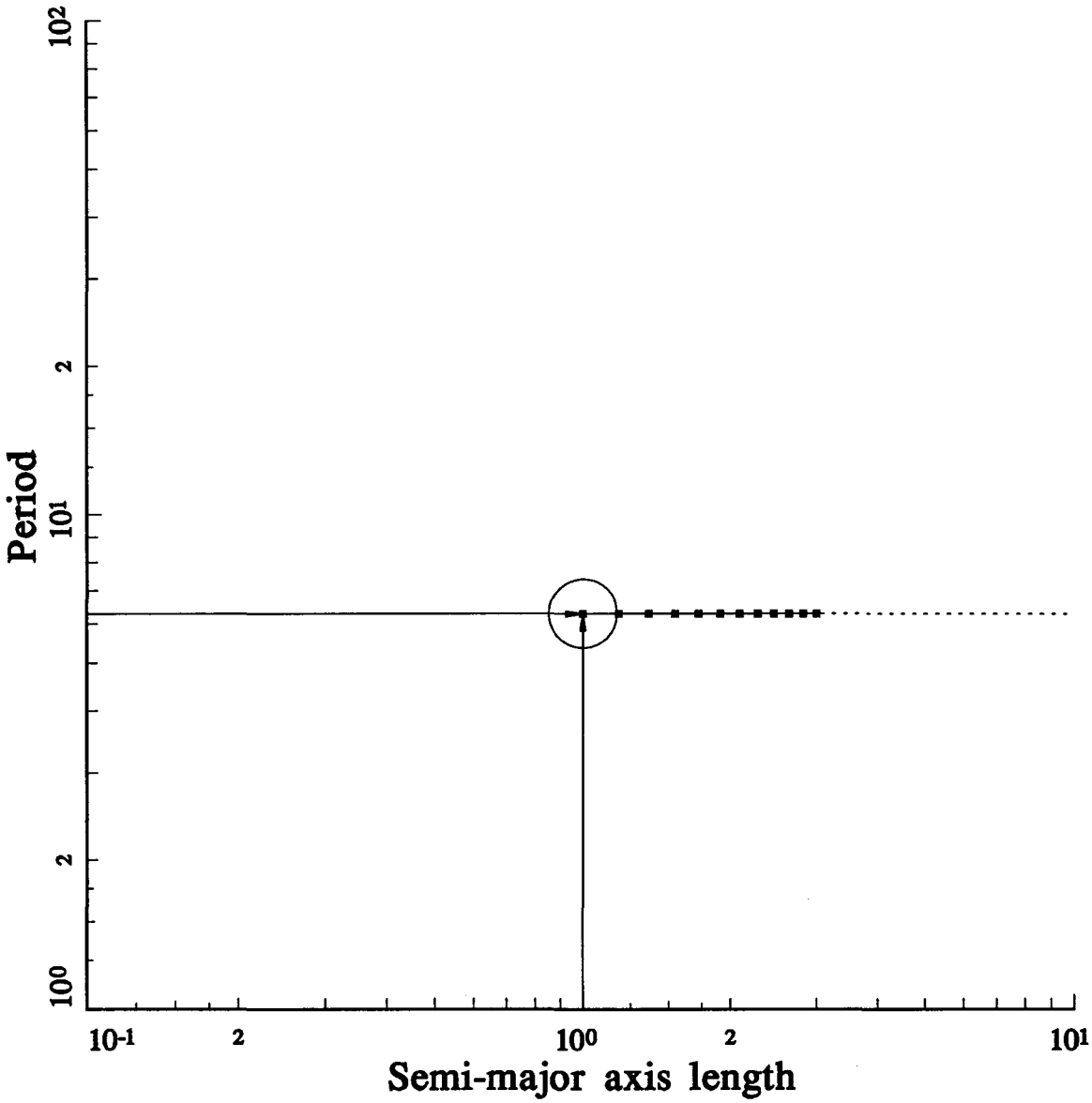


Figure 1.7.11. The periodic time versus the semi–major axis length for the family of oscillator orbital ellipses shown in Figure 1.7.10. The slope of the curve is 0 and the $y-$intercept is 2π, *i.e.* the period is constant at 2π. The period is independent of the eccentricity.

where the subscripts k and o correspond to the Kepler problem and the oscillator respectively. It is possible to solve the above equations for E_o in terms of E_k,

$$E_o = \frac{2{L_o}^2}{\mu^2}{E_k}^2 - \frac{{L_o}^2}{{L_k}^2}E_k, \tag{1.7.52}$$

and then using the expression for E_o (1.7.52) in (1.7.51) to obtain an expression for λ^2 in terms of E_k, *i.e.*,

$$\lambda^2 = \frac{-8{E_k}^3}{\mu^2}\left(\frac{L_o}{L_k}\right)^2 = \frac{\mu}{{a_k}^3}\left(\frac{L_o}{L_k}\right)^2. \tag{1.7.53}$$

If we set $L_o = L_k = L$, it is clear that the periodic time of the Kepler problem

$$\ddot{\boldsymbol{r}} + \frac{\mu}{r^3}\boldsymbol{r} = \boldsymbol{0} \tag{1.7.54}$$

is the same as that for the periodic time of the equivalent oscillator

$$\ddot{\boldsymbol{r}} + \frac{\mu}{a_k^3}\boldsymbol{r} = \boldsymbol{0}, \tag{1.7.55}$$

in which the magnitude of $\boldsymbol{r}$ in (1.7.54) has been replaced by the semi–major axis length of (1.7.54) to give (1.7.55). Equation (1.7.55) has a period given by (1.7.48), where λ is now $(\mu/a_k^3)^{\frac{1}{2}}$, and hence Kepler's third law follows, *i.e.*,

$$T = \frac{2\pi}{\lambda} = 2\pi\left(\frac{a_k^3}{\mu}\right)^{\frac{1}{2}}. \tag{1.7.56}$$

Figure 1.7.12 shows an elliptical oscillator orbit superimposed over the corresponding Kepler orbit. The constants are chosen according to equations (1.7.54) and (1.7.55) so that the orbits are the same size (ignoring the differences in origin) and have the same period. The symbols show the respective displacements at regular time intervals. The origins of the respective ellipses do not coincide which would of course violate Kepler's second law. Notice that the angular velocity is greater for the Kepler problem at $\theta = 0$ than for the oscillator, however, at $\theta = \pi$ the angular velocity for the oscillator is now larger. This should be obvious from the angular velocity expression $\dot{\theta} = L/r^2$ since in the first instance the radius for the Kepler problem is measured from the focus on the right and is thus smaller than the semi–major axis of the oscillator. In the second instance the radius for the Kepler problem is now larger, since it is still measured from the focus on the right, than the semi–major axis of the oscillator.

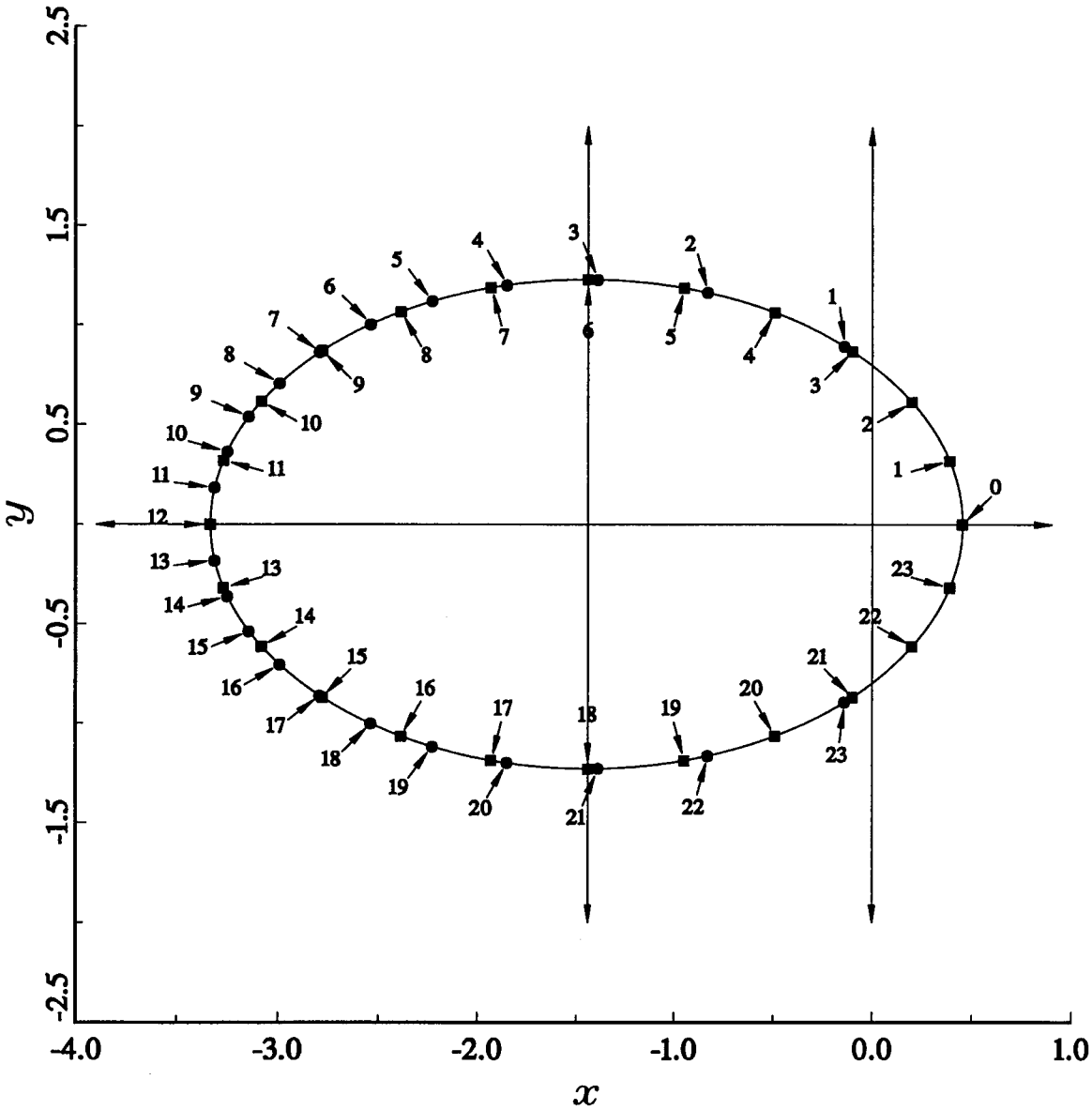


Figure 1.7.12. The elliptical oscillator orbit superimposed over the corresponding Kepler orbit. The circles (–•–•–•–) show the displacements of the Keplerian particle at the time intervals $iT/24$ (indicated by the numbered arrows) and the squares (–■–■–■–) the equivalent oscillator displacements for the same time intervals. The period T is 14.6479. Note that the origins do not coincide which would of course be a violation of Kepler's second law. The constants are chosen as for Figures 1.5.1 and 1.7.1.

1.8 The First Integrals Associated with the Self–Similar Symmetry

The results of §§1.8–1.9 are described in Gorringe and Leach [40]. In §4.3 it is shown that the equation of motion

$$\ddot{\boldsymbol{r}} + \mu r^{-\frac{2}{\alpha}} \boldsymbol{r} = \boldsymbol{0} \tag{1.8.1}$$

is invariant under the action of the symmetry generator

$$G_2 = t\frac{\partial}{\partial t} + \alpha r \frac{\partial}{\partial r} \tag{1.8.2}$$

in addition to the usual time and rotation symmetries. It is of interest to calculate the first integrals associated with (1.8.2) and thereby establish a connection with Hamilton–Jacobi theory.

For appropriate values of the constants μ and α, (1.8.1) includes the free particle and the three–dimensional isotropic harmonic oscillator, which have many more symmetries, and have already been studied in detail by Leach [72], Prince and Eliezer [109] and Gorringe and Leach [38]. We can therefore restrict our attention to cases where μ is non–zero and α is finite. On closer examination of (1.8.1), for $\alpha \neq 1$ and μ non–zero we obtain a Hamiltonian

$$H = \frac{1}{2}\boldsymbol{p}\cdot\boldsymbol{p} + \frac{\alpha\mu}{2\alpha - 2} r^{2-\frac{2}{\alpha}} \tag{1.8.3}$$

and in the case $\alpha = 1$, the logarithmic potential Hamiltonian

$$H = \frac{1}{2}\boldsymbol{p}\cdot\boldsymbol{p} + \mu \log r, \tag{1.8.4}$$

where the momentum canonically conjugate to $\boldsymbol{r}$ is $\boldsymbol{p} = \dot{\boldsymbol{r}}$, and for convenience the mass of the particle has been rescaled to unity. As the treatment of (1.8.3) and (1.8.4) is very similar, the details will be discussed in some detail for (1.8.3) and, where appropriate, just quoted for (1.8.4).

When $\alpha = \frac{2}{3}$, equation (1.8.1) describes the Kepler problem for which the relationship between the conserved energy, the angular momentum and Laplace–Runge–Lenz vectors and the Lie symmetries has been studied in some detail by Prince and Eliezer [110] and Leach [72]. Lévy–Leblond [82] has also obtained the Laplace–Runge–Lenz vector for the Kepler problem using a variation of Noether's theorem. In Chapter 2 (§§2.15 and 2.17) the link between the self–similar symmetry of the Kepler problem (1.8.2) and the period of elliptical motion is extended. It would thus seem sensible to investigate the first integrals for general α.

The Lie symmetry generator G can be written in plane polar coordinates as

$$G = \tau(t,r,\theta)\frac{\partial}{\partial t} + \xi(t,r,\theta)\frac{\partial}{\partial r} + \eta(t,r,\theta)\frac{\partial}{\partial \theta} \tag{1.8.5}$$

which has the first extension

$$G^{[1]} = G + (\dot{\xi} - \dot{r}\dot{\tau})\frac{\partial}{\partial \dot{r}} + (\dot{\eta} - \dot{\theta}\dot{\tau})\frac{\partial}{\partial \dot{\theta}}. \tag{1.8.6}$$

According to the Lie method as described in §P3.2, a function $I(t,r,\theta,\dot{r},\dot{\theta})$ which is associated with a symmetry G is a first integral if

$$G^{[1]}I = 0 \tag{1.8.7}$$

and

$$\left.\frac{\mathrm{d}I}{\mathrm{d}t}\right|_{\boldsymbol{E}=\boldsymbol{0}} = 0, \tag{1.8.8}$$

where $\boldsymbol{E}\,(t,r,\theta,\dot{r},\dot{\theta}) = \boldsymbol{0}$ is the equation of motion (1.8.1). Substituting the first extension (1.8.6) of the self–similar symmetry G_2 in (1.8.7) leads to the equation

$$t\,\frac{\partial I}{\partial t} + \alpha r\,\frac{\partial I}{\partial r} + 0\,\frac{\partial I}{\partial \theta} + (\alpha - 1)\dot{r}\,\frac{\partial I}{\partial \dot{r}} - \dot{\theta}\,\frac{\partial I}{\partial \dot{\theta}} = 0, \tag{1.8.9}$$

which gives the characteristics as solutions to the associated Lagrange's system

$$\frac{\mathrm{d}t}{t} = \frac{\mathrm{d}r}{\alpha r} = \frac{\mathrm{d}\theta}{0} = \frac{\mathrm{d}\dot{r}}{(\alpha-1)\dot{r}} = \frac{\mathrm{d}\dot{\theta}}{-\dot{\theta}}. \tag{1.8.10}$$

They are

$$\begin{aligned} u_1 &= rt^{-\alpha} \quad & v_1 &= \dot{r}t^{1-\alpha} \\ u_2 &= \theta & v_2 &= \dot{\theta}t, \end{aligned} \tag{1.8.11}$$

which are individually invariant under the infinitesimal transformation generated by $G^{[1]}$.

Rewriting I in terms of the characteristics and imposing the condition for a first integral (1.8.8) gives

$$\dot{u}_1\,\frac{\partial I}{\partial u_1} + \dot{u}_2\,\frac{\partial I}{\partial u_2} + \dot{v}_1\,\frac{\partial I}{\partial v_1} + \dot{v}_2\,\frac{\partial I}{\partial v_2} = 0. \tag{1.8.12}$$

The equation of motion (1.8.1) can be separated into radial and angular parts, which are

$$\ddot{r} = r\dot{\theta}^2 - \mu r^{1-\frac{2}{\alpha}} \qquad \ddot{\theta} = -2\dot{r}\dot{\theta}/r, \tag{1.8.13}$$

so that

$$\begin{aligned} \dot{u}_1 &= t^{-1}(v_1 - \alpha u_1) \quad & \dot{v}_1 &= t^{-1}\left[(1-\alpha)v_1 + u_1 v_2^2 - \mu u_1^{1-\frac{2}{\alpha}}\right] \\ \dot{u}_2 &= t^{-1} v_2 & \dot{v}_2 &= t^{-1}[v_2 - 2v_1 v_2/u_1], \end{aligned} \tag{1.8.14}$$

and so the characteristics of (1.8.12) are solutions of the associated Lagrange's system

$$\frac{\mathrm{d}u_1}{v_1 - \alpha u_1} = \frac{\mathrm{d}u_2}{v_2} = \frac{\mathrm{d}v_1}{(1-\alpha)v_1 + u_1 v_2^2 - \mu u_1^{1-\frac{2}{\alpha}}} = \frac{\mathrm{d}v_2}{v_2 - 2v_1 v_2/u_1} = \frac{\mathrm{d}t}{t}, \tag{1.8.15}$$

where the term $\mathrm{d}t/t$ has been added as an auxiliary variable (see Ince [55]). To solve (1.8.15) for the characteristics involves somewhat more complex combinations than were used to solve (1.8.10). It is convenient to label the ith member of (1.8.15) as (1.8.15.i, $i = 1, 5$).

The combination $\left(u_1 v_2^2 + \mu u_1^{1-\frac{2}{\alpha}}\right)$ (1.8.15.1) + v_1(1.8.15.3) + $u_1^2 v_2$(1.8.15.4) gives

$$\frac{\mathrm{d}\left[\frac{1}{2}\, v_1^2 + \frac{1}{2}\, u_1^2 v_2^2 + \frac{\alpha\mu}{2(\alpha-1)}\, u_1^{2-\frac{2}{\alpha}}\right]}{2(1-\alpha)\left[\frac{1}{2}\, v_1^2 + \frac{1}{2}\, u_1^2 v_2^2 + \frac{\alpha}{2(\alpha-1)}\, \mu u_1^{2-\frac{2}{\alpha}}\right]} = \frac{\mathrm{d}t}{t} \tag{1.8.16}$$

which can be easily integrated to give the first integral

$$w_1 = \left[\frac{1}{2}\, v_1^2 + \frac{1}{2}\, u_1^2 v_2^2 + \frac{\alpha\mu}{2(\alpha-1)}\, u_1^{2-\frac{2}{\alpha}}\right] t^{2(\alpha-1)}, \tag{1.8.17}$$

which in terms of the original variables becomes

$$w_1 = \frac{1}{2}\, \dot{r}^2 + \frac{1}{2}\, r^2\dot{\theta}^2 + \frac{\alpha\mu}{2(\alpha-1)}\, r^{2-\frac{2}{\alpha}}. \tag{1.8.18}$$

This is easily recognised as the conserved energy. For the case $\alpha = 1$ the last term of (1.8.18) is replaced by $\mu \log r$.

The combination $2u_1 v_2$(1.8.15.1) + u_1^2(1.8.15.4) reduces to

$$\frac{\mathrm{d}(u_1^2 v_2)}{(1-2\alpha)u_1^2 v_2} = \frac{\mathrm{d}t}{t} \tag{1.8.19}$$

which gives the second first integral

$$w_2 = u_1^2 v_2 t^{2\alpha-1} \tag{1.8.20}$$

or, in terms of the original variables,

$$w_2 = r^2\dot{\theta}, \tag{1.8.21}$$

the one component of the conserved angular momentum which we did not make zero when going from three dimensions to two dimensions. In three dimensions it would be easier to find the components of the angular momentum in cartesian components.

In the construction of both the energy and angular momentum first integrals, it has been necessary to introduce the auxiliary time variable t in (1.8.15.5). This has been due to a non–zero denominator in the left hand members of (1.8.16) and (1.8.19). One can in fact construct a zero denominator by taking the combination $t(1.8.15.1) - (v_1 - \alpha u_1)(1.8.15.5)$ which gives

$$\frac{t\mathrm{d}u_1 + \alpha u_1 \mathrm{d}t - v_1 \mathrm{d}t}{0}. \tag{1.8.22}$$

As the denominator is zero in (1.8.22) the numerator must be the differential of a characteristic up to an integrating factor. The characteristic remains obscure in its present form, but on multiplication of (1.8.22) by $t^{\alpha-1}(v_1 t^{\alpha-1})^{-1}$ it becomes

$$\frac{-\mathrm{d}t + [v_1 t^{\alpha-1}]^{-1}\mathrm{d}(u_1 t^{\alpha})}{0}. \tag{1.8.23}$$

On substituting for v_2 from (1.8.20) in (1.8.17), rearrangement gives

$$\left(v_1 t^{\alpha-1}\right)^2 = 2w_1 - \frac{w_2^2}{(u_1 t^{\alpha})^2} - \frac{\alpha\mu}{(\alpha-1)}\,(u_1 t^{\alpha})^{2-\frac{2}{\alpha}} \tag{1.8.24}$$

which gives the characteristic for (1.8.23) as

$$w_3 = -t + \int^{u_1 t^{\alpha}} \left[2w_1 - \frac{w_2^2}{\eta^2} - \frac{\alpha\mu}{\alpha-1}\,\eta^{2-\frac{2}{\alpha}}\right]^{-\frac{1}{2}} \mathrm{d}\eta. \tag{1.8.25}$$

Equation (1.8.25) can be rewritten in terms of the original coordinates to become

$$w_3 = -t + \int^{r} \left[2w_1 - \frac{w_2^2}{\eta^2} - \frac{\alpha\mu}{\alpha-1}\,\eta^{2-\frac{2}{\alpha}}\right]^{-\frac{1}{2}} \mathrm{d}\eta. \tag{1.8.26}$$

For the case $\alpha = 1$ the last term in crochets is replaced by $-2\mu \log \eta$.

In principle the solution of the orbit equation for the original equation of motion can be reduced to the quadrature

$$\theta = \int^{t} \frac{w_2}{r^2}\,\mathrm{d}t', \tag{1.8.27}$$

where r is replaced in (1.8.27) by $r(t)$ from (1.8.26). For general α the integral in (1.8.26) cannot be evaluated in closed form, but can be expressed in terms of elliptic or circular functions for the fourteen values of α given by Whittaker [129, §48 p80ff], Broucke [13] and Taff [123, p40].

1.9 The Connection with Hamilton–Jacobi Theory and with a Laplace–Runge–Lenz Vector Analogue

It is interesting to note that (1.8.26) is reminiscent of Hamilton's characteristic function of Hamilton–Jacobi theory. For the Hamiltonian (1.8.3) (or using the relevant substitution for (1.8.4)) the solution to the Hamilton Jacobi equation

$$\frac{1}{2}\left[\left(\frac{\partial S}{\partial r}\right)^2+\frac{1}{r^2}\left(\frac{\partial S}{\partial \theta}\right)^2+\frac{\alpha\mu}{\alpha-1}\,r^{2-\frac{2}{\alpha}}\right]+\frac{\partial S}{\partial t}=0 \tag{1.9.1}$$

is, in the notation of this paper,

$$\begin{aligned} S(r,\theta,t) = -w_1 t \;&+\; \int^r \left[2w_1-\frac{w_2^2}{\eta^2}-\frac{\alpha\mu}{\alpha-1}\,\eta^{2-\frac{2}{\alpha}}\right]^{\frac{1}{2}} \mathrm{d}\eta \\ &+\; w_2\theta. \end{aligned} \tag{1.9.2}$$

Clearly (1.9.1) is cyclic in θ and so (1.9.2) is linear in θ. Now,

$$w_3=\frac{\partial S}{\partial w_1} \tag{1.9.3}$$

is a constant as predicted by the theory. In using the symmetries of the differential equation (1.8.1) we have used the following argument, albeit by roundabout means. If w_3 is a constant we may write

$$w_3=-t+\int^t \mathrm{d}t. \tag{1.9.4}$$

Now $\mathrm{d}t=\mathrm{d}r(\mathrm{d}t/\mathrm{d}r)=\mathrm{d}r/\dot{r}$, and so (1.9.4) becomes

$$w_3=-t+\int^r \frac{\mathrm{d}r}{\dot{r}} \tag{1.9.5}$$

and (1.8.26) follows since $\dot{r}$ can be expressed in terms of w_1, w_2 and r.

As yet we have still to consider analogues of the Laplace–Runge–Lenz vector stemming from G_2. For this purpose it is more appropriate to use the cartesian representation of (1.8.2)

$$G_2=t\frac{\partial}{\partial t}+\alpha\left(x\frac{\partial}{\partial x}+y\frac{\partial}{\partial y}\right). \tag{1.9.6}$$

If we consider the case $\alpha=\frac{2}{3}$ which is the Kepler problem, the characteristics arising from (1.8.7) are

$$\begin{aligned} u_1 &= xt^{-\frac{2}{3}} \qquad v_1=\dot{x}t^{\frac{1}{3}} \\ u_2 &= yt^{-\frac{2}{3}} \qquad v_2=\dot{y}t^{\frac{1}{3}}, \end{aligned} \tag{1.9.7}$$

and the corresponding Lagrange's system arising from (1.8.8) is

$$\frac{\mathrm{d}u_1}{v_1 - \frac{2}{3}u_1} = \frac{\mathrm{d}u_2}{v_2 - \frac{2}{3}u_2} = \frac{\mathrm{d}v_1}{\frac{1}{3}v_1 - \mu u_1 P^{-3}} = \frac{\mathrm{d}v_2}{\frac{1}{3}v_2 - \mu u_1 P^{-3}} = \frac{\mathrm{d}t}{t}, \tag{1.9.8}$$

where $P^2 = u_1^2 + u_2^2$. Using the same numbering convention as for (1.8.15) the combination $(v^2 - \mu u_2^2 P^{-3})(1.9.8.1) - (v_1 v_2 - \mu u_1 u_2 P^{-3})(1.9.8.2) - u_2 v_2(1.9.8.3) + (2u_1 v_2 - u_2 v_1)(1.9.8.4)$ gives

$$\frac{\mathrm{d}(u_1 v_2^2 - u_2 v_1 v_2 - \mu u_1 P^{-1})}{0} \tag{1.9.9}$$

and so the characteristic is

$$\begin{aligned} w_4 &= (u_1 v_2 - u_2 v_1)v_2 - \frac{\mu u_1}{P} \\ &= (x\dot{y} - y\dot{x})\dot{y} - \frac{\mu x}{r} \end{aligned} \tag{1.9.10}$$

which is readily recognized as one of the components of the Laplace–Runge–Lenz vector in two dimensions. The combination $-(v_1 v_2 - \mu u_1 u_2 P^{-3})(1.9.8.1) + (v_1^2 - \mu u_1^2 P^{-3})(1.9.8.2) - (u_1 v_2 - 2u_2 v_1)(1.9.8.3) - u_1 v_1(1.9.8.4)$ gives the other component

$$\begin{aligned} w_5 &= -(u_1 v_2 - u_2 v_1)v_2 - \frac{\mu u_2}{P} \\ &= -(x\dot{y} - y\dot{x})\dot{x} - \frac{\mu y}{r}. \end{aligned} \tag{1.9.11}$$

The virtues of the Laplace–Runge–Lenz vector have been explained at length. However, it is not vital for the integration of (1.8.1) (see Kaplan [59]). For general α an analogue of the Laplace–Runge–Lenz vector will certainly not be quadratic in the velocity. The reason for this is simple. Ignoring the free particle and the three–dimensional isotropic harmonic oscillator, the only central force problem apart from the Kepler problem which admits a second integral quadratic in the velocity is in the case $\alpha = \frac{1}{2}$. This can be shown as follows. The Hamiltonian (see Leach [73])

$$H = \frac{1}{2}\boldsymbol{p}\cdot\boldsymbol{p} - \frac{1}{2}\frac{\ddot{\rho}}{\rho}r^2 + \frac{1}{\rho^2}U\left(\frac{r}{\rho}\right), \tag{1.9.12}$$

where $\rho = \rho(t)$ is an arbitrary function of time and U an arbitrary function of its argument, has a first integral which is quadratic in the velocity given by

$$I = \frac{1}{2}(\rho p_r - \dot{\rho}r)^2 + \frac{1}{2}r^{-2}p_\theta^2\rho^2 + U\left(\frac{r}{\rho}\right). \tag{1.9.13}$$

When $\alpha = \frac{1}{2}$, (1.8.3) becomes

$$H = \frac{1}{2}\boldsymbol{p}\cdot\boldsymbol{p} - \frac{1}{2}\mu r^{-2}. \tag{1.9.14}$$

The potential in (1.9.14) can be obtained from that in (1.9.12) in two ways: (i) set $\rho = 1$, $U = -\frac{1}{2}\,\mu r^{-2}$ and (ii) let $U = -\frac{1}{2}\,\mu(r/\rho)^{-2} - \frac{1}{8}(r/\rho)^2$ and set $\ddot{\rho}/\rho + 1/(4\rho^4) = 0$, *i.e.*, $\rho = t^{\frac{1}{2}}$. Corresponding to (i) there is the usual energy integral, but for (ii) we obtain

$$\begin{aligned} w_6 &= tw_1 - \frac{1}{2}\,r\dot{r} \\ &= -w_1 w_3 \end{aligned} \tag{1.9.15}$$

which can be verified from (1.8.26) with $\alpha = \frac{1}{2}$. The choice of $U(r/\rho)$ and the solution $\rho = r^{\frac{1}{2}}$ have been constructed to give w_6 in terms of w_1 and w_3. The case $\alpha = \frac{1}{2}$ is a particular example from the class of monopole problems for which the symmetry algebra is $sl(2,R) \oplus so(3)$ (see §4.3). The additional symmetry gives rise to an integral which is quadratic in t, but, as one would expect, it is not algebraically independent of w_1, w_2 or w_3.

Thus it can be seen that for a general central force power law the additional symmetry generator gives rise to the usual laws of energy and angular momentum, as well as a time–dependent first integral from the Hamilton–Jacobi equation, which involves the other two first integrals. It would appear that, in the case of the Kepler problem when $\alpha = \frac{2}{3}$, the existence of a Laplace–Runge–Lenz vector is anomolous in the wider context of the general central force power law, although various analogues are known for other types of force laws as will be demonstrated in Chapters 2 and 3. For general α it would appear that no such conserved quantity which is quadratic in the velocities does exist, although there is a possibility of a non–autonomous first integral being present.

1.10 The Conserved Hamilton and Laplace–Runge–Lenz Vector Analogues for the Non–Autonomous Equation of Motion $\ddot{\boldsymbol{r}} + f(r,\theta,t)\boldsymbol{r} = \boldsymbol{0}$

Using a direct method Katzin and Levine [61] and Leach [73], using a variant of Noether's theorem, have shown that a time–dependent central force

$$\ddot{\boldsymbol{r}} = F(r,t)\hat{\boldsymbol{r}}, \tag{1.10.1}$$

admits a time–dependent vector first integral of the form

$$\boldsymbol{J} = U(r,t)(\boldsymbol{L}\times\dot{\boldsymbol{r}}) + Z(r,t)(\boldsymbol{L}\times\boldsymbol{r}) + W(r,t)\boldsymbol{r} \tag{1.10.2}$$

provided

$$\begin{aligned} U &= u(t) \neq 0 \\ Z &= -\dot{u}(t) \\ W &= \frac{\mu}{r} \\ F &= \left(\frac{\ddot{u}r}{u}\right) - \left(\frac{\mu}{ur^2}\right). \end{aligned} \tag{1.10.3}$$

The system described by (1.10.1) and (1.10.3) encompasses both a time–dependent Kepler type problem, when $\mu = 1$ and $u = (\alpha t + \beta)/\lambda$, with α, β and λ all constant (which has been also been studied by Katzin and Levine [60]), and a particular case of the time–dependent harmonic oscillator, when $\mu = 0$, which has been solved in one dimension using Kruskal's method, by Lewis [83, 84]. Lewis and Riesenfeld [86] using a noncanonical transformation to a time–dependent harmonic oscillator have constructed an invariant for a charged particle moving in a time–dependent electromagnetic field. Other techniques which have been developed to construct invariants for explicitly time–dependent classical Hamiltonians are those of Lewis and Leach [85], and also Moreira [98, 99]. Günther and Leach [46] extended these results to include the three–dimensional isotropic time–dependent harmonic oscillator and, generalising the invariant found by Lewis [83, 84] to three dimensions, discovered a tensor invariant analogous to the Jauch–Hill–Fradkin tensor for the time independent oscillator. It is also interesting to note that in the case $\mu = 0$, (1.10.1) with (1.10.3) has both a tensor analogue as described by Günther and Leach [46] as well as a Laplace–Runge–Lenz analogue which is described below. In the case of the three–dimensional isotropic harmonic oscillator, the conserved tensor is obtained using elementary operations on the

equation of motion whereas the Laplace–Runge–Lenz analogue is arrived at by rather contrived manipulations. For this particular time–dependent case ($\mu = 0$), however, the Laplace–Runge–Lenz vector is obtained naturally and the tensor is obtained in a more involved fashion, as is the case in the Kepler problem.

Previous techniques for solving (1.10.1) with (1.10.3) have been algebraically rather complex, as is usual in a direct approach. The approach adopted below is algebraically much simpler and involves only simple vector manipulations of the equation of motion. The technique of solution is an appropriate generalization of the work of Collinson [21, 22] on the Kepler problem and in the spirit of the work of Sarlet and Bahar [115] on a variety of classical systems. The results of section §§1.10–1.12 are described in Gorringe and Leach [34, 36] and Leach and Gorringe [77].

The first integrals and orbit equation for the dynamical system described by the Newtonian equation of motion $\ddot{\boldsymbol{r}} = \ddot{g}\boldsymbol{r}/g - \mu\boldsymbol{r}/(gr^3)$ are derived and also generalised. The algebraic properties of the integrals with respect to the Poisson Bracket are also given.

Let us consider the equation of motion

$$\ddot{\boldsymbol{r}} + f(r, \theta, t)\boldsymbol{r} = \boldsymbol{0} \tag{1.10.4}$$

for which (1.10.1) combined with (1.10.3) is a special case. It is a simple matter to establish the conservation of angular momentum directly from the equation of motion. Taking the vector product of $\boldsymbol{r}$ with (1.10.4) gives the angular momentum first integral

$$\boldsymbol{L} = \boldsymbol{r} \times \dot{\boldsymbol{r}}. \tag{1.10.5}$$

The construction of a Hamilton–like vector for (1.10.4) is slightly more involved. It is possible to integrate (1.10.4) to obtain a Hamilton vector analogue provided we can find an integrating factor g. Writing

$$g\ddot{\boldsymbol{r}} = (g\dot{\boldsymbol{r}} - \dot{g}\boldsymbol{r})^{\cdot} + \ddot{g}\boldsymbol{r} \tag{1.10.6}$$

and multiplying (1.10.4) by g we see that

$$(g\dot{\boldsymbol{r}} - \dot{g}\boldsymbol{r})^{\cdot} + (\ddot{g} + gf)\boldsymbol{r} = \boldsymbol{0}. \tag{1.10.7}$$

For a conserved vector other than the angular momentum to exist, it must be possible to express the second term of (1.10.7) as a quadrature. The presence of $\hat{\boldsymbol{r}}$ which is a function of θ signals the requirement that

$$(\ddot{g} + gf)r = v(\theta)\dot{\theta}, \tag{1.10.8}$$

for some function $v(\theta)$. Making use of the expression for the magnitude of the angular momentum $L = r^2\dot{\theta}$, (1.10.8) becomes

$$(\ddot{g} + gf)r^3 = Lv(\theta) \tag{1.10.9}$$

from which it follows upon rearrangement that

$$f = \frac{Lv(\theta)}{gr^3} - \frac{\ddot{g}}{g}. \tag{1.10.10}$$

Since f was assumed to be a function of r, θ and t to begin with, we conclude that $g = g(t)$. Replacing f in (1.10.4) using (1.10.10) we obtain

$$\ddot{\boldsymbol{r}} + \frac{Lv(\theta)}{g(t)r^3}\boldsymbol{r} - \frac{\ddot{g}(t)}{g(t)}\boldsymbol{r} = \boldsymbol{0} \tag{1.10.11}$$

where L is treated as a constant in the equation of motion although it is expressed as $r^2\dot{\theta}$ during calculations. Consequently the equation of motion (1.10.11) possesses the Hamilton–like vector

$$\boldsymbol{K} = g\dot{\boldsymbol{r}} - \dot{g}\boldsymbol{r} + z'(\theta)\hat{\boldsymbol{r}} - z(\theta)\hat{\boldsymbol{\theta}} \tag{1.10.12}$$

where $z(\theta)$ and $z'(\theta)$ are given by (1.1.19) and (1.1.20) as described in detail in §1.1. The Laplace–Runge–Lenz analogue is given by

$$\begin{aligned} \boldsymbol{J} &= \boldsymbol{K} \times \hat{\boldsymbol{L}} \\ &= (g\dot{\boldsymbol{r}} - \dot{g}\boldsymbol{r}) \times \hat{\boldsymbol{L}} - z(\theta)\hat{\boldsymbol{r}} - z'(\theta)\hat{\boldsymbol{\theta}}. \end{aligned} \tag{1.10.13}$$

1.11 The Orbit Equation

Due to the presence of $\boldsymbol{r}$ in the Hamilton–like vector $\boldsymbol{K}$ it does not appear possible to express the velocity hodograph in any recognisable or useful form.

The orbit equation is obtained in the usual way by taking the scalar product of $\boldsymbol{J}$ (1.10.13) with $\boldsymbol{r}$ which gives

$$r(\theta) = \frac{Lg(t)}{z(\theta) + J\cos(\theta - \theta_0)}. \tag{1.11.1}$$

Unfortunately (1.11.1) contains an explicit function of time and consequently is not the required orbit equation. To obtain the orbit equation the function of time is eliminated as follows. Using the expression for the angular momentum

$$L = r^2\,\frac{\mathrm{d}\theta}{\mathrm{d}t} = \frac{L^2g^2(t)}{(z(\theta) + J\cos(\theta - \theta_0))^2}\,\frac{\mathrm{d}\theta}{\mathrm{d}t}, \tag{1.11.2}$$

equation (1.11.2) can be rearranged and integrated to give

$$\int_0^t \frac{\mathrm{d}t}{g^2(t)} = \int_{\theta_0}^{\theta} \frac{L\mathrm{d}\theta}{(z(\theta) + J\cos(\theta - \theta_0))^2}. \tag{1.11.3}$$

If we further assume that (1.11.3) can be inverted to give

$$t = N(\theta) \tag{1.11.4}$$

which, from the implicit function theorem, is the case provided the integrands are continuous and non–zero, we can rewrite (1.11.1) using (1.11.4) as

$$r(\theta) = \frac{Lg \circ N(\theta)}{z(\theta) + J\cos(\theta - \theta_0)}, \tag{1.11.5}$$

where $g \circ N$ represents the composition of the functions g and N.

1.12 Examples

1.) $v(\theta) = 0$
The equation of motion (1.10.11) can be written as

$$\ddot{\boldsymbol{r}} = \frac{\ddot{g}}{g}\boldsymbol{r}. \tag{1.12.1}$$

The conserved vectors are given by (1.10.12) and (1.10.13)

$$\begin{aligned} \boldsymbol{K} &= g\dot{\boldsymbol{r}} - \dot{g}\boldsymbol{r} \\ \boldsymbol{J} &= (g\dot{\boldsymbol{r}} - \dot{g}\boldsymbol{r}) \times \hat{\boldsymbol{L}}. \end{aligned} \tag{1.12.2}$$

The following energy–like first integral can also be constructed

$$\begin{aligned} I &= \frac{1}{2}\boldsymbol{K} \cdot \boldsymbol{K} \\ &= \frac{1}{2}(g\dot{\boldsymbol{r}} - \dot{g}\boldsymbol{r})^2. \end{aligned} \tag{1.12.3}$$

The Hamiltonian for this system is given by

$$H = \frac{1}{2}\boldsymbol{p}^2 - \frac{\ddot{g}}{2g}r^2. \tag{1.12.4}$$

The orbit equation is given by (1.11.5)

$$r(\theta) = \frac{Lg \circ N(\theta)}{J\cos(\theta - \theta_0)}. \tag{1.12.5}$$

Now using (1.11.3)

$$\int_0^t \frac{\mathrm{d}t}{g^2(t)} = M(t) = \int_{\theta_0}^{\theta} \frac{L\mathrm{d}\theta}{J^2\cos^2(\theta-\theta_0)} = \frac{L\tan(\theta-\theta_0)}{J^2} \tag{1.12.6}$$

and so the orbit equation can be written as

$$r(\theta) = \frac{Lg \circ M^{-1} \circ (L\tan(\theta-\theta_0)/J^2)}{J\cos(\theta-\theta_0)}. \tag{1.12.7}$$

2.) $v(\theta) = \mu/L$

The equation of motion (1.10.11) can be written as

$$\ddot{\boldsymbol{r}} = \frac{\ddot{g}}{g}\boldsymbol{r} - \frac{\mu}{gr^3}\boldsymbol{r}. \tag{1.12.8}$$

The conserved vectors are given by (1.10.12) and (1.10.13)

$$\begin{aligned} \boldsymbol{K} &= g\dot{\boldsymbol{r}} - \dot{g}\boldsymbol{r} - \frac{\mu}{L}(\hat{\boldsymbol{\theta}} - \hat{\boldsymbol{\theta}}_0) \\ \boldsymbol{J} &= (g\dot{\boldsymbol{r}} - \dot{g}\boldsymbol{r}) \times \hat{\boldsymbol{L}} - \frac{\mu}{L}(\hat{\boldsymbol{r}} - \hat{\boldsymbol{r}}_0), \end{aligned} \tag{1.12.9}$$

where $\boldsymbol{J}$ in (1.12.9) agrees with (1.10.2) up to an additive constant term after scaling. The energy–like first integral is given by

$$\begin{aligned} I &= \frac{1}{2}\boldsymbol{K}\cdot\boldsymbol{K} \\ &= \frac{1}{2}(g\dot{\boldsymbol{r}} - \dot{g}\boldsymbol{r})^2 - \frac{\mu g}{r} \end{aligned} \tag{1.12.10}$$

up to an additive constant where, in order to simplify things, any constant terms in $\boldsymbol{K}$ have been neglected. The Hamiltonian for this system is given by

$$H = \frac{1}{2}\boldsymbol{p}^2 - \frac{\ddot{g}}{2g}r^2 - \frac{\mu}{gr}. \tag{1.12.11}$$

The orbit equation is given by (1.11.5)

$$r(\theta) = \frac{L^2 g \circ N(\theta)}{\mu + (JL-\mu)\cos(\theta-\theta_0)}. \tag{1.12.12}$$

In Leach [73] a simple example of an orbit was computed for

$$g(t) = (a + b\cos t)^{\frac{1}{2}}. \tag{1.12.13}$$

Rather more complex orbits are shown in the figures below. The function $g(t)$ is

$$g(t) = (a + b\cos(t/2))^{\frac{1}{2}}, \tag{1.12.14}$$

with $a^2 > b^2$ and $\mu^2 > (JL - \mu)^2$ which in terms of θ gives using G&R [43, 2.553.3 case $a^2 > b^2$ and 2.554.3]

$$u(t) = a^{\frac{1}{2}}\left[1 + k\cos\left(2\arctan\left(\left(\frac{1+k}{1-k}\right)^{\frac{1}{2}}\tan\left(\frac{a(1-k^2)^{\frac{1}{2}}L^3}{4\mu^2(1-l^2)}\left(\frac{-l\sin(\theta-\theta_0)}{1+l\cos(\theta-\theta_0)}\right.\right.\right.\right.\right.$$
$$\left.\left.\left.\left.\left.+\frac{2}{(1-l^2)^{\frac{1}{2}}}\arctan\left(\left(\frac{1-l}{1+l}\right)^{\frac{1}{2}}\tan\left(\frac{1}{2}(\theta-\theta_0)\right)\right)\right)\right)\right)\right)\right]^{\frac{1}{2}}, \qquad (1.12.15)$$

where $b = ka$ and $J = \mu(1 + l)/L$. The figures described below have all been made to close by adjusting the value of L. Figure 1.12.1 shows a simple orbit and Figure 1.12.2 is the corresponding velocity hodograph. Figure 1.12.3 is a more complicated orbit and Figure 1.12.4 is the corresponding velocity hodograph. Figure 1.12.5 is a more erratic orbit with the velocity hodograph shown in Figure 1.12.6.

As the mass has been taken as unity we may identify the momentum $\boldsymbol{p}$ with $\dot{\boldsymbol{r}}$. Calculating the Poisson Bracket relations (a task made easier using a simple REDUCE [112] procedure) we find for both Examples 1 and 2 that

$$[L_i, L_j]_{PB} = \varepsilon_{ijk}L_k$$
$$[J_i, J_j]_{PB} = (-2I)\varepsilon_{ijk}L_k$$
$$[J_i, L_j]_{PB} = \varepsilon_{ijk}J_k$$
$$[L_i, H]_{PB} = 0$$
$$[J_i, I]_{PB} = 0, \qquad (1.12.16)$$

where the Hamiltonian is given by (1.12.4) for Example 1 and (1.12.11) for Example 2. Thus the Hamiltonian has the symmetry group $so(3)$ and the symmetry group $so(4)$ of the time–independent Kepler problem has been transferred to the energy–like first integral I.

3.) One other related system for which an energy–like integral can also be found is given by the equation of motion

$$\ddot{\boldsymbol{r}} = \frac{\ddot{g}}{g}\boldsymbol{r} - \frac{\mu}{g^3 r}\boldsymbol{r}. \qquad (1.12.17)$$

Taking the scalar product of $g \times$ (1.12.17) with $(g\dot{\boldsymbol{r}} - \dot{g}\boldsymbol{r})$ and integrating gives

$$I = \frac{1}{2}(g\dot{\boldsymbol{r}} - \dot{g}\boldsymbol{r})^2 + \frac{\mu r}{g}. \qquad (1.12.18)$$

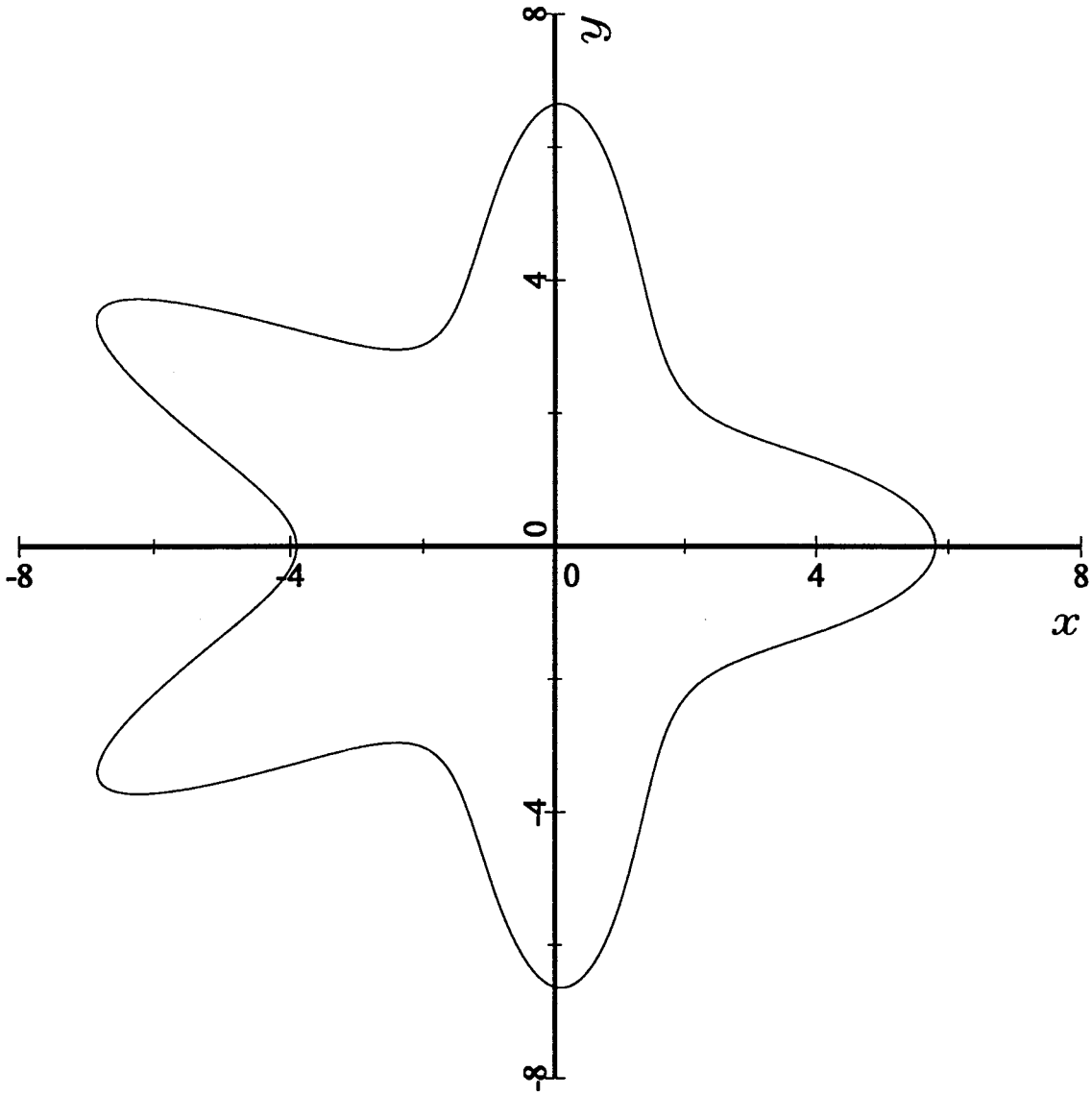


Figure 1.12.1. The orbit for $\mu = 1$, $a = 1$, $b = 0.6$, $\theta_0 = 0$, $K = J = 0.5$ and $L = 2.295$ which was selected to close the orbit.

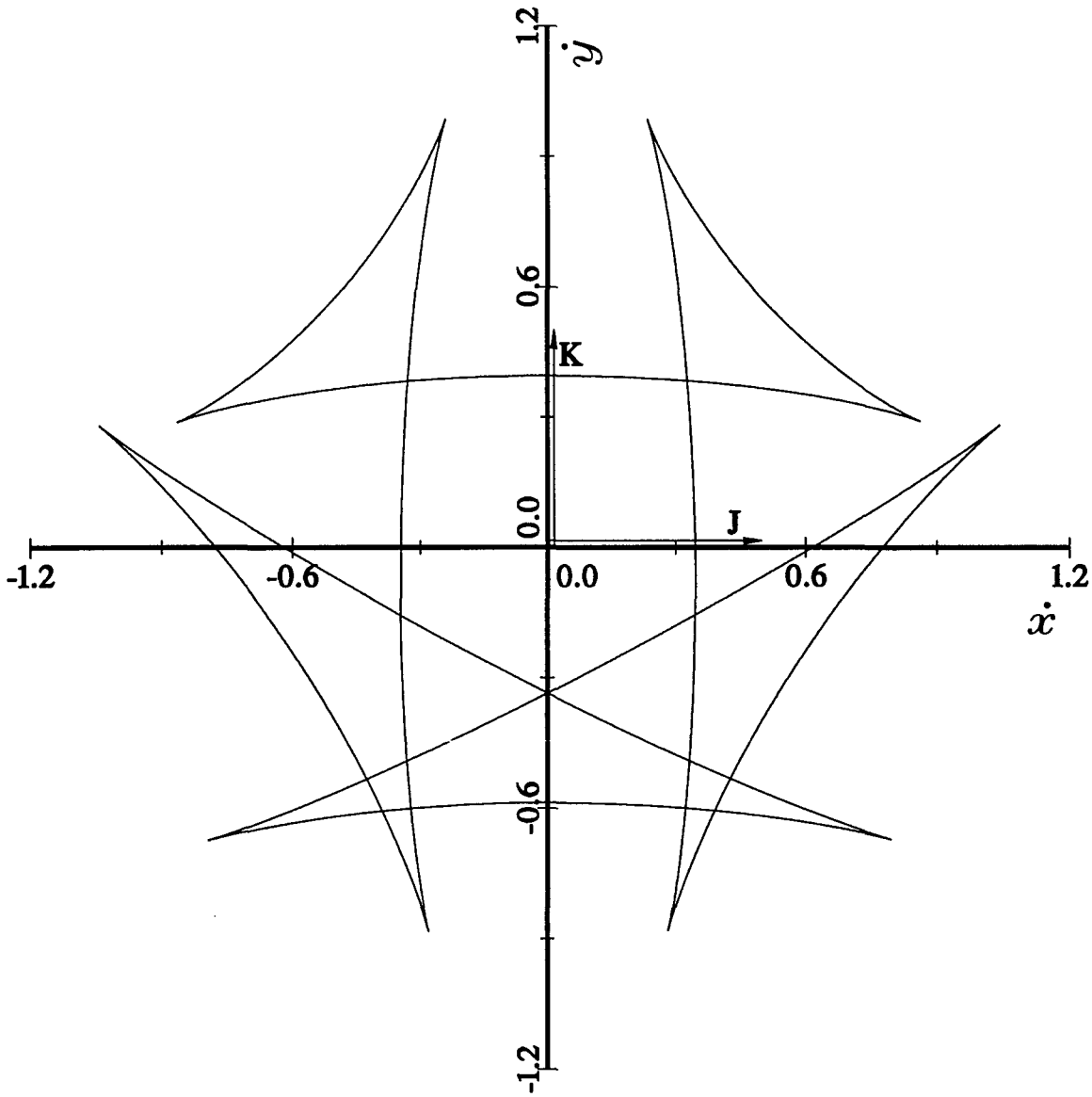


Figure 1.12.2. The velocity hodograph associated with Figure 1.12.1.

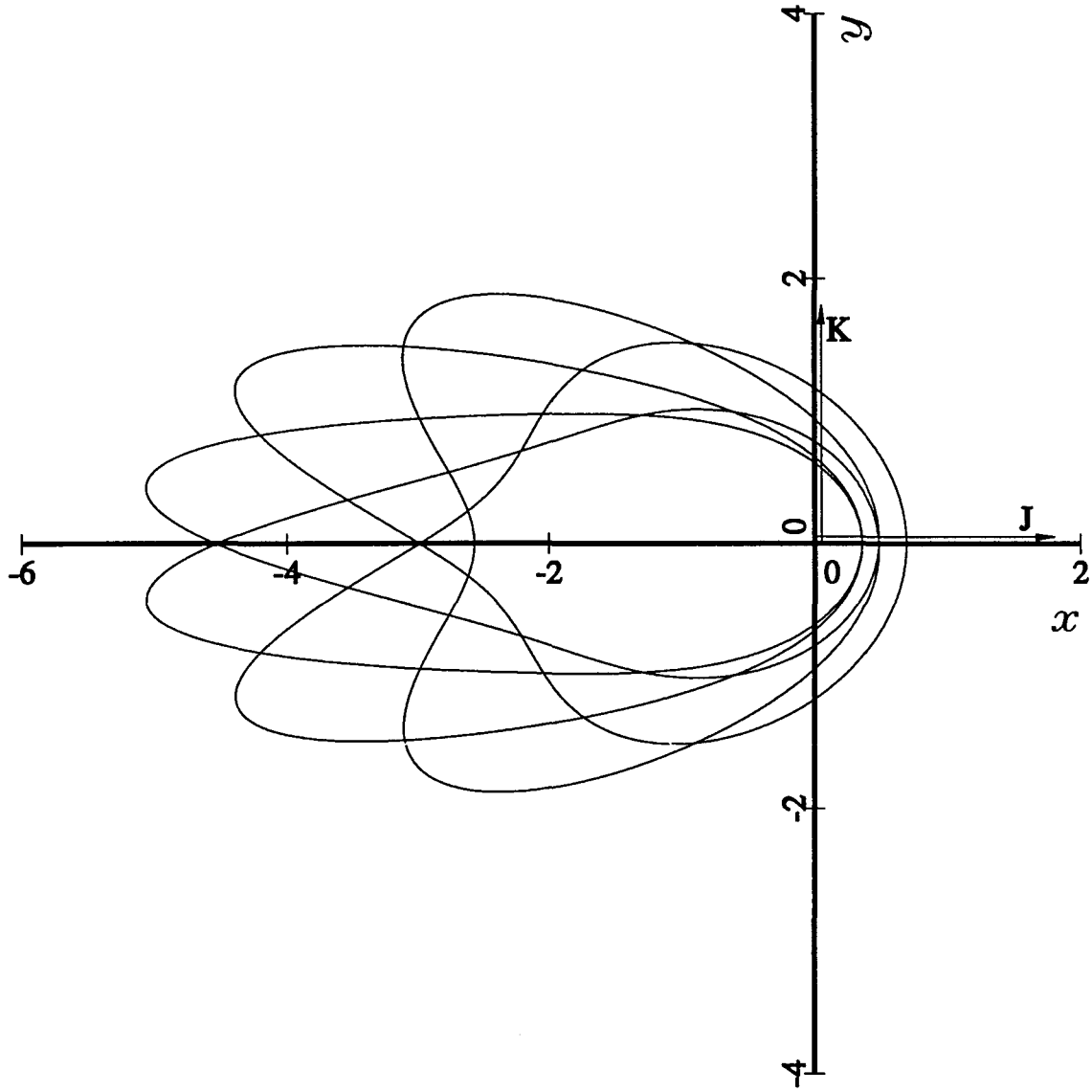


Figure 1.12.3. The orbit for $\mu = 1$, $a = 1$, $b = 0.6$, $\theta_0 = 0$, $K = J = 1.8$ and $L = 0.9799$ which was selected to close the orbit.

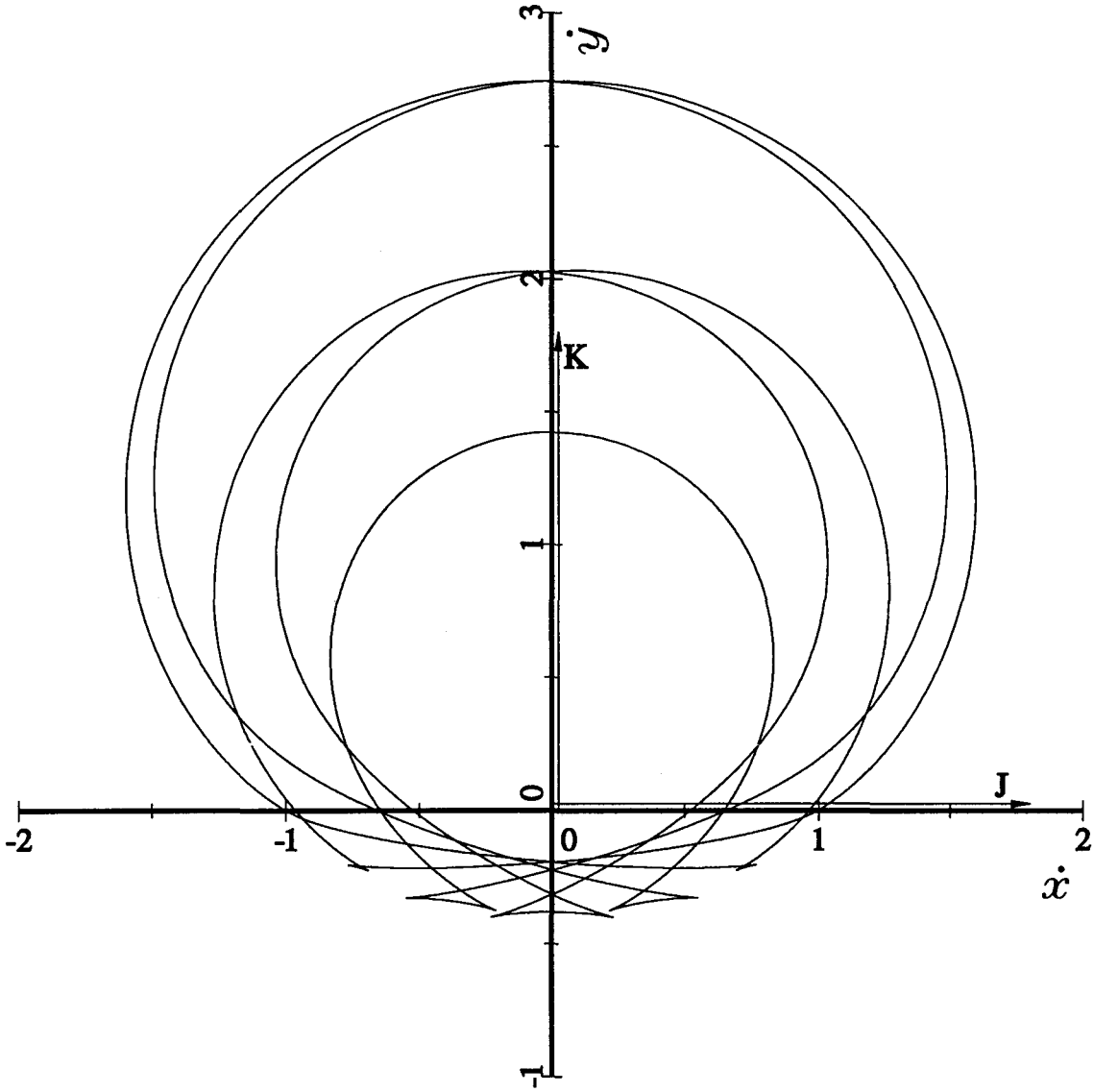


Figure 1.12.4. The velocity hodograph associated with Figure 1.12.3.

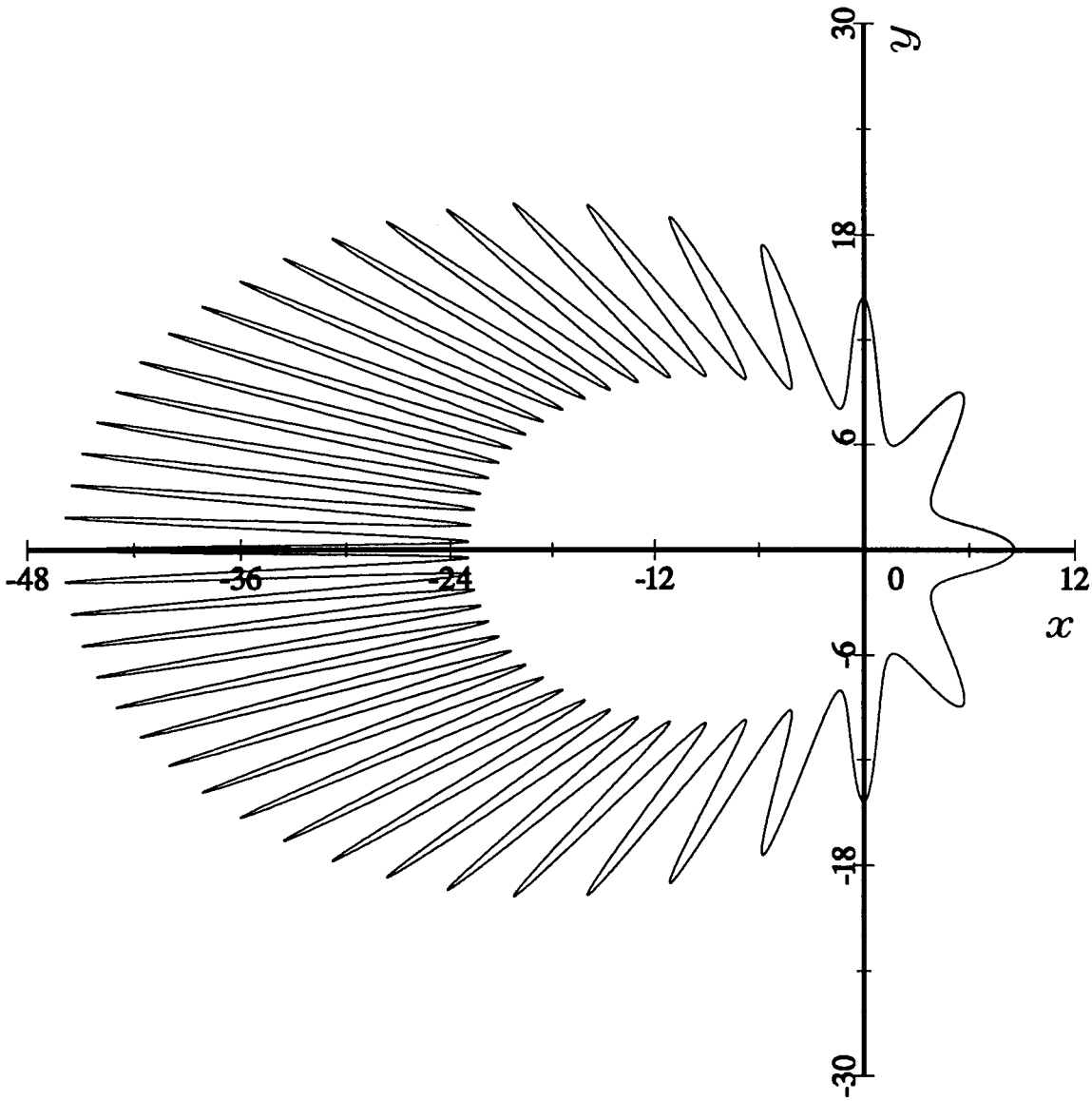


Figure 1.12.5. The orbit for $\mu = 1$, $a = 1$, $b = 0.6$, $\theta_0 = 0$, $K = J = 0.5$ and $L = 3.3736$ which was selected to close the orbit.

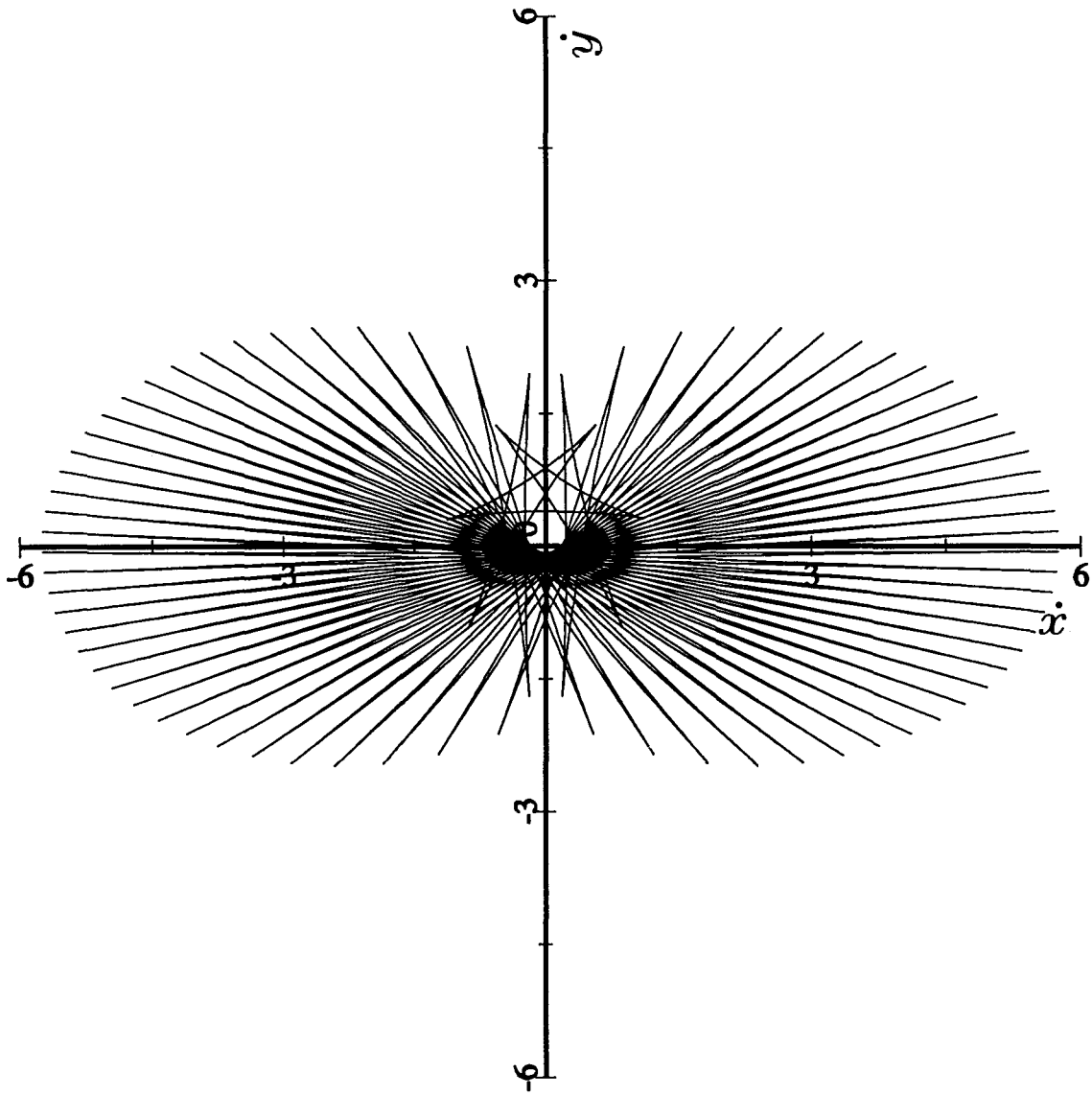


Figure 1.12.6. The velocity hodograph associated with Figure 1.12.5.

The Hamiltonian for the system is given by

$$H = \frac{1}{2}\boldsymbol{p}^2 - \frac{\ddot{g}}{2g}r^2 + \frac{\mu r}{g^3}. \tag{1.12.19}$$

It does not seem possible to construct either a Hamilton–like vector or a Laplace–Runge–Lenz vector for a general function g, although it may be possible in specific cases.

CHAPTER 2

MOTION WITH CONSERVED $\hat{\boldsymbol{L}}$

2.1 The Conserved Hamilton and Laplace–Runge–Lenz Vector Analogues for the Equation of Motion $\ddot{\boldsymbol{r}} + g\hat{\boldsymbol{r}} + h\hat{\boldsymbol{\theta}} = \boldsymbol{0}$

The contents of §§2.1–2.5 are described in Gorringe and Leach [35]. Relaxation of the condition on the angular momentum used in Chapter 1, by only requiring that $\hat{\boldsymbol{L}}$ be constant, gives

$$\dot{\boldsymbol{L}} = \dot{L}\hat{\boldsymbol{L}} \tag{2.1.1}$$

using (P1.11). The vector product of (2.1.1) with $\boldsymbol{L}$ gives

$$\dot{\boldsymbol{L}} \times \boldsymbol{L} = \boldsymbol{0} \tag{2.1.2}$$

using (P1.4). Equation (2.1.2) implies that $\dot{\boldsymbol{L}}$ and $\boldsymbol{L}$ are collinear and so

$$\dot{\boldsymbol{L}} + h_1 \boldsymbol{L} = \boldsymbol{0}, \tag{2.1.3}$$

where at this stage h_1 remains an arbitrary function. Since we assumed that $\hat{\boldsymbol{L}}$ was constant, we may take the origin to lie in the plane and use plane polar coordinates (r, θ) to describe the motion in the plane. In this representation $\hat{\boldsymbol{L}} = \hat{\boldsymbol{r}} \times \hat{\boldsymbol{\theta}}$. Equation (2.1.3) can be rewritten as

$$\boldsymbol{r} \times \ddot{\boldsymbol{r}} + g_1 \boldsymbol{r} \times \boldsymbol{r} + \frac{h_1 L}{r} \boldsymbol{r} \times \hat{\boldsymbol{\theta}} = \boldsymbol{0}, \tag{2.1.4}$$

where again g_1 is an arbitrary function. It now follows that the equation of motion

$$\ddot{\boldsymbol{r}} + g\hat{\boldsymbol{r}} + h\hat{\boldsymbol{\theta}} = \boldsymbol{0}, \tag{2.1.5}$$

where $g = g_1 r$ and $h = h_1 L/r$ describe motion in a plane with $\hat{\boldsymbol{L}}$ conserved. Equation (2.1.5) should not be regarded as the most general equation of motion in the plane, but one such class of problems for which the techniques discussed below can be applied. It is indeed possible to introduce more unrestricted functions into (2.1.5), and express the angular momentum with terms such as $e\boldsymbol{r} \times \dot{\boldsymbol{r}}$. In §2.10, equation (2.1.3) is rewritten in terms of a different set of vector products and shown to describe a model for the motion of low altitude artificial satellites in the atmosphere.

We now employ a direct method attributed to J. Bertrand (see Whittaker [129, p332 §152]) to find a Laplace–Runge–Lenz analogue for the equation of motion (2.1.5). To simplify matters we assume that $g = g(r,\theta)$ and $h = h(r,\theta)$. The severe restrictions placed on the functions above are vital to insure the separation of the partial differential equation obtained from enforcing the constraint that the time derivative of a first integral be zero.

By taking the vector product of $\boldsymbol{r}$ with (2.1.5) we obtain

$$\dot{L} = -hr. \tag{2.1.6}$$

The vector product of (2.1.5) with $\boldsymbol{L}$ gives

$$\ddot{\boldsymbol{r}}\times\boldsymbol{L} - gL\hat{\boldsymbol{\theta}} + hL\hat{\boldsymbol{r}} = \boldsymbol{0} \tag{2.1.7}$$

which can be rewritten as

$$\frac{\mathrm{d}}{\mathrm{d}t}(\dot{\boldsymbol{r}}\times\boldsymbol{L}) - \dot{\boldsymbol{r}}\times\dot{\boldsymbol{L}} - gL\hat{\boldsymbol{\theta}} + hL\hat{\boldsymbol{r}} = \boldsymbol{0}. \tag{2.1.8}$$

A Laplace–Runge–Lenz analogue of the form

$$\boldsymbol{J} = \dot{\boldsymbol{r}}\times\boldsymbol{L} - u(r,\theta)\hat{\boldsymbol{r}} - v(r,\theta)\hat{\boldsymbol{\theta}} \tag{2.1.9}$$

exists, provided

$$\frac{\mathrm{d}}{\mathrm{d}t}\left(-u\hat{\boldsymbol{r}} - v\hat{\boldsymbol{\theta}}\right) = hr\dot{\boldsymbol{r}}\times\hat{\boldsymbol{L}} - gL\hat{\boldsymbol{\theta}} + hL\hat{\boldsymbol{r}}. \tag{2.1.10}$$

By equating the coefficients of $\hat{\boldsymbol{r}}$ and $\hat{\boldsymbol{\theta}}$ separately to zero and using $L = r^2\dot{\theta}$ we have

$$\begin{aligned} \hat{\boldsymbol{r}}: &\quad \dot{u} - v\dot{\theta} = -2r^2h\dot{\theta} \\ \hat{\boldsymbol{\theta}}: &\quad u\dot{\theta} + \dot{v} = r\dot{r}h + gr^2\dot{\theta}. \end{aligned} \tag{2.1.11}$$

Since g, h, u and v depend only on r and θ, we may separate by coefficients of $\dot{r}$ and $\dot{\theta}$ to obtain the set of four partial differential equations

$$\begin{aligned} \dot{r}\hat{\boldsymbol{r}}: &\quad \frac{\partial u}{\partial r} = 0 \\ \dot{\theta}\hat{\boldsymbol{r}}: &\quad \frac{\partial u}{\partial \theta} - v = -2hr^2 \\ \dot{r}\hat{\boldsymbol{\theta}}: &\quad \frac{\partial v}{\partial r} = hr \\ \dot{\theta}\hat{\boldsymbol{\theta}}: &\quad \frac{\partial v}{\partial \theta} + u = gr^2. \end{aligned} \tag{2.1.12}$$

The set of equations (2.1.12) can easily be solved to give

$$\begin{aligned} u &= U(\theta) \\ v &= U'(\theta) + 2r^{\frac{1}{2}}V(\theta) \\ h &= r^{-\frac{3}{2}}V(\theta) \\ g &= \frac{1}{r^2}\left[U''(\theta) + U(\theta) + 2r^{\frac{1}{2}}V'(\theta)\right], \end{aligned} \tag{2.1.13}$$

where $U(\theta)$ and $V(\theta)$ are arbitrary functions. Thus the system which has the equation of motion

$$\ddot{\boldsymbol{r}} + \left[\frac{U''(\theta) + U(\theta)}{r^2} + \frac{2V'(\theta)}{r^{\frac{3}{2}}}\right]\hat{\boldsymbol{r}} + \frac{V(\theta)}{r^{\frac{3}{2}}}\hat{\boldsymbol{\theta}} = \boldsymbol{0} \tag{2.1.14}$$

has the conserved vector

$$\boldsymbol{J} = \dot{\boldsymbol{r}} \times \boldsymbol{L} - U(\theta)\hat{\boldsymbol{r}} - \left[U'(\theta) + 2r^{\frac{1}{2}}V(\theta)\right]\hat{\boldsymbol{\theta}}. \tag{2.1.15}$$

A Hamilton vector analogue can be constructed from the Laplace–Runge–Lenz vector analogue by taking the vector product of $\hat{\boldsymbol{L}}$ with $\boldsymbol{J}$,

$$\begin{aligned} \boldsymbol{K} &= \hat{\boldsymbol{L}} \times \boldsymbol{J} \\ &= L\dot{\boldsymbol{r}} - u\hat{\boldsymbol{\theta}} + v\hat{\boldsymbol{r}}. \end{aligned} \tag{2.1.16}$$

It should be appreciated that it is not possible to scale either (2.1.15) or (2.1.16) by L as was done in §1.5 and since L is no longer conserved.

2.2 The Velocity Hodograph and the Orbit Equation

The velocity hodograph can be calculated using the techniques of §1.2. Using the expression (2.1.16) for $\boldsymbol{K}$ the velocity hodograph can be shown to take the general form

$$(L\dot{x} + K\sin\theta_0)^2 + (L\dot{y} - K\cos\theta_0)^2 = U^2 + \left(U' + 2r^{\frac{1}{2}}V\right)^2. \tag{2.2.1}$$

Both L and r can in theory be expressed in terms of θ using (2.2.7) and (2.2.8). Equation (2.2.1) does not appear to possess any well–known geometry. There may, of course, be certain choices for the unknown functions where (2.2.1) does reduce to something recognisable, such as the characteristic circle for the standard Kepler problem.

As before the orbit equation is constructed from $\boldsymbol{J}$. If we let θ_0 be the fixed angle between $\boldsymbol{J}$ and the cartesian unit vector $\boldsymbol{i}$, taking the scalar product of $\boldsymbol{J}$ with $\boldsymbol{r}$ gives

$$Jr\cos(\theta - \theta_0) = L^2 - Ur, \tag{2.2.2}$$

which can be rearranged to give

$$r = \frac{L^2}{U + J\cos(\theta - \theta_0)}. \tag{2.2.3}$$

Since L is no longer constant, we must try to express L in terms of θ. Writing

$$\dot{L} = \frac{\mathrm{d}L}{\mathrm{d}\theta}\dot{\theta} = \frac{\mathrm{d}L}{\mathrm{d}\theta}\frac{L}{r^2} \tag{2.2.4}$$

and using (2.1.6) and the third equation of (2.1.13) we obtain

$$L\frac{\mathrm{d}L}{\mathrm{d}\theta} = -r^{\frac{3}{2}}V(\theta). \tag{2.2.5}$$

Using the orbit equation (2.2.3) and rearranging we obtain

$$-\frac{\mathrm{d}L}{L^2} = \frac{V(\theta)\mathrm{d}\theta}{\left[U(\theta) + J\cos(\theta - \theta_0)\right]^{\frac{3}{2}}} \tag{2.2.6}$$

or

$$\frac{1}{L} = \frac{1}{L_0} + \int_{\theta_0}^{\theta} \frac{V(\eta)\mathrm{d}\eta}{\left[U(\eta) + J\cos(\eta - \theta_0)\right]^{\frac{3}{2}}}. \tag{2.2.7}$$

The orbit equation (2.2.3) then becomes

$$r(\theta) = \frac{1}{U(\theta) + J\cos(\theta - \theta_0)} \times \left[\frac{1}{L_0} + \int_{\theta_0}^{\theta} \frac{V(\eta)\mathrm{d}\eta}{\left[U(\eta) + J\cos(\eta - \theta_0)\right]^{\frac{3}{2}}}\right]^{-2}. \tag{2.2.8}$$

The standard Kepler orbit equation is recovered when $U(\theta) = U_0$ and $V(\theta) = 0$.

2.3 The Motion in Time

A solution to the radial motion in time is not possible in general, unless θ can be expressed in terms of r. Differentiating (2.2.3) and using (2.1.6) to replace $\dot{L}$ and (2.2.3) itself give

$$\dot{r} = -\frac{2hr^2}{L} - \frac{1}{L}\big(U' - J\sin(\theta - \theta_0)\big). \tag{2.3.1}$$

Unless the right hand side of (2.3.1) can be expressed entirely in terms of r, the radial motion can only be evaluated numerically.

The angular motion in time can be calculated using the scalar equation for the angular momentum

$$\dot{\theta} = \frac{\big(U(\theta) + J\cos(\theta - \theta_0)\big)^2}{L^3}. \tag{2.3.2}$$

Provided L in (2.3.2) can be expressed in terms of θ using (2.2.7), the angular motion can in theory be determined. All the problems associated with the inversion of the radial and angular equations dealt with in §§1.5 and 1.7 still apply.

The calculation of the areal velocity also poses serious problems. Since L is no longer constant, an attempt must be made to express L in terms of t. Assuming the angular motion in time can be solved using (2.3.2) allows us to write

$$t = f_1(\theta). \tag{2.3.3}$$

Provided (2.3.3) can be inverted to give

$$\theta = f_2(t) \tag{2.3.4}$$

and then using

$$\frac{\mathrm{d}A}{\mathrm{d}t} = \frac{1}{2}L\left(f_2(t)\right), \tag{2.3.5}$$

where L is calculated using (2.2.7), the areal velocity can in principle be determined. For most practical purposes a numerical solution is probably more suitable since the determination of (2.3.5) will usually be involved.

2.4 Examples

1.) The orbit equation (2.2.8) can give rise to a wide variety of orbits. If $V \equiv 0$ and U is an increasing function of θ and $U(0) > J > 0$, the orbit spirals inward. Conversely, if $V \equiv 0$ and U is a decreasing function of θ with $U(0) > J > 0$ the orbit spirals outward. For $V \equiv 0$ and U periodic with a period not commensurate with 2π, the orbit does not close. For appropriate values of the energy, the orbit does close with period 2π if U has the period $2\pi/n$, $n \in N$. On the other hand, if U has a period $2n\pi$, $n \in N$, the orbit circles the origin n times before closing. If we choose

$$U(\theta) = a \sin k(\theta - \theta_0) + b, \tag{2.4.1}$$

then the corresponding equation of motion (2.1.14) is

$$\ddot{\boldsymbol{r}} + \left(\frac{a(1-k^2)\sin k(\theta-\theta_0)+b}{r^2}\right)\hat{\boldsymbol{r}} = \boldsymbol{0}, \tag{2.4.2}$$

and the conserved vectors $\boldsymbol{K}$ and $\boldsymbol{J}$ are given by (2.1.16) and (2.1.15) which become

$$\boldsymbol{K} = L\dot{\boldsymbol{r}} - \big(a\sin k(\theta-\theta_0)+b\big)\hat{\boldsymbol{\theta}} + ak\cos k(\theta-\theta_0)\hat{\boldsymbol{r}} \tag{2.4.3}$$

and

$$\boldsymbol{J} = \dot{\boldsymbol{r}}\times\boldsymbol{L} - \big(a\sin k(\theta-\theta_0)+b\big)\hat{\boldsymbol{r}} - ak\cos k(\theta-\theta_0)\hat{\boldsymbol{\theta}}. \tag{2.4.4}$$

The orbit equation and velocity hodograph are then given by (2.2.8) and (2.2.1) respectively. Figures 2.4.1 and 2.4.2 show the orbit and the corresponding velocity hodograph for a particular choice of the constants a, b and k. In this case U has a period of $\pi/4$ radians. Figure 2.4.3 shows the variation in the magnitude of the angular momentum vector along the orbit corresponding with Figures 2.4.1 and 2.4.2. In this case the angular momentum remains constant both in magnitude and direction.

Figures 2.4.4 and 2.4.5 show the orbit and the corresponding velocity hodograph for a different choice of the constants a, b and k. In this case U has a period of 16π and consequently the orbit circles the origin 8 times before closing. Figures 2.4.6 and 2.4.7 show a 'scattering' orbit and the corresponding velocity hodograph when $b=0$. The orbit approaches asymptotically and 'circles' the origin several times before leaving asymptotically.

2.) In the case when U is constant and V is periodic with period $2n\pi, n\in N/\{1\}$, we see that for classically bound states, the orbit circles the origin n times before closing. If we choose

$$U=a,\quad V=b\sin k(\theta-\theta_0), \tag{2.4.5}$$

then the corresponding equation of motion (2.1.14) is

$$\ddot{\boldsymbol{r}} + \left(\frac{a}{r^2}+\frac{2bk\cos k(\theta-\theta_0)}{r^{\frac{3}{2}}}\right)\hat{\boldsymbol{r}} + \frac{b\sin k(\theta-\theta_0)}{r^{\frac{3}{2}}}\hat{\boldsymbol{\theta}} = \boldsymbol{0} \tag{2.4.6}$$

which has the conserved vectors

$$\boldsymbol{K} = L\dot{\boldsymbol{r}} + \big(2r^{\frac{1}{2}}b\sin k(\theta-\theta_0)\big)\hat{\boldsymbol{r}} - a\hat{\boldsymbol{\theta}} \tag{2.4.7}$$

and

$$\boldsymbol{J} = \dot{\boldsymbol{r}}\times\boldsymbol{L} - \big(2r^{\frac{1}{2}}b\sin k(\theta-\theta_0)\big)\hat{\boldsymbol{\theta}} - a\hat{\boldsymbol{r}}. \tag{2.4.8}$$

The orbit equation and velocity hodograph are then given by (2.2.8) and (2.2.1) after making suitable substitutions. Figures 2.4.8 and 2.4.9 show the orbit and the corresponding velocity hodograph for a particular choice of the constants a, b and k. Figure 2.4.10 shows the variation in the magnitude of the angular momentum vector along the orbit corresponding with Figures 2.4.8 and 2.4.9. In this case the angular momentum is constant only in direction but not in magnitude.

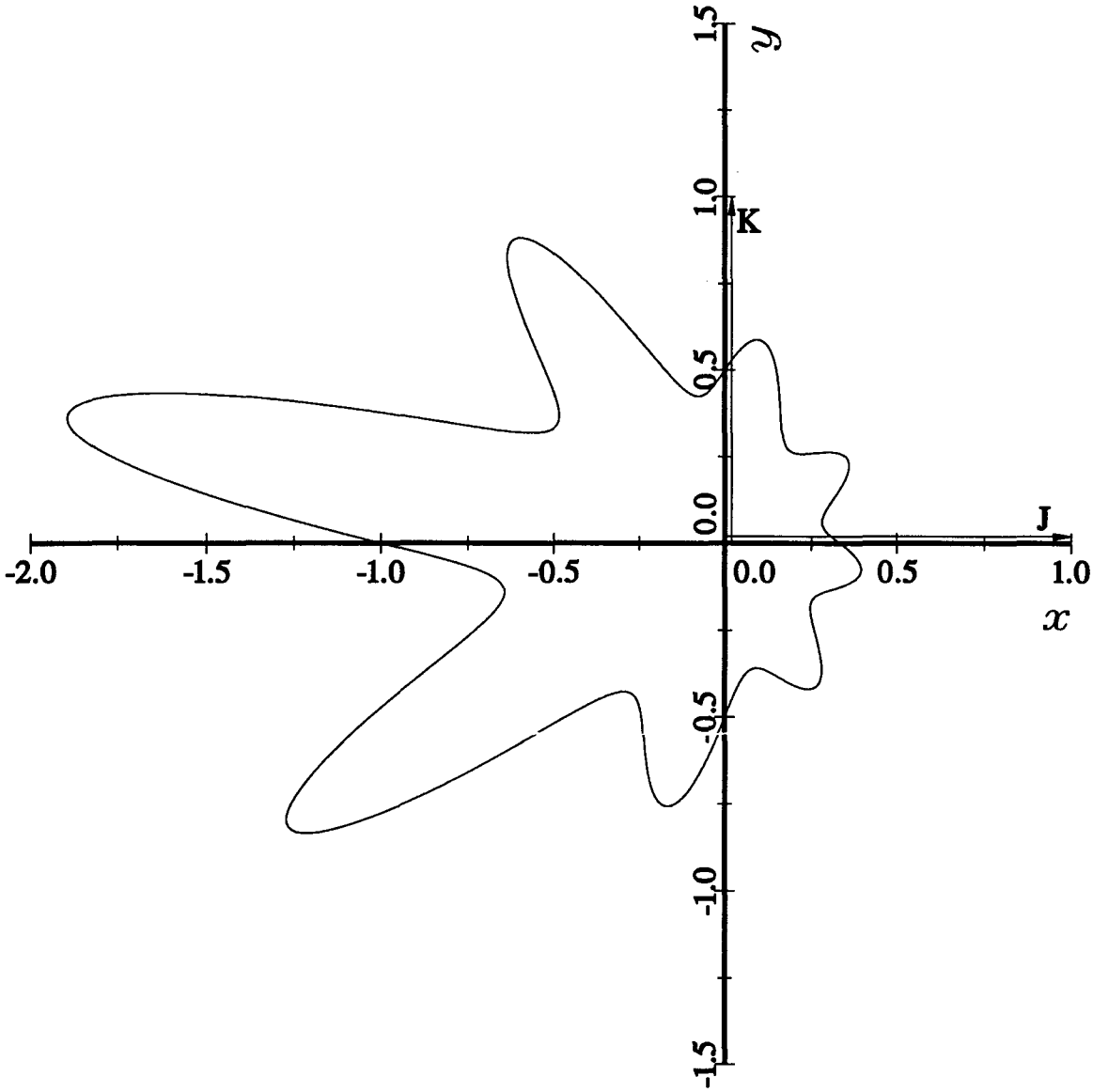


Figure 2.4.1. The orbit for $U(\theta) = a \sin k(\theta - \theta_0) + b$, $V(\theta) = 0$, $a = 1/2$, $b = 2$, $k = 8$, $\theta_0 = 0$, $K = J = 1$ and $L_0 = 1$. $U(\theta)$ has a period of $\pi/4$ radians which is reflected in the eight bulges in the orbit.

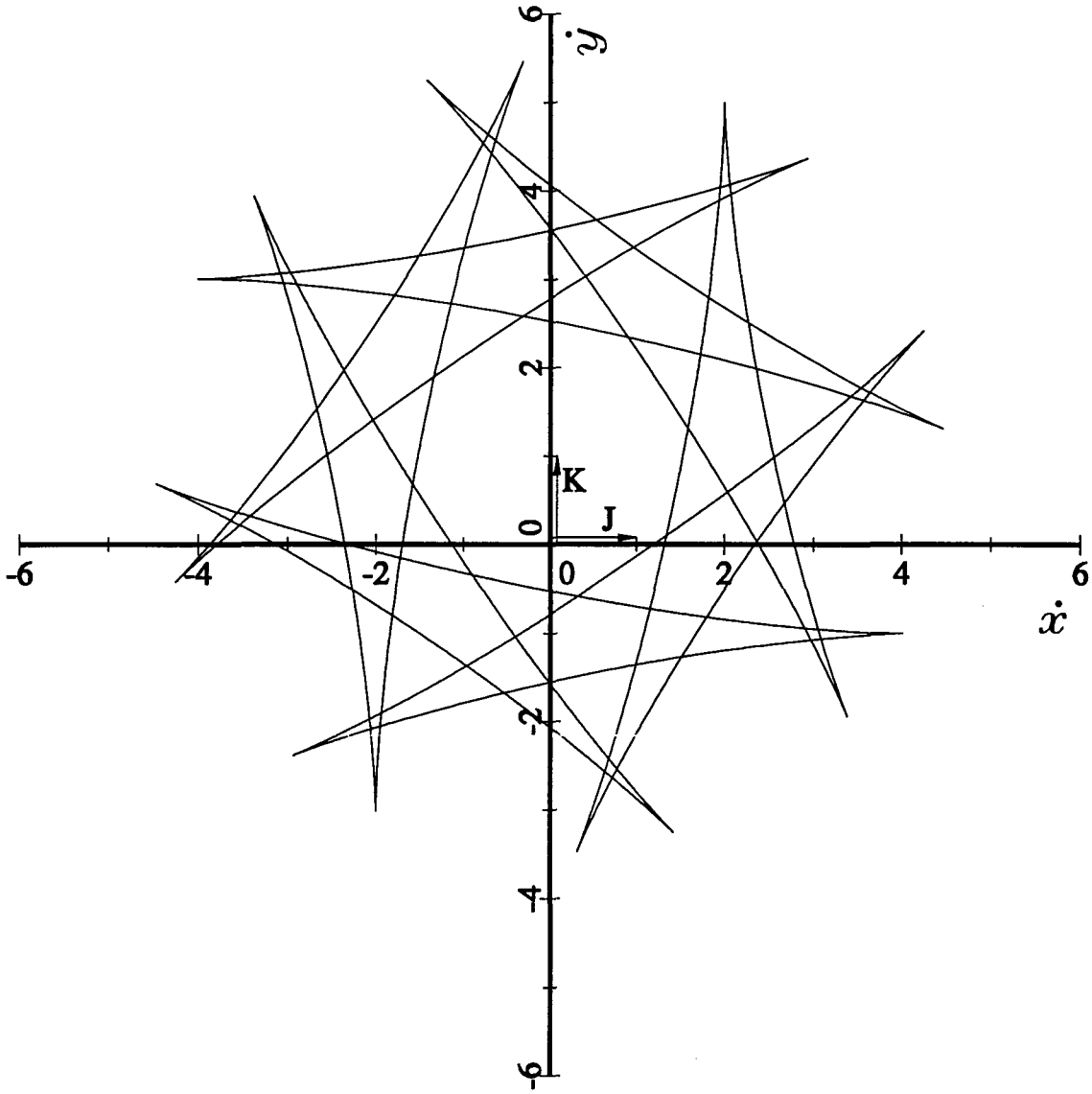


Figure 2.4.2. The velocity hodograph associated with Figure 2.4.1. $U(\theta)$ has a period of $\pi/4$ radians which is reflected in the sixteen vertices of the velocity hodograph.

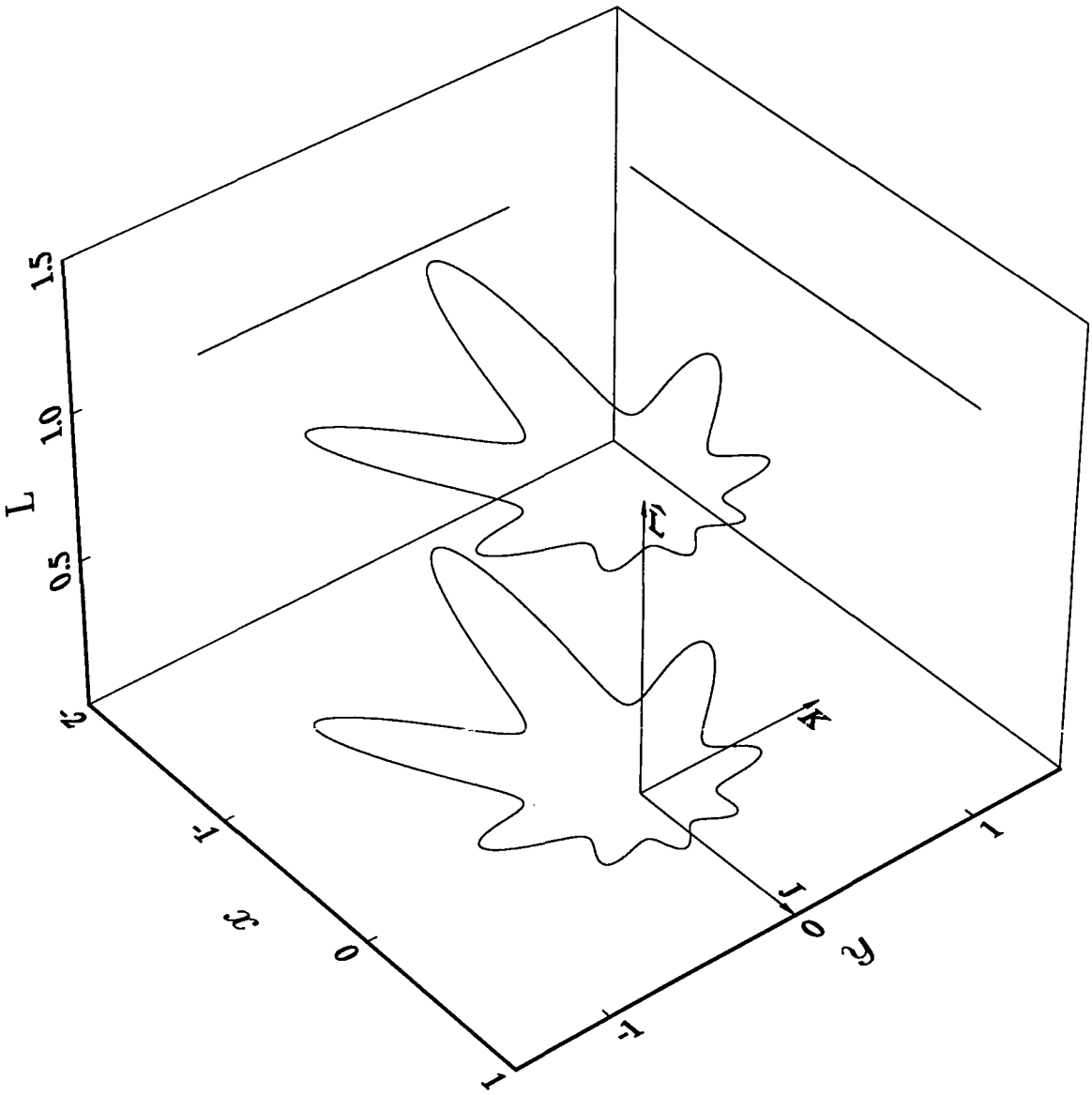


Figure 2.4.3. The variation in the magnitude of the angular momentum vector along the orbit corresponding with Figures 2.4.1 and 2.4.2. The projections of the angular momentum curve onto planes parallel to the xy, xL and yL planes are also shown. In this example the angular momentum is constant both in magnitude and direction.

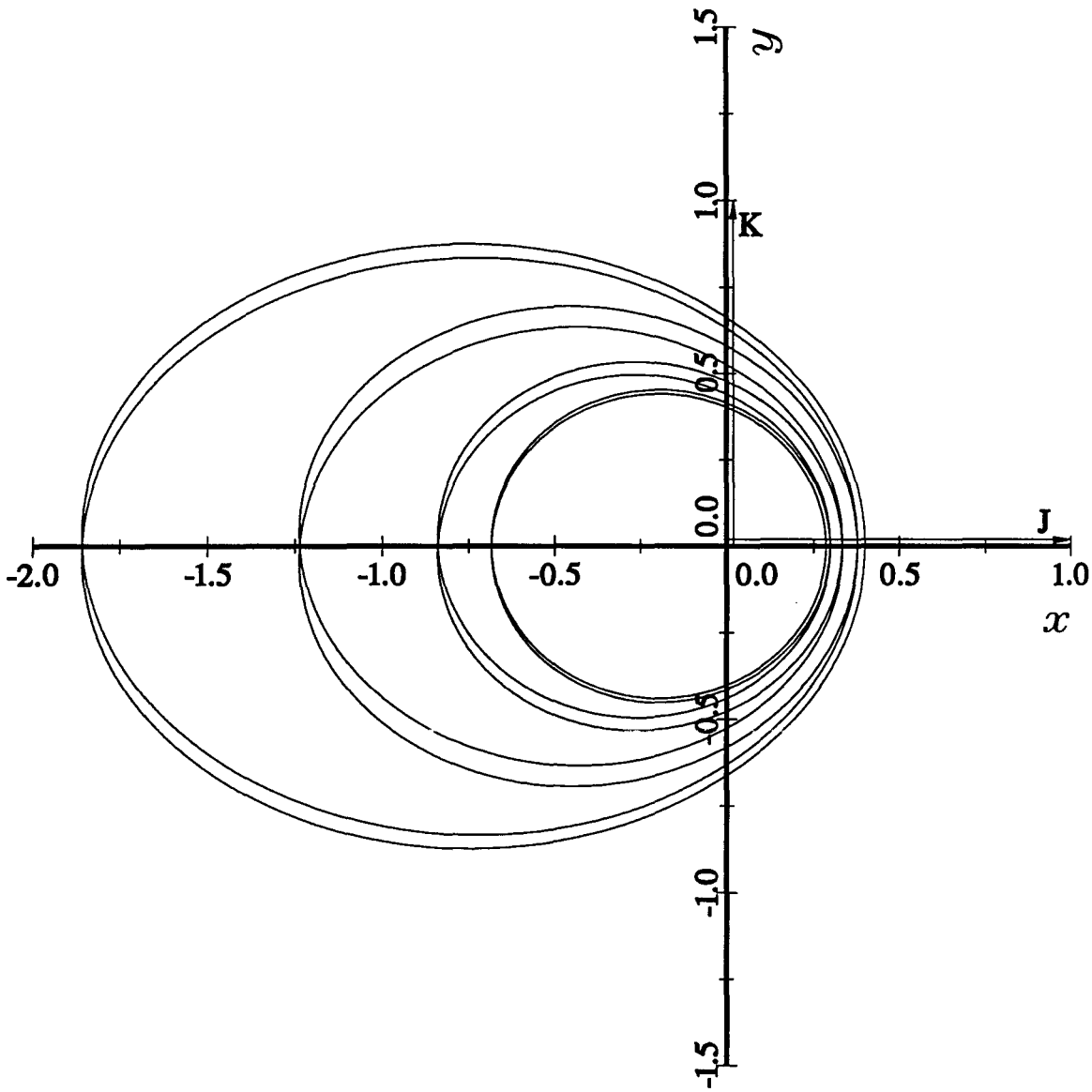


Figure 2.4.4. The orbit for $U(\theta) = a \sin k(\theta - \theta_0) + b$, $V(\theta) = 0$, $a = 1/2$, $b = 2$, $k = 1/8$, $\theta_0 = 0$, $K = J = 1$ and $L_0 = 1$. $U(\theta)$ has a period of 16π radians and consequently the orbit circles the origin eight times before closing. In this example the angular momentum is constant both in magnitude and direction.

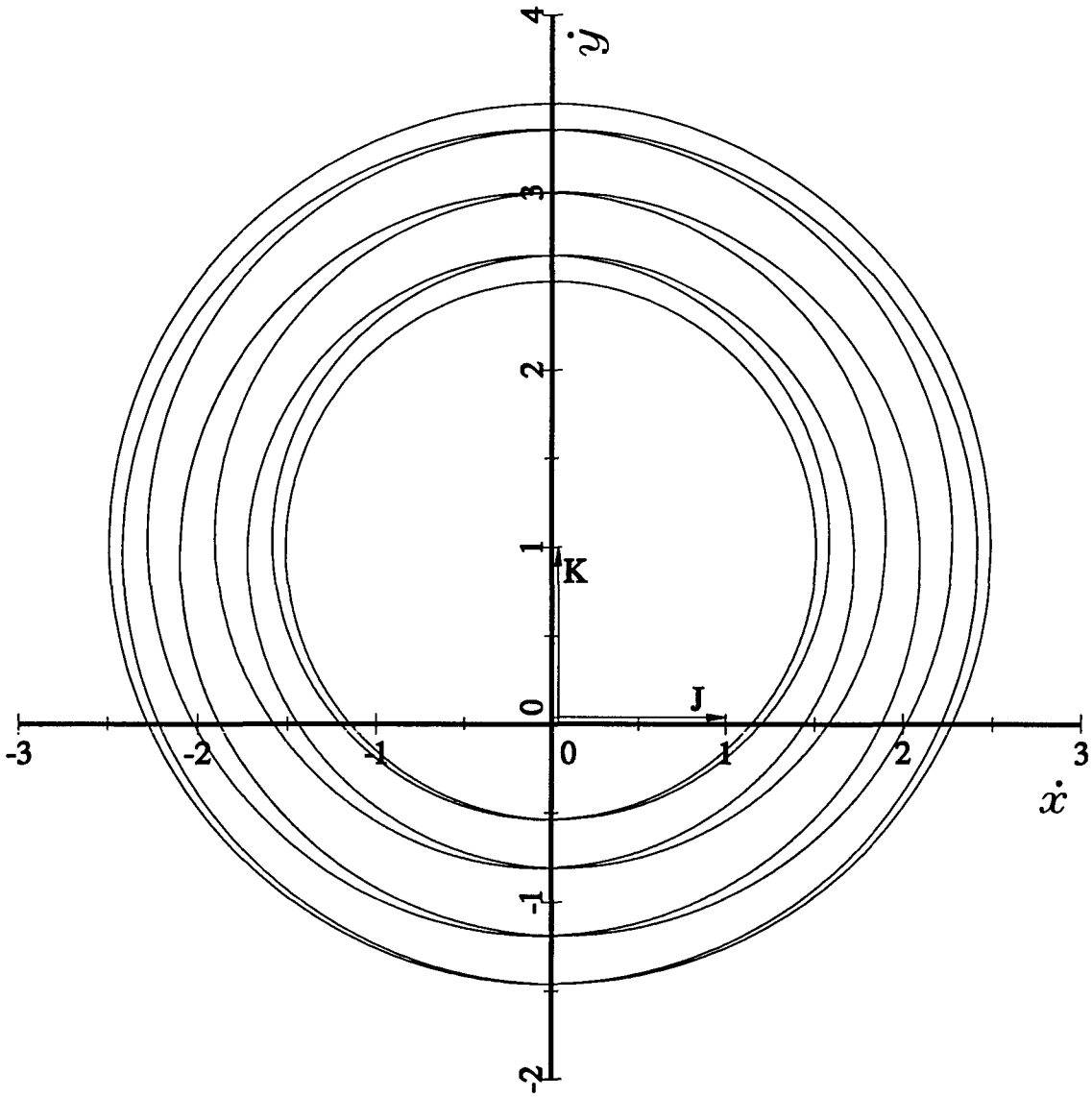


Figure 2.4.5. The velocity hodograph associated with Figure 2.4.4. Since $U(\theta)$ has a period of 16π radians the velocity hodograph also circles the origin eight times before closing.

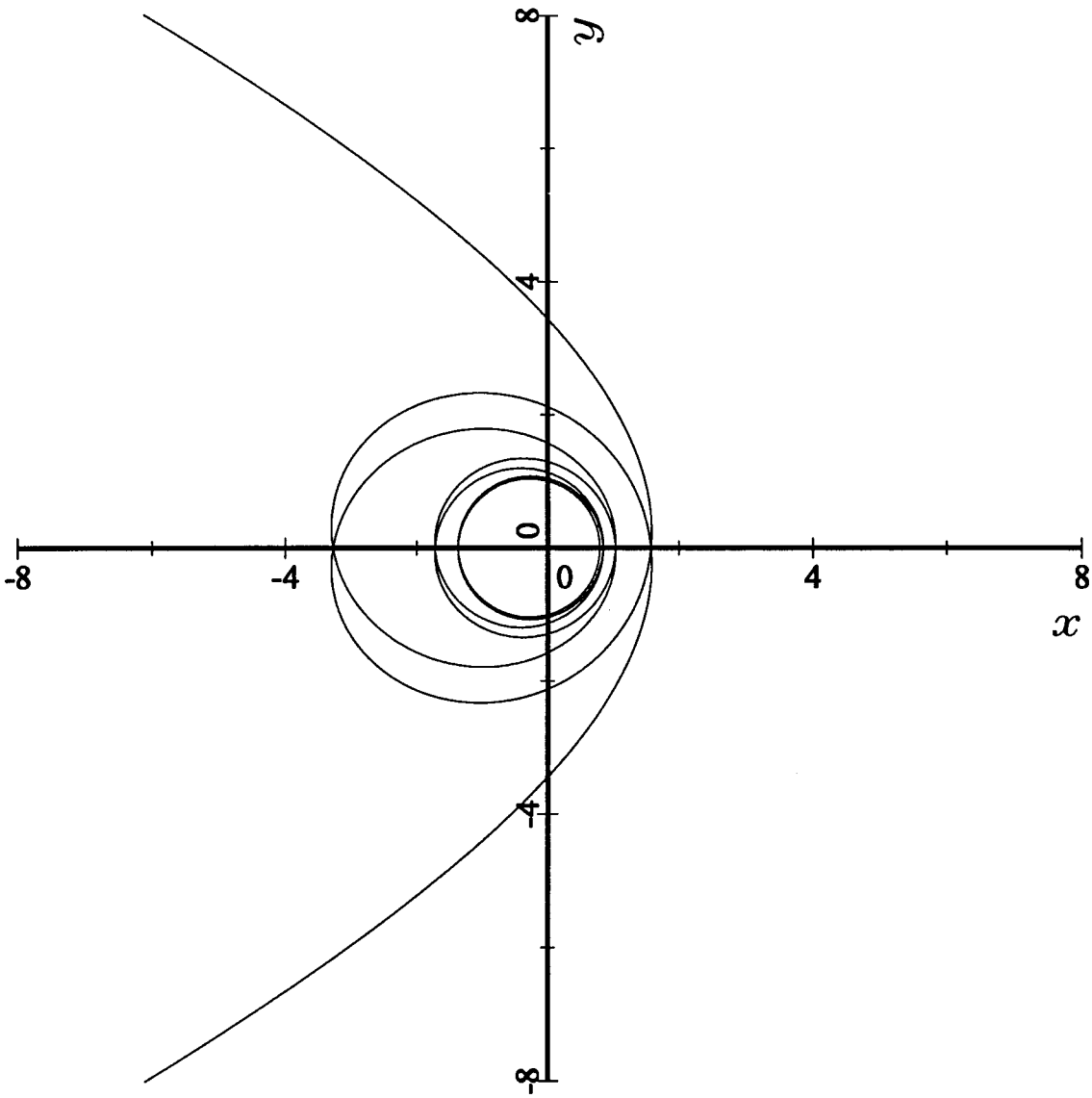


Figure 2.4.6. The orbit for $U(\theta) = a \sin k(\theta - \theta_0) + b$, $V(\theta) = 0$, $a = 1$, $b = 0$, $k = 1/16$, $\theta_0 = 0$, $K = J = 1/4$ and $L_0 = 1$. The orbit approaches asymptotically, circles the origin six times before leaving asymptotically. In this example the angular momentum is constant both in magnitude and direction.

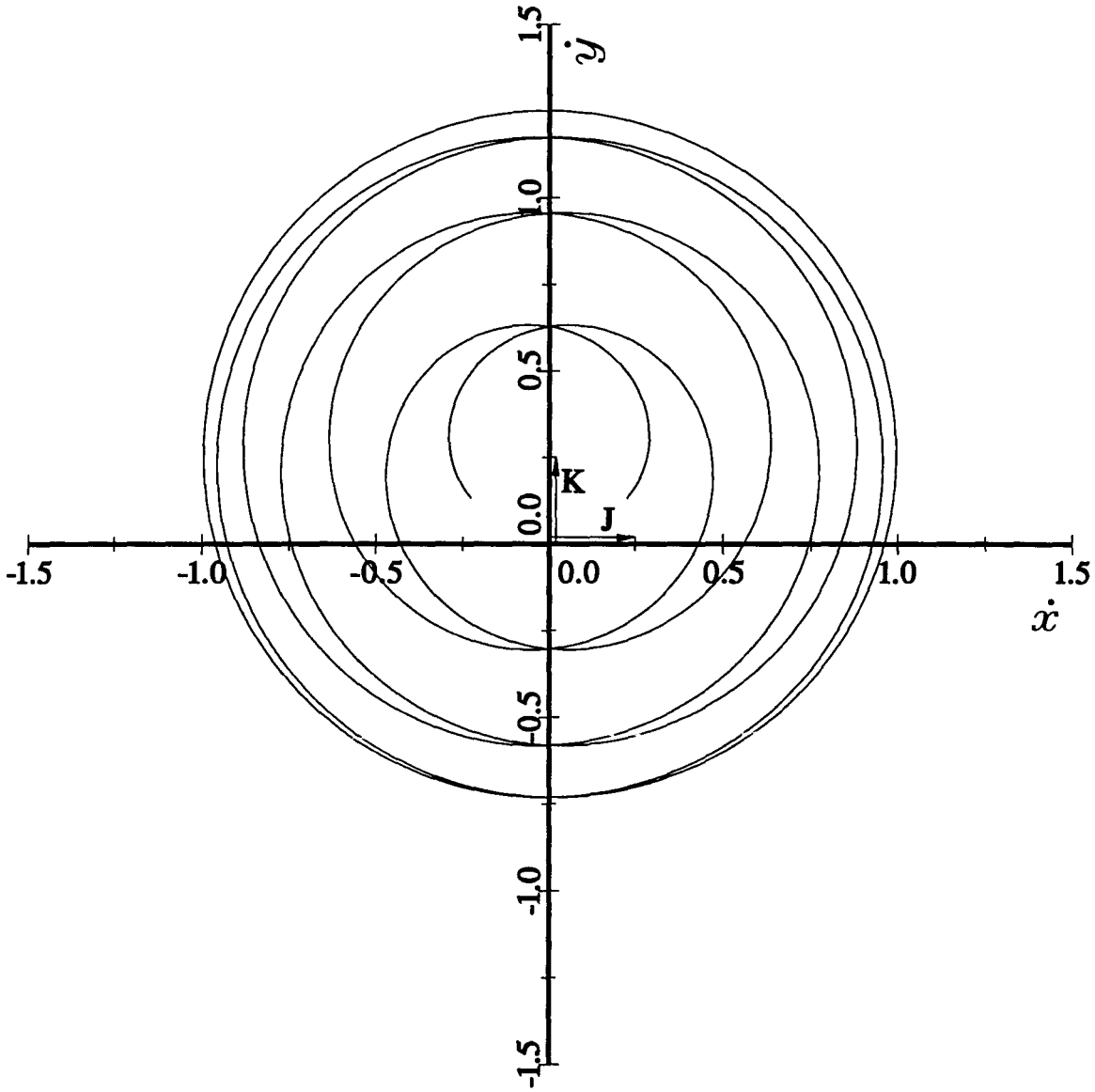


Figure 2.4.7. The velocity hodograph associated with Figure 2.4.6. The velocity hodograph is bounded at one end by the corresponding asymptote to the orbit (with the intersection of the two asymptotes relocated to the origin) and circles the origin six times before being bounded by the opposite asymptote.

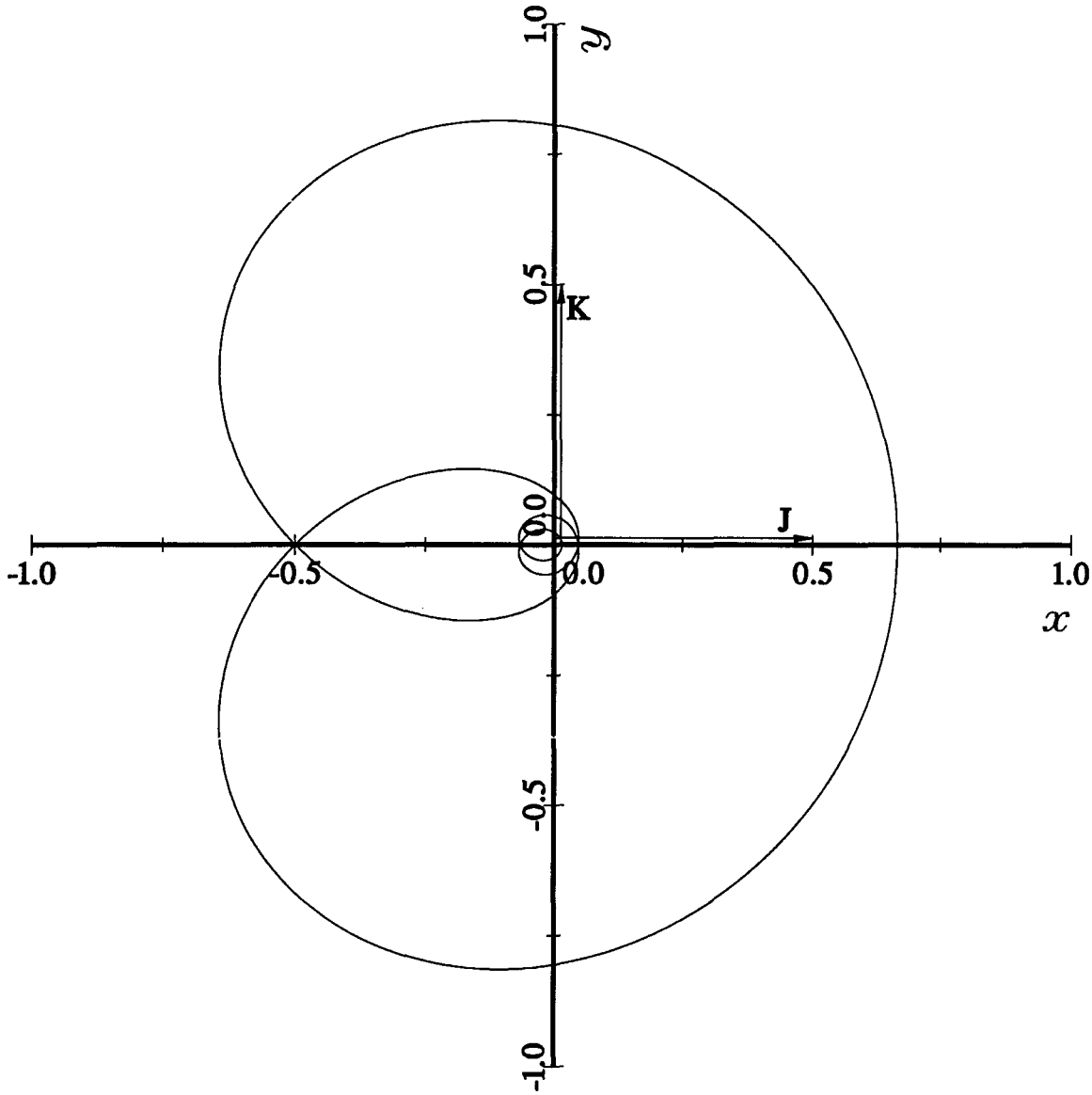


Figure 2.4.8. The orbit for $U(\theta) = a$, $V(\theta) = b \sin k(\theta - \theta_0)$, $a = 1$, $b = 1/2$, $k = 1/4$, $\theta_0 = 0$, $K = J = 1/2$ and $L_0 = 1$. $V(\theta)$ has a period of 8π radians and consequently the orbit circles the origin four times before closing.

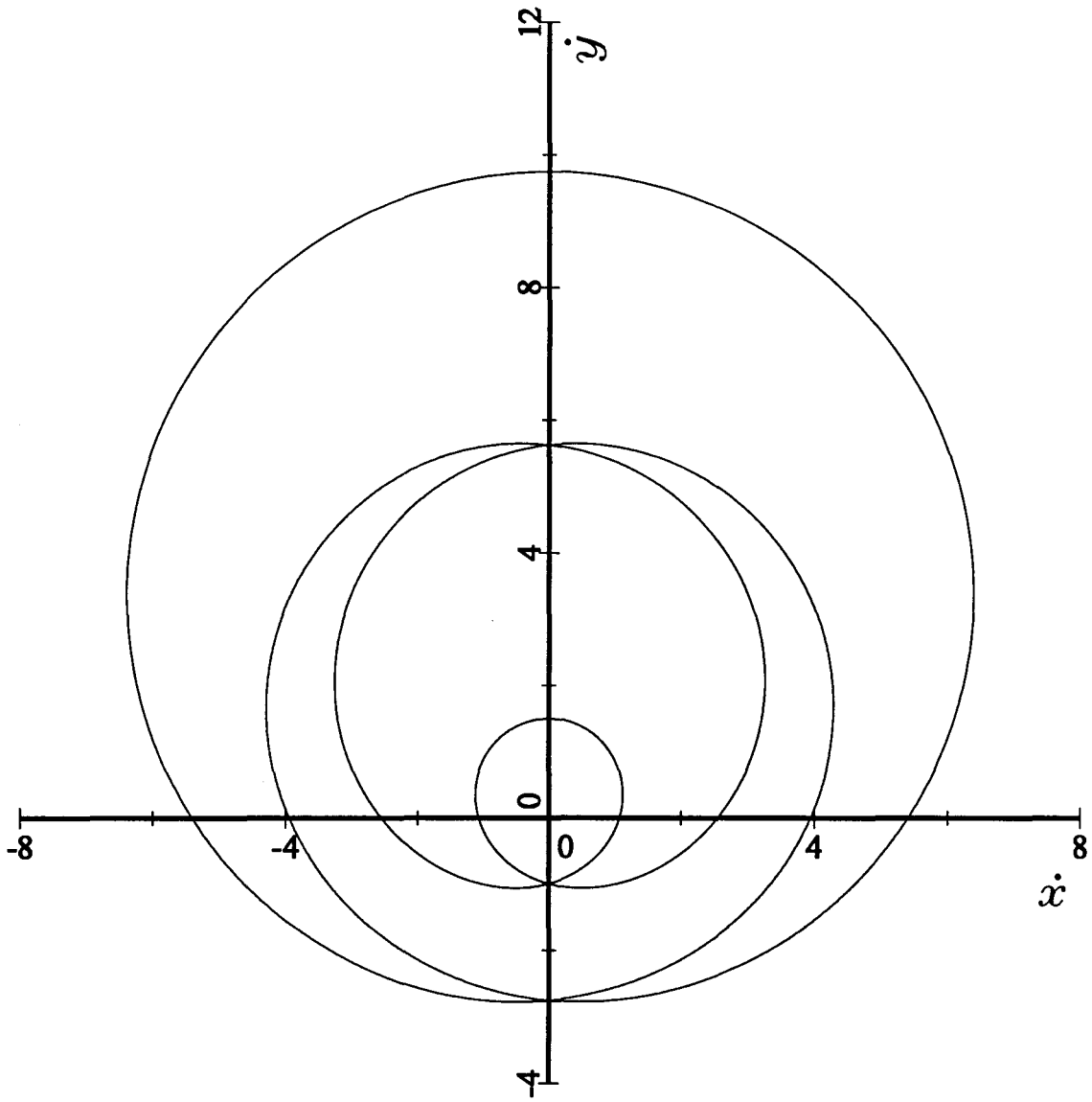


Figure 2.4.9. The velocity hodograph associated with Figure 2.4.8. Since $V(\theta)$ has a period of 8π radians the velocity hodograph also circles the origin four times before closing.

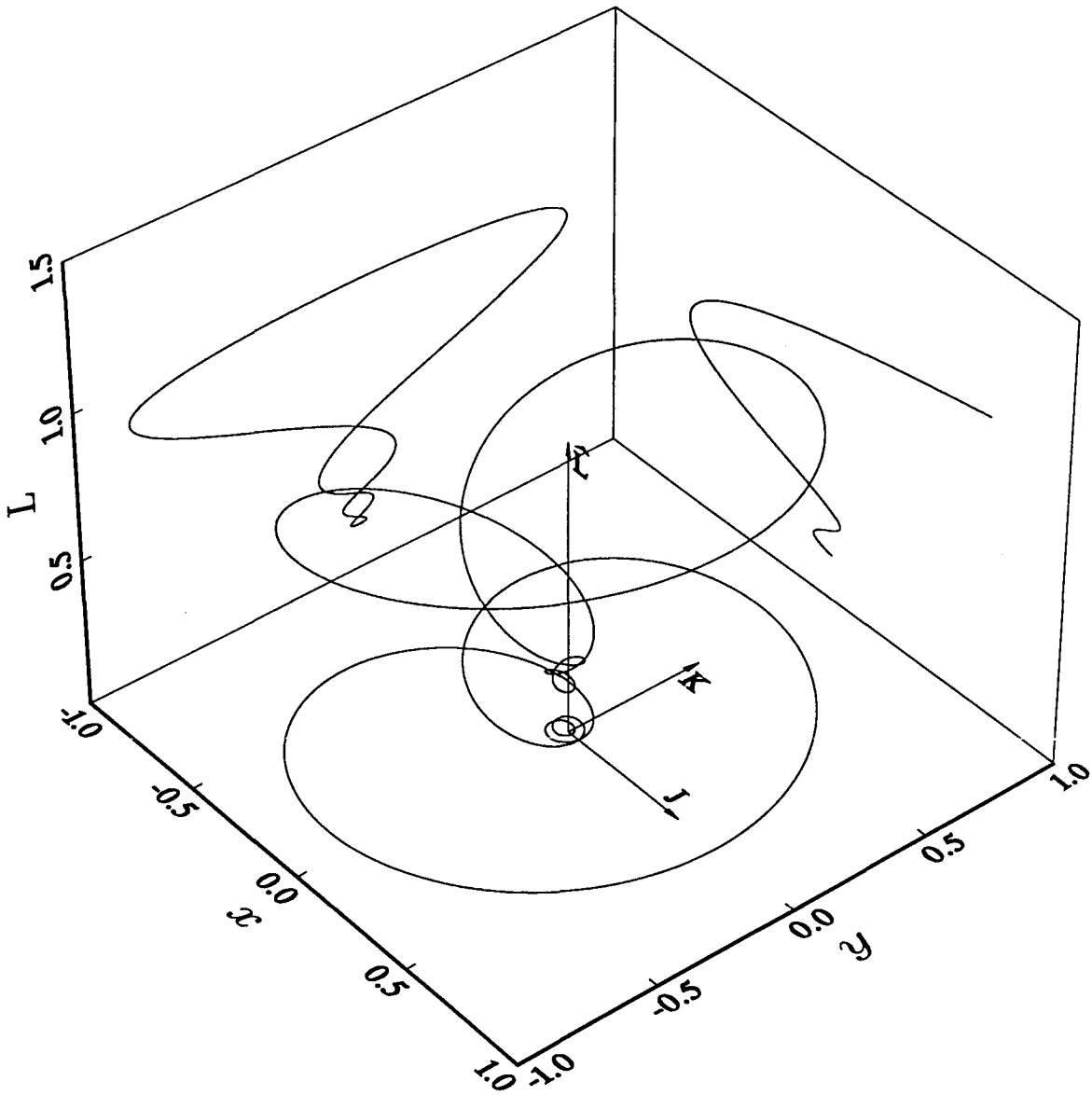


Figure 2.4.10. The variation in the magnitude of the angular momentum vector along the orbit corresponding with Figures 2.4.8 and 2.4.9. The projections of the angular momentum curve onto planes parallel to the the xy, xL and yL planes are also shown. In this example the angular momentum is constant in direction but not in magnitude.

2.5 The Conserved Hamilton and Laplace–Runge–Lenz Vector Analogues for a Related Hamiltonian System

Let us now consider the most general autonomous Hamiltonian which possesses a Laplace–Runge–Lenz vector which belongs to the class of problems given by equation (2.1.14). Assume a general form for the Hamiltonian

$$H = \frac{1}{2}\boldsymbol{p}\cdot\boldsymbol{p} + W(r,\theta). \tag{2.5.1}$$

The Newtonian equation of motion corresponding to (2.5.1) can be calculated from

$$\ddot{\boldsymbol{r}} = -\boldsymbol{\nabla}W(r,\theta) = \boldsymbol{F}(r,\theta). \tag{2.5.2}$$

The gradient of the potential in plane polar coordinates takes the form

$$\boldsymbol{\nabla}W(r,\theta) = \frac{\partial W}{\partial r}\hat{\boldsymbol{r}} + \frac{1}{r}\frac{\partial W}{\partial \theta}\hat{\boldsymbol{\theta}} \tag{2.5.3}$$

and the Newtonian equation of motion can now be written as

$$\ddot{\boldsymbol{r}} + \frac{\partial W}{\partial r}\hat{\boldsymbol{r}} + \frac{1}{r}\frac{\partial W}{\partial \theta}\hat{\boldsymbol{\theta}} = \boldsymbol{0}. \tag{2.5.4}$$

Thus, in the notation of (2.1.5)

$$\begin{aligned} g(r,\theta) &= \frac{\partial W}{\partial r} \\ h(r,\theta) &= \frac{1}{r}\frac{\partial W}{\partial \theta}. \end{aligned} \tag{2.5.5}$$

Now comparing (2.5.5) with (2.1.13) gives

$$\frac{\partial W}{\partial r} = \frac{1}{r^2}\left[U''(\theta) + U(\theta)\right] + 2r^{-\frac{3}{2}}V'(\theta) \tag{2.5.6}$$

and

$$\frac{1}{r}\frac{\partial W}{\partial \theta} = r^{-\frac{3}{2}}V(\theta). \tag{2.5.7}$$

Solving for $W(r,\theta)$ in (2.5.6) gives

$$W = -\frac{1}{r}\left[U''(\theta) + U(\theta)\right] - 4r^{-\frac{1}{2}}V'(\theta). \tag{2.5.8}$$

Differentiating (2.5.8) partially with respect to θ and equating with (2.5.7) yields

$$\begin{aligned} r^{-\frac{1}{2}} &: \ 4V''(\theta) + V(\theta) = 0 \\ r^{-1} &: \ U'''(\theta) + U'(\theta) = 0, \end{aligned} \tag{2.5.9}$$

which have the solution

$$\begin{aligned} U &= \mu + \gamma \sin(\theta - \delta) \\ V &= \frac{\alpha}{2} \sin\left(\frac{1}{2}(\theta - \beta)\right), \end{aligned} \tag{2.5.10}$$

where the constant $\alpha/2$ is introduced to simplify the expressions at a later stage and μ, γ, δ and β are also constants. Using (2.5.10) we find that

$$\begin{aligned} \boldsymbol{J} &= \dot{\boldsymbol{r}} \times \boldsymbol{L} - \left(\mu + \gamma \sin(\theta - \delta)\right)\hat{\boldsymbol{r}} \\ &\quad - \left(\gamma \cos(\theta - \delta) + \alpha r^{\frac{1}{2}} \sin\left(\frac{1}{2}(\theta - \beta)\right)\right)\hat{\boldsymbol{\theta}} \end{aligned} \tag{2.5.11}$$

and

$$H = \frac{1}{2}\left({p_r}^2 + \frac{{p_\theta}^2}{r^2}\right) - \frac{\mu}{r} - \alpha r^{-\frac{1}{2}} \cos\left(\frac{1}{2}(\theta - \beta)\right). \tag{2.5.12}$$

Equation (2.5.11) can be simplified on realising that

$$-\gamma \sin(\theta - \delta)\hat{\boldsymbol{r}} - \gamma \cos(\theta - \delta)\hat{\boldsymbol{\theta}} = \gamma(\boldsymbol{i} \sin\delta - \boldsymbol{j} \cos\delta) \tag{2.5.13}$$

is an ignorable constant vector. Thus with no loss of generality we may set $\gamma = 0$ in (2.5.10). The corresponding Newtonian equation of motion (2.5.4) now becomes

$$\ddot{\boldsymbol{r}} + \left(\frac{\mu}{r^2} + \frac{\alpha \cos\frac{1}{2}(\theta - \beta)}{2r^{\frac{3}{2}}}\right)\hat{\boldsymbol{r}} + \frac{\alpha \sin\frac{1}{2}(\theta - \beta)}{2r^{\frac{3}{2}}}\hat{\boldsymbol{\theta}} = \boldsymbol{0}. \tag{2.5.14}$$

The conserved vectors $\boldsymbol{K}$ and $\boldsymbol{J}$ are given by (2.1.16) and (2.5.11) after substituting for u, v, U and V and become

$$\boldsymbol{K} = L\dot{\boldsymbol{r}} + \alpha r^{\frac{1}{2}} \sin\frac{1}{2}(\theta - \beta)\hat{\boldsymbol{r}} - \mu\hat{\boldsymbol{\theta}} \tag{2.5.15}$$

and

$$\boldsymbol{J} = \dot{\boldsymbol{r}} \times \boldsymbol{L} - \mu\hat{\boldsymbol{r}} - \alpha r^{\frac{1}{2}} \sin\frac{1}{2}(\theta - \beta)\hat{\boldsymbol{\theta}}. \tag{2.5.16}$$

The orbit equation is then given by (2.2.8) and the velocity hodograph by (2.2.1). Figure 2.5.1 shows the velocity hodograph (left) and the orbit (right) in the case $\mu > J$ for a particular choice of the constants. Note that both the orbit and the velocity hodograph have a period of 4π. Figure 2.5.2 shows the variation in the magnitude of the angular momentum vector along the orbit corresponding with Figure 2.5.1. In this case the angular momentum is constant in direction but varies in magnitude. Figure 2.5.3 shows the velocity hodograph (loop–shaped) and the orbit (bean–shaped) in the case $\mu = J$. The orbit has a singularity at the origin and correspondingly the $\dot{x}$ component of the velocity hodograph tends to infinity. Figure 2.5.4 shows the variation in the magnitude of the the angular momentum vector along the orbit corresponding with Figure 2.5.3. Note that the angular momentum

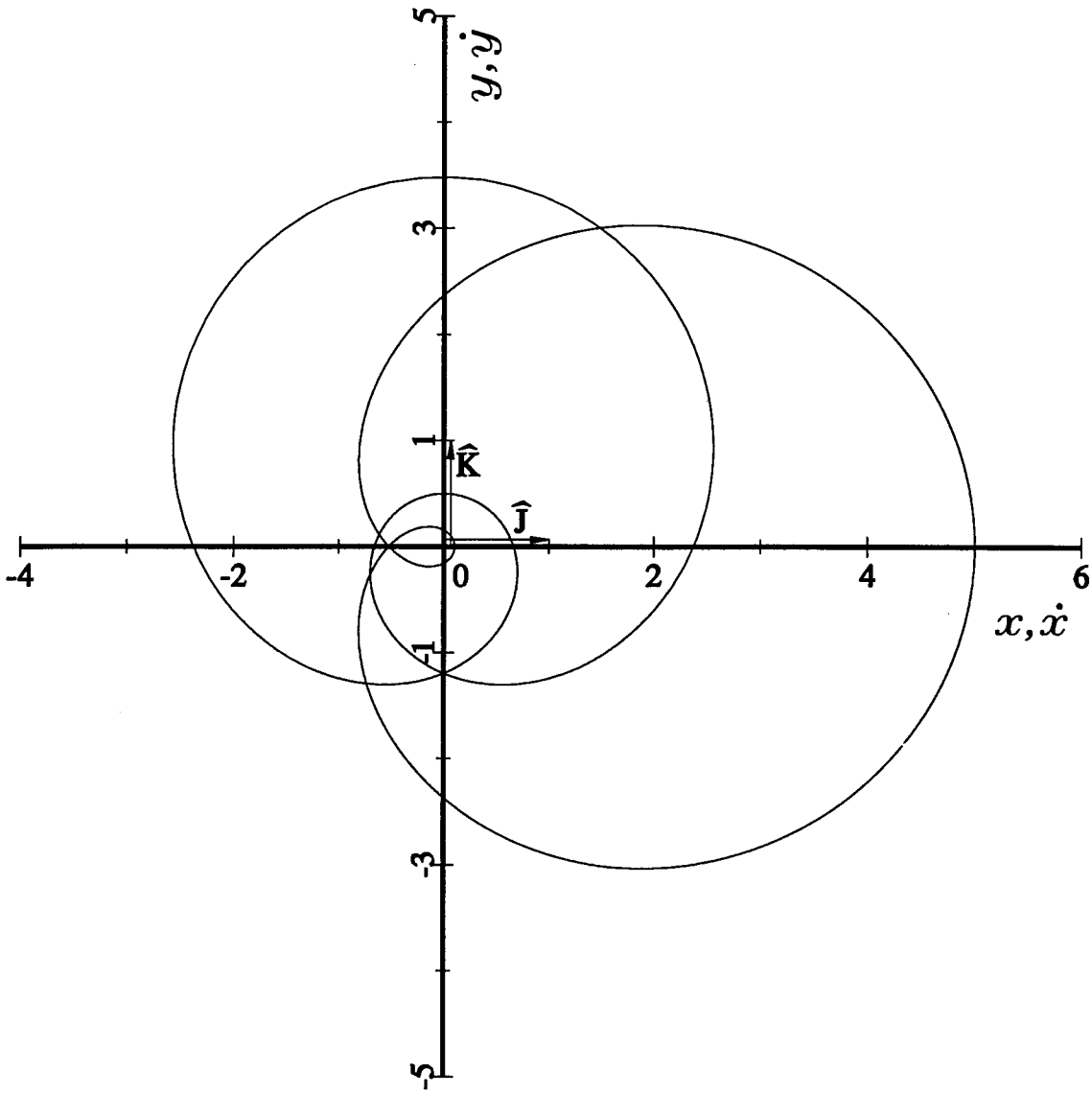


Figure 2.5.1. The velocity hodograph (left) and the orbit (right) for $U = \mu$, $V = \alpha \sin\big((\theta - \beta)/2\big)/2$, $\mu = 1$, $\alpha = 1$, $\beta = 0$, $\theta_0 = 0$, $K = J = 0.25$ and $L_0 = 2.5$. Note that both the orbit and the velocity hodograph have a period of 4π.

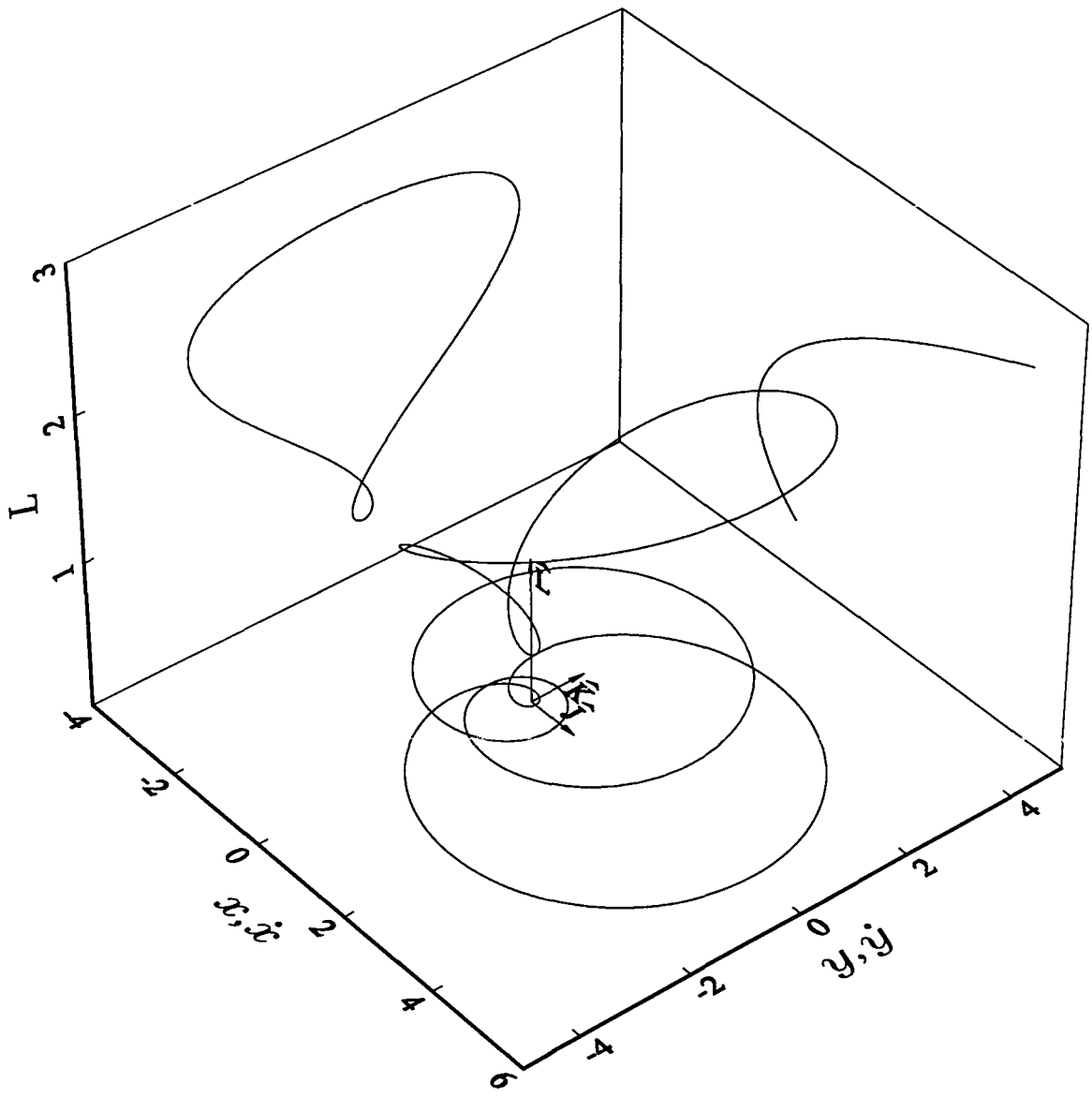


Figure 2.5.2. The variation in the magnitude of the angular momentum vector along the orbit corresponding with Figure 2.5.1. The projections of the angular momentum curve onto planes parallel to the xy, xL and yL planes are also shown. In this example the angular momentum is constant in direction but varies in magnitude.

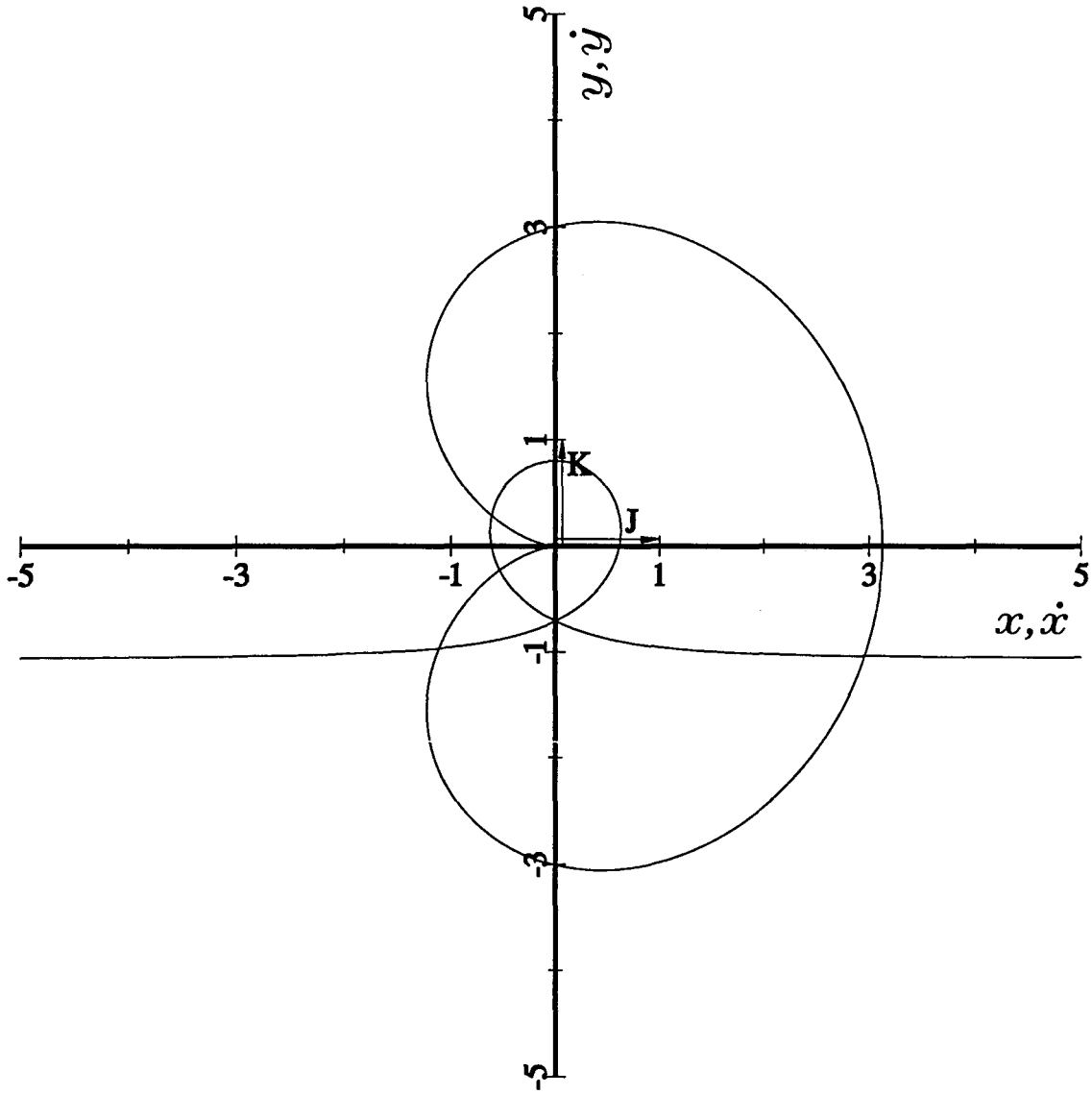


Figure 2.5.3. The velocity hodograph (loop–shaped) and the orbit (bean–shaped) for $U = \mu$, $V = \alpha \sin\big((\theta - \beta)/2\big)/2$, $\mu = 1$, $\alpha = 1$, $\beta = 0$, $\theta_0 = 0$, $K = J = 1$ and $L_0 = 2.5$. The orbit has a singularity at the origin and correspondingly the $\dot{x}-$components of the velocity hodograph become infinite at this point.

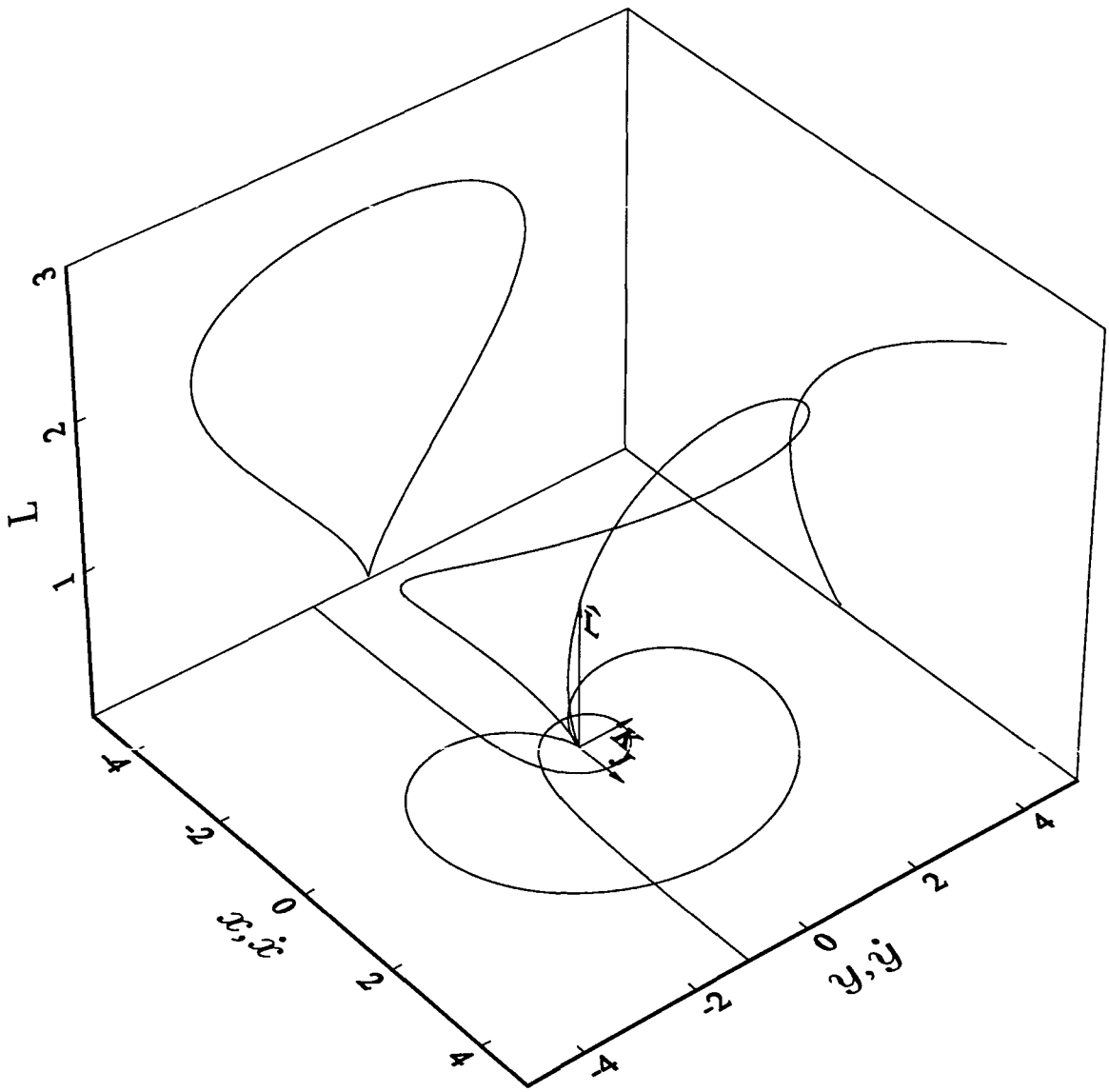


Figure 2.5.4. The variation in the magnitude of the angular momentum vector along the orbit corresponding with Figure 2.5.3. The projections of the angular momentum curve onto planes parallel to the xy, xL and yL planes are also shown. Note that the angular momentum is zero at the singularity. The angular momentum is only constant in direction but not in magnitude.

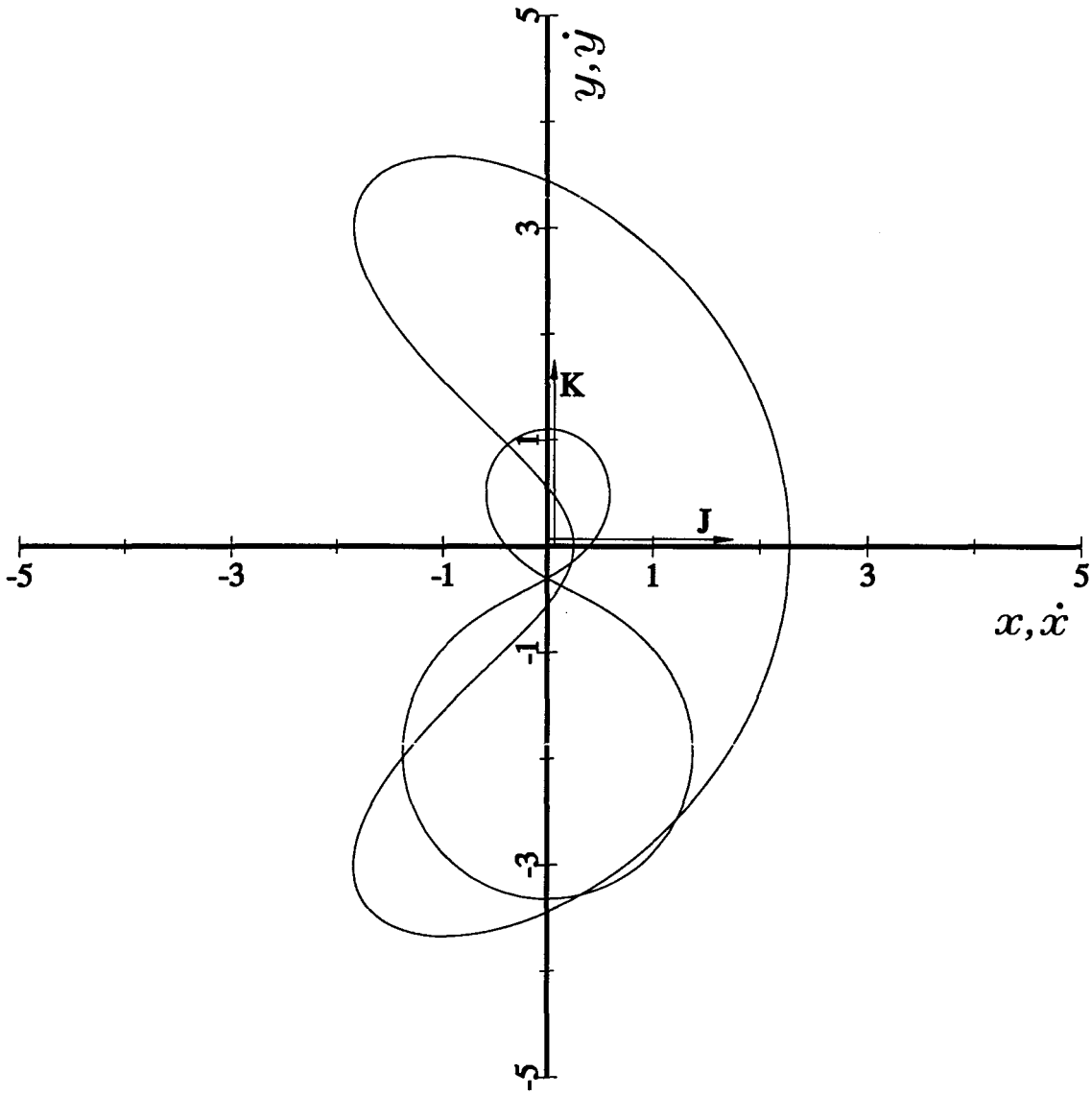


Figure 2.5.5. The velocity hodograph (figure–of–eight shaped) and the orbit (bean–shaped) for $U = \mu$, $V = \alpha \sin\big((\theta - \beta)/2\big)/2$, $\mu = 1$, $\alpha = 1$, $\beta = 0$, $\theta_0 = 0$, $K = J = 1.75$ and $L_0 = 2.5$. Note that the origin is outside the orbit but inside the velocity hodograph.

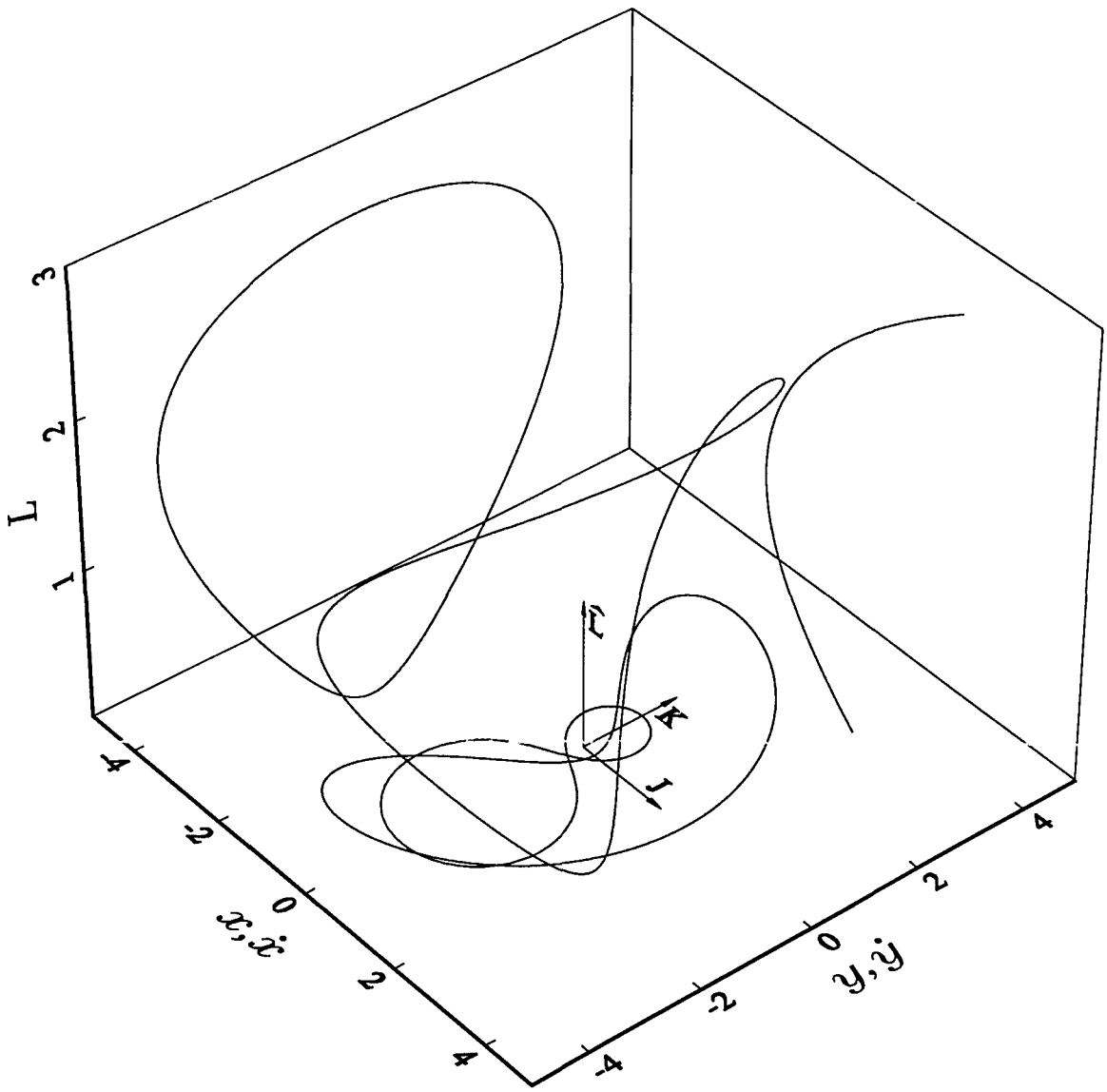


Figure 2.5.6. The variation in the magnitude of the angular momentum vector along the orbit corresponding with Figure 2.5.5. The projections of the angular momentum curve onto planes parallel to the xy, xL and yL planes are also shown. Note that the angular momentum changes direction at two places along the orbit.

is zero at the singularity. The angular momentum is only constant in direction but not in magnitude. Figure 2.5.5 shows the velocity hodograph (figure–of–eight shaped) and the orbit (bean–shaped) in the case $\mu < J$. Both the velocity hodograph and the orbit are closed. Note also that the origin is outside the orbit whilst inside the velocity hodograph. Figure 2.5.6 shows the variation in the magnitude of the angular momentum vector along the orbit corresponding with Figure 2.5.5. Note that the angular momentum changes direction at two points along the orbit. Note also that the analytic solution (2.2.8) breaks down when $\hat{\boldsymbol{L}}$ points downwards.

2.6 The Lie Algebras of the First Integrals

The two non–zero Cartesian components of (2.5.16) are

$$\begin{aligned} J_1 &= p_r p_\theta \sin\theta + \frac{{p_\theta}^2}{r}\cos\theta - \mu\cos\theta \\ &\quad + \alpha r^{\frac{1}{2}} \sin\frac{1}{2}(\theta-\beta)\ \sin\theta \end{aligned} \tag{2.6.1}$$

$$\begin{aligned} J_2 &= -p_r p_\theta \cos\theta + \frac{{p_\theta}^2}{r}\sin\theta - \mu\sin\theta \\ &\quad - \alpha r^{\frac{1}{2}} \sin\frac{1}{2}(\theta-\beta)\ \cos\theta, \end{aligned} \tag{2.6.2}$$

where for convenience we have written the Cartesian representation in terms of the usual polar coordinates r and θ. An alternative derivation of (2.6.1) and (2.6.2) would have been to use the structure for H (2.5.1) and $\boldsymbol{J}$ (2.1.9) and impose the requirement that the Poisson bracket of H with each of J_1 and J_2 be zero. The result is the same although the machinery used is quite different. For a detailed treatment see Gorringe and Leach [42].

The two components of the Laplace–Runge–Lenz vector (2.6.1) and (2.6.2) can be used to generate a third integral using Poisson's theorem (see [129, p320 §145] and Poisson's paper cited there).

$$\begin{aligned} [J_1, J_2]_{PB} &= \frac{\partial J_1}{\partial r}\frac{\partial J_2}{\partial p_r} + \frac{\partial J_1}{\partial \theta}\frac{\partial J_2}{\partial p_\theta} - \frac{\partial J_1}{\partial p_r}\frac{\partial J_2}{\partial r} - \frac{\partial J_1}{\partial p_\theta}\frac{\partial J_2}{\partial \theta} \\ &= -2p_\theta H - p_r \alpha r^{\frac{1}{2}} \sin\frac{1}{2}(\theta-\beta) - p_\theta \alpha r^{-\frac{1}{2}} \cos\frac{1}{2}(\theta-\beta) \end{aligned} \tag{2.6.3}$$

and we define the third integral I to be

$$I = 2p_\theta H + p_r \alpha r^{\frac{1}{2}} \sin\frac{1}{2}(\theta-\beta) + p_\theta \alpha r^{-\frac{1}{2}} \cos\frac{1}{2}(\theta-\beta). \tag{2.6.4}$$

The algebra of the Poisson Brackets of J_1, J_2 and I is

$$\begin{aligned}
[J_1, J_2]_{PB} &= -I \\
[J_1, I]_{PB} &= -2H\, J_2 - \frac{1}{2}\,\alpha^2 \sin\beta \\
[J_2, I]_{PB} &= 2H\, J_1 + \frac{1}{2}\,\alpha^2 \cos\beta.
\end{aligned} \tag{2.6.5}$$

The bracket relations (2.6.5) are not very tidy. For negative energy we define

$$\begin{aligned}
A_- &= (-2H)^{-\frac{1}{2}} \left(J_1 + \frac{\alpha^2 \cos\beta}{4H} \right) \\
B_- &= (-2H)^{-\frac{1}{2}} \left(J_2 + \frac{\alpha^2 \sin\beta}{4H} \right) \\
C_- &= \frac{I}{2H}
\end{aligned} \tag{2.6.6}$$

so that using (2.6.5) we find that

$$\begin{aligned}
[A_-, B_-]_{PB} &= C_- \\
[B_-, C_-]_{PB} &= A_- \\
[C_-, A_-]_{PB} &= B_-
\end{aligned} \tag{2.6.7}$$

which is immediately recognisable as the Lie algebra $so(3)$. For positive energy we define

$$\begin{aligned}
A_+ &= (2H)^{-\frac{1}{2}} \left(J_1 + \frac{\alpha^2 \cos\beta}{4H} \right) \\
B_+ &= (2H)^{-\frac{1}{2}} \left(J_2 + \frac{\alpha^2 \sin\beta}{4H} \right) \\
C_+ &= \frac{I}{2H}
\end{aligned} \tag{2.6.8}$$

so that

$$\begin{aligned}
[A_+, B_+]_{PB} &= -C_+ \\
[B_+, C_+]_{PB} &= A_+ \\
[C_+, A_+]_{PB} &= B_+
\end{aligned} \tag{2.6.9}$$

which are the Poisson Bracket relations for the non-compact Lie algebra $so(2,1)$. It is well-known for the Kepler problem that the angular momentum, Laplace-Runge-Lenz vector and the Hamiltonian are not independent (see equation (1.5.19)). For this problem a similar relationship can be found after some manipulation. It is

$$\frac{1}{2H} \left\{ \left(J_1 + \frac{\alpha^2 \cos\beta}{4H} \right)^2 + \left(J_2 + \frac{\alpha^2 \sin\beta}{4H} \right)^2 - \left(\mu - \frac{\alpha^2}{4H} \right)^2 \right\} = \left(\frac{I}{2H} \right)^2. \tag{2.6.10}$$

The relationship (2.6.10) is also not very neat. If we define

$$\begin{aligned} \mu- &= (-2H)^{-\frac{1}{2}}\left(\mu - \frac{\alpha^2}{4H}\right) \\ \mu+ &= (2H)^{-\frac{1}{2}}\left(\mu - \frac{\alpha^2}{4H}\right) \end{aligned} \tag{2.6.11}$$

for negative and positive energies respectively, (2.6.10) can be rewritten as

$$\mu_-^2 = A_-^2 + B_-^2 + C_-^2 \tag{2.6.12}$$

for negative energies, and

$$\mu_+^2 = A_+^2 + B_+^2 - C_+^2 \tag{2.6.13}$$

for positive energies. In the space of first integrals equation (2.6.12) represents a sphere which is naturally associated with $so(3)$ symmetry and (2.6.13) a hyperboloid of one sheet, the natural geometric object associated with $so(2,1)$ symmetry.

When H takes on the particular value of zero, the analysis following (2.6.3) no longer holds true. The third integral is now

$$I = p_r \alpha r^{\frac{1}{2}} \sin\frac{1}{2}(\theta - \beta) + p_\theta \alpha r^{-\frac{1}{2}} \cos\frac{1}{2}(\theta - \beta) \tag{2.6.14}$$

which is no longer a true first integral but, rather, a configurational invariant as discussed by Hall [47] and Sarlet *et al.* [116], since it is only invariant for that particular value of H. Introducing the unit vector $\hat{\boldsymbol{\beta}}$ which is given by

$$\hat{\boldsymbol{\beta}} = \hat{\boldsymbol{j}}_1 \cos\beta + \hat{\boldsymbol{j}}_2 \sin\beta, \tag{2.6.15}$$

where $\hat{\boldsymbol{j}}_1$ and $\hat{\boldsymbol{j}}_2$ are the unit vectors along which J_1 and J_2 lie respectively, it is now possible to show that

$$\boldsymbol{J} \cdot \hat{\boldsymbol{\beta}} = \frac{I^2}{\alpha^2} - \mu \tag{2.6.16}$$

or equivalently that

$$J_1 \cos\beta + J_2 \sin\beta = \frac{I^2}{\alpha^2} - \mu. \tag{2.6.17}$$

Equation (2.6.17) represents the natural geometric object associated with the case $H = 0$ which describes a right parabolic cylinder with $\hat{\boldsymbol{\beta}}$ lying along the axis of symmetry.

A distinction can now be drawn with the standard Kepler problem, where, for $H = 0$, $J = \pm\mu$ from (1.5.19). This is the equation for a plane, unlike (2.6.17). This discrepancy is also reflected in the form of the algebra. We define

$$\begin{aligned} A_0 &= -J_1 \sin\beta + J_2 \cos\beta \\ B_0 &= \frac{2I}{\alpha^2} \\ C_0 &= 1. \end{aligned} \tag{2.6.18}$$

The combination $J_1 \cos\beta + J_2 \sin\beta$ cannot be used as this is a function of I from (2.6.17). The Poisson bracket relations are

$$\begin{aligned} [A_0, B_0]_{PB} &= C_0 \\ [B_0, C_0]_{PB} &= 0 \\ [C_0, A_0]_{PB} &= 0 \end{aligned} \tag{2.6.19}$$

which represent the Weyl algebra $W(3,1)$. The standard Kepler problem has the algebra $E(2)$ when $H = 0$.

For $H \neq 0$, the Hamiltonian can be expressed as a function of the three first integrals, J_1, J_2 and I, and is

$$H = \frac{1}{2\left(J^2 - \mu^2\right)} \left[I^2 - \alpha^2(J_1 \cos\beta + J_2 \sin\beta + \mu)\right]. \tag{2.6.20}$$

2.7 The Connection with Sen's Results

An alternate derivation of the integrals for the Hamiltonian was proposed by Sen [118] which is an extension of the work done on first integrals polynomial in the velocities for a variety of Hamiltonian systems by amongst others Gascón *et al.* [30], Grammaticos *et al.* [44], Thompson [125], Hietarinta [53], Leach [74] and also the work done on time-dependent systems by Lewis and Leach [85]. Essentially Sen assumes a polynomial structure for the first integral

$$I_S = \sum_{i=0} \sum_{j=0} d_{ij}(x,y) {p_x}^i {p_y}^j, \quad i + j \leq n, \tag{2.7.1}$$

where $i+j$ is either even or odd in sympathy with n since autonomous first integrals for an autonomous Hamiltonian of even degree in the momenta are either even or odd in the momenta (see Thompson [125]). He takes this idea further by making a point transformation to a complex coordinate system using

$$\begin{aligned} z &= 2^{-1/2}(x+iy), \qquad \bar{z} = 2^{-1/2}(x-iy) \\ p_z &= 2^{-1/2}(p_x - ip_y), \quad p_{\bar{z}} = 2^{-1/2}(p_x + ip_y). \end{aligned} \tag{2.7.2}$$

In these new coordinates, H_S is now of the form

$$H_S = 2p_z p_{\bar{z}} + V(z,\bar{z}) \tag{2.7.3}$$

and the invariant becomes

$$\begin{aligned} I_S = (zp_z - \bar{z}p_{\bar{z}})^{n-2} p_z p_{\bar{z}} \;+\; & \sum_{i=0}\sum_{j=0} e_{ij}(z,\bar{z}) p_z^i p_{\bar{z}}^j, \\ & i+j \leq n-2. \end{aligned} \tag{2.7.4}$$

Imposing the condition that the Poisson bracket of (2.7.4) with H_S (2.7.3) must vanish results in a system of equations obtained by equating the coefficients of different powers of p_z and $p_{\bar{z}}$ to zero. The solution of this set of equations for a particular n determines the invariants and the integrable potential. The integrable Hamiltonian

$$H_{IS} = 2p_z p_{\bar{z}} + az^{-\frac{1}{2}} + b\bar{z}^{-\frac{1}{2}} + c(z\bar{z})^{-\frac{1}{2}} \tag{2.7.5}$$

gives rise to the third order invariant

$$\begin{aligned} I_3 = (zp_z - \bar{z}p_{\bar{z}})p_z p_{\bar{z}} \;+\; & \frac{1}{2}\left[b\bar{z}^{-\frac{1}{2}} + c(z\bar{z})^{-\frac{1}{2}}\right] zp_z \\ - \; & \frac{1}{2}\left[az^{-\frac{1}{2}} + c(z\bar{z})^{-\frac{1}{2}}\right] \bar{z}p_{\bar{z}} \end{aligned} \tag{2.7.6}$$

as well as the two quadratic invariants

$$I_1 = (zp_z - \bar{z}p_{\bar{z}})p_z + \frac{1}{2}\left[b\bar{z}^{\frac{1}{2}} - az^{-\frac{1}{2}}\bar{z} - cz^{-\frac{1}{2}}\bar{z}^{\frac{1}{2}}\right] \tag{2.7.7}$$

$$I_2 = (zp_z - \bar{z}p_{\bar{z}})p_{\bar{z}} + \frac{1}{2}\left[bz\bar{z}^{-\frac{1}{2}} - az^{\frac{1}{2}} + cz^{\frac{1}{2}}\bar{z}^{-\frac{1}{2}}\right]. \tag{2.7.8}$$

It is easy to show that, when

$$b = \bar{a} = a_1 - ia_2, \tag{2.7.9}$$

$$\begin{aligned} H_{IS} &= 2H \\ -2^{-1/2}(I_1 - I_2) &= J_1 \\ -2^{-1/2}\, i(I_1 + I_2) &= J_2 \\ 2iI_3 &= I, \end{aligned} \tag{2.7.10}$$

where H is given in (2.5.12) and J_1 and J_2 in (2.6.1) and (2.6.2). Now $a = a_1 + ia_2$ and c can be expressed in terms of the constants appearing in J_1, J_2 and I, as follows

$$\begin{aligned} a_1 &= -2^{-1/4}\alpha \cos\frac{1}{2}\beta \\ a_2 &= -2^{-1/4}\alpha \sin\frac{1}{2}\beta \\ c &= -2^{1/2}\mu. \end{aligned} \tag{2.7.11}$$

For convenience, Sen defined

$$\begin{aligned} A_S &= \left(\frac{\varepsilon}{2H_{IS}}\right)^{\frac{1}{2}}\left[I_1 - I_2 - \frac{1}{2H_{IS}}\left(a^2 + \bar{a}^2\right)\right] \\ &= -2^{\frac{1}{2}}\left(\frac{\varepsilon}{4H}\right)^{\frac{1}{2}}\left(J_1 + \alpha^2\frac{\cos\beta}{4H}\right) \\ B_S &= i\left(\frac{\varepsilon}{2H_{IS}}\right)^{\frac{1}{2}}\left[I_1 + I_2 + \frac{1}{2H_{IS}}\left(a^2 - \bar{a}^2\right)\right] \\ &= -2^{\frac{1}{2}}\left(\frac{\varepsilon}{4H}\right)^{\frac{1}{2}}\left(J_2 + \alpha^2\frac{\sin\beta}{4H}\right) \\ C_S &= -\frac{2i}{H_{IS}}I_3 \\ &= -\frac{I}{2H}, \end{aligned} \tag{2.7.12}$$

where $\varepsilon = \operatorname{sgn} H$ and (2.7.12) is in agreement with the equations (2.6.6) and (2.6.8) obtained earlier. The relationship between the integrals is given by

$$\left(I_1 I_2 + \frac{1}{4}c^2\right)H_{IS} + \frac{1}{2}\left(a^2 I_1 - \bar{a}^2 I_2\right) + \frac{1}{2}a\bar{a}c = 2{I_3}^2 \tag{2.7.13}$$

and, using

$$I_1 I_2 = -\frac{1}{2}\left({J_1}^2 + {J_2}^2\right) \tag{2.7.14}$$

and

$$a^2 I_1 - \bar{a}^2 I_2 = -2^{-1/2}a^2(J_1 - iJ_2) - 2^{-1/2}\bar{a}^2(J_1 + iJ_2), \tag{2.7.15}$$

(2.7.13) reduces to (2.6.10).

2.8 The Extension of the Hamiltonian Treatment to Three Dimensions

It would at this stage seem sensible to extend these results to three dimensions. In terms of spherical polar coordinates

$$H = \frac{1}{2}\left(p_r^2 + \frac{p_\theta^2}{r^2} + \frac{p_\phi^2}{r^2 \sin^2\theta}\right) + V(r,\theta,\phi) \tag{2.8.1}$$

$$J_1 = \frac{1}{r}\left(p_\theta^2 + \frac{p_\phi^2}{\sin^2\theta}\right)\sin\theta\cos\phi - p_r p_\theta \cos\theta\cos\phi$$
$$+\frac{p_r p_\phi}{\sin\theta}\sin\phi + f(r,\theta,\phi) \tag{2.8.2}$$

$$J_2 = \frac{1}{r}\left(p_\theta^2 + \frac{p_\phi^2}{\sin^2\theta}\right)\sin\theta\sin\phi - p_r p_\theta \cos\theta\sin\phi$$
$$-\frac{p_r p_\phi}{\sin\theta}\cos\phi + g(r,\theta,\phi) \tag{2.8.3}$$

$$J_3 = \frac{1}{r}\left(p_\theta^2 + \frac{p_\phi^2}{\sin^2\theta}\right)\cos\theta + p_r p_\theta \sin\theta$$
$$+h(r,\theta,\phi). \tag{2.8.4}$$

Using the requirement that J_1, J_2 and J_3 have zero Poisson Bracket with H, rather than using the equation of motion directly as was done previously, gives rise to nine equations for the r, θ and ϕ derivatives of f, g and h. Imposing the consistency condition between the mixed derivatives of f, g and h leads to nine equations for the potential V. These can then be rearranged to give

$$\frac{\partial}{\partial r}\left(r^2 \frac{\partial V}{\partial \theta}\right) = 0 \tag{2.8.5}$$

$$\frac{\partial}{\partial r}\left(r^2 \frac{\partial V}{\partial \phi}\right) = 0 \tag{2.8.6}$$

$$\frac{\partial}{\partial \theta}\left(\frac{1}{\sin\theta}\frac{\partial V}{\partial \phi}\right) = 0 \tag{2.8.7}$$

$$\frac{\partial}{\partial r}\left(r^2 \frac{\partial V}{\partial r}\right) - \frac{\partial^2 V}{\partial \theta^2} = 0 \tag{2.8.8}$$

$$\frac{\partial}{\partial r}\left(2r \frac{\partial V}{\partial \theta}\right) - \frac{\partial V}{\partial \theta} = 0 \tag{2.8.9}$$

$$\frac{\partial}{\partial r}\left(2r\,\frac{\partial V}{\partial \phi}\right) - \frac{\partial V}{\partial \phi} = 0 \tag{2.8.10}$$

$$\sin\theta\left[\frac{\partial}{\partial r}\left(r^2\frac{\partial V}{\partial r}\right) - \frac{1}{\sin^2\theta}\frac{\partial^2 V}{\partial \phi^2}\right] - \cos\theta\,\frac{\partial V}{\partial \theta} = 0 \tag{2.8.11}$$

(two equations become identically zero).

Making the combination $2\times(2.8.5) - r\times(2.8.9)$ gives

$$\frac{\partial V}{\partial \theta} = 0. \tag{2.8.12}$$

Similarily the combination $2\times(2.8.6) - r\times(2.8.10)$ yields

$$\frac{\partial V}{\partial \phi} = 0. \tag{2.8.13}$$

Equation (2.8.7) is then immediately satisfied. Equations (2.8.8) and (2.8.11) reduce to

$$\frac{\partial}{\partial r}\left(r^2\frac{\partial V}{\partial r}\right) = 0. \tag{2.8.14}$$

The only nontrivial solution to (2.8.14) is

$$V = -\frac{\mu}{r}, \tag{2.8.15}$$

which is, of course, the potential for the standard Kepler problem. Thus it would seem that the only autonomous Hamiltonian of the form $H = T + V$ describing a three–dimensional motion which possesses a Laplace–Runge–Lenz vector of the form

$$\boldsymbol{J} = \dot{\boldsymbol{r}}\times\boldsymbol{L} + \boldsymbol{f}(r,\theta,\phi), \tag{2.8.16}$$

is the Kepler problem. It also appears that the two–dimensional problem considered is singularly unique. Sen [118] further considered the quantum mechanical represenations of the two–dimensional Hamiltonian. The presence of the quadratic invariants in the classical case implies that the quantum mechanical version of this potential is also integrable (see Hietarinta [52]). He then proceeded to obtain the quantum invariants, the identical algebra to the classical case and the bound state energy spectrum using the Casimir operator for $so(3)$. This should not be suprising in view of equation (2.6.12).

2.9 The First Integrals Associated with the Time Invariance Symmetry

The contents of §2.9 are also described in Gorringe and Leach [42]. For completeness, as well as to correct a misconception by Sen, it would seem worthwhile to construct the integrals, H, J_1 and J_2 of §§2.5 and 2.6 using the Lie symmetry generator. Sen has shown that the differential equation (2.5.14)

$$\ddot{\boldsymbol{r}} + \left(\frac{\mu}{r^2} + \frac{\alpha \cos \frac{1}{2}(\theta - \beta)}{2r^{\frac{3}{2}}}\right)\hat{\boldsymbol{r}} + \frac{\alpha \sin \frac{1}{2}(\theta - \beta)}{2r^{\frac{3}{2}}}\,\hat{\boldsymbol{\theta}} = \mathbf{0} \tag{2.9.1}$$

gives rise to the single generator $G_1 = \partial/\partial t$. He incorrectly interprets this as giving rise to only the conservation of energy. Leach [72] in his study of the Kepler problem constructs the energy (in this case the Hamiltonian), the angular momentum and the components of the Laplace–Runge–Lenz vector from this symmetry. Of course a system having N degrees of freedom can at most have only $2N - 1$ independent autonomous first integrals (see Kaplan [59]).

The Lie symmetry generator G can be written in plane polar coordinates as

$$G = \tau(t, r, \theta)\frac{\partial}{\partial t} + \xi(t, r, \theta)\frac{\partial}{\partial r} + \eta(t, r, \theta)\frac{\partial}{\partial \theta} \tag{2.9.2}$$

which has the first extension

$$G^{[1]} = G + (\dot{\xi} - \dot{r}\dot{\tau})\frac{\partial}{\partial \dot{r}} + (\dot{\eta} - \dot{\theta}\dot{\tau})\frac{\partial}{\partial \dot{\theta}}. \tag{2.9.3}$$

According to the Lie method as described in §P3.2, a function $I(t, r, \theta, \dot{r}, \dot{\theta})$ which is associated with a symmetry G is a first integral if

$$G^{[1]}I = 0 \tag{2.9.4}$$

and

$$\left.\frac{\mathrm{d}I}{\mathrm{d}t}\right|_{\boldsymbol{E}=\mathbf{0}} = 0, \tag{2.9.5}$$

where $\boldsymbol{E}\,(t, r, \theta, \dot{r}, \dot{\theta}) = \mathbf{0}$ is the equation of motion (2.9.1). Substituting the first extension (2.9.3) of the time invariance symmetry $G = \partial/\partial t$ in (2.9.4) leads to the equation

$$\frac{\partial I}{\partial t} + 0\,\frac{\partial I}{\partial r} + 0\,\frac{\partial I}{\partial \theta} + 0\,\frac{\partial I}{\partial \dot{r}} + 0\,\frac{\partial I}{\partial \dot{\theta}} = 0, \tag{2.9.6}$$

which gives the characteristics as solutions to the associated Lagrange's system

$$\frac{\mathrm{d}t}{1} = \frac{\mathrm{d}r}{0} = \frac{\mathrm{d}\theta}{0} = \frac{\mathrm{d}\dot{r}}{0} = \frac{\mathrm{d}\dot{\theta}}{0}. \tag{2.9.7}$$

They are

$$\begin{aligned} u_1 &= r \qquad v_1 = \dot{r} \\ u_2 &= \theta \qquad v_2 = \dot{\theta}, \end{aligned} \tag{2.9.8}$$

which are individually invariant under the infinitesimal transformation generated by $G^{[1]}$.

Rewriting I in terms of the characteristics and imposing the condition for a first integral (2.9.5) gives

$$\dot{u}_1 \frac{\partial I}{\partial u_1} + \dot{u}_2 \frac{\partial I}{\partial u_2} + \dot{v}_1 \frac{\partial I}{\partial v_1} + \dot{v}_2 \frac{\partial I}{\partial v_2} = 0. \tag{2.9.9}$$

Substituting for the equation of motion reveals

$$\begin{aligned} \dot{u}_1 &= v_1 \\ \dot{v}_1 &= u_1 v_2^2 - \frac{\mu}{u_1^2} - \frac{\alpha \cos \frac{1}{2}(u_2 - \beta)}{2u_1{}^{\frac{3}{2}}} \\ \dot{u}_2 &= v_2 \\ \dot{v}_2 &= -\frac{2v_1 v_2}{u_1} - \frac{\alpha \sin \frac{1}{2}(u_2 - \beta)}{2u_1{}^{\frac{5}{2}}}, \end{aligned} \tag{2.9.10}$$

and the characteristics of (2.9.9) are found from

$$\begin{aligned} \frac{\mathrm{d}u_1}{v_1} &= \frac{\mathrm{d}u_2}{v_2} = \frac{\mathrm{d}v_1}{u_1 v_2^2 - \frac{\mu}{u_1^2} - \frac{\alpha \cos \frac{1}{2}(u_2 - \beta)}{2u_1^{3/2}}} \\ &= \frac{\mathrm{d}v_2}{\frac{-2v_1 v_2/u_1 - \frac{1}{2}\alpha \sin \frac{1}{2}(u_2 - \beta)}{u_1^{5/2}}}. \end{aligned} \tag{2.9.11}$$

Numbering the ith element of (2.9.11) as (2.9.11.i), $i = 1, \ldots, 4$ the combination

$$\begin{aligned} &\left(u_1 v_2^2 + \frac{\mu}{u_1^2} + \frac{\alpha \cos \frac{1}{2}(u_2 - \beta)}{2u_1{}^{\frac{3}{2}}}\right)(2.9.11.1) \\ &+ \frac{\alpha \sin \frac{1}{2}(u_2 - \beta)}{2u_1{}^{\frac{1}{2}}}(2.9.11.2) + v_1(2.9.11.3) + u_1^2 v_2(2.9.11.4) \end{aligned} \tag{2.9.12}$$

gives

$$\frac{\mathrm{d}\left[\frac{1}{2}(v_1^2 + u_1^2 v_2^2) - \frac{\mu}{u_1} - \frac{\alpha \cos \frac{1}{2}(u_2 - \beta)}{u_1{}^{\frac{1}{2}}}\right]}{0}. \tag{2.9.13}$$

The term in crochets is a characteristic and hence a first integral. On reverting to the original coodinates, it is easy to verify that (2.9.13) is in fact the energy, which in this case is the Hamiltonian. Similarly the components of the Laplace–Runge–Lenz are obtained from the combinations

$$\begin{aligned}
&\left(2u_1v_1v_2\sin u_2 + 3u_1^2v_2^2\cos u_2 + \frac{1}{2}\,\alpha u_1^{-\frac{1}{2}}\sin\frac{1}{2}(u_2-\beta)\sin u_2\right)\text{(2.9.11.1)}\\
+\;&\left(u_1^2v_1v_2\cos u_2 - u_1^3v_2^2\sin u_2 + \mu\sin u_2 + \frac{1}{2}\,\alpha u_1^{\frac{1}{2}}\cos\frac{1}{2}(u_2-\beta)\sin u_2\right.\\
+\;&\left.\alpha u_1^{\frac{1}{2}}\sin\frac{1}{2}(u_2-\beta)\cos u_2\right)\text{(2.9.11.2)} + \left(u_1^2v_2\sin u_2\right)\text{(2.9.11.3)}\\
+\;&\left(u_1^2v_1\sin u_2 + 2u_1^3v_2\cos u_2\right)\text{(2.9.11.4)} \qquad\qquad (2.9.14)
\end{aligned}$$

for J_1 and

$$\begin{aligned}
&\left(-2u_1v_1v_2\cos u_2 + 3u_1^2v_2^2\sin u_2 - \frac{1}{2}\,\alpha u_1^{-\frac{1}{2}}\sin\frac{1}{2}(u_2-\beta)\cos u_2\right)\text{(2.9.11.1)}\\
+\;&\left(u_1^2v_1v_2\sin u_2 + u_1^3v_2^2\cos u_2 - \mu\cos u_2 - \frac{1}{2}\,\alpha u_1^{\frac{1}{2}}\cos\frac{1}{2}(u_2-\beta)\cos u_2\right.\\
+\;&\left.\alpha u_1^{\frac{1}{2}}\sin\frac{1}{2}(u_2-\beta)\sin u_2\right)\text{(2.9.11.2)} + \left(-u_1^2v_2\cos u_2\right)\text{(2.9.11.3)}\\
+\;&\left(-u_1^2v_1\cos u_2 + 2u_1^3v_2\sin u_2\right)\text{(2.9.11.4)} \qquad\qquad (2.9.15)
\end{aligned}$$

for J_2. Finally I comes from the combination

$$\begin{aligned}
&\left(4u_1v_2H + \frac{1}{2}\,u_1^{-\frac{1}{2}}v_1\alpha\sin\frac{1}{2}(u_2-\beta) + \frac{3}{2}\,u_1^{\frac{1}{2}}v_2\alpha\cos\frac{1}{2}(u_2-\beta)\right)\text{(2.9.11.1)}\\
+\;&\left(\frac{1}{2}\,u_1^{\frac{1}{2}}v_1\alpha\cos\frac{1}{2}(u_2-\beta) - \frac{1}{2}\,u_1^{\frac{3}{2}}v_2\alpha\sin\frac{1}{2}(u_2-\beta)\right)\text{(2.9.11.2)} \qquad (2.9.16)\\
+\;&\left(u_1^{\frac{1}{2}}\alpha\sin\frac{1}{2}(u_2-\beta)\right)\text{(2.9.11.3)} + \left(2u_1^2H + u_1^{\frac{3}{2}}\alpha\cos\frac{1}{2}(u_2-\beta)\right)\text{(2.9.11.4)},
\end{aligned}$$

where the fact that $\mathrm{d}H{=}0$ is used. Since (2.9.11) can have at most three independent characteristics, it is not surprising that H, J_1, J_2 and I are related by (2.6.10). Although it can be argued that the solution of (2.9.11) is not necessarily transparent, it is one possible method where it is not essential to have an *a priori* ansatz for the structure of the first integrals.

2.10 The Conserved Hamilton and Laplace–Runge–Lenz Vector Analogues for the Equation of Motion $\ddot{\boldsymbol{r}} + f\dot{\boldsymbol{r}} + g\boldsymbol{r} = \boldsymbol{0}$

The contents of §§2.10 and 2.11 are described in Gorringe and Leach [39]. In §2.1 we had that

$$\dot{\boldsymbol{L}} + h_1\boldsymbol{L} = \boldsymbol{0} \tag{2.10.1}$$

which we can alternatively rewrite as

$$\boldsymbol{r} \times \ddot{\boldsymbol{r}} + g_1\boldsymbol{r} \times \boldsymbol{r} + h_1\boldsymbol{r} \times \dot{\boldsymbol{r}} = \boldsymbol{0} \tag{2.10.2}$$

where g_1 and h_1 are again arbitrary functions. It now follows that the equation of motion

$$\ddot{\boldsymbol{r}} + f\dot{\boldsymbol{r}} + g\boldsymbol{r} = \boldsymbol{0}, \tag{2.10.3}$$

where $f = h_1$ and $g = g_1$, describes motion in a plane with $\hat{\boldsymbol{L}}$ conserved. It should be noted that (2.10.3) should not be regarded as the most general equation of motion in the plane, but one further class of physical interest. Equation (2.10.3) is a generalisation of the equation of motion describing low altitude satellites proposed by Brouwer and Hori [14]. They obtained a closed–form solution which included first–order corrections for drag acceleration involving a quadratic velocity dependent term to account for atmospheric effects on satellites sufficiently close to the Earth. Danby [25] modified this assumption and used a resistive term which was proportional to the vector velocity and inversely proportional to the square of the radial distance. For small values of this constant he obtained a first–order perturbation solution. Mittleman and Jezewski [95] gave an exact analytic solution to the same problem and in a later paper [58] they further demonstrated the existence of direct analogues of the angular momentum, energy and Laplace–Runge–Lenz vector of the classical Kepler problem for the Danby problem. The approach used was to manipulate the equation of motion as had been done by Collinson [21, 22], Pollard [108] and also Sarlet and Bahar [115] on various non–linear problems. The work done by Mittleman and Jezewski [95] is unneccessarily complicated and the techniques demonstrated previously in Chapter 1 lend themselves to an elegant and natural progression in the construction of conserved vector analogues and the subsequent solution of the orbit.

We now establish conditions on the functional forms of f and g and ascertain whether the law proposed by Danby [25] is indeed unique, or an introduction to a whole class of problems admitting conserved vector analogues.

Taking the vector product of $\boldsymbol{r}$ with (2.10.3) gives

$$\dot{L} = -fL. \tag{2.10.4}$$

The initial assumption was that $\hat{\boldsymbol{L}}$ was constant. Thus the orbit is planar with $\hat{\boldsymbol{L}}$ directed from the origin perpendicular to the plane of the orbit. Using (2.10.4), f can be eliminated from (2.10.3) giving

$$\ddot{\boldsymbol{r}} - \frac{\dot{L}}{L}\dot{\boldsymbol{r}} + g\boldsymbol{r} = \boldsymbol{0}. \tag{2.10.5}$$

Equation (2.10.5) can be written as

$$\frac{\mathrm{d}}{\mathrm{d}t}\left(\frac{\dot{\boldsymbol{r}}}{L}\right) + \frac{g\boldsymbol{r}}{L} = \boldsymbol{0} \tag{2.10.6}$$

on dividing throughout by L. Provided $\int g\boldsymbol{r}/L \, \mathrm{d}t$ can determined without a knowledge of $r(t)$ and $\theta(t)$, we can find a conserved vector which is the analogue of Hamilton's vector for the Kepler problem without solving (2.10.6) directly. Denoting the integral by the vector $\boldsymbol{u}$, we obtain

$$\boldsymbol{K} = \frac{\dot{\boldsymbol{r}}}{L} + \boldsymbol{u}. \tag{2.10.7}$$

The Laplace–Runge–Lenz vector analogue is obtained by taking the vector product of (2.10.7) with $\hat{\boldsymbol{L}}$ and is given by

$$\boldsymbol{J} = \frac{\dot{\boldsymbol{r}} \times \hat{\boldsymbol{L}}}{L} + \boldsymbol{u} \times \hat{\boldsymbol{L}}. \tag{2.10.8}$$

2.11 The Velocity Hodograph and the Orbit Equation

The velocity hodograph is obtained by rewriting the expression for $\boldsymbol{K}$ (2.10.7) and squaring both sides of the equation as described above in §1.2. By separating $\boldsymbol{u}$ in terms of the polar unit vectors $\hat{\boldsymbol{r}}$ and $\hat{\boldsymbol{\theta}}$ and denoting the radial and angular coefficients as u_r and u_θ respectively, we obtain

$$\left(\frac{\dot{x}}{L} + K\sin\theta_0\right)^2 + \left(\frac{\dot{y}}{L} - K\cos\theta_0\right)^2 = {u_r}^2 + {u_\theta}^2, \tag{2.11.1}$$

where, as before, the angle between $\boldsymbol{K}$ and $\boldsymbol{j}$ is θ_0.

The orbit equation is obtained from (2.10.8) by taking the scalar product with $\boldsymbol{r}$, giving

$$r = \frac{1}{-u_\theta + J\cos(\theta - \theta_0)}. \tag{2.11.2}$$

To solve for $\boldsymbol{u}$, we make use of the cartesian representation for $\hat{\boldsymbol{r}}$,

$$\begin{aligned} \boldsymbol{u} &= \int \frac{g\boldsymbol{r}}{L}\,\mathrm{d}t \\ &= \boldsymbol{i}\int \frac{gr}{L}\cos\theta\,\mathrm{d}t + \boldsymbol{j}\int \frac{gr}{L}\sin\theta\,\mathrm{d}t. \end{aligned} \tag{2.11.3}$$

The two integrals in (2.11.3) can be evaluated provided

$$\frac{gr}{L} = v(\theta)\dot{\theta}. \tag{2.11.4}$$

Equation (2.11.3) then reduces to

$$\begin{aligned} \boldsymbol{u} &= \boldsymbol{i}\int_{\theta_0}^{\theta} v(\eta)\cos\eta\,\mathrm{d}\eta + \boldsymbol{j}\int_{\theta_0}^{\theta} v(\eta)\sin\eta\,\mathrm{d}\eta \\ &= \hat{\boldsymbol{r}}\int_{\theta_0}^{\theta} v(\eta)\cos(\theta-\eta)\mathrm{d}\eta - \hat{\boldsymbol{\theta}}\int_{\theta_0}^{\theta} v(\eta)\sin(\theta-\eta)\mathrm{d}\eta \\ &= z'(\theta)\hat{\boldsymbol{r}} - z(\theta)\hat{\boldsymbol{\theta}}, \end{aligned} \tag{2.11.5}$$

where

$$z(\theta) = \int_{\theta_0}^{\theta} v(\eta)\sin(\theta-\eta)\mathrm{d}\eta, \tag{2.11.6}$$

or, alternatively,

$$z''(\theta) + z(\theta) = v(\theta) \tag{2.11.7}$$

with initial conditions

$$z(\theta_0) = 0, \qquad z'(\theta_0) = 0. \tag{2.11.8}$$

Using (2.11.5) to replace $\boldsymbol{u}$ in (2.10.7) and (2.10.8) gives

$$\boldsymbol{K} = \frac{\dot{\boldsymbol{r}}}{L} + z'(\theta)\hat{\boldsymbol{r}} - z(\theta)\hat{\boldsymbol{\theta}} \tag{2.11.9}$$

and

$$\boldsymbol{J} = \frac{\dot{\boldsymbol{r}}\times\hat{\boldsymbol{L}}}{L} - z(\theta)\hat{\boldsymbol{r}} - z'(\theta)\hat{\boldsymbol{\theta}}. \tag{2.11.10}$$

By comparing (2.11.9) with (2.10.7) the radial and angular components of $\boldsymbol{u}$ are found to be

$$u_r = z'(\theta), \qquad u_\theta = -z(\theta). \tag{2.11.11}$$

Using (2.11.11) to substitute for u_r and u_θ, the velocity hodograph (2.11.1) becomes

$$\left(\frac{\dot{x}}{L} + K\sin\theta_0\right)^2 + \left(\frac{\dot{y}}{L} - K\cos\theta_0\right)^2 = z'^2(\theta) + z^2(\theta), \tag{2.11.12}$$

and the orbit equation (2.11.2) is given by

$$r = \frac{1}{z(\theta) + J\cos(\theta - \theta_0)}. \tag{2.11.13}$$

If f in (2.10.3) has the form

$$f = \frac{B(L,r,\theta)\dot{r} + C(L,r,\theta)\dot{\theta}}{LA(L,r,\theta)}, \tag{2.11.14}$$

where

$$\begin{aligned} A &= \frac{\partial M(L,r,\theta)}{\partial L} \\ B &= \frac{\partial M(L,r,\theta)}{\partial r} \\ C &= \frac{\partial M(L,r,\theta)}{\partial \theta}, \end{aligned} \tag{2.11.15}$$

equation (2.10.4) can be integrated to give

$$M(L,r,\theta) = h, \tag{2.11.16}$$

where h is a constant. Assuming (2.11.16) can be inverted to obtain L, we may write

$$L = N(h,r,\theta). \tag{2.11.17}$$

Rewriting (2.11.4) as

$$\frac{gr^3}{L^2} = v(\theta), \tag{2.11.18}$$

where $\dot{\theta}$ has been replaced by L/r^2, we obtain

$$g = \frac{1}{r^3}N^2(h,r,\theta)v(\theta). \tag{2.11.19}$$

Equations (2.11.14) and (2.11.19) prescribe one possible form of (2.10.3) for which the conserved vectors $\boldsymbol{K}$ and $\boldsymbol{J}$ (2.11.9) and (2.11.10) as well as the orbit equation (2.11.13) and the velocity hodograph (2.11.12) exist.

It is also possible to obtain a scalar energylike first integral that is a direct generalisation of that obtained by Jezewski and Mittleman [58] for the motion of the low level satellite.

$$\begin{aligned} \boldsymbol{I} &= \frac{1}{2}\boldsymbol{K}\cdot\boldsymbol{K} = \frac{1}{2}\boldsymbol{J}\cdot\boldsymbol{J} \\ &= \frac{1}{2}\frac{\dot{\boldsymbol{r}}\cdot\dot{\boldsymbol{r}}}{L^2} + \frac{1}{L}\left[\dot{r}z'(\theta) - r\dot{\theta}z(\theta)\right] + \frac{1}{2}\left[z^2(\theta) + z'^2(\theta)\right]. \end{aligned} \tag{2.11.20}$$

The derivation of (2.11.20) shown above is, incidentally, much simpler and more general than that used by Jezewski and Mittleman [58].

2.12 The Motion in Time

The radial motion in time can be found by differentiating (2.11.13) and then using the orbit equation to remove the $\sin(\theta - \theta_0)$ term. The resultant expression is then

$$\dot{r} = -L\left(z'(\theta) - \frac{1}{r}\Big((J^2 - z^2(\theta))r^2 + 2z(\theta)r - 1\Big)^{\frac{1}{2}}\right) \tag{2.12.1}$$

where $L = r^2\dot{\theta}$ has been used to eliminate $\dot{\theta}$. Equation (2.12.1) will only be solvable analytically provided $z(\theta)$, $z'(\theta)$ and L can be expressed entirely as functions of r. If this is possible, (2.12.1) can be reduced to the form

$$t = f_1(r). \tag{2.12.2}$$

One class of problems where this is possible is developed in the examples below (see §2.14).

The angular motion in time is obtained from the two-dimensional angular momentum equation $L = r^2\dot{\theta}$ using (2.11.13) to eliminate r to give

$$\dot{\theta} = L\Big(z(\theta) + J\cos(\theta - \theta_0)\Big)^2. \tag{2.12.3}$$

Provided L can be expressed in terms of θ, the differential equation (2.12.3) can be separated and solved to give

$$t = f_2(\theta). \tag{2.12.4}$$

The areal velocity is obtained from the equation

$$\dot{A} = \frac{1}{2}L(t), \tag{2.12.5}$$

where $L(t)$ can in theory be obtained by inverting either (2.12.2) or (2.12.3) to replace functions of r or θ in L.

2.13 Examples

The contents of this section are described in Leach [75] and Gorringe and Leach [37]. More recently Mavraganis [92] has considered equations of the form (2.10.3) where the resistive term varies very slowly with time. By using a Taylor series expansion about the initial velocity he obtained expressions for the orbit equation and the Hamilton and Laplace–Runge–Lenz analogues which are similar in structure to those described by Jezewski and Mittleman [58] and Leach [75] for the Danby [25] problem.

1.) It is now possible to apply the above techniques to the solution of the Danby problem [25]. The equation of motion is given by

$$\ddot{\boldsymbol{r}} + \frac{\alpha \dot{\boldsymbol{r}}}{r^2} + \frac{\mu \boldsymbol{r}}{r^3} = \boldsymbol{0}. \tag{2.13.1}$$

By comparing (2.13.1) with (2.10.3) we find that

$$f = \frac{\alpha}{r^2}, \qquad g = \frac{\mu}{r^3}. \tag{2.13.2}$$

Using (2.10.4) it can be shown that

$$-\frac{\dot{L}}{L} = \frac{\alpha}{r^2} = \frac{\alpha \dot{\theta}}{L}. \tag{2.13.3}$$

Solving (2.13.3) for L gives

$$L = k - \alpha\theta, \tag{2.13.4}$$

where k is some arbitrary constant, which agrees with the result obtained by Jezewski and Mittleman [58, eq3]. Using (2.11.19) we can show that $v(\theta)$ is given by

$$v(\theta) = \frac{\mu}{(k - \alpha\theta)^2} \tag{2.13.5}$$

and $z(\theta)$ by the integral (2.11.6)

$$z(\theta) = \mu \int_{\theta_0}^{\theta} \frac{\sin(\theta - \eta)\mathrm{d}\eta}{(k - \alpha\eta)^2}. \tag{2.13.6}$$

By making the substitution $x = \theta - \eta$, (2.13.6) can be integrated using G&R [43, 2.641.2–2.641.3] to give

$$z(\theta) = \frac{\mu}{\alpha^2}\left[\frac{\sin(u - u_0)}{u_0} - \sin u\big(\mathrm{si}(u) - \mathrm{si}(u_0)\big) - \cos u\big(\mathrm{Ci}(u) - \mathrm{Ci}(u_0)\big)\right] \tag{2.13.7}$$

and using (1.1.20) and G&R [43, 2.641.1,4]

$$\begin{aligned} z'(\theta) &= \int_{\theta_0}^{\theta} v(\eta)\cos(\theta - \eta)\mathrm{d}\eta \\ &= -\frac{\mu}{\alpha^2}\left[\frac{\cos(u - u_0)}{u_0} - \frac{1}{u} + \sin u\big(\mathrm{Ci}(u) - \mathrm{Ci}(u_0)\big)\right. \\ &- \left.\cos u\big(\mathrm{si}(u) - \mathrm{si}(u_0)\big)\right], \end{aligned} \tag{2.13.8}$$

where

$$u = \left(\frac{k}{\alpha} - \theta\right), \qquad u_0 = \left(\frac{k}{\alpha} - \theta_0\right). \tag{2.13.9}$$

The usual sine and cosine integrals are given by

$$\mathrm{si}(x) = -\frac{\pi}{2} + \int_0^x \frac{\sin t}{t}\mathrm{d}t \tag{2.13.10}$$

and

$$\mathrm{Ci}(x) = \gamma + \ln x + \int_0^x \frac{\cos t - 1}{t}\mathrm{d}t \tag{2.13.11}$$

and Euler's constant in (2.13.11) has the numerical value

$$\gamma = 0.57721566490\cdots . \tag{2.13.12}$$

The conserved vectors $\boldsymbol{K}$ and $\boldsymbol{J}$ for this problem are then given by (2.11.9) and (2.11.10), using (2.13.7) and (2.13.8) to substitute for $z(\theta)$ and $z'(\theta)$ and are given by

$$\begin{aligned}\boldsymbol{K} &= \frac{\dot{\boldsymbol{r}}}{L} + \frac{\mu}{\alpha^2}\left(\frac{1}{u} - \sin u\ \mathrm{Ci}(u) + \cos u\ \mathrm{si}(u)\right)\hat{\boldsymbol{r}} \\ &+ \frac{\mu}{\alpha^2}\Big(\sin u\ \mathrm{si}(u) + \cos u\ \mathrm{Ci}(u)\Big)\hat{\boldsymbol{\theta}} \\ &- \frac{\mu}{\alpha^2}\left(\frac{\hat{\boldsymbol{r}}_{\theta_0}}{u_0} + \mathrm{si}(u_0)\ \hat{\boldsymbol{r}}_{k/\alpha} + \mathrm{Ci}(u_0)\ \hat{\boldsymbol{\theta}}_{k/\alpha}\right)\end{aligned} \tag{2.13.13}$$

and

$$\begin{aligned}\boldsymbol{J} &= \frac{\dot{\boldsymbol{r}} \times \hat{\boldsymbol{L}}}{L} + \frac{\mu}{\alpha^2}\Big(\sin u\ \mathrm{si}(u) + \cos u\ \mathrm{Ci}(u)\Big)\hat{\boldsymbol{r}} \\ &- \frac{\mu}{\alpha^2}\left(\frac{1}{u} - \sin u\ \mathrm{Ci}(u) + \cos u\ \mathrm{si}(u)\right)\hat{\boldsymbol{\theta}} \\ &+ \frac{\mu}{\alpha^2}\left(\frac{\hat{\boldsymbol{\theta}}_{\theta_0}}{u_0} + \mathrm{si}(u_0)\ \hat{\boldsymbol{\theta}}_{k/\alpha} - \mathrm{Ci}(u_0)\ \hat{\boldsymbol{r}}_{k/\alpha}\right).\end{aligned} \tag{2.13.14}$$

Figure 2.13.1 shows a typical inwardly spiralling orbit. In practice the spiralling would not be so severe. The distances between successive zeroes from left to right along the $x-$axis is seen to decrease up until the origin and then to slowly increase. This effect can be more clearly observed in Figure 2.13.3. Figure 2.13.2 shows the outwardly spiralling velocity hodograph associated with Figure 2.13.1. Figure 2.13.3 shows the variation in the magnitude of the angular momentum vector along the orbit corresponding with Figures 2.13.1 and 2.13.2 which is very reminiscent of a 'tornado'. Note that the envelope enclosing the L_xL_z projection is concave downward on both sides of the origin which means that the distances between successive zeroes along the $x-$axis decrease from left to right up until the origin and then increase again. It should be remembered that L is a linear function of θ from (2.13.4) and so L decreases by a constant amount from one zero to the next from left to right along the $x-$axis until the origin at which point L begins to increase by the same amount.

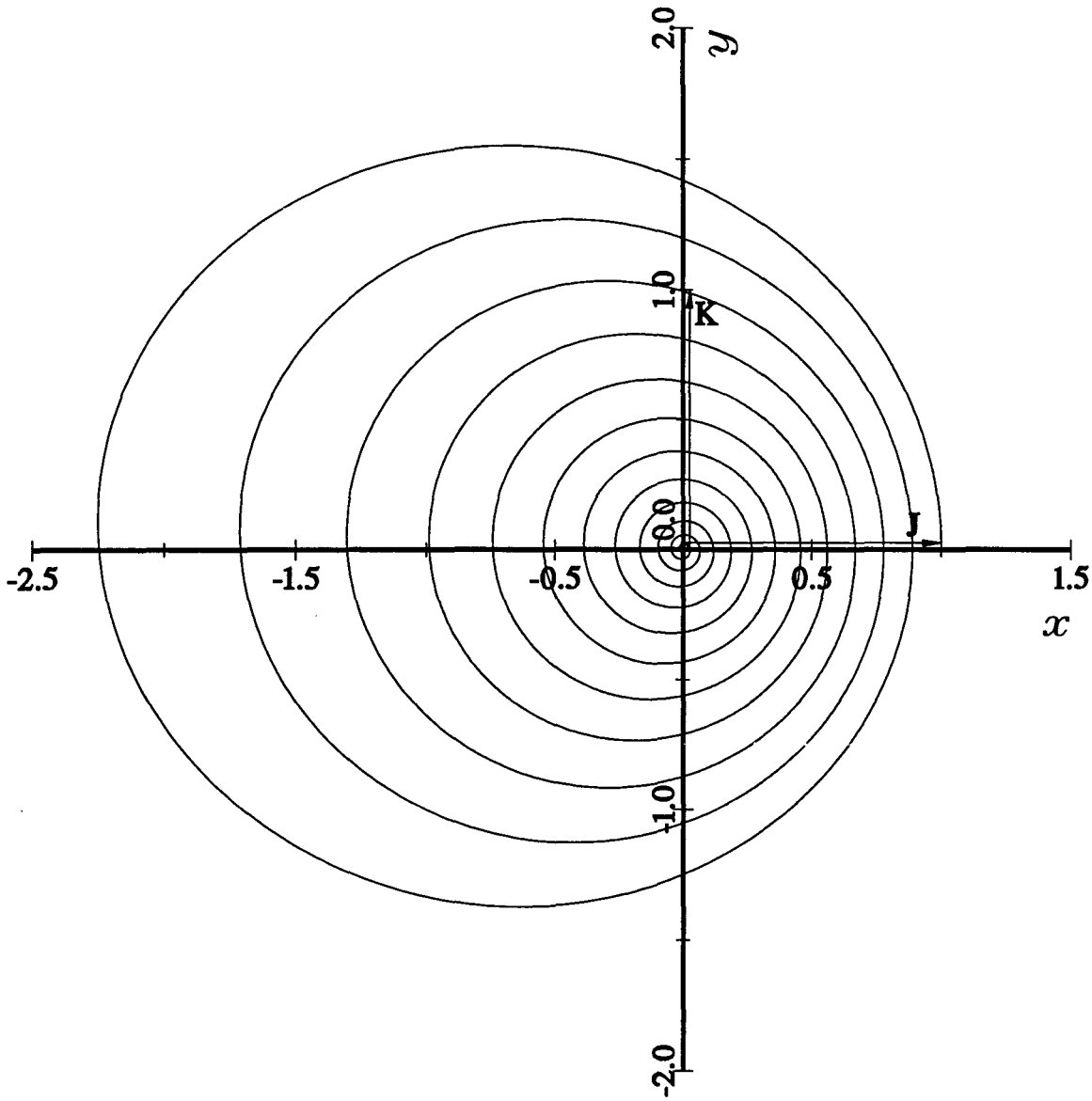


Figure 2.13.1. The spiralling orbit of the Danby problem for $f = \alpha/r^2$, $g = \mu/r^3$, $\alpha = 0.015$, $\mu = 1$, $k = 1.2$, $\theta_0 = 0$ and $K = J = 1$.

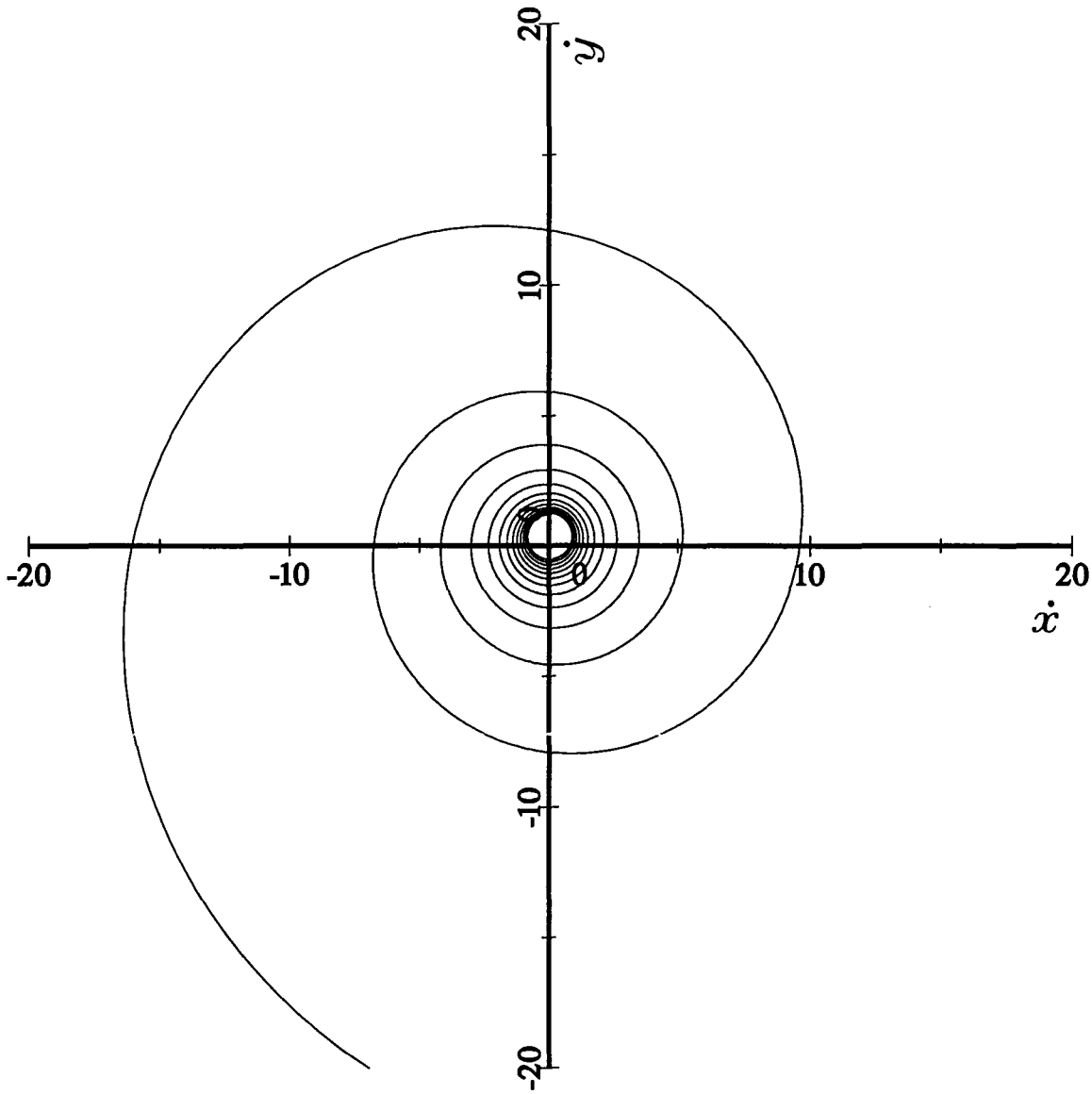


Figure 2.13.2. The hodograph associated with Figure 2.13.1. Note that the orbit spirals inward in a counter–clockwise fashion towards the origin, whilst the hodograph spirals outward in a counter–clockwise fashion.

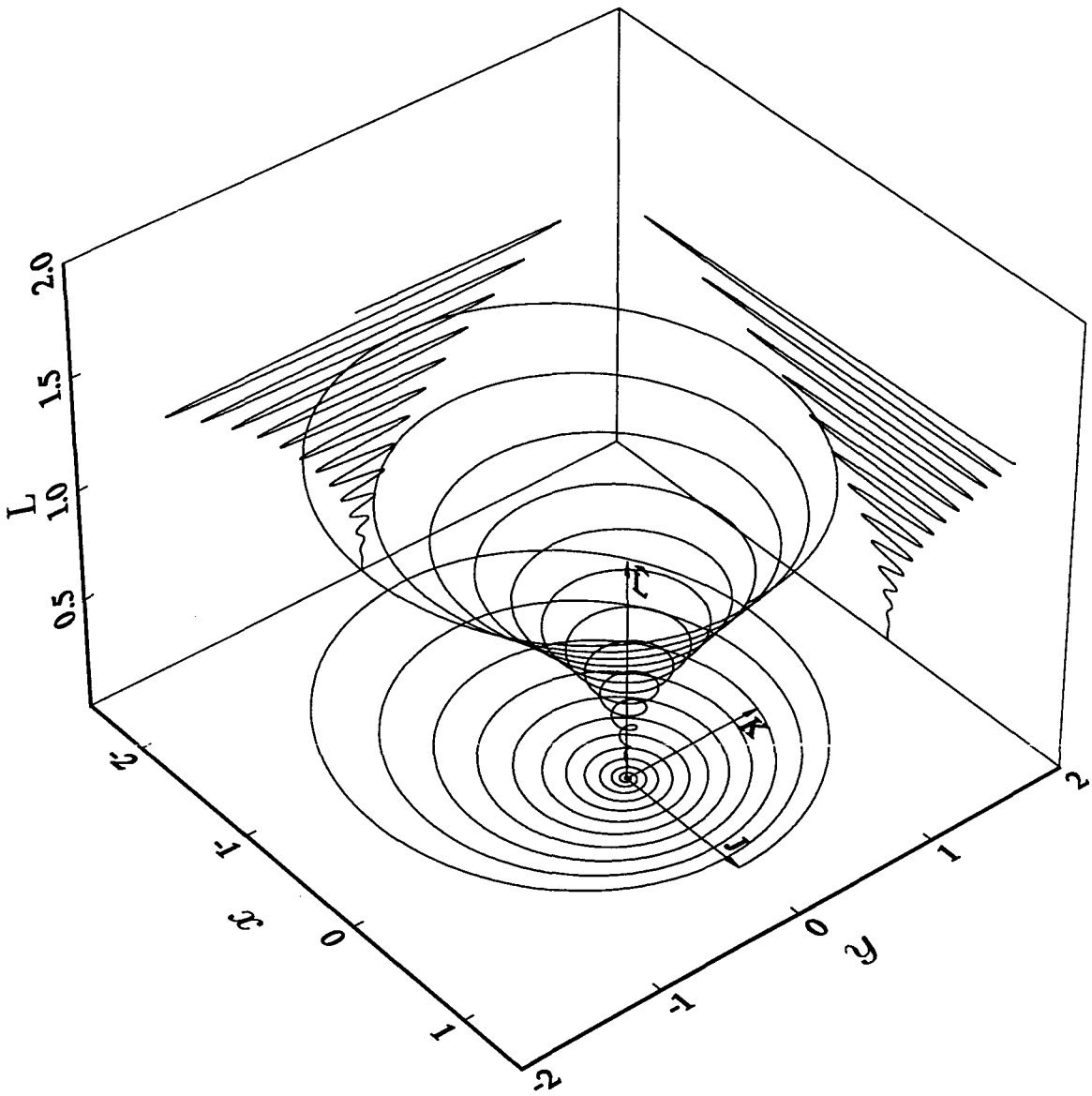


Figure 2.13.3. The variation in the magnitude of the angular momentum vector along the orbit corresponding with Figures 2.13.1 and 2.13.2. The projections of the angular momentum curve onto planes parallel to the xy, xL and yL planes are also shown. Note that the envelope enclosing the xL projection is concave downward on both sides of the origin, *i.e.* the distances between successive zeroes along the $x-$axis decrease from left to right and then increase again. The angular momentum is only constant in direction but not in magnitude.

Since the final term in both (2.13.13) and (2.13.14) is a constant vector it can be ignored in order to simplify matters. Making use of the notation employed by Mittleman and Jezewski [95, 58] for purposes of comparison and letting

$$g(u) = -\sin u\ \mathrm{si}(u) - \cos u\ \mathrm{Ci}(u) \tag{2.13.15}$$

then

$$g' = \frac{\mathrm{d}g}{\mathrm{d}u} = -\frac{1}{u} + \sin u\ \mathrm{Ci}(u) - \cos u\ \mathrm{si}(u). \tag{2.13.16}$$

Equations (2.13.13) and (2.13.14) can be rewritten as

$$\boldsymbol{K} = \frac{\dot{\boldsymbol{r}}}{L} - \frac{\mu}{\alpha^2} g'\,\hat{\boldsymbol{r}} - \frac{\mu}{\alpha^2} g\,\hat{\boldsymbol{\theta}} \tag{2.13.17}$$

and

$$\boldsymbol{J} = \frac{\dot{\boldsymbol{r}} \times \hat{\boldsymbol{L}}}{L} - \frac{\mu}{\alpha^2} g\,\hat{\boldsymbol{r}} + \frac{\mu}{\alpha^2} g'\,\hat{\boldsymbol{\theta}}. \tag{2.13.18}$$

The expression (2.13.18) is then identical to that obtained by Jezewski and Mittleman in [58, eq16] who employed a more complicated procedure involving the use of an integrating factor. The velocity hodograph is obtained from $\boldsymbol{K}$ (2.13.17) by squaring both sides of the rearranged equation as described in §1.2 which gives

$$\left(\frac{\dot{x}}{L} + K\sin\theta_0\right)^2 + \left(\frac{\dot{y}}{L} - K\cos\theta_0\right)^2 = \frac{\mu^2}{\alpha^4}\left(g(u)^2 + g'(u)^2\right). \tag{2.13.19}$$

The orbit equation is found by taking the scalar product of $\boldsymbol{J}$ (2.13.18) with $\boldsymbol{r}$ and rearranging to obtain

$$r = \frac{1}{\mu g(u)/\alpha^2 + J\cos(\theta - \theta_0)} \tag{2.13.20}$$

which was also obtained in [95, eq16] using a more *ad hoc* technique. Finally the energylike first integral I can then easily be constructed using either (2.13.17) or (2.13.18) to give

$$\begin{aligned} I &= \frac{1}{2}\boldsymbol{K}\cdot\boldsymbol{K} = \frac{1}{2}\boldsymbol{J}\cdot\boldsymbol{J} \\ &= \frac{\dot{\boldsymbol{r}}\cdot\dot{\boldsymbol{r}}}{2L^2} - \frac{\mu}{\alpha^2 L}\left(\dot{r}g'(u) + r\dot{\theta}g(u)\right) + \frac{\mu^2}{2\alpha^4}\left(g(u)^2 + g'(u)^2\right), \end{aligned} \tag{2.13.21}$$

where $g' = \mathrm{d}g/\mathrm{d}u$, which was also obtained in [58, eq12] using a less general approach.

2.) A more realistic resistive force for satellite motion which takes into account the variation in the thickness of the atmosphere could perhaps be given by

$$f = \frac{a\cos\theta + b}{r^2}, \qquad g = \frac{\mu}{r^3}. \tag{2.13.22}$$

The function $z(\theta)$ is given by

$$z(\theta) = \mu \int_{\theta_0}^{\theta} \frac{\sin(\theta - \eta)\mathrm{d}\eta}{(k - a\sin\eta - b\eta)^2}. \tag{2.13.23}$$

Figure 2.13.4 shows a typical inwardly spiralling orbit. The distances between successive zeroes from left to right along the $x-$axis are seen to decrease up until the origin, then to increase for a few zeroes and then finally decrease. This effect can be more clearly observed in Figure 2.13.6. Figure 2.13.5 shows the outwardly spiralling velocity hodograph associated with Figure 2.13.4. Figure 2.13.6 shows the variation in the magnitude of the angular momentum vector along the orbit corresponding with Figures 2.13.4 and 2.13.5 which is also reminiscent of a 'tornado'. Note that the envelope enclosing the L_xL_z projection is concave downward on the left side of the origin and for a small distance past the origin, *i.e.* the distances between successive zeroes along the $x-$axis decrease from left to right up until the origin and then increase again for a little while before slowly decreasing again, *i.e.* the envelope becomes concave upward. L decreases by a constant amount from one zero to the next from left to right along the $x-$axis and on reaching the origin begins to increase again by the same amount as a consequence of the choice of f.

3.) If we make the choice

$$f = \frac{a\cos\theta + b}{Lr^2}, \qquad g = \frac{\mu}{r^3}, \tag{2.13.24}$$

then

$$z(\theta) = \frac{\mu}{2} \int_{\theta_0}^{\theta} \frac{\sin(\theta - \eta)\mathrm{d}\eta}{k - a\sin\eta - b\eta}. \tag{2.13.25}$$

Figure 2.13.7 shows the orbit which revolves laterally before leaving asymptotically. The distances between successive zeroes from left to right along the $x-$axis are seen to decrease up until the origin and then start to increase. This effect can be more clearly observed in Figure 2.13.9. Figure 2.13.8 shows the velocity hodograph associated with Figure 2.13.7 which revolves longitudinally and tends to a limiting value which is bounded both in magnitude and direction. Figure 2.13.9 shows the variation in the magnitude of the angular momentum vector along the orbit corresponding with Figures 2.13.7 and 2.13.8. Note that the envelope enclosing the L_xL_z projection is concave downward left of the origin but concave upwards right of the origin due to the lateral motion of the orbit to the right. L decreases by slowly increasing amounts on both sides of the origin from one zero to the next from left to right along the $x-$axis.

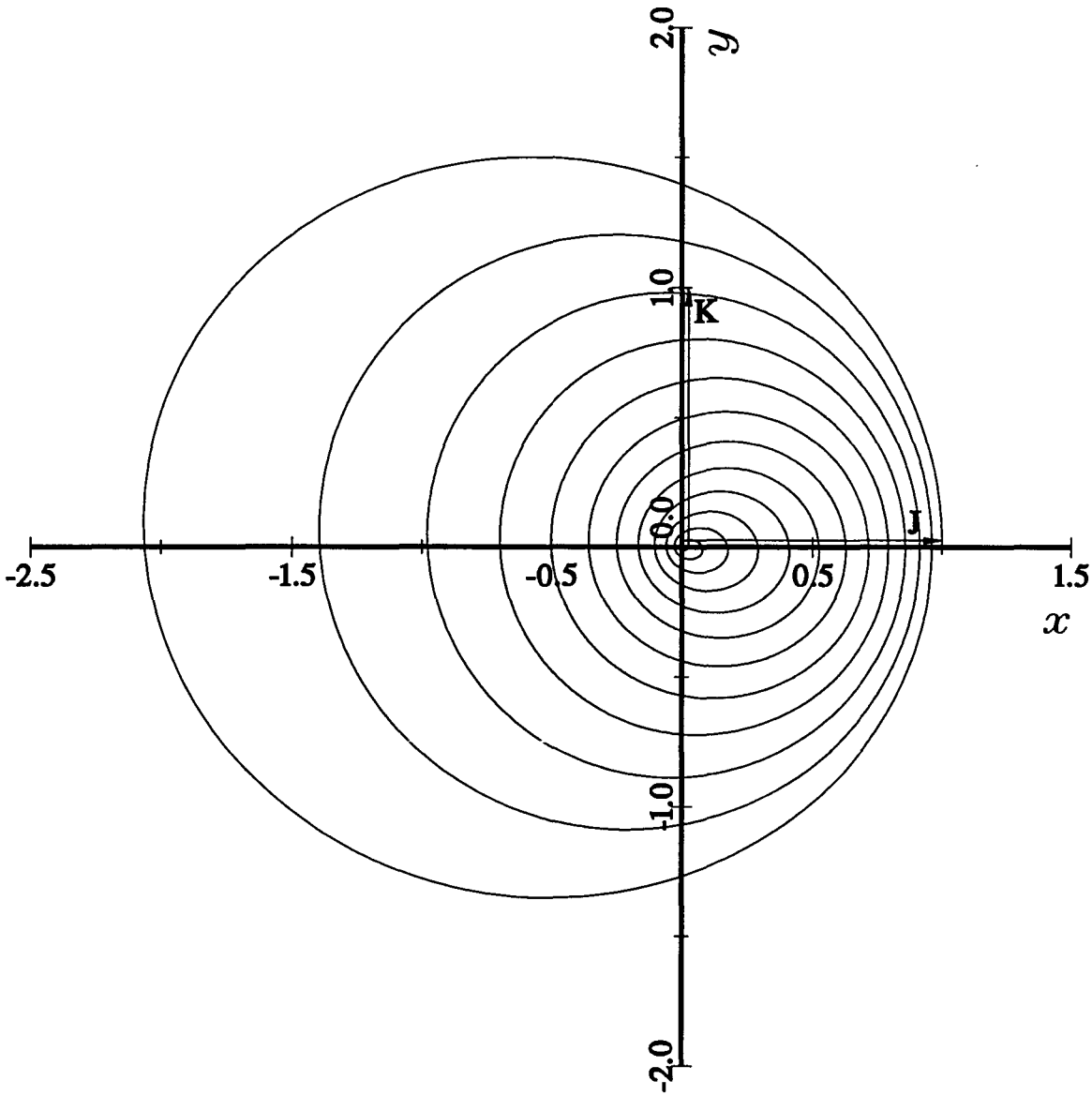


Figure 2.13.4. The spiralling orbit for $f = (a\cos\theta + b)/r^2$, $g = \mu/r^3$, $a = 0.02$, $b = 0.015$, $\mu = 1$, $k = 1.2$, $\theta_0 = 0$ and $K = J = 1$.

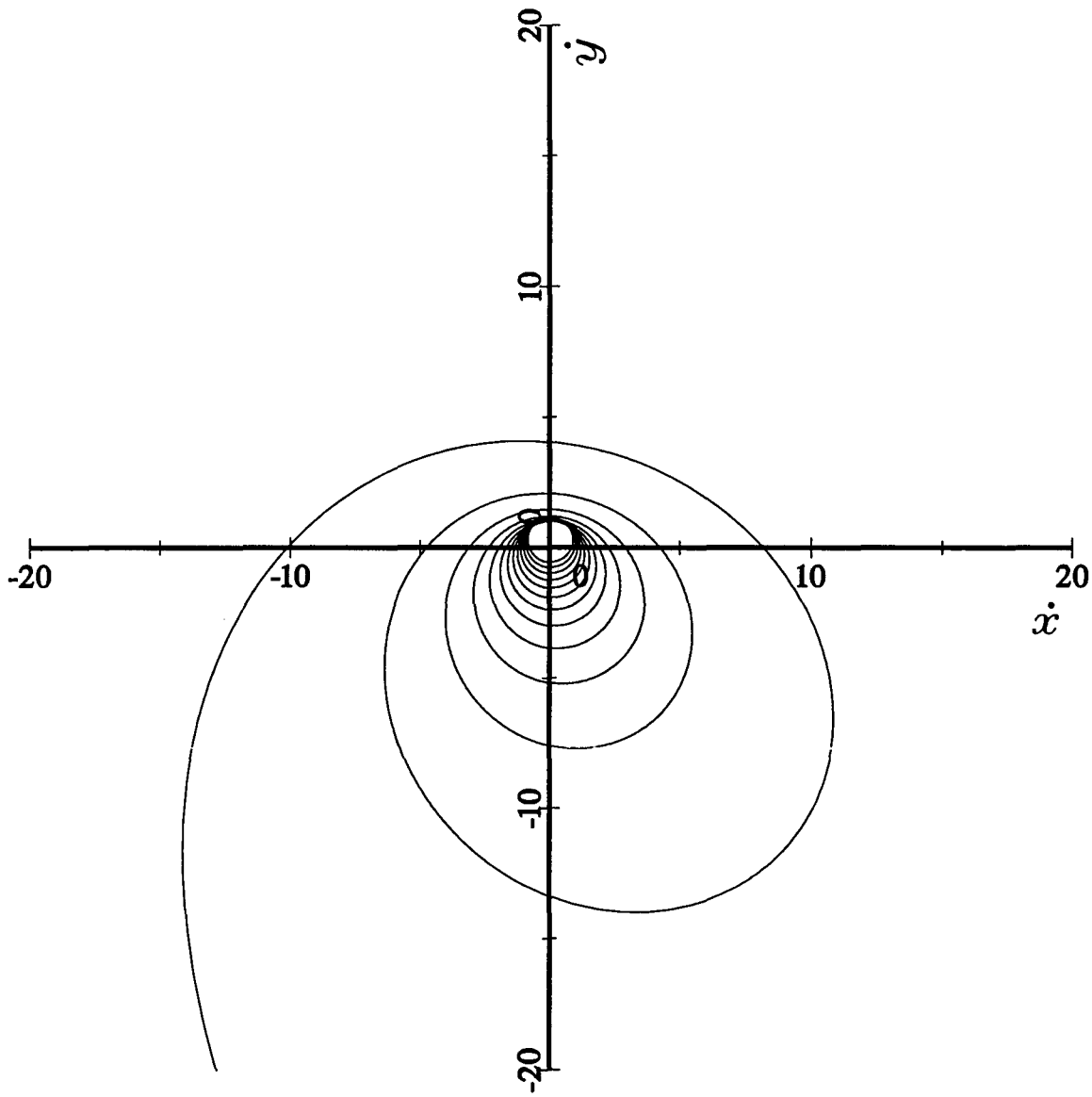


Figure 2.13.5. The hodograph associated with Figure 2.13.4. Note that the orbit spirals inward in a counter–clockwise fashion towards the origin, whilst the hodograph spirals outward in a counter–clockwise fashion.

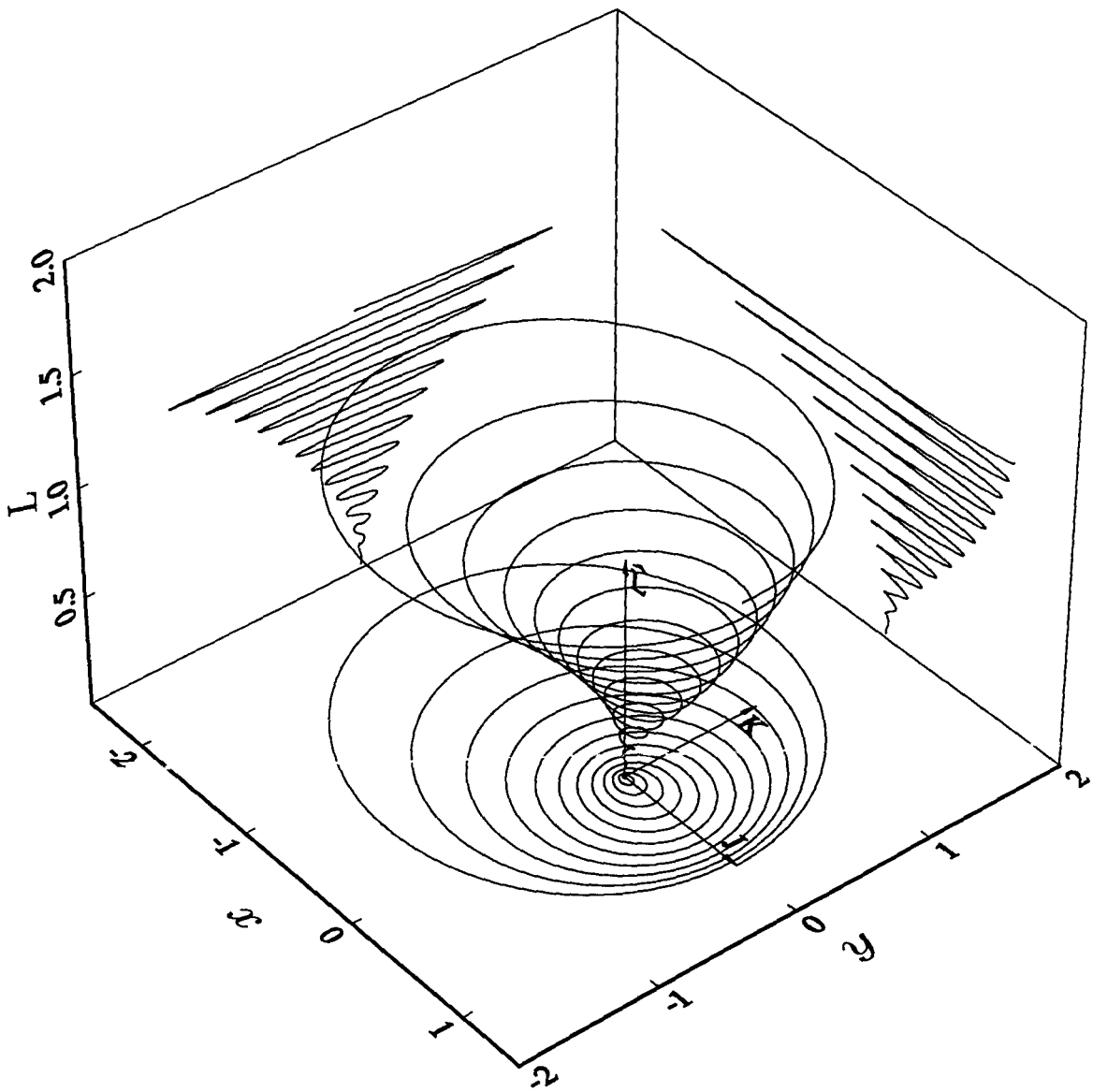


Figure 2.13.6. The variation in the magnitude of the angular momentum vector along the orbit corresponding with Figures 2.13.4 and 2.13.5. The projections of the angular momentum curve onto planes parallel to the xy, xL and yL planes are also shown. Note that the envelope enclosing the xL projection is concave downward on the left side of the origin and for a small distance past the origin, *i.e.* the distances between successive zeroes along the $x-$axis decrease from left to right and then increase again for a little while before slowly decreasing again, *i.e.* the envelope becomes concave upward. The angular momentum is only constant in direction but not in magnitude.

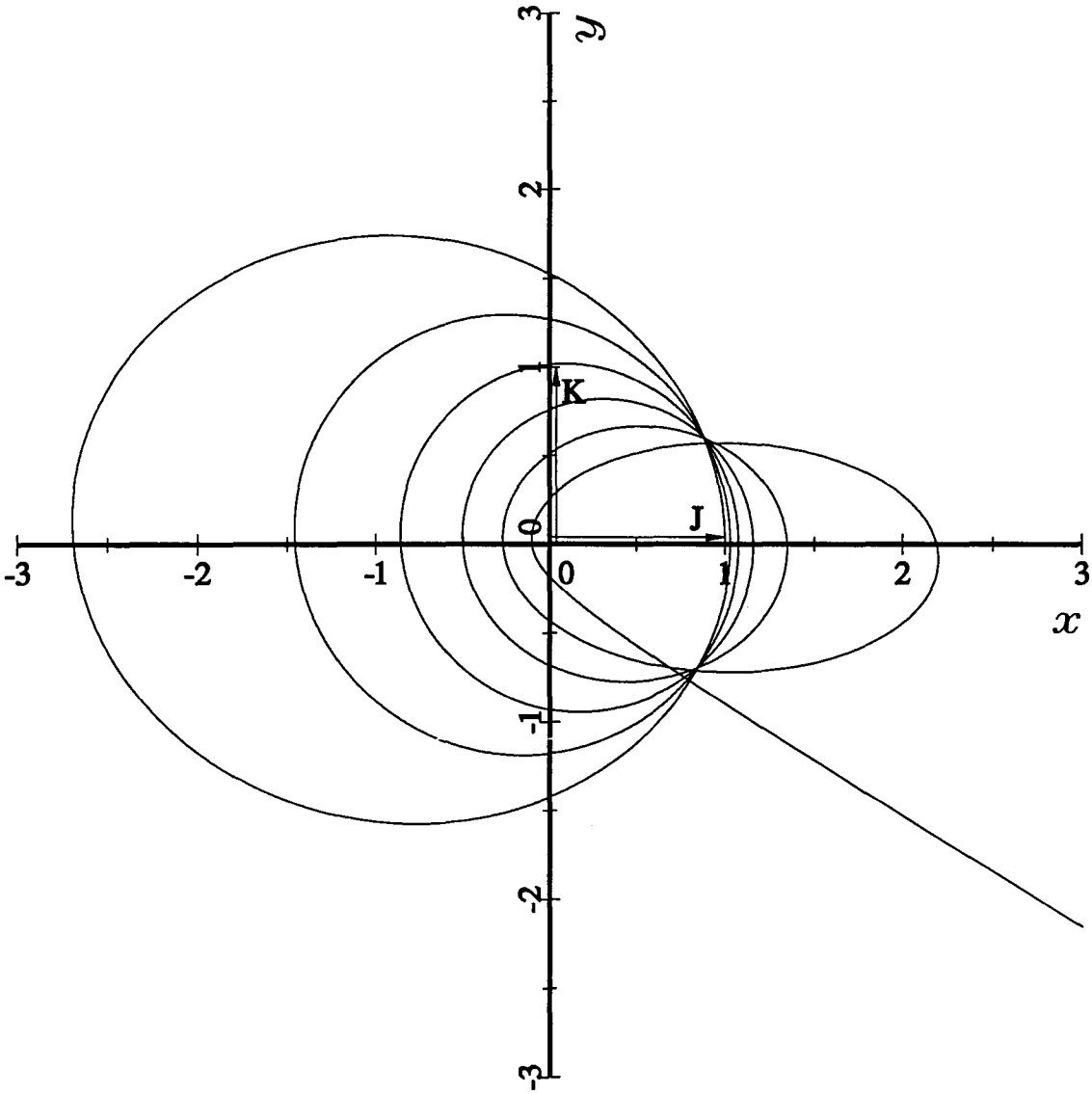


Figure 2.13.7. The orbit for $f = (a\cos\theta + b)/(Lr^2)$, $g = \mu/r^3$, $a = 0.05$, $b = 0.02$, $\mu = 1$, $k = 0.8$, $\theta_0 = 0$ and $K = J = 1$. The orbit circles the origin five times before leaving asymptotically.

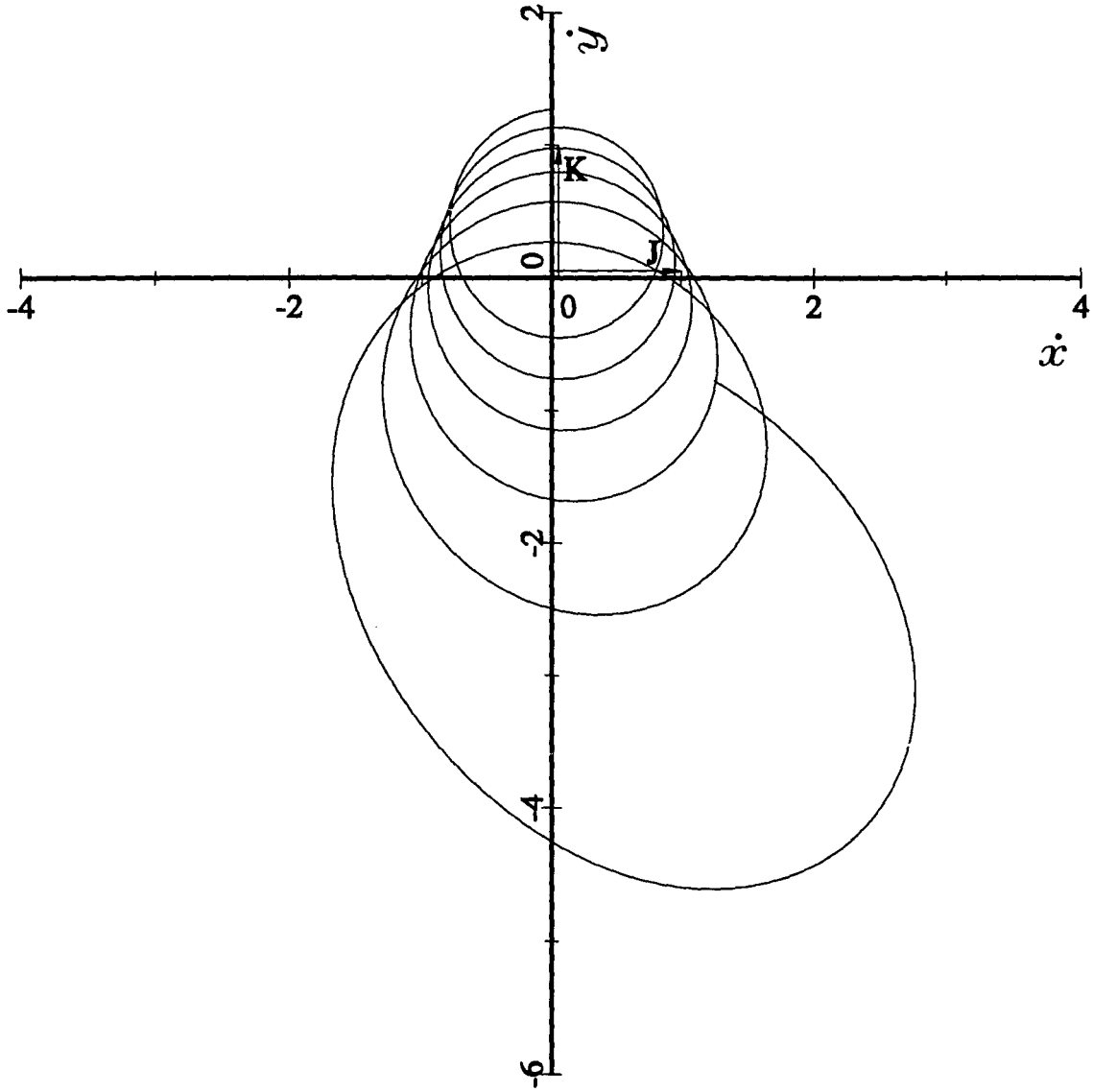


Figure 2.13.8. The hodograph associated with Figure 2.13.7. Note that the hodograph circles the origin five times before tending to a limiting value (bounded in magnitude and direction).

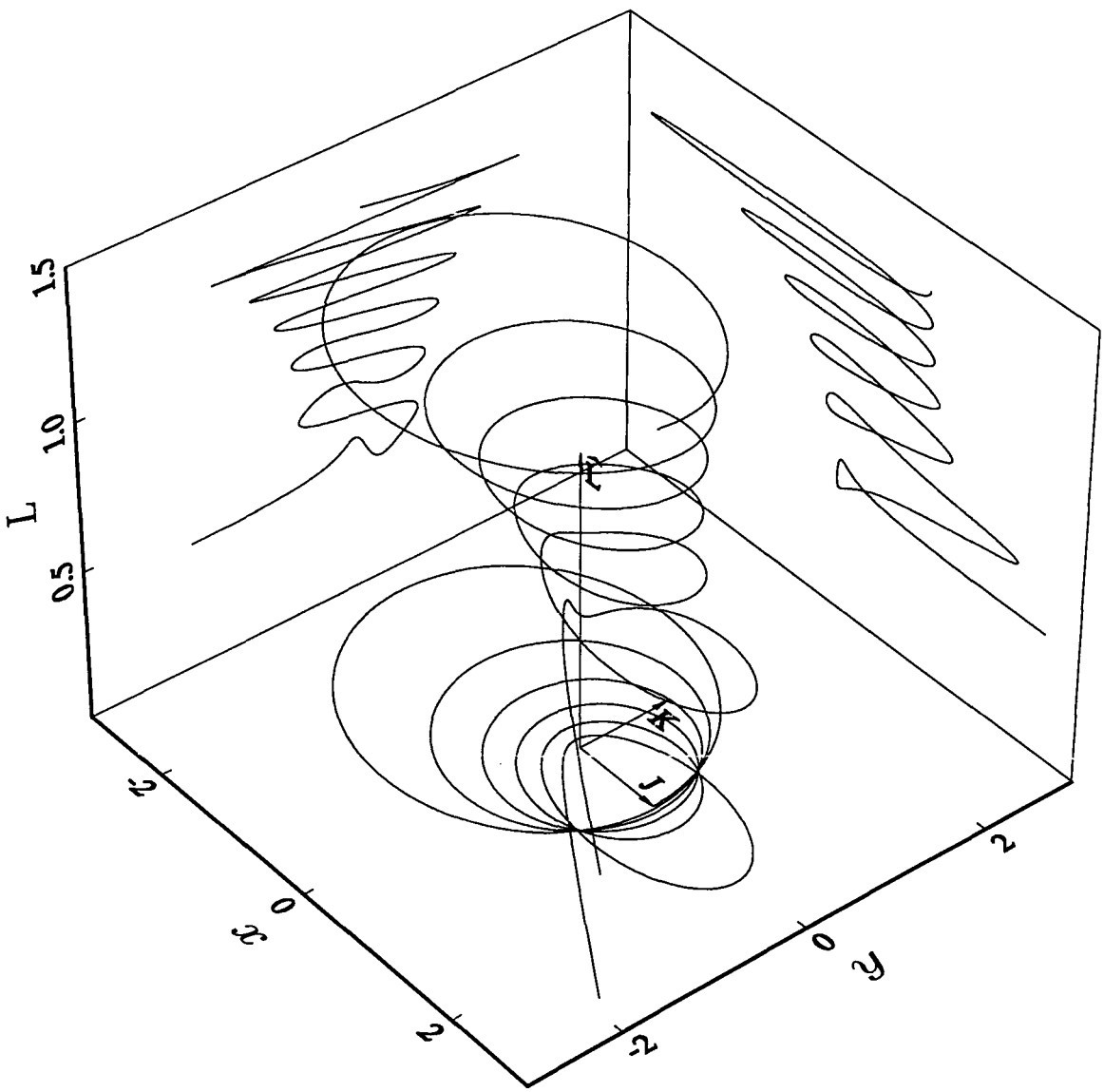


Figure 2.13.9. The variation in the magnitude of the angular momentum vector along the orbit corresponding with Figures 2.13.7 and 2.13.8. The projections of the angular momentum curve onto planes parallel to the xy, xL and yL planes are also shown. Note that the envelope enclosing the xL projection is concave downward on the left hand side of the origin and concave upward on the right hand side due to the lateral motion of the orbit to the right. The angular momentum is only constant in direction but not in magnitude.

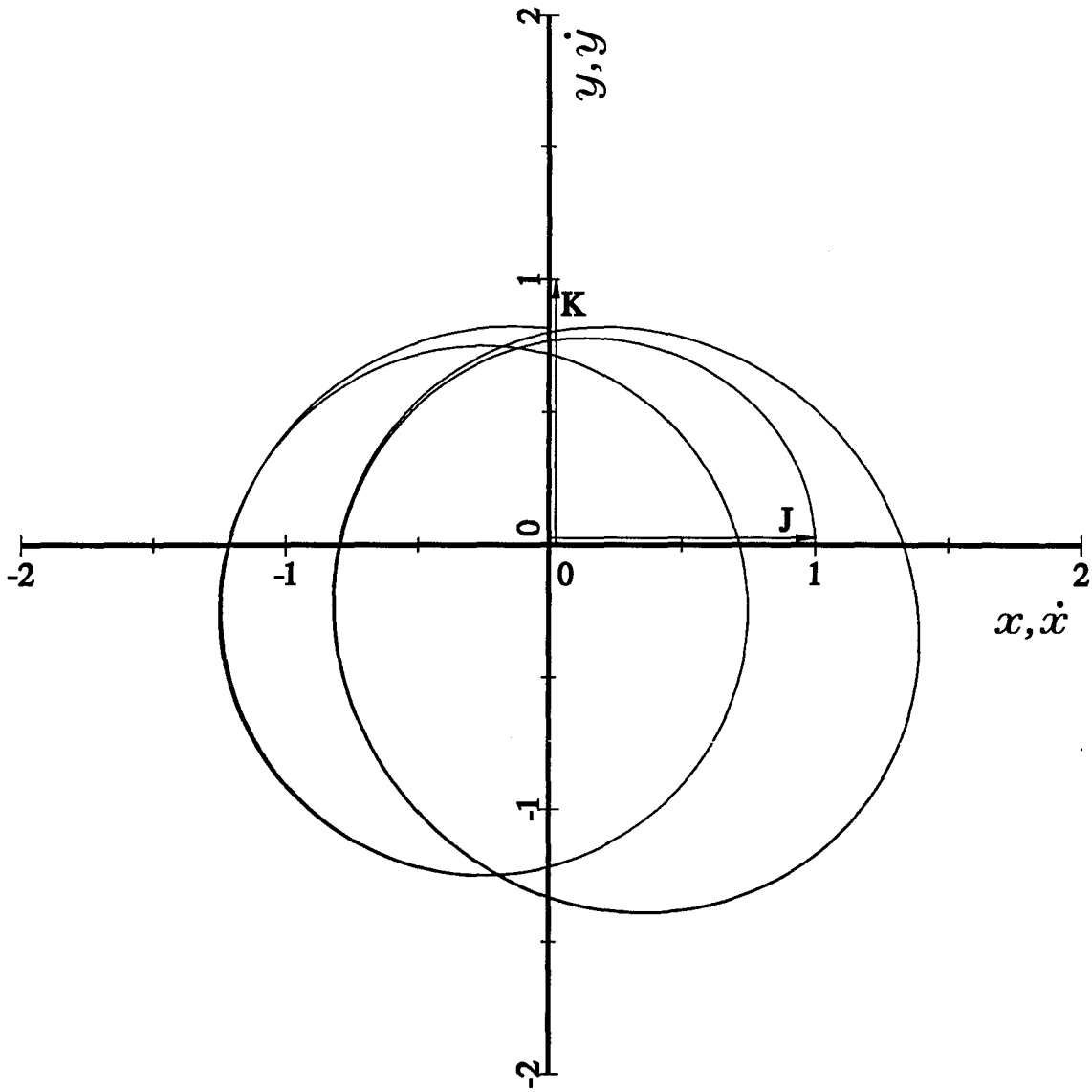


Figure 2.13.10. The hodograph (left) and the orbit (right) for $f = -ae^{-(\theta-\theta_0)}L^3/(2r^2)$, $g = \mu/r^3$, $a = 1/2$, $b = 1$, $\mu = 1$, $\theta_0 = 0$ and $K = J = 1$. Note that the hodograph grows inwards in a counter–clockwise fashion towards its limit cycle while the orbit grows outwards in a counter–clockwise fashion towards its limit cycle.

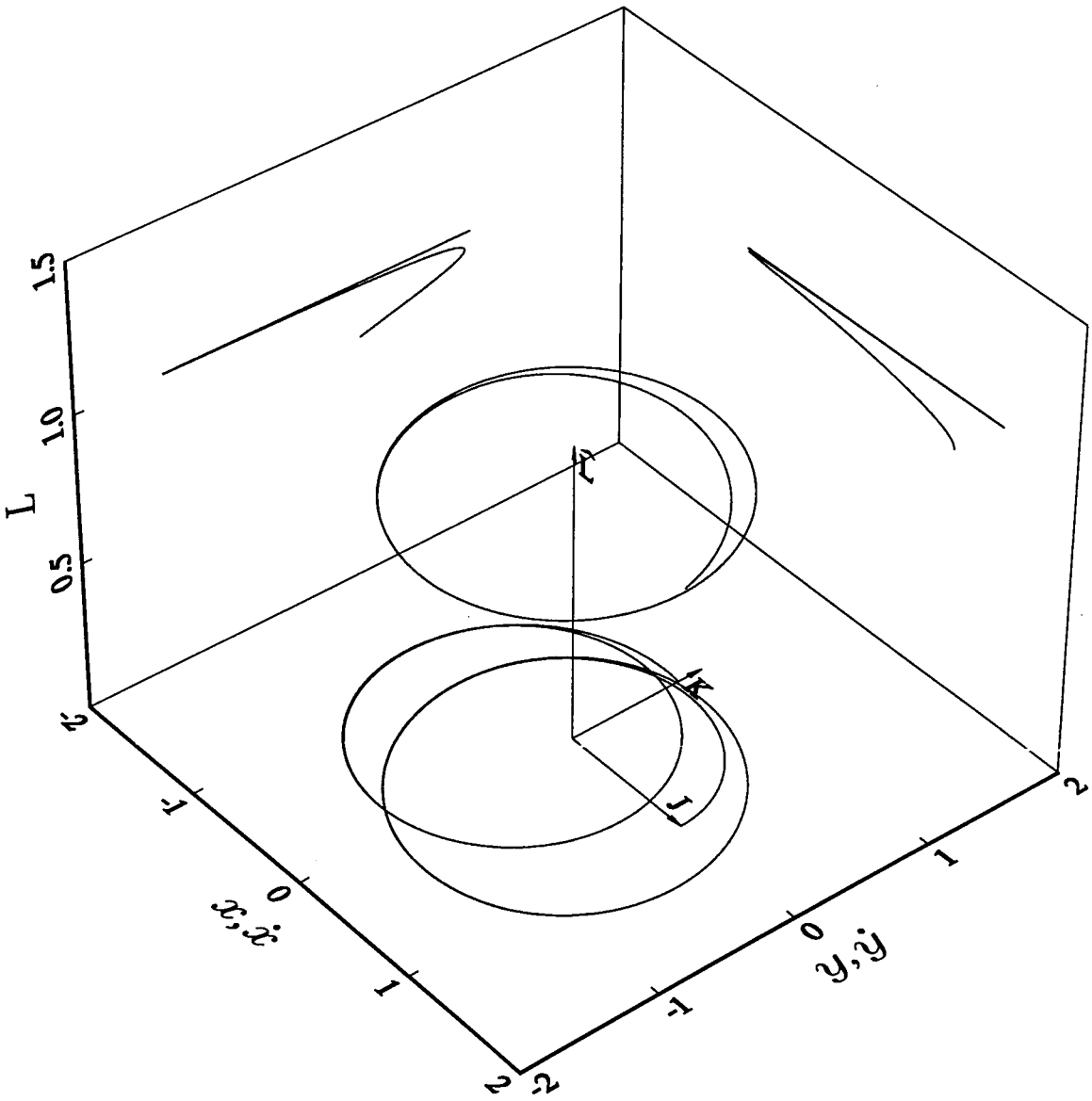


Figure 2.13.11. The variation in the magnitude of the angular momentum vector along the orbit corresponding with Figure 2.13.10. The projections of the angular momentum curve onto planes parallel to the xy, xL and yL planes are also shown. In this example the angular momentum is constant in direction but varies in magnitude.

4.) For the choice

$$f = \frac{-ae^{-(\theta-\theta_0)}L^3}{2r^2}, \qquad g = \frac{\mu}{r^3}, \tag{2.13.26}$$

$$z(\theta) = \frac{\mu a}{2}\Big(e^{-(\theta-\theta_0)} + \sin(\theta-\theta_0) - \cos(\theta-\theta_0)\Big) + \mu b\Big(1 - \cos(\theta-\theta_0)\Big). \tag{2.13.27}$$

Figure 2.13.10 shows the velocity hodograph (left) and the orbit equation (right). The limit cycle behaviour is evident in both the velocity hodograph and the orbit. Figure 2.13.11 shows the variation in the magnitude of the angular momentum vector along the orbit corresponding with Figure 2.13.10. Note that the angular momentum increases and reaches a limiting value of unity.

2.14 The Conserved Hamilton and Laplace–Runge–Lenz Vector Analogues for General Keplerian Orbits

Motivated by the results of Bertrand's theorem [7] which apply specifically to central force orbits, we will construct the most general Keplerian orbits from (2.10.3). We are not specifically concerned with the inverse problem of finding the most general equation of motion for a given orbit, which has a long history (see Whittaker [129] and more recently Broucke [12] and the references cited).

If we assume that the Keplerian orbit has its origin at one of the foci and referring to (2.11.13), it is easy to show that

$$z(\theta) = A\Big(1 - \cos(\theta-\theta_0)\Big), \tag{2.14.1}$$

since $z(\theta_0) = 0$, where A is some constant. The velocity hodograph can now be written using (2.11.12) as

$$\left(\frac{\dot{x}}{L} + (K-A)\sin\theta_0\right)^2 + \left(\frac{\dot{y}}{L} - (K-A)\cos\theta_0\right)^2 = A^2 \tag{2.14.2}$$

and, since L is not constant, the path is no longer circular as was the case in §1.5. Using (2.14.1) for $z(\theta)$ in (2.11.7) gives

$$v(\theta) = A. \tag{2.14.3}$$

Using (2.11.19) to construct g gives

$$g = \frac{AL^2}{r^3}. \tag{2.14.4}$$

Rearranging (2.14.4) to obtain an expression for L^2 and differentiating gives

$$2L\dot{L} = \frac{\dot{g}r^3}{A} + \frac{3r^2\dot{r}g}{A}. \tag{2.14.5}$$

Dividing (2.14.5) by $-2L^2$ gives

$$f = -\frac{\dot{g}}{2g} - \frac{3\dot{r}}{2r}. \tag{2.14.6}$$

Thus the most general equation of motion possessing the conserved vectors $\boldsymbol{K}$ and $\boldsymbol{J}$ given by (2.11.9) and (2.11.10) and in addition an orbit equation which is a conic section is given by f and g in (2.14.6) and (2.14.4). It should be pointed out that it does not seem possible to construct an acceleration hodograph in any recognisable form for this equation of motion as $\boldsymbol{L}$ is no longer conserved.

It is of further interest to consider a time transformation of (2.10.3) for the orbit with f described by (2.14.6), *i.e.*,

$$\ddot{\boldsymbol{r}} - \left(\frac{\dot{g}}{2g} + \frac{3\dot{r}}{2r}\right)\dot{\boldsymbol{r}} + g\boldsymbol{r} = \boldsymbol{0}. \tag{2.14.7}$$

Making use of the transformation $t \to \rho(t)$ (2.14.7) becomes

$$\dot{\rho}^2\frac{\mathrm{d}^2\boldsymbol{r}}{\mathrm{d}\rho^2} + \left(\ddot{\rho} - \left(\frac{\dot{g}}{2g} + \frac{3\dot{r}}{2r}\right)\dot{\rho}\right)\frac{\mathrm{d}\boldsymbol{r}}{\mathrm{d}\rho} + g\boldsymbol{r} = \boldsymbol{0}. \tag{2.14.8}$$

If we set the middle term of (2.14.8) to zero we obtain

$$\frac{\mathrm{d}^2\boldsymbol{r}}{\mathrm{d}\rho^2} + \frac{g}{\dot{\rho}^2}\boldsymbol{r} = \boldsymbol{0}, \tag{2.14.9}$$

with

$$\dot{\rho}^2 = \frac{gr^3}{\mu} = \frac{AL^2}{\mu} = \frac{4A}{\mu}\dot{S}^2 = \frac{4}{\bar{L}^2}\dot{S}^2 \tag{2.14.10}$$

where μ is an arbitrary constant, $\dot{S} = L/2$ is the areal velocity of (2.14.7) and $\bar{L}$ the angular momentum of the Kepler problem (2.14.11). As expected (2.14.7) has been transformed into the equivalent Kepler problem

$$\frac{\mathrm{d}^2\boldsymbol{r}}{\mathrm{d}\rho^2} + \frac{\mu}{r^3}\boldsymbol{r} = \boldsymbol{0} \tag{2.14.11}$$

using the area swept out in the orbit described by (2.14.7). Equation (2.14.10) is consistent with that obtained by equating the area $S(t)$ swept out in the orbit described by (2.14.7) at time t with the same area swept out in the Kepler problem at time $\rho(t)$ as given by Kepler's second law, *i.e.* $\rho(t) = 2S(t)/\bar{L}$.

The conserved vectors $\boldsymbol{K}$ (2.11.9) and $\boldsymbol{J}$ (2.11.10) associated with (2.14.7) are form invariant under the transformation $t \rightarrow \rho(t)$ since the term $\dot{\boldsymbol{r}} \times \boldsymbol{L}/L^2 = \boldsymbol{r}' \times \boldsymbol{L}_t/{L_t}^2$, where the prime denotes differentiation with respect to ρ and $L_t = r^2\theta'$, and so

$$\boldsymbol{K} = \frac{\boldsymbol{r}'}{L_t} - A\left(\hat{\boldsymbol{\theta}} - \hat{\boldsymbol{\theta}}_{\theta_0}\right) \tag{2.14.12}$$

and

$$\boldsymbol{J} = \frac{\boldsymbol{r}' \times \hat{\boldsymbol{L}}_t}{L_t} - A\left(\hat{\boldsymbol{r}} - \hat{\boldsymbol{r}}_{\theta_0}\right), \tag{2.14.13}$$

where $\hat{\boldsymbol{r}}_{\theta_0} = \boldsymbol{i}\cos\theta_0 + \boldsymbol{j}\sin\theta_0$ and $\hat{\boldsymbol{\theta}}_{\theta_0} = -\boldsymbol{i}\sin\theta_0 + \boldsymbol{j}\cos\theta_0$.

The angular momentum is obtained by taking the vector product of $\boldsymbol{r}$ with (2.14.7) to give

$$\dot{\boldsymbol{L}} - \left(\frac{\dot{g}}{2g} + \frac{3\dot{r}}{2r}\right)\boldsymbol{L} = \boldsymbol{0} \tag{2.14.14}$$

and, since $\hat{\boldsymbol{L}}$ is constant, the scalar part of (2.14.14) gives

$$L = kg^{\frac{1}{2}}r^{\frac{3}{2}}. \tag{2.14.15}$$

Using $L = r^2\dot{\theta}$,

$$k = \frac{r^{\frac{1}{2}}\dot{\theta}}{g^{\frac{1}{2}}} \tag{2.14.16}$$

is also a constant of the motion and $\boldsymbol{k} = k\hat{\boldsymbol{L}}$ can be regarded as a generalised angular momentum.

The scalar energylike first integral for (2.14.7) is obtained by simplifing (2.11.20) using (2.14.1) to substitute for $z(\theta)$ as well as its derivative and is given by

$$I = \frac{1}{2}\boldsymbol{J}^2 = A\frac{\dot{\boldsymbol{r}}\cdot\dot{\boldsymbol{r}}}{2gr^3} - \frac{A}{r} + AJ. \tag{2.14.17}$$

Alternatively taking the scalar product of $(gr^3)^{-1}\dot{\boldsymbol{r}}$ with (2.14.7) and integrating give the conserved quantity

$$E = \frac{\dot{\boldsymbol{r}}\cdot\dot{\boldsymbol{r}}}{2gr^3} - \frac{1}{r} = \frac{J^2}{2A} - J. \tag{2.14.18}$$

The radial motion in time can be calculated as follows. By differentiating (2.11.13) and then expressing L in terms of r by solving (2.10.4) and rewriting $\sin(\theta - \theta_0)$ in terms of r through the orbit equation (2.11.13) we obtain

$$\dot{r} = \frac{g^{\frac{1}{2}}r^{\frac{1}{2}}}{A^{\frac{1}{2}}}\left(2AEr^2 + 2Ar - 1\right)^{\frac{1}{2}}, \tag{2.14.19}$$

which can in theory be solved provided g can be expressed entirely as a function of r. The angular motion in time is found by solving

$$\dot{\theta} = \frac{g^{\frac{1}{2}}}{A^{\frac{1}{2}}}\Big(A + (J - A)\cos(\theta - \theta_0)\Big)^{\frac{1}{2}} \tag{2.14.20}$$

which can in principle also be solved if g can be expressed entirely as a function of θ. The areal velocity is found from the equation

$$\dot{A} = \frac{1}{2}L(t) = \frac{1}{2}kg^{\frac{1}{2}}r^{\frac{3}{2}} \tag{2.14.21}$$

provided g and r can be expressed in terms of time only which possibly involves inverting either (2.14.19) or (2.14.20). See §2.15 for some examples.

2.15 The Geometry of the Generalised Kepler Problem

The contents of §2.15 are described in Gorringe and Leach [41]. In general an expression for the area swept out by the radius vector in time cannot be found explicitly due to global inversion problems. However, the periodic time expressions can be found rather elegantly for the power law central force type potentials $g = \mu r^{\alpha}$. The equation of motion (2.14.7) now becomes

$$\ddot{\boldsymbol{r}} - \frac{1}{2}(\alpha + 3)\frac{\dot{r}}{r}\dot{\boldsymbol{r}} + \mu r^{\alpha}\boldsymbol{r} = \boldsymbol{0}. \tag{2.15.1}$$

To be consistent with the conserved vectors used for the standard Kepler problem in Chapter 1 it is necessary to remove the additional constant terms in (2.14.12) and (2.14.13).

The vector product of $\boldsymbol{r}$ with (2.15.1) gives

$$\dot{\boldsymbol{L}} - \frac{1}{2}(\alpha + 3)\frac{\dot{r}}{r}\boldsymbol{L} = \boldsymbol{0}. \tag{2.15.2}$$

Since $\hat{\boldsymbol{L}}$ is conserved, the scalar part of (2.15.2) can be solved to give

$$L = kr^{\frac{(\alpha+3)}{2}}. \tag{2.15.3}$$

Now using $L = r^2\dot{\theta}$ we find that

$$k = r^{\frac{-(\alpha-1)}{2}}\dot{\theta}, \tag{2.15.4}$$

which is of course a constant of the motion and $\boldsymbol{k} = k\hat{\boldsymbol{L}}$ can be regarded as a generalised angular momentum. Division of (2.15.1) by L and making use of (2.15.4) gives rise to an exact derivative which can be integrated to give the Hamilton–like vector

$$\boldsymbol{K} = \frac{\dot{\boldsymbol{r}}}{L} - \frac{\mu}{k^2}\hat{\boldsymbol{\theta}}. \tag{2.15.5}$$

The Laplace–Runge–Lenz vector follows from

$$\begin{aligned} \boldsymbol{J} &= \boldsymbol{K} \times \hat{\boldsymbol{L}} \\ &= \frac{\dot{\boldsymbol{r}} \times \boldsymbol{L}}{L^2} - \frac{\mu}{k^2}\hat{\boldsymbol{r}}. \end{aligned} \tag{2.15.6}$$

The velocity hodograph is obtained as described in §1.2 and is given by

$$\left(\frac{\dot{x}}{L} + K\sin\theta_0\right)^2 + \left(\frac{\dot{y}}{L} - K\cos\theta_0\right)^2 = \frac{\mu^2}{k^4}. \tag{2.15.7}$$

Note that L is no longer conserved and the path is no longer circular as was the case in the standard Kepler problem (see §1.5). The scalar product of $\boldsymbol{J}$ and $\boldsymbol{r}$ leads to the equation of the orbit

$$r = \frac{1}{\mu/k^2 + J\cos(\theta - \theta_0)}, \tag{2.15.8}$$

where as usual the angle between $\boldsymbol{J}$ and $\boldsymbol{i}$ is θ_0. It does not seem possible to express the acceleration hodograph in any useful or recognisable form since L is no longer constant except when $\alpha = -3$.

The ellipses shown throughout the remainder of this chapter are chosen to have the same size as those used in §§1.5 and 1.7 for purposes of comparison. Figure 2.15.1 shows the elliptic Keplerian orbit and the construction of the corresponding velocity hodograph for the generalised problem when $\alpha = -6$ and $A > J$. Note that the circular velocity hodograph in the Kepler problem ($\alpha = -3$) is now distorted into an egg–shaped curve. The origin still remains inside the velocity hodograph and is also situated in the bottom half of the velocity hodograph. Figure 2.15.2 shows the parabolic Keplerian orbit and the construction of the corresponding velocity hodograph for the generalised problem when $\alpha = -6$ and $A = J$. Again the velocity hodograph is egg–shaped and unlike the Kepler problem differs in size from the velocity hodograph for the elliptical case. As with the Kepler problem the velocity hodograph closes and touches the origin as t ranges from negative through positive infinity or equivalently when $\theta - \theta_0$ ranges from $-\pi$ through π radians. Figure 2.15.3 shows the hyperbolic Keplerian orbit and the construction of the corresponding velocity hodograph for the generalised problem when $\alpha = -6$ and $A < J$. As in the previous two cases the velocity hodograph is egg–shaped and also differs in size from

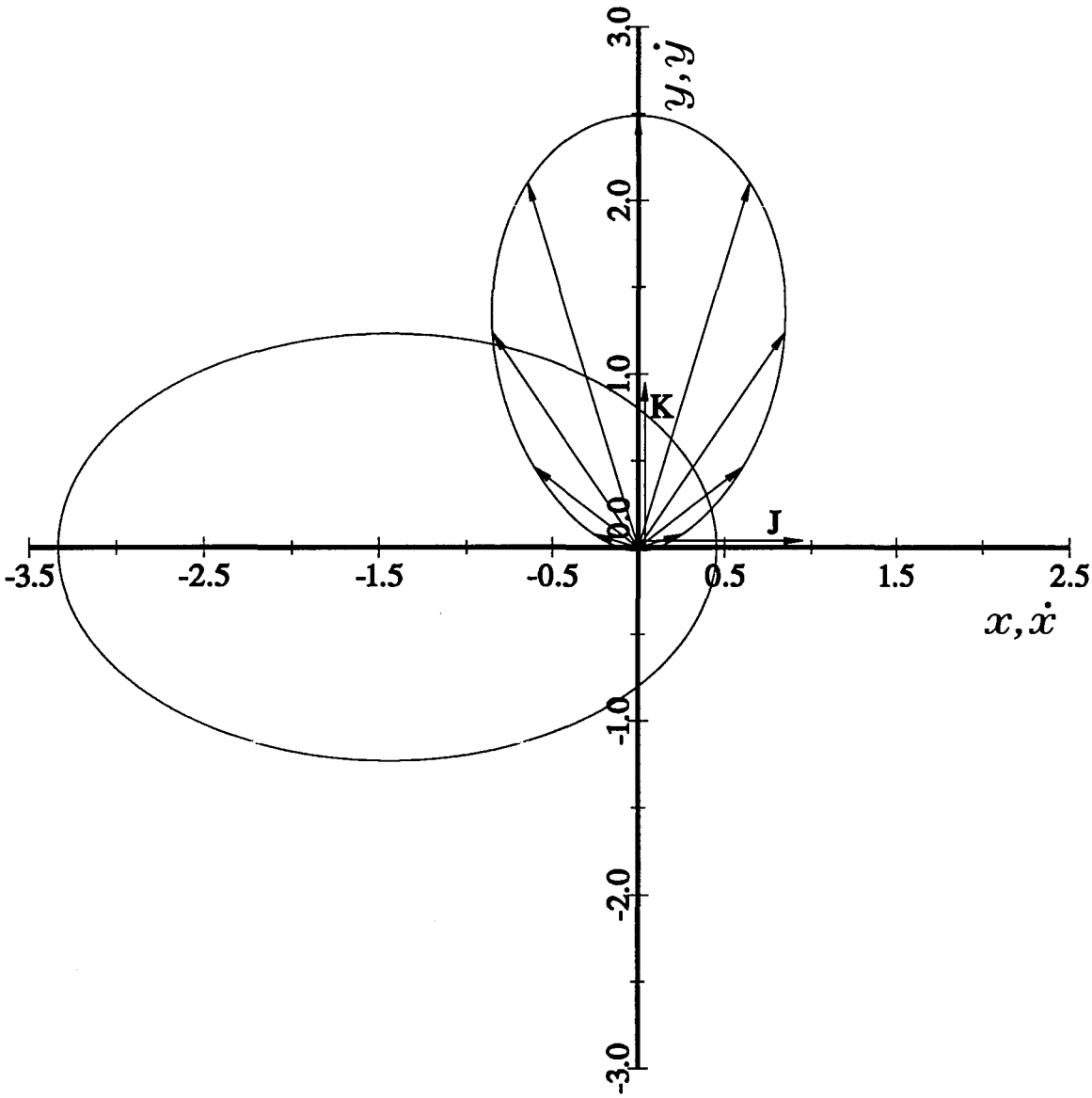


Figure 2.15.1. The elliptical Keplerian orbit and the construction of the corresponding velocity hodograph for the generalised Kepler problem with a selection of velocity vectors drawn from the origin on the same set of axes as the displacement. The constants have the values $\alpha = -6$, $\mu = 0.15$, $A = 1.25$, $\theta_0 = 0$ and $K = J = 0.95$. The origin lies inside the velocity hodograph.

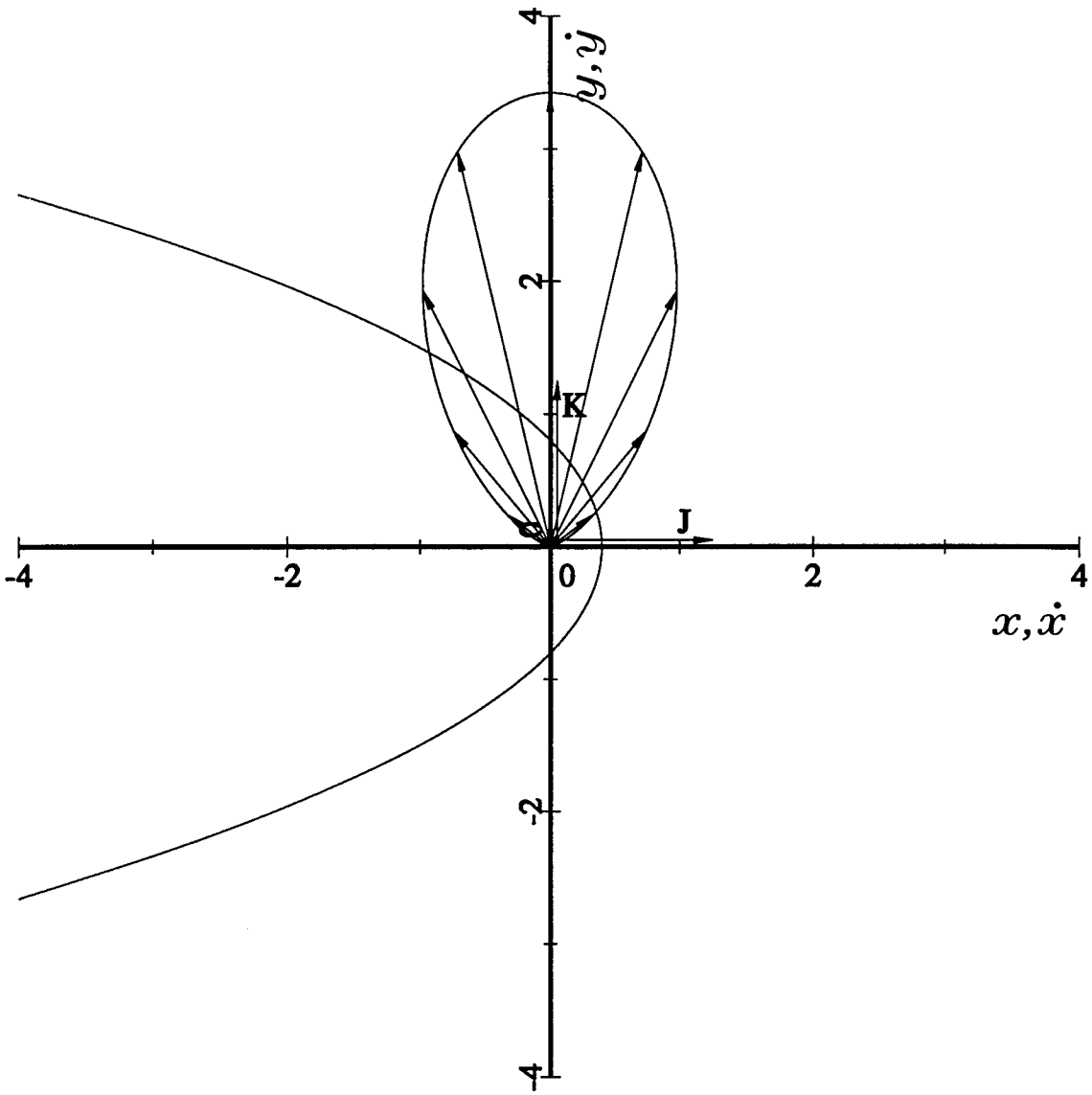


Figure 2.15.2. The parabolic Keplerian orbit and the construction of the corresponding velocity hodograph for the generalised Kepler problem with a selection of velocity vectors drawn from the origin on the same set of axes as the displacement. The constants have the values $\alpha = -6$, $\mu = 0.15$, $A = 1.25$, $\theta_0 = 0$ and $K = J = 1.25$. The origin touches the velocity hodograph. Note that as with the Kepler problem the velocity hodograph is only completed as t ranges from negative through positive infinity.

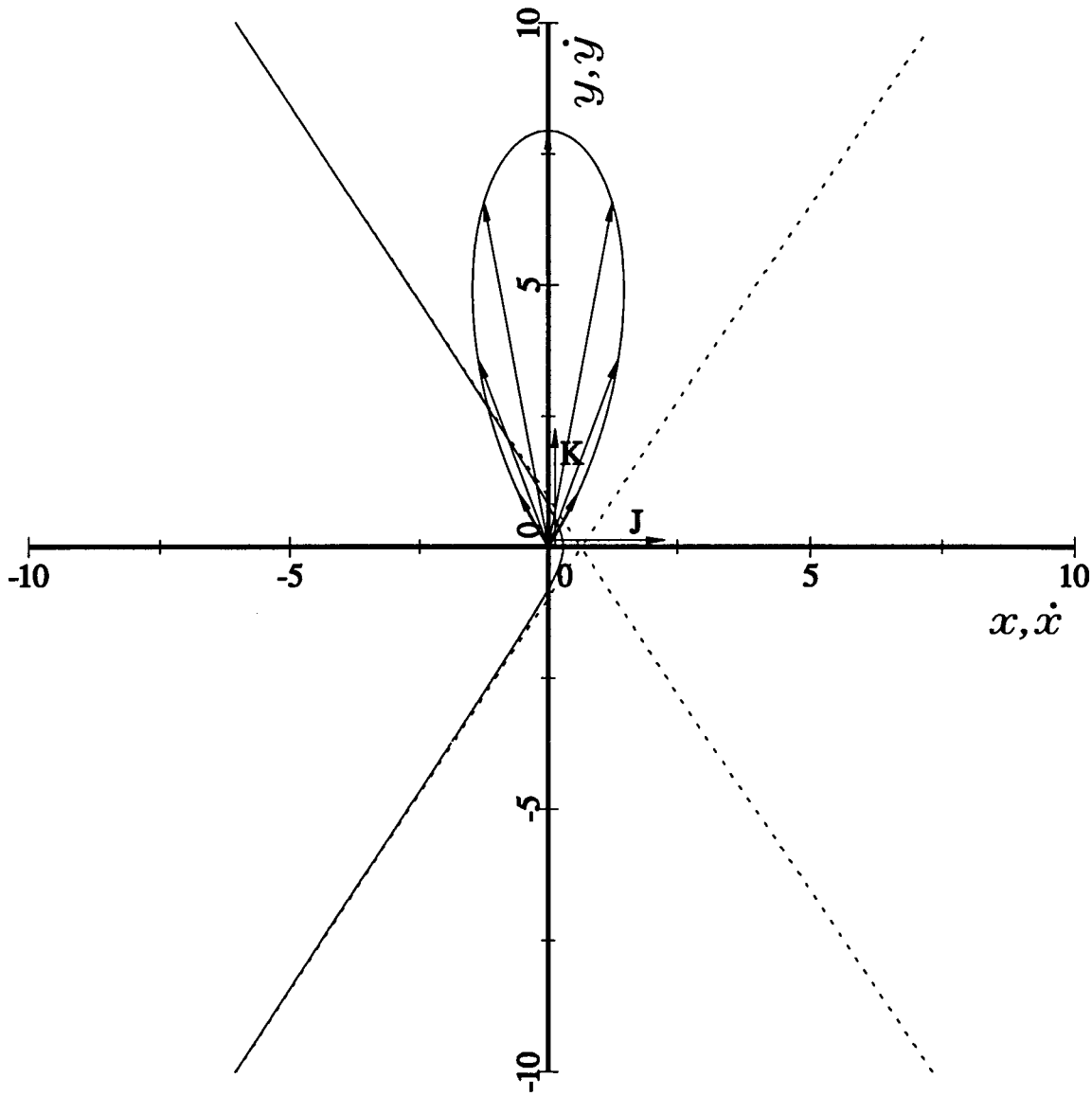


Figure 2.15.3. The hyperbolic Keplerian orbit and the construction of the corresponding velocity hodograph for the generalised Kepler problem with a selection of velocity vectors drawn from the origin on the same set of axes as the displacement. The constants have the values $\alpha = -6$, $\mu = 0.15$, $A = 1.25$, $\theta_0 = 0$ and $K = J = 2.25$. The origin touches the velocity hodograph. Note that unlike the Kepler problem the velocity hodograph is completed as t ranges from negative through positive infinity.

the elliptical and parabolic cases, unlike the Kepler problem. The velocity hodograph also closes as t ranges from negative through positive infinity or equivalently when $\theta - \theta_0$ ranges from $\arccos(1/e) - \pi$ through $\pi - \arccos(1/e)$ radians unlike the Kepler problem where the velocity hodograph does not close. This is because the curve of the velocity hodograph does not intersect with the asymptotes to the orbit when they are shifted so that the intersection of the asymptotes to the hyperbola is centred on the origin unlike the corresponding Kepler problem where there is an intersection.

Figure 2.15.4 shows the variation in the magnitude of the angular momentum vector along the orbit corresponding with Figure 2.15.1. Note that the angular momentum is largest where r is smallest and *vice versa*. This should be the case since $L = \frac{1}{2}kr^{\frac{\alpha+3}{2}}$.

Figure 2.15.5 geometrically demonstrates the construction of $\boldsymbol{L}$ corresponding with Figures 2.15.1 and 2.15.4. The shaded parallelograms represent the magnitude of $\boldsymbol{L} = \boldsymbol{r} \times \dot{\boldsymbol{r}}$.

Figure 2.15.6 shows both the displacements and corresponding velocities at regular time intervals for the elliptical case $\alpha = -6$ and $A > J$. Kepler's second law is now invalid as the area enclosed between the orbit and any two vectors drawn from the origin to two consecutive solid round time markers on the orbit is clearly not constant for every pair of solid round time markers over the entire length of the orbit. It should be obvious that the initial phase difference between the displacement and velocity vectors is $\pi/2$ radians as the displacement lies along the $+x-$axis at $t = 0$ while the velocity is purely along the $+\dot{y}-$axis. The phase difference in general between the displacement and velocity vectors is not constant since $\boldsymbol{r} \cdot \dot{\boldsymbol{r}} = r\dot{r}$ which is nonzero except when $\dot{r} = 0$, *i.e.* at the extremities of the motion. This is also evident by comparing the angle between the corresponding displacement and velocity vectors for a range of time intervals using the solid round time markers on the orbit and the corresponding solid square time markers on the velocity hodograph and counting the number of round markers from the rightmost vertex of the ellipse in a counter–clockwise direction to the displacement of interest and then counting off the same number of square markers on the velocity hodograph starting from the square marker at the top of the velocity hodograph (since at $t = 0$ the velocity is purely along the $+\dot{y}-$axis) in a counter–clockwise direction to obtain the corresponding velocity or *vice versa*. Note, however, that the phase difference between the radial vector $\boldsymbol{r}$ and the vector directed from the head of the Hamilton–like vector $\boldsymbol{K}$ to the head of the vector $\dot{\boldsymbol{r}}/L$, *i.e.* $\dot{\boldsymbol{r}}/L - \boldsymbol{K}$ is a constant $\pi/2$ radians since $\boldsymbol{r} \cdot (\dot{\boldsymbol{r}}/L - \boldsymbol{K}) = 0$. In summary, the phase difference between $\boldsymbol{r}$ and $\dot{\boldsymbol{r}}$ is not constant in the generalised Kepler problem

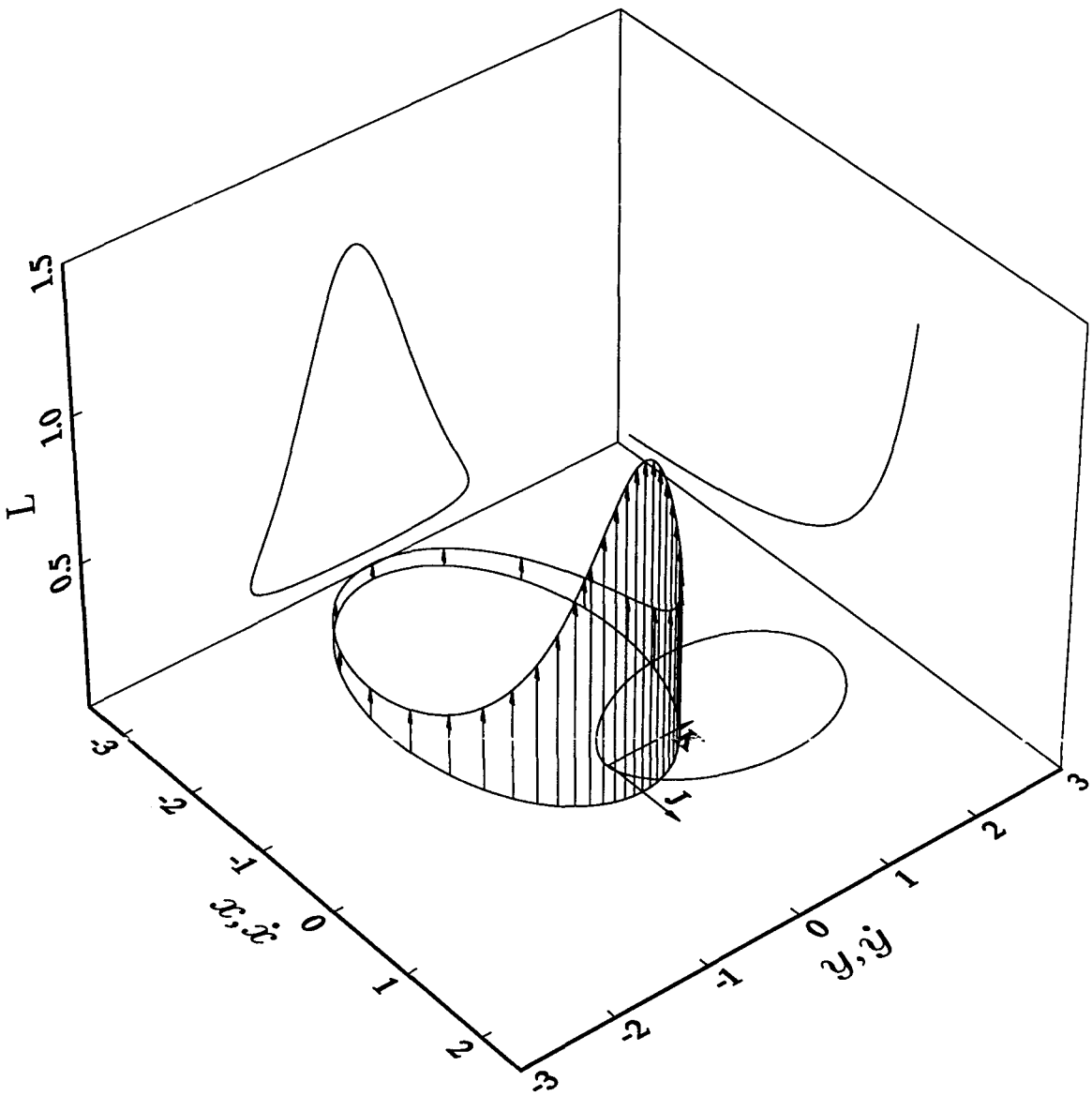


Figure 2.15.4. The variation in the magnitude of the angular momentum vector along the orbit corresponding with Figure 2.15.1. The projections of the angular momentum curve onto planes parallel to the xy, xL and yL planes are also shown. In this example the angular momentum is constant in direction but not in magnitude.

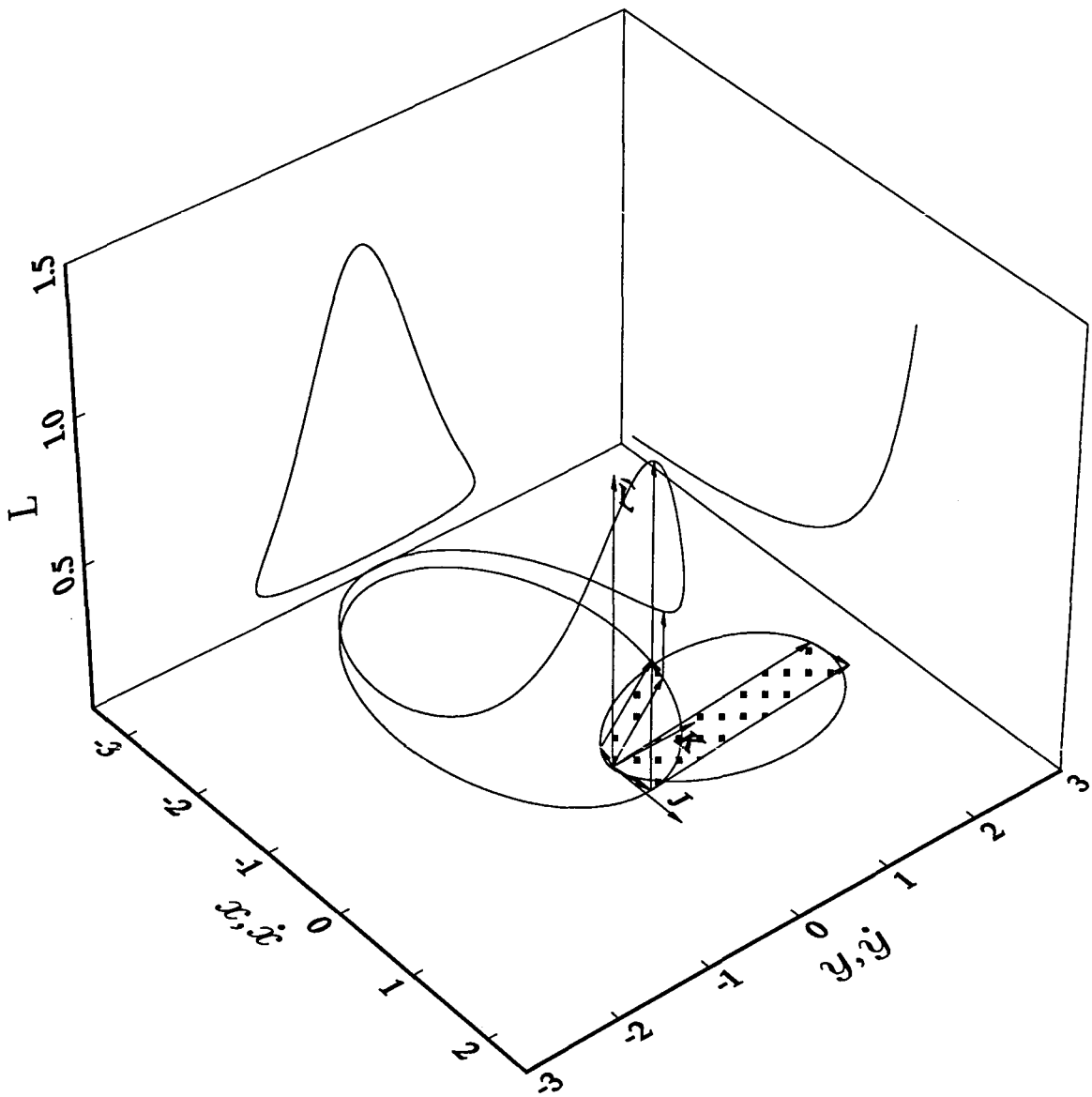


Figure 2.15.5. The elliptical Keplerian orbit with its corresponding velocity hodograph associated with Figures 2.15.1 and 2.15.4 demonstrating the construction of $\boldsymbol{L}$. The height of the angular momentum vector placed at the vertex of the shaded parallelogram touching the orbit is equal in magnitude to the shaded area.

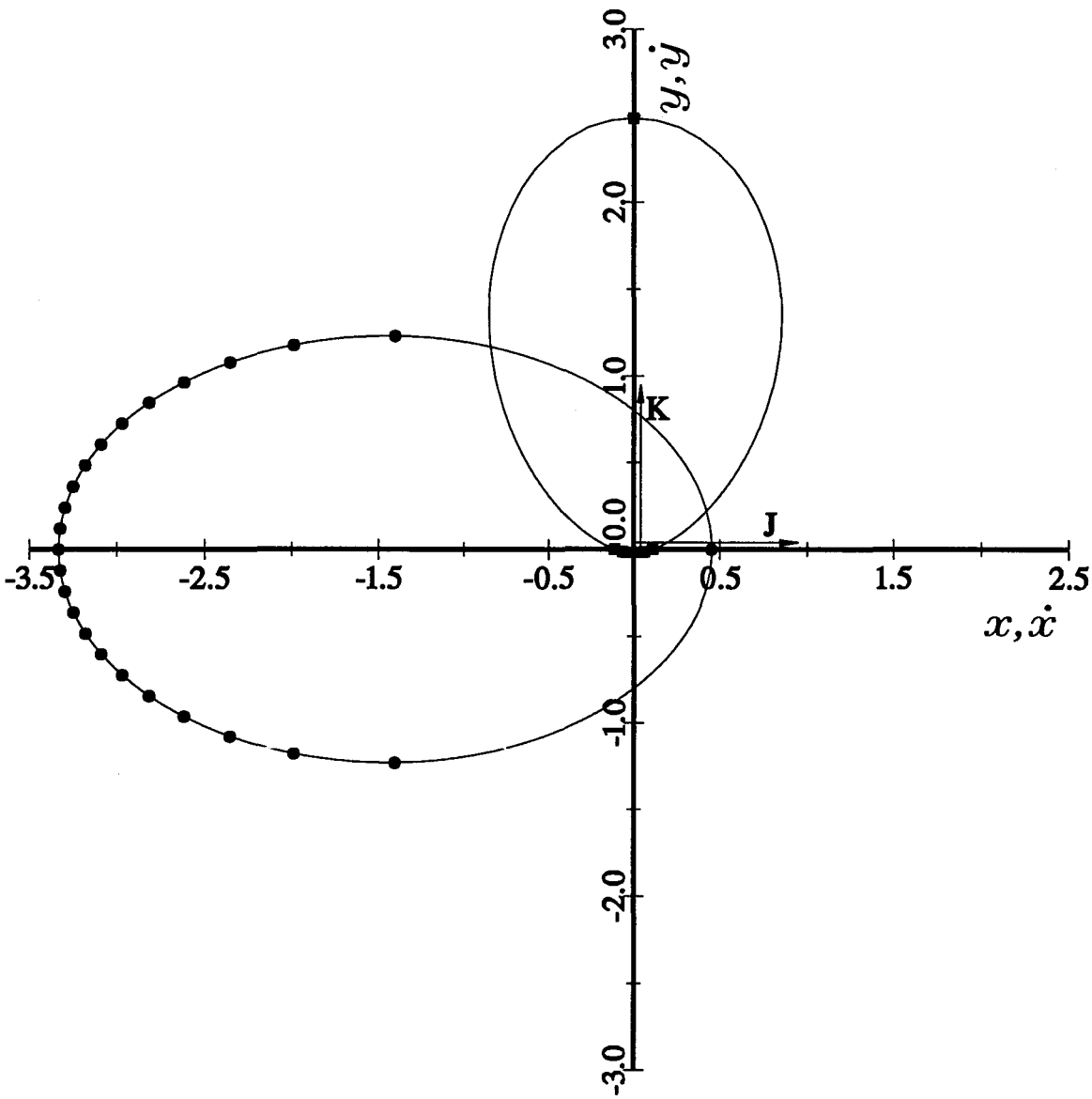


Figure 2.15.6. The elliptical Keplerian orbit with its corresponding velocity hodograph. The circles (–●–●–●–) show the displacements of the particle at the time intervals $iT/24$, $i = 0, \ldots, 24$ and the squares (–■–■–■–) give the corresponding velocities. Kepler's second law is now invalid as equal areas are not swept out in equal times. The phase difference between the velocity and displacement vectors is not constant. The constants are chosen as for Figure 2.15.1.

but the phase difference between $\boldsymbol{r}$ and $\dot{\boldsymbol{r}}/L - \boldsymbol{K}$ is constant at $\pi/2$ radians or, in other words, the radial vector directed from the origin which is also a focus of the ellipse in the plane moves in phase with an offset scaled velocity vector directed from the head of the Hamilton–like vector. Note also that the velocity decreases rapidly as the particle moves a short distance from the perihelion and then increases again rapidly a short distance before returning to the perihelion (the increase is faster than for the Kepler problem).

Figure 2.15.7 shows the elliptic Keplerian orbit and the construction of the corresponding velocity hodograph for the generalised problem when $\alpha = 3$ and $A > J$. Note that the circular velocity hodograph in the Kepler problem ($\alpha = -3$) is now distorted into a kidney–shaped curve. The origin still remains inside the velocity hodograph, but is now situated in the top half of the velocity hodograph. Figure 2.15.8 shows the parabolic Keplerian orbit and the construction of the corresponding velocity hodograph for the generalised problem when $\alpha = 3$ and $A = J$. Unlike the Kepler problem the velocity hodograph does not close as t ranges from negative through positive infinity or equivalently when $\theta - \theta_0$ ranges from $-\pi$ through π radians and the origin lies below the tip of the velocity hodograph. Figure 2.15.9 shows the hyperbolic Keplerian orbit and the construction of the corresponding velocity hodograph for the generalised problem when $\alpha = 3$ and $A < J$. The velocity hodograph is now V–shaped and lies parallel to the asymptotes of the orbit. The velocity hodograph is unbounded as t ranges from negative through positive infinity or equivalently when $\theta - \theta_0$ ranges from $\arccos(1/e) - \pi$ through $\pi - \arccos(1/e)$ radians unlike the Kepler problem where the velocity hodograph is bounded. This is because the curve of the velocity hodograph becomes collinear with the asymptotes to the orbit when they are shifted so that the intersection of the asymptotes to the hyperbola is centred on the origin unlike the corresponding Kepler problem where there is an intersection.

Figure 2.15.10 shows the variation in the magnitude of the angular momentum vector along the orbit corresponding with Figure 2.15.7. Note that the angular momentum is greatest where r is largest and *vice versa*. This should be the case since $L = \frac{1}{2}kr^{\frac{\alpha+3}{2}}$. Figure 2.15.11 geometrically demonstrates the construction of $\boldsymbol{L}$ corresponding with Figures 2.15.7 and 2.15.10. The shaded parallelograms represent the magnitude of $\boldsymbol{L} = \boldsymbol{r} \times \dot{\boldsymbol{r}}$.

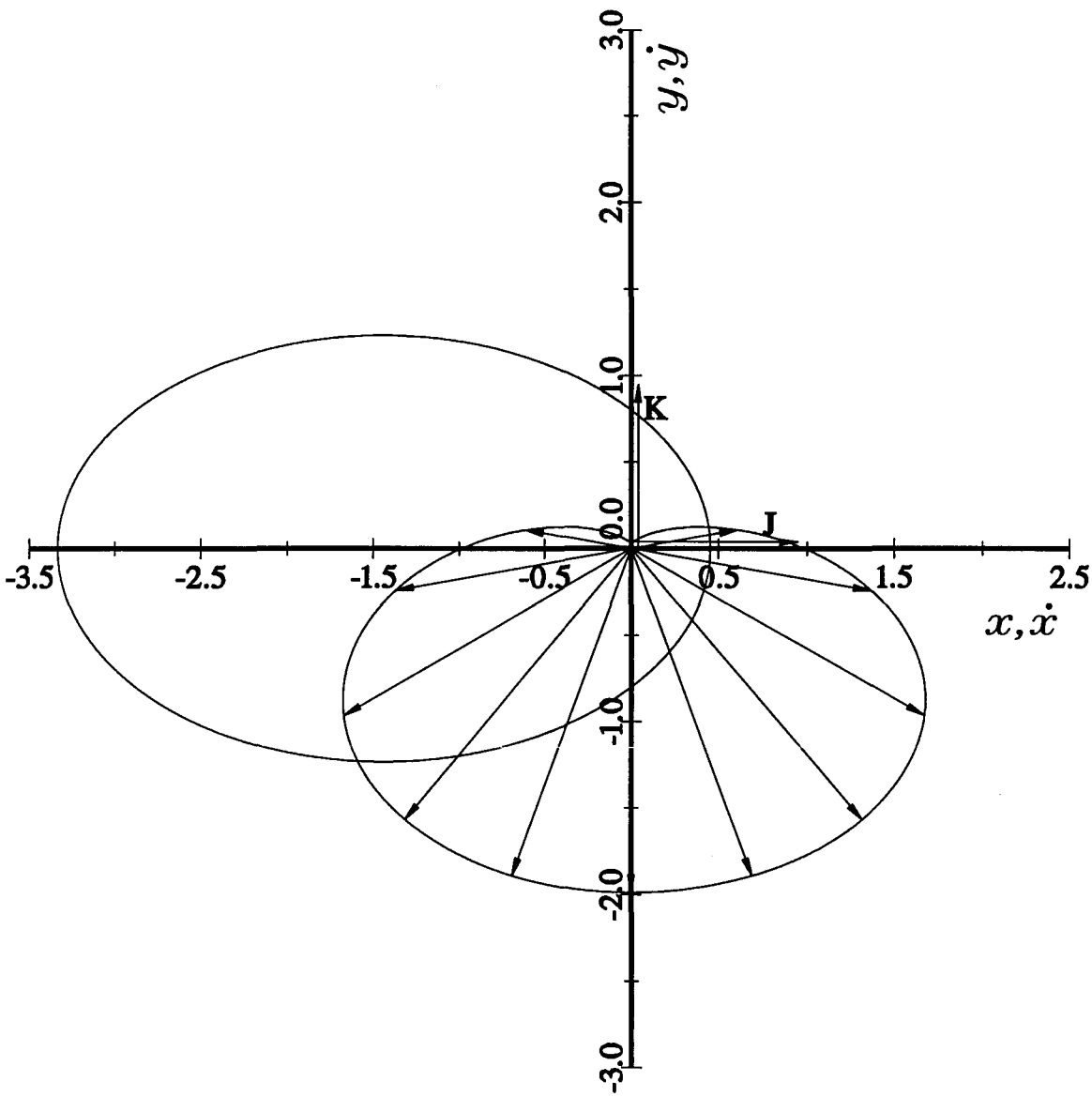


Figure 2.15.7. The elliptical Keplerian orbit and the construction of the corresponding velocity hodograph for the generalised Kepler problem with a selection of velocity vectors drawn from the origin on the same set of axes as the displacement. The constants have the values $\alpha = 3$, $\mu = 0.04$, $A = 1.25$, $\theta_0 = 0$ and $K = J = 0.95$. The origin lies inside the velocity hodograph.

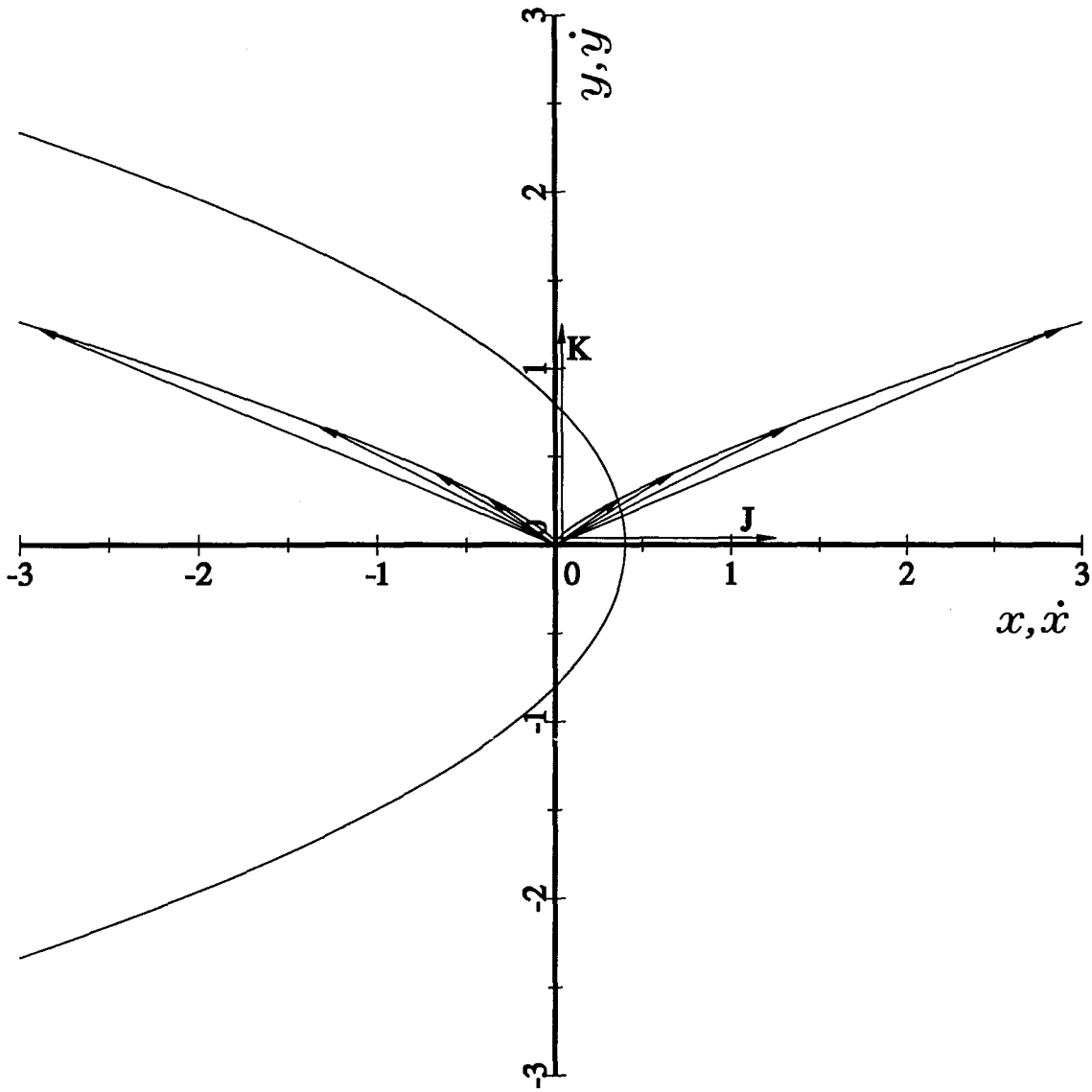


Figure 2.15.8. The parabolic Keplerian orbit and the construction of the corresponding velocity hodograph for the generalised Kepler problem with a selection of velocity vectors drawn from the origin on the same set of axes as the displacement. The constants have the values $\alpha = 3$, $\mu = 0.04$, $A = 1.25$, $\theta_0 = 0$ and $K = J = 1.25$. The origin lies below the tip of the velocity hodograph. Note that unlike the Kepler problem the velocity hodograph is unbounded as t ranges from negative through positive infinity.

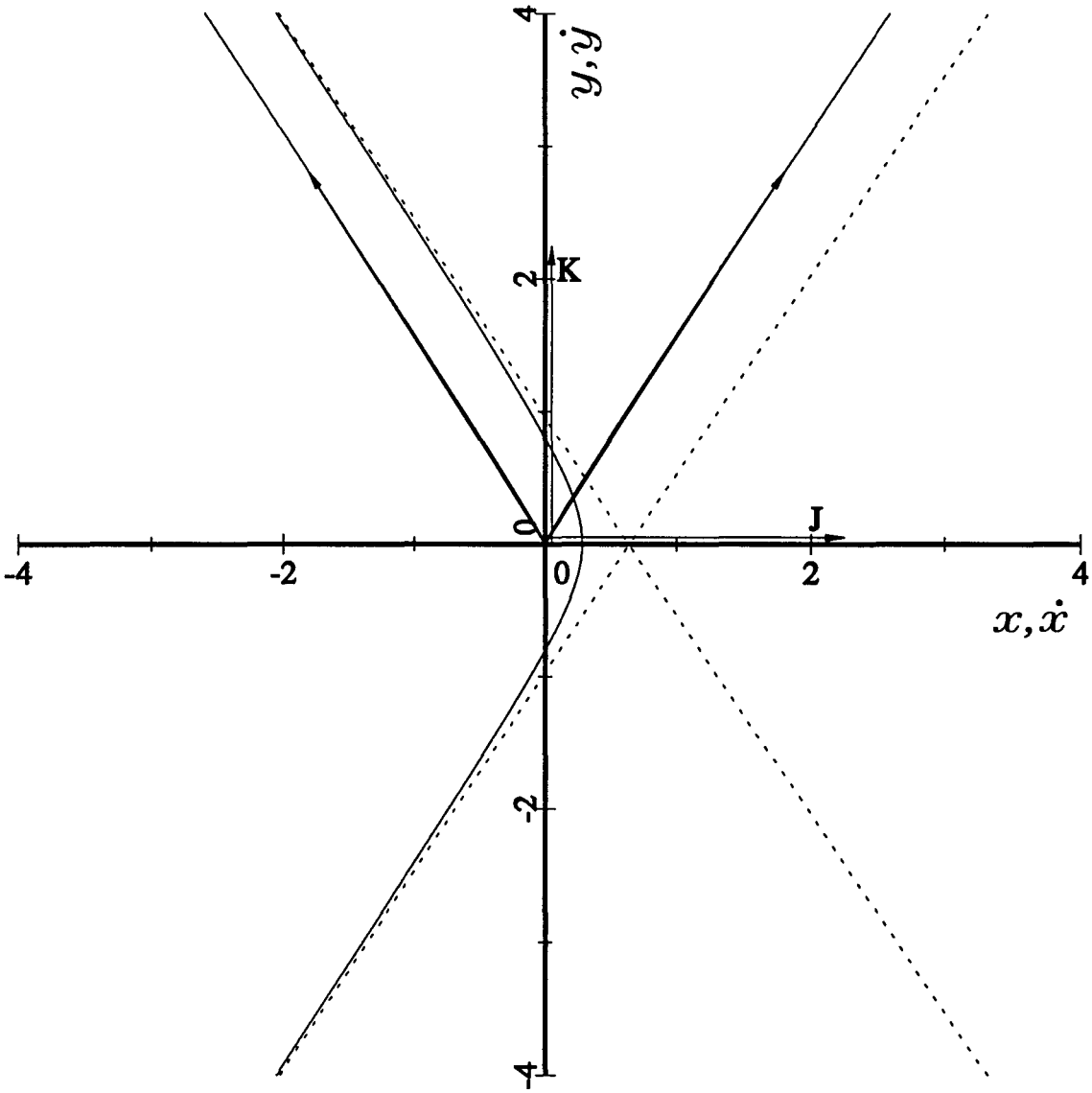


Figure 2.15.9. The hyperbolic Keplerian orbit and the construction of the corresponding velocity hodograph for the generalised Kepler problem with a selection of velocity vectors drawn from the origin on the same set of axes as the displacement. The constants have the values $\alpha = 3$, $\mu = 0.04$, $A = 1.25$, $\theta_0 = 0$ and $K = J = 2.25$. The origin lies below the tip of the velocity hodograph. Note that unlike the Kepler problem the velocity hodograph is unbounded as t ranges from negative through positive infinity.

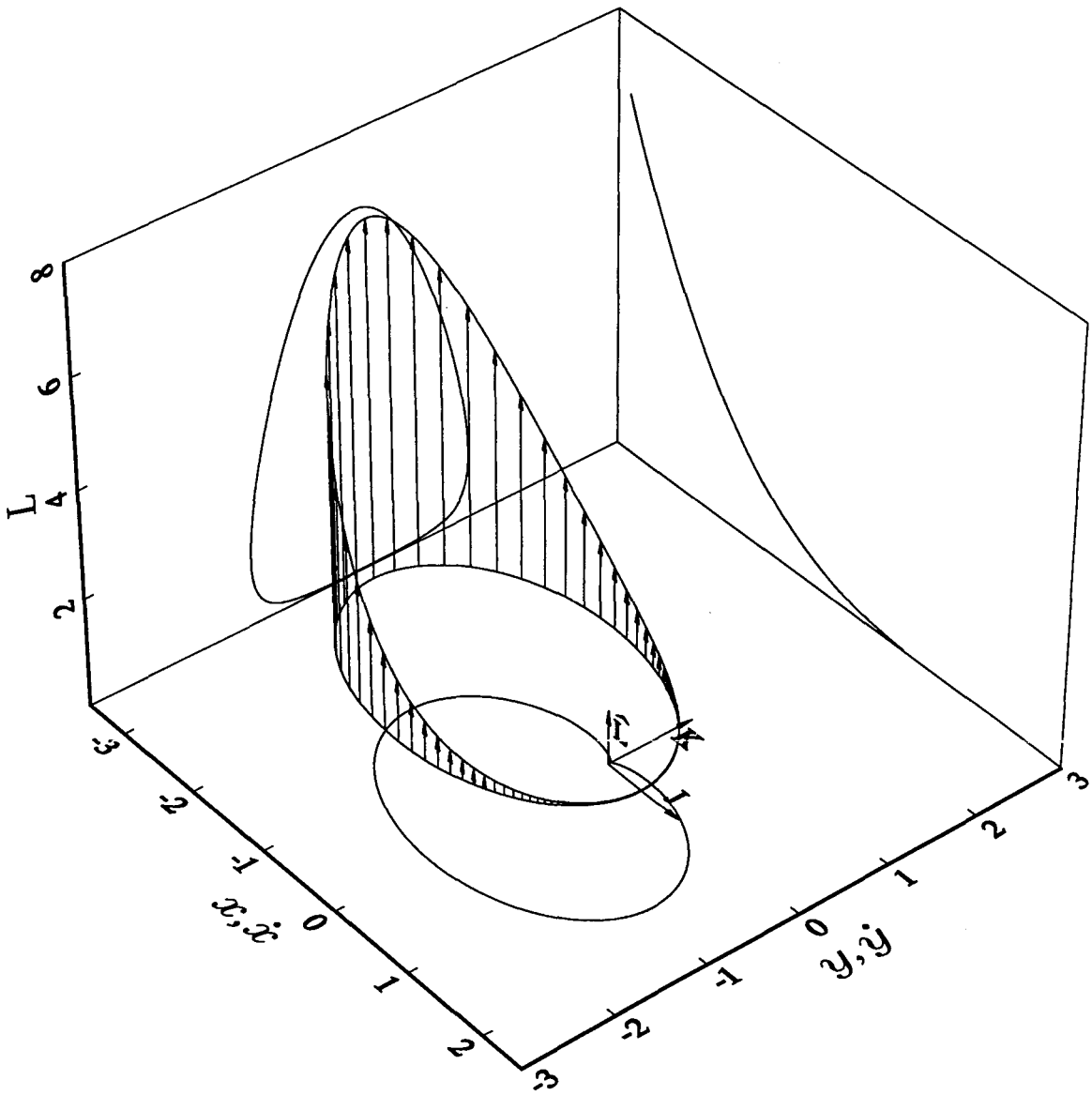


Figure 2.15.10. The variation in the magnitude of the angular momentum vector along the orbit corresponding with Figure 2.15.7. The projections of the angular momentum curve onto planes parallel to the xy, xL and yL planes are also shown. In this example the angular momentum is constant in direction but not in magnitude.

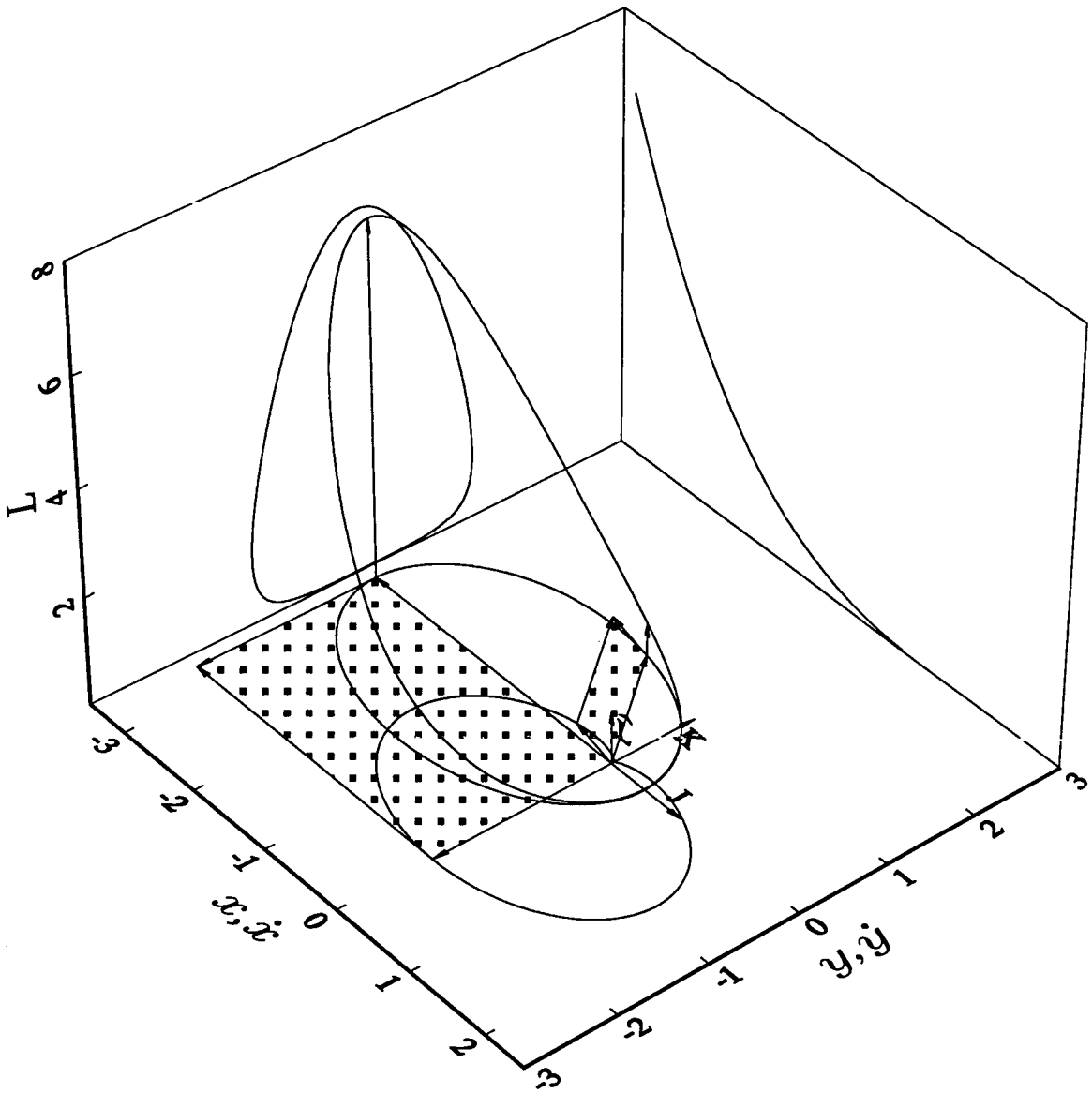


Figure 2.15.11. The elliptical Keplerian orbit with its corresponding velocity hodograph associated with Figures 2.15.7 and 2.15.10 demonstrating the construction of $\boldsymbol{L}$. The height of the angular momentum vector placed at the vertex of the shaded parallelogram touching the orbit is equal in magnitude to the shaded area.

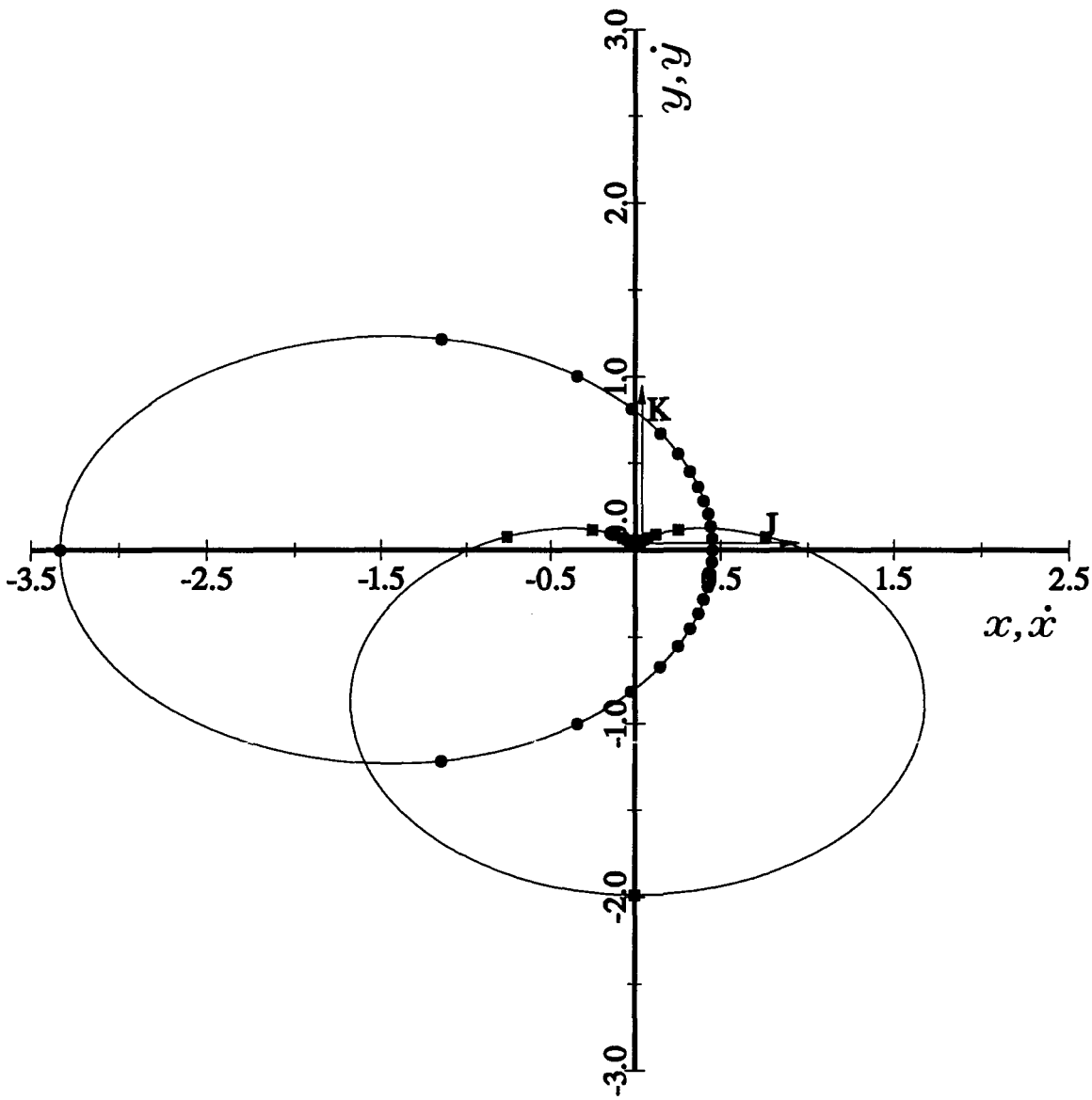


Figure 2.15.12. The elliptical Keplerian orbit with its corresponding velocity hodograph. The circles (–•–•–•–) show the displacements of the particle at the time intervals $iT/24$, $i = 0, \ldots, 24$ and the squares (–■–■–■–) give the corresponding velocities. Kepler's second law is now invalid as equal areas are not swept out in equal times. The phase difference between the velocity and displacement vectors is not constant. The constants are chosen as for Figure 2.15.7.

Figure 2.15.12 shows both the displacements and corresponding velocities at regular time intervals for the elliptical case $\alpha = 3$ and $A > J$. Kepler's second law is now invalid as the area enclosed between the orbit and any two vectors drawn from the origin to two consecutive solid round time markers on the orbit is clearly not constant for every pair of solid round time markers over the entire length of the orbit. It should be obvious that the initial phase difference between the displacement and velocity vectors is $\pi/2$ radians as the displacement lies along the $+x-$axis at $t = 0$ while the velocity is purely along the $+\dot{y}-$axis. The phase difference in general between the displacement and velocity vectors is not constant since $\boldsymbol{r} \cdot \dot{\boldsymbol{r}} = r\dot{r}$ which is nonzero except when $\dot{r} = 0$, *i.e.* at the extremities of the motion. This is also evident by comparing the angle between the corresponding displacement and velocity vectors for a range of time intervals using the solid round time markers on the orbit and the corresponding solid square time markers on the velocity hodograph and counting the number of round markers from the rightmost vertex of the ellipse in a counter–clockwise direction to the displacement of interest and then counting off the same number of square markers on the velocity hodograph starting from the square marker at the top of the velocity hodograph (since at $t = 0$ the velocity is purely along the $+\dot{y}-$axis) in a counter–clockwise direction to obtain the corresponding velocity or *vice versa*. Note, however, that the phase difference between the radial vector $\boldsymbol{r}$ and the vector directed from the head of the Hamilton–like vector $\boldsymbol{K}$ to the head of the vector $\dot{\boldsymbol{r}}/L$, *i.e.* $\dot{\boldsymbol{r}}/L - \boldsymbol{K}$ is a constant $\pi/2$ radians since $\boldsymbol{r} \cdot (\dot{\boldsymbol{r}}/L - \boldsymbol{K}) = 0$. In summary, the phase difference between $\boldsymbol{r}$ and $\dot{\boldsymbol{r}}$ is not constant in the generalised Kepler problem but the phase difference between $\boldsymbol{r}$ and $\dot{\boldsymbol{r}}/L - \boldsymbol{K}$ is constant at $\pi/2$ radians or, in other words, the radial vector directed from the origin which is also a focus of the ellipse in the plane moves in phase with an offset scaled velocity vector directed from the head of the Hamilton–like vector. Note also that the velocity increases rapidly as the particle moves a short distance from the perihelion and then decreases again rapidly a short distance before returning to the perihelion (the opposite behaviour to that of the Kepler problem).

The scalar product of $r^{-(\alpha+3)}\dot{\boldsymbol{r}}$ and (2.15.1) gives rise to the energy–like integral upon integration

$$E = \frac{1}{2}\frac{\dot{\boldsymbol{r}} \cdot \dot{\boldsymbol{r}}}{r^{\alpha+3}} - \frac{\mu}{r}. \tag{2.15.9}$$

The conserved quantities J, k and E are not of course independent but related by the formula

$$J^2 = K^2 = \frac{2E}{k^2} + \frac{\mu^2}{k^4}. \tag{2.15.10}$$

The period of the motion T is found using (2.15.4) and the orbit equation (2.15.8) to be

$$T = \frac{2}{k}\int_{\theta_0}^{\pi+\theta_0} \left(\frac{\mu}{k^2} + J\cos(\theta-\theta_0)\right)^{\frac{(\alpha-1)}{2}} \mathrm{d}\theta. \tag{2.15.11}$$

Using (2.15.10)

$$\frac{\mu}{k^2} + J\cos(\theta-\theta_0) = \left(\frac{-2E}{k^2}\right)^{\frac{1}{2}} \left\{ \frac{\mu}{k(-2E)^{\frac{1}{2}}} + \left[\left(\frac{\mu}{k(-2E)^{\frac{1}{2}}}\right)^2 - 1\right]^{\frac{1}{2}} \cos(\theta-\theta_0)\right\}. \tag{2.15.12}$$

Using G&R [43, 8.822.1] we observe that

$$P_v(z) = \frac{1}{\pi}\int_0^{\pi} \frac{\mathrm{d}\xi}{\left[z + (z^2-1)^{\frac{1}{2}}\cos\xi\right]^{v+1}} = \frac{1}{\pi}\int_0^{\pi} \left[z + \left(z^2-1\right)^{\frac{1}{2}}\cos\xi\right]^{v} \mathrm{d}\xi, \tag{2.15.13}$$

where $P_v(z)$ is the Legendre function of the first kind which becomes the Legendre polynomial for v an integer.

Remembering that $E < 0$ for an elliptical orbit, equation (2.15.11) can be rewritten using (2.15.13) as

$$T = \frac{2\pi}{k}\left(\frac{-2E}{k^2}\right)^{\frac{(\alpha-1)}{4}} P_{\frac{(\alpha-1)}{2}}(z), \tag{2.15.14}$$

where

$$z = \frac{\mu}{k(-2E)^{\frac{1}{2}}}. \tag{2.15.15}$$

The semi–major axis length a is found from the orbit equation (2.15.8) and (2.15.10)

$$\begin{aligned} a &= \frac{1}{2}\left[r(0) + r(\pi)\right] \\ &= \frac{\mu}{-2E}. \end{aligned} \tag{2.15.16}$$

We recall that for an ellipse the length of the semi–latus rectum is

$$l = \frac{b^2}{a} = a(1-e^2), \tag{2.15.17}$$

where a is the semi–major axis length, b the semi–minor axis length and e is the eccentricity. The semi–minor axis length is given by (2.15.8) as

$$l = r\left(\frac{\pi}{2}\right) = \frac{k^2}{\mu} \tag{2.15.18}$$

so that z, the argument of the generalised Kepler's third law becomes

$$z = (1-e^2)^{-\frac{1}{2}}, \tag{2.15.19}$$

using (2.15.16)–(2.15.18). The generalised Kepler's third law can now be written as

$$Ta^{\frac{\alpha}{2}} = \frac{2\pi}{\mu^{\frac{1}{2}}}\left(1-e^2\right)^{-\frac{(\alpha+1)}{4}} P_{\frac{(\alpha-1)}{2}}\left[(1-e^2)^{-\frac{1}{2}}\right]. \tag{2.15.20}$$

Figures 2.15.13 and 2.15.14 show two families of focus–centred Keplerian ellipses with differing semi–major axis lengths for two different values of the eccentricity. Figure 2.15.15 shows the relationship between the periodic time of the orbit and the eccentricity for the elliptical Keplerian orbits as given by equation (2.15.20). The Legendre functions were calculated from the first definite integral expression in (2.15.13) for $\nu < -1/2$ and the second expression for $\nu \geq -1/2$ using an adaptive numerical technique. The two different definite integral expressions were used in order to improve the convergence of the integration algorithm although they are both valid for any value of ν. In order to verify the results from the integration, the Legendre functions were also calculated in Maple [90] using $P_\nu(z) = F(-\nu, \nu+1; 1; (1-z)/2)$, where F is the hypergeometric function and the results were found to agree up until the tenth decimal place over the interval of convergence of the hypergeometric series, *i.e.* $-1 < (1-z)/2 < 1$ or $-1 < z < 3$. The definite integral expressions (2.15.13) are preferable in this case since they can be used over the whole domain of interest, *i.e.* $z \geq 1$ (see Ince [55, §7·24 pp164*ff*]). For eccentricities equal to zero (which imply circular orbits) the period is given by equation (2.15.20) which reduces to $2\pi R^{-\frac{\alpha}{2}}/\mu^{\frac{1}{2}}$ since $P_\nu(1) = 1$, while for eccentricities equal to unity (which imply parabolic orbits) and $\alpha = 3$ the period tends to infinity while for $\alpha = -6$ the period tends to a limiting value (see Figure 2.15.15). The period was calculated for eccentricities between zero and one.

It is straightforward to show that the differential equation (2.15.1) is invariant under the similarity transformation

$$(t, \boldsymbol{r}) \rightarrow (\bar{t}, \bar{\boldsymbol{r}} : t = \gamma\bar{t}, \boldsymbol{r} = \gamma^{-\frac{2}{\alpha}}\bar{\boldsymbol{r}}). \tag{2.15.21}$$

Since the energy integral (2.15.9) transforms as

$$E = \gamma^{\frac{2}{\alpha}}\bar{E}, \tag{2.15.22}$$

and using (2.15.16)

$$a = \gamma^{-\frac{2}{\alpha}}\bar{a}, \tag{2.15.23}$$

it follows that the quantity

$$\frac{a^{-\frac{\alpha}{2}}}{t} = \frac{\gamma\bar{a}^{-\frac{\alpha}{2}}}{\gamma\bar{t}} = \frac{\bar{a}^{-\frac{\alpha}{2}}}{\bar{t}} \tag{2.15.24}$$

is invariant, or alternatively that $Ta^{\frac{\alpha}{2}}$ is invariant.

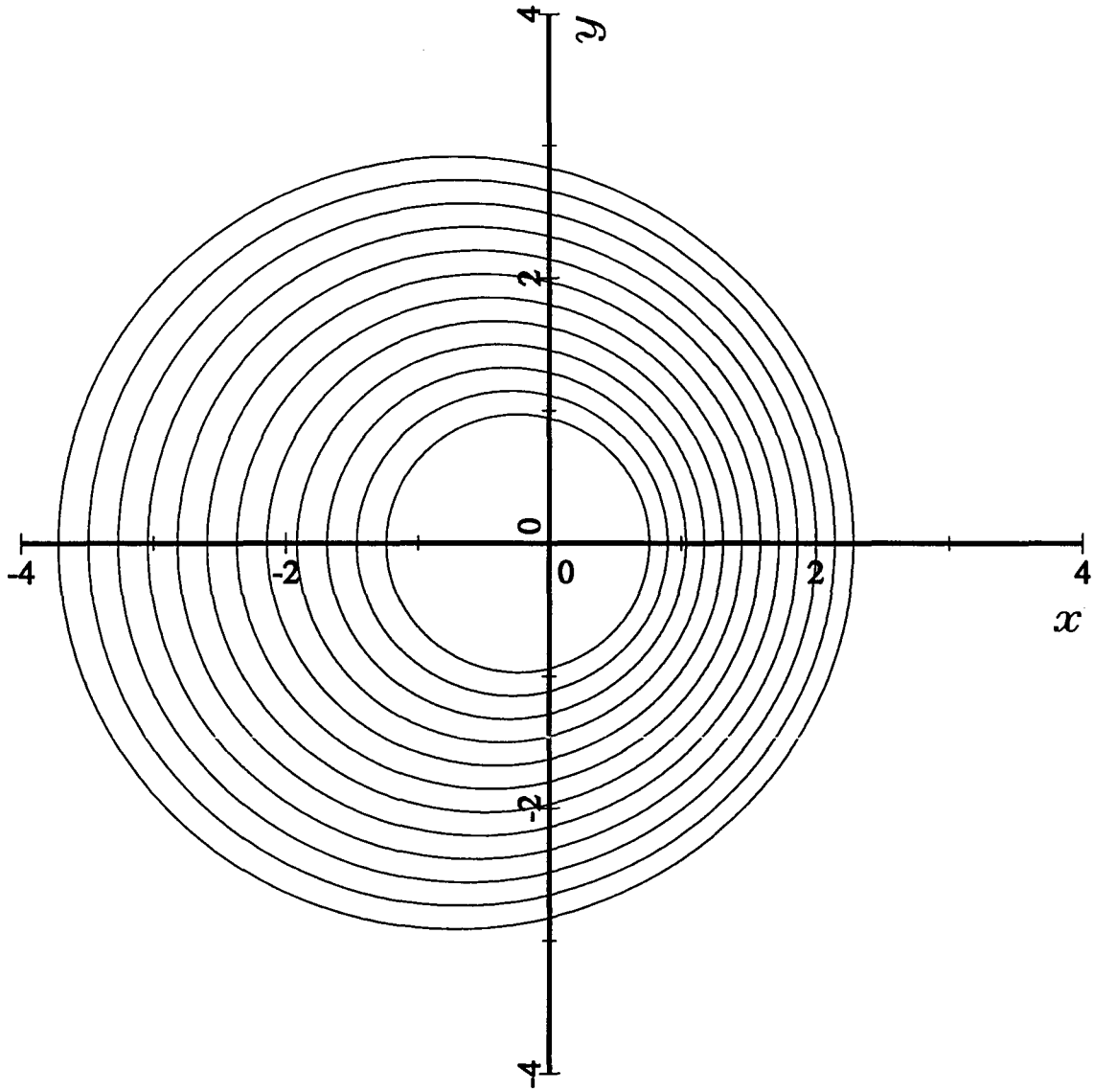


Figure 2.15.13. A family of Keplerian orbital ellipses with differing semi–major axis lengths for a fixed value of the eccentricity. The constants have the values $e = 0.24$ and $a = 2i/11 + 1$, $i = 0, \ldots, 11$.

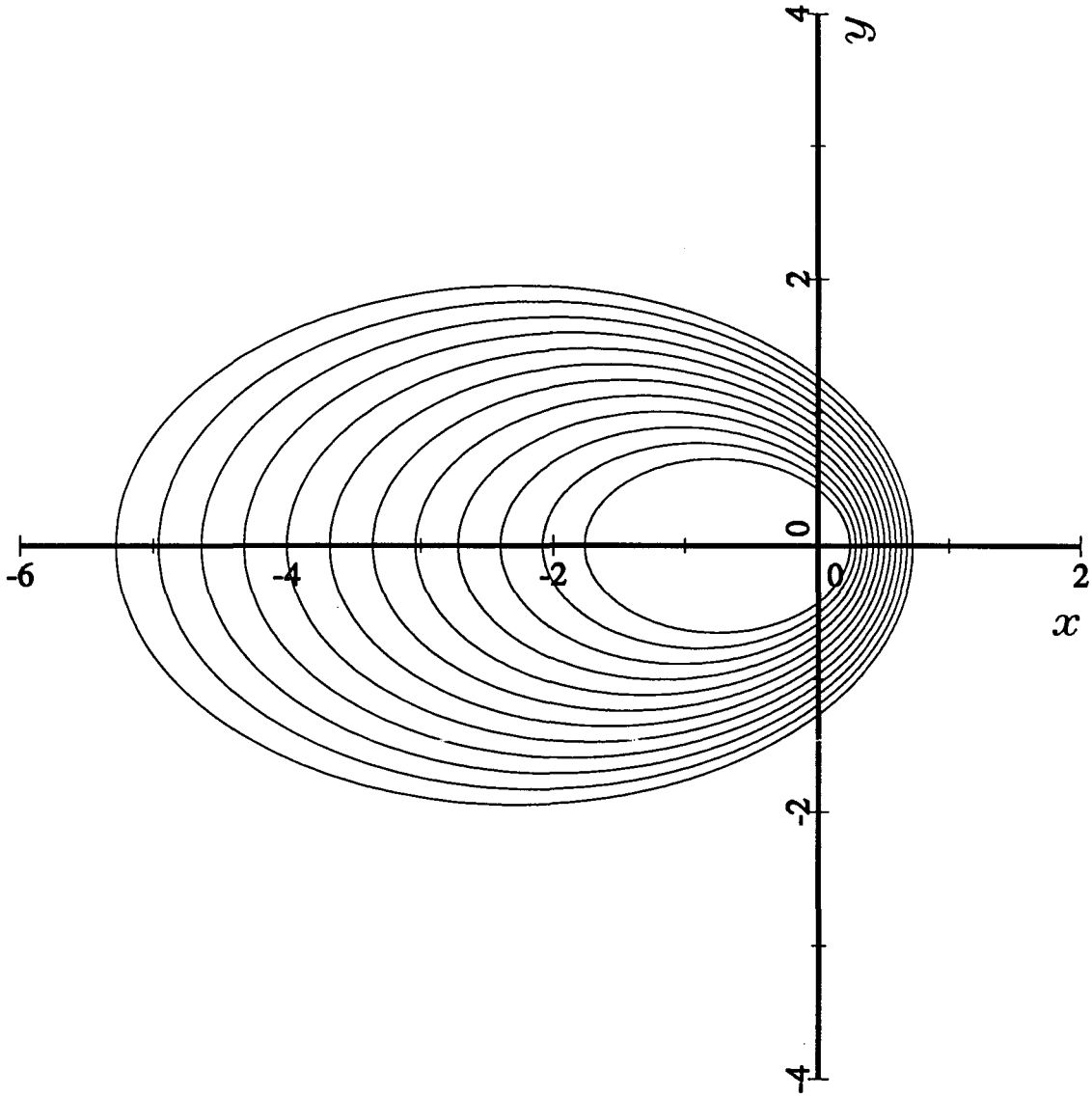


Figure 2.15.14. A family of Keplerian orbital ellipses with differing semi–major axis lengths for a fixed value of the eccentricity. The constants have the values $e = 0.76$ and $a = 2i/11 + 1$, $i = 0, \ldots, 11$.

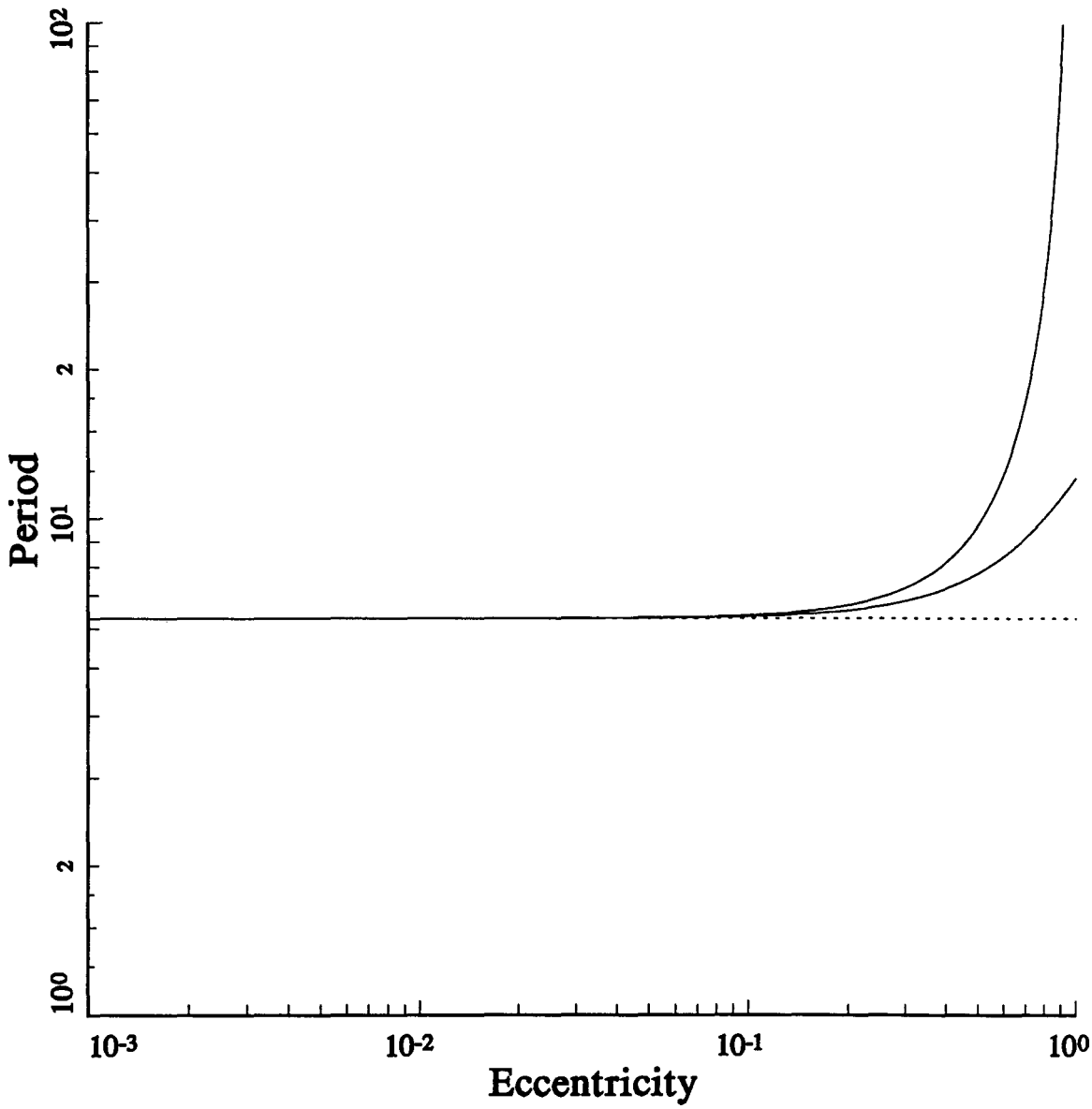


Figure 2.15.15. The periodic time versus the eccentricity for the generalised Kepler problem. The steeper curve corresponds to the choice of constants $\alpha = 3$, $\mu = 1$, $a = 1$ whilst the shallower curve corresponds to the choice $\alpha = -6$, $\mu = 1$ and $a = 1$. The dotted line indicates a constant period of 2π radians independent of the eccentricity, which is the case when $\alpha = -3$ or -1.

The angular momentum transforms as

$$L = r^2\dot{\theta} = \frac{\gamma^{-\frac{4}{\alpha}}\bar{r}^2}{\gamma}\left(\frac{\mathrm{d}\bar{\theta}}{\mathrm{d}\bar{t}}\right) = \gamma^{-\frac{4}{\alpha}-1}\bar{L} \tag{2.15.25}$$

and so using (2.15.18) and (2.15.3)

$$l = \gamma^{-\frac{2}{\alpha}}\bar{l}. \tag{2.15.26}$$

It now follows that the ratio

$$(1-e^2) = \frac{l}{a} = \frac{\gamma^{-\frac{2}{\alpha}}\bar{l}}{\gamma^{-\frac{2}{\alpha}}\bar{a}} = \frac{\bar{l}}{\bar{a}} \tag{2.15.27}$$

is invariant and the eccentricity, z from (2.15.19) and the right hand side of (2.15.20) are all invariant. Alternatively we could, of course, have used the infinitesimal generator of the transformation

$$G = t\frac{\partial}{\partial t} - \frac{2}{\alpha}r\frac{\partial}{\partial r} \tag{2.15.28}$$

to show the invariance of (2.15.20) under the first extension of G, $G^{[1]}$. The task is simplified somewhat, by rewriting the $G^{[1]}(t, r, \dot{r}, \dot{\theta})$ in terms of the relevant conserved quantities, *i.e.*, $G^{[1]}(T, a, l)$. In the new coordinates,

$$G^{[1]} = t\frac{\partial}{\partial t} - \frac{2}{\alpha}r\frac{\partial}{\partial r} - \frac{\alpha+2}{\alpha}\dot{r}\frac{\partial}{\partial \dot{r}} - \dot{\theta}\frac{\partial}{\partial \dot{\theta}} \tag{2.15.29}$$

becomes

$$G^{[1]} = T\frac{\partial}{\partial T} - \frac{2}{\alpha}a\frac{\partial}{\partial a} - \frac{2}{\alpha}l\frac{\partial}{\partial l} \tag{2.15.30}$$

when acting on functions of T, a and l. Using (2.15.20) it is easy to show that

$$G^{[1]}\left(Ta^{\frac{\alpha}{2}}\right) = G^{[1]}\left((1-e^2)^{-\frac{1}{2}}\right) = G^{[1]}\left(\frac{a}{l}\right)^{\frac{1}{2}} = 0, \tag{2.15.31}$$

which illustrates the invariance.

To summarise, the equation

$$\ddot{\boldsymbol{r}} - \frac{1}{2}(\alpha+3)\frac{\dot{r}}{r}\dot{\boldsymbol{r}} + \mu r^{\alpha}\boldsymbol{r} = 0, \tag{2.15.32}$$

describes motion in the plane which has the following properties.

(i) The orbit is a conic section with the origin at a focus (Kepler–like),

(ii) the areal velocity is $\frac{1}{2}kr^{\frac{\alpha+3}{2}}$ and

(iii) in the case of an elliptical orbit the period and semi–major axis are related by (with R in place of a)

$$TR^{\frac{\alpha}{2}} = \frac{2\pi}{\mu^{\frac{1}{2}}}\left(1-e^2\right)^{-\left(\frac{\alpha+1}{4}\right)} P_{\frac{(\alpha-1)}{2}}\left[(1-e^2)^{-\frac{1}{2}}\right]. \tag{2.15.33}$$

For $\alpha = -3$ in (2.15.32) we obtain the usual Kepler's laws of planetary motion and, in particular, we see that $T^2 \propto R^3$ irrespective of the value of the eccentricity of the ellipse. Using the relation

$$P_v(z) = P_{-v-1}(z) \tag{2.15.34}$$

$P_{-2}(z) = P_1(z) = z$. For general α in (2.15.32) the value of the energy integral is of course always negative. This follows from the requirement that the orbit equation (2.15.8) remain finite and the semi–major axis length (2.15.16) remain positive. The areal velocity is in general not constant. Equation (2.15.33) is the generalised Kepler's third law for a power law central force plus a resistive term. It is interesting to note that the constant of proportionality depends explicitly on the eccentricity of the orbit. When $\alpha = -3$, the self–similar transformation (2.15.28) maps solutions onto solutions of the same eccentricity (see Prince and Eliezer [110]). This is not reflected in the period semi–major axis relation. However, for general α, not only does the symmetry map solutions onto solutions of the same eccentricity, but the period semi–major axis relation now depends explicitly on the eccentricity. It is also worth noting that several cases arise where the constant of proportionality of (2.15.33) does not depend on the eccentricity. This occurs when $\alpha = -3$ (Kepler problem), and $\alpha = -1$. In the cases $\alpha = 1$ and $\alpha = 3$ the constant of proportionality can be made independent of the eccentricity if the semi–latus rectum $l = R(1-e^2)$ is used instead of the semi–major axis length. When $\alpha = 1$,

$$Tl^{\frac{1}{2}} = \frac{2\pi}{\mu^{\frac{1}{2}}} \tag{2.15.35}$$

and when $\alpha = 3$,

$$Tl^{\frac{3}{2}} = \frac{2\pi}{\mu^{\frac{1}{2}}}. \tag{2.15.36}$$

If we further set $\alpha = 0$ in (2.15.32), we obtain an oscillator with an additional velocity dependent force. The additional force changes the usual geometric–centred oscillator ellipse into a Kepler one and isochronism is only preserved for orbits of the same eccentricity.

Rewriting the energy equation (2.15.9) in terms of $\dot{r}$ gives

$$\dot{r} = r^{\frac{\alpha+1}{2}}\left(2Er^2 + 2\mu r - k^2\right)^{\frac{1}{2}}. \tag{2.15.37}$$

Referring to G&R [43, 2.26ff] it should be evident that (2.15.37) can be solved and subsequently inverted to give r as a function of time for the two cases $\alpha = -1,\ 1$. Correspondingly it is possible to obtain expressions for both θ and the area swept out in the ellipse as functions of time as described in §2.14.

1.) $\alpha = -1$

$$r = \frac{k^2 J}{2E}\cos\left((-2E)^{\frac{1}{2}}(t - t_0)\right) - \frac{\mu}{2E} \tag{2.15.38}$$

$$\theta = 2\arctan\left(\frac{k(-2E)^{\frac{1}{2}}}{(\mu - k^2 J)}\tan\left(\frac{(-2E)^{\frac{1}{2}}(t - t_0)}{2}\right)\right) + \theta_0. \tag{2.15.39}$$

The area swept out by the orbit is given by

$$S = \frac{k^3 J}{4E\,(-2E)^{\frac{1}{2}}}\sin\left((-2E)^{\frac{1}{2}}(t - t_0)\right) - \frac{\mu k\,(t - t_0)}{4E}. \tag{2.15.40}$$

2.) $\alpha = 1$

$$r = \frac{1}{\mu/k^2 + J\cos\left(k(t - t_0)\right)} \tag{2.15.41}$$

$$\theta = k(t - t_0) + \theta_0. \tag{2.15.42}$$

The area of the orbit is given by G&R [43, 2.554.3 and 2.2553.3 (case $a^2 > b^2$)]

$$S = \frac{k^2 J \sin p}{4E(\mu/k^2 + J\cos p)} - \frac{\mu k}{2E\,(-2E)^{\frac{1}{2}}}\arctan\left(\frac{k\,(-2E)^{\frac{1}{2}}\tan(p/2)}{\mu + k^2 J}\right), \tag{2.15.43}$$

where $p = k(t - t_0)$. It is rather interesting that in this case θ increases linearly with time. It should also be noted that the function $\rho(t)$ described above in (2.14.8) can be obtained explicitly in these two cases using $\rho(t) = 2S(t)/\bar{L}$ from (2.14.10). Since the orbit is elliptical and the area swept out in the corresponding Kepler problem is constant, it seems intuitive that the time transformation required to convert (2.15.32) to the equivalent Kepler equation of motion should involve the area swept out in the original elliptical orbit.

2.16 The Connection with Central Force Problems and the Conserved Hamilton and Laplace–Runge–Lenz Vector Analogues and a Conserved Jauch–Hill–Fradkin Tensor Analogue for General Oscillator Orbits

Consider the equation of motion

$$\ddot{\boldsymbol{r}} + f\dot{\boldsymbol{r}} + g\boldsymbol{r} = \boldsymbol{0}. \tag{2.16.1}$$

The vector product of $\boldsymbol{r}$ with (2.16.1) gives the scalar equation

$$f = -\frac{\dot{L}}{L}. \tag{2.16.2}$$

Equation (2.16.1) can be rewritten in terms of the plane polar unit vectors

$$\hat{\boldsymbol{r}}: \quad \ddot{r} - r\dot{\theta}^2 + f\dot{r} + gr = 0 \tag{2.16.3}$$

$$\hat{\boldsymbol{\theta}}: \quad r\ddot{\theta} + 2\dot{r}\dot{\theta} + fr\dot{\theta} = 0. \tag{2.16.4}$$

Using the transformation

$$u(\theta) = \frac{1}{r(\theta)}, \qquad L = r^2\dot{\theta}, \tag{2.16.5}$$

equation (2.16.3) becomes

$$-L^2u^2\frac{\mathrm{d}^2u}{\mathrm{d}\theta^2} - \dot{L}\frac{\mathrm{d}u}{\mathrm{d}\theta} - L^2u^3 - fL\frac{\mathrm{d}u}{\mathrm{d}\theta} + \frac{g}{u} = 0. \tag{2.16.6}$$

Substituting (2.16.2) for f and simplifying, gives the differential equation of the orbit

$$\frac{\mathrm{d}^2u}{\mathrm{d}\theta^2} + u - \frac{g}{L^2u^3} = 0. \tag{2.16.7}$$

The general central force problem

$$\ddot{\boldsymbol{r}} + \bar{g}\boldsymbol{r} = \boldsymbol{0} \tag{2.16.8}$$

has the corresponding differential equation for the orbit

$$\frac{\mathrm{d}^2u}{\mathrm{d}\theta^2} + u - \frac{\bar{g}}{\bar{L}^2u^3} = 0 \tag{2.16.9}$$

which is identical to (2.16.7) except that $\bar{L}$ is constant. It is thus possible to construct equations of motion with standard central force orbits by making certain choices of g. As an example we consider the equation of motion for the three-dimensional isotropic harmonic oscillator. In this case $\bar{g}/\bar{L}^2$ is constant.

Equating (2.16.9) with (2.16.7) gives

$$g = \frac{\bar{g}L^2}{\bar{L}^2}, \tag{2.16.10}$$

where, of course, L is no longer constant. Differentiating both sides of (2.16.10) with respect to time gives

$$\dot{g} = \frac{2L\dot{L}\bar{g}}{\bar{L}^2}. \tag{2.16.11}$$

Dividing (2.16.11) by twice (2.16.10) gives

$$\frac{\dot{g}}{2g} = \frac{\dot{L}}{L} = -f. \tag{2.16.12}$$

Hence, the equation of motion

$$\ddot{\boldsymbol{r}} - \frac{\dot{g}}{2g}\dot{\boldsymbol{r}} + g\boldsymbol{r} = \boldsymbol{0} \tag{2.16.13}$$

has the orbit equation of the three–dimensional isotropic harmonic oscillator for suitable choices of g.

As was done in §2.14 and using the transformation $t \to \rho(t)$, (2.16.13) becomes

$$\dot{\rho}^2\frac{\mathrm{d}^2\boldsymbol{r}}{\mathrm{d}\rho^2} + \left(\ddot{\rho} - \frac{\dot{g}}{2g}\dot{\rho}\right)\frac{\mathrm{d}\boldsymbol{r}}{\mathrm{d}\rho} + g\boldsymbol{r} = \boldsymbol{0}. \tag{2.16.14}$$

If we set the middle term of (2.16.14) to zero we obtain

$$\frac{\mathrm{d}^2\boldsymbol{r}}{\mathrm{d}\rho^2} + \frac{g}{\dot{\rho}^2}\boldsymbol{r} = \boldsymbol{0} \tag{2.16.15}$$

with

$$\dot{\rho}^2 = \frac{g}{\mu} = \frac{L^2}{\bar{L}^2} = \frac{4}{\bar{L}^2}\dot{S}^2, \tag{2.16.16}$$

where μ is an arbitrary constant, $\dot{S} = L/2$ is the areal velocity of (2.16.13) and $\bar{L}$ is the angular momentum of the three–dimensional isotropic harmonic oscillator (2.16.17). As expected (2.16.13) has been transformed into the equivalent three–dimensional isotropic harmonic oscillator

$$\frac{\mathrm{d}^2\boldsymbol{r}}{\mathrm{d}\rho^2} + \mu\boldsymbol{r} = \boldsymbol{0} \tag{2.16.17}$$

using the area swept out in the orbit described by (2.16.13). Equation (2.16.16) is consistent with that obtained by equating the area $S(t)$ swept out in the orbit described by (2.16.13) at time t with the same area swept out in the three–dimensional isotropic harmonic oscillator at time $\rho(t)$ as given by the analogue of Kepler's second law, *i.e.* $\rho(t) = 2S(t)/\bar{L}$.

The conserved vectors for (2.16.13) are readily constructed using Fradkin's method (suitably modified for this non–conservative system, see §§1.6 and 1.7) and are identical in structure to those of the three–dimensional isotropic harmonic oscillator. However, L is no longer conserved, *i.e.*

$$\boldsymbol{J} = \pm J \frac{1}{e\left(r^2 - b^2\right)^{\frac{1}{2}}}\left(\boldsymbol{r} - \frac{b^2}{L^2}\dot{\boldsymbol{r}} \times \boldsymbol{L}\right) \tag{2.16.18}$$

$$\begin{aligned} \boldsymbol{K} &= \hat{\boldsymbol{L}} \times \boldsymbol{J} \\ &= \pm J \frac{\left(1 - e^2\right)^{\frac{1}{2}}}{e\left(a^2 - r^2\right)^{\frac{1}{2}}}\left(\frac{a^2}{L^2}\dot{\boldsymbol{r}} \times \boldsymbol{L} - \boldsymbol{r}\right), \end{aligned} \tag{2.16.19}$$

where

$$J = \left(E^2 - k^2\right)^{\frac{1}{2}}. \tag{2.16.20}$$

The same restrictions apply as for the three–dimensional isotropic harmonic oscillator regarding the discontinuities and the choice of sign.

As was shown before in §2.14 for the generalised Kepler problem, the conserved vectors $\boldsymbol{K}$ (2.16.19) and $\boldsymbol{J}$ (2.16.18) associated with (2.16.13) are also form invariant under the transformation $t \to \rho(t)$, since the term $\dot{\boldsymbol{r}} \times \boldsymbol{L}/L^2 = \boldsymbol{r}' \times \boldsymbol{L}_t/{L_t}^2$ where the prime denotes differentiation with respect to ρ and $L_t = r^2\theta'$.

The vector product of $\boldsymbol{r}$ with (2.16.13) gives

$$\dot{\boldsymbol{L}} - \frac{\dot{g}}{2g}\boldsymbol{L} = \boldsymbol{0} \tag{2.16.21}$$

from which it follows that

$$L = kg^{\frac{1}{2}} \tag{2.16.22}$$

or alternatively that

$$k = \frac{r^2\dot{\theta}}{g^{\frac{1}{2}}} \tag{2.16.23}$$

is a constant of the motion and $\boldsymbol{k} = k\hat{\boldsymbol{L}}$ can be regarded as a generalised angular momentum. The analogue of the Jauch–Hill–Fradkin tensor is easily obtained from the cartesian form of (2.16.13) (or alternatively using Fradkin's method suitably modified for this non–conservative system) namely

$$\ddot{x}_i - \frac{\dot{g}}{2g}\dot{x}_i + gx_i = 0, \quad i = 1, 2, 3. \tag{2.16.24}$$

Making the combination $(2.16.24)_i\ \dot{x}_j + \dot{x}_i(2.16.24)_j$ gives

$$\ddot{x}_i\dot{x}_j + \dot{x}_i\ddot{x}_j - \frac{\dot{g}}{g}\dot{x}_i\dot{x}_j + g(x_i\dot{x}_j + \dot{x}_i x_j) = 0, \tag{2.16.25}$$

which on division by g can be integrated to give the conserved tensor

$$A_{ij} = \frac{\dot{x}_i\dot{x}_j}{g} + x_i x_j. \tag{2.16.26}$$

The energylike integral is

$$\begin{aligned} E &= \frac{1}{2}\operatorname{tr}(A_{ij}) \\ &= \frac{1}{2}\frac{\dot{\boldsymbol{r}}\cdot\dot{\boldsymbol{r}}}{g} + \frac{1}{2}r^2, \end{aligned} \tag{2.16.27}$$

which can also be obtained by taking the scalar product of $g^{-1}\dot{\boldsymbol{r}}$ with (2.16.13) and integrating.

The equation of the velocity hodograph is given by

$$\dot{\boldsymbol{r}}^T(2EI - A)\dot{\boldsymbol{r}} = L^2. \tag{2.16.28}$$

Since $\hat{\boldsymbol{L}}$ is constant, the motion is planar and conveniently we assign x_3 to be the variable in the direction of $\hat{\boldsymbol{L}}$. The 2x2 matrix in (2.16.28) has two distinct eigenvalues that determine the velocity hodograph in the plane, which are

$$\lambda = E \mp \left(E^2 - k^2\right)^{\frac{1}{2}} \tag{2.16.29}$$

and, if we rotate the velocity hodograph (2.16.28) so that the cartesian unit vectors $\boldsymbol{i}$ and $\boldsymbol{j}$ become the principal axes,

$$\frac{\dot{x}^2}{\left(E + (E^2 - k^2)^{\frac{1}{2}}\right)} + \frac{\dot{y}^2}{\left(E - (E^2 - k^2)^{\frac{1}{2}}\right)} = \frac{L^2}{k^2}. \tag{2.16.30}$$

Equation (2.16.30) can be expressed more compactly as

$$\frac{\dot{x}^2}{a^2} + \frac{\dot{y}^2}{b^2} = \frac{L^2}{k^2} \tag{2.16.31}$$

which is an ellipse only when L is constant.

The equation of the orbit is given by

$$\boldsymbol{r}^T[2EI - A]\boldsymbol{r} = k^2 \tag{2.16.32}$$

and, after a suitable rotation so that the cartesian unit vectors $\boldsymbol{i}$ and $\boldsymbol{j}$ become the principal axes,

$$\frac{x^2}{a^2} + \frac{y^2}{b^2} = 1, \tag{2.16.33}$$

which is the equation of an ellipse. Expressing (2.16.33) in terms of plane polar coordinates where the angle between $\boldsymbol{J}$ and $\boldsymbol{i}$ is θ_0 gives

$$r^2 = \frac{k^2}{E - (E^2 - k^2)^{\frac{1}{2}} \cos 2(\theta - \theta_0)} \tag{2.16.34}$$

which has the same structure as the orbit equation for the three–dimensional isotropic harmonic oscillator (see (1.7.16)). The equation for the acceleration hodograph is given by

$$\ddot{\boldsymbol{r}}^T(2EI - A)\ddot{\boldsymbol{r}} = \frac{L^4}{k^2} + \dot{L}^2 \tag{2.16.35}$$

which can be rotated onto principal axes to give

$$\left(\frac{\ddot{x}}{a}\right)^2 + \left(\frac{\ddot{y}}{b}\right)^2 = \frac{L^4}{k^4} + \frac{\dot{L}^2}{k^2}, \tag{2.16.36}$$

which is only recognisable as an ellipse when L is constant or $L^4/k^4 + \dot{L}^2/k^2$ is constant. The radial motion in time is found by rewriting the energy integral in terms of $\dot{r}$ using (2.16.22) to replace L^2 and making the substitution $q = r^2$ which results in

$$\dot{q} = 2g^{\frac{1}{2}}\left(-q^2 + 2Eq - k^2\right)^{\frac{1}{2}}, \tag{2.16.37}$$

which can be solved provided g can be expressed entirely as a function of r. The angular motion in time is obtained by solving

$$\dot{\theta} = \frac{g^{\frac{1}{2}}}{k}\left(E - (E - k^2\cos 2\theta)^{\frac{1}{2}}\right) \tag{2.16.38}$$

provided g can be expressed entirely as a function of θ. The areal velocity is found by solving

$$\dot{A} = \frac{1}{2}L(t) = \frac{1}{2}kg^{\frac{1}{2}} \tag{2.16.39}$$

provided g can be expressed in terms of time only, possibly through inversion of either (2.16.37) or (2.16.38).

2.17 The Geometry of the Generalised Harmonic Oscillator

In general an expression for the area swept out by the radius vector in time cannot be found due to global inversion problems. The periodic time expressions can be found rather elegantly for the power law central force type potentials $g = \mu r^{\alpha}$. The contents of §2.17 are also described in Gorringe and Leach [41]. Equation (2.16.13) becomes

$$\ddot{\boldsymbol{r}} - \frac{1}{2}\alpha\frac{\dot{r}}{r}\dot{\boldsymbol{r}} + \mu r^{\alpha}\boldsymbol{r} = \boldsymbol{0}. \tag{2.17.1}$$

For $\alpha = 0$, (2.17.1) reduces to the three–dimensional isotropic harmonic oscillator.

The vector product of $\boldsymbol{r}$ with (2.17.1) gives

$$\dot{\boldsymbol{L}} - \frac{1}{2}\alpha\frac{\dot{r}}{r}\boldsymbol{L} = \boldsymbol{0}. \tag{2.17.2}$$

As before it follows that $\hat{\boldsymbol{L}}$ is constant and

$$L = kr^{\frac{\alpha}{2}} \tag{2.17.3}$$

for some constant k. Using the expression $L = r^2\dot{\theta}$, (2.17.3) can be rearranged to give

$$k = r^{\frac{(4-\alpha)}{2}}\dot{\theta} \tag{2.17.4}$$

and k can be viewed as a generalised angular momentum $\boldsymbol{k} = k\hat{\boldsymbol{L}}$.

The Hamilton vector and Laplace–Runge–Lenz vector analogues are given by equations (2.16.19) and (2.16.18) using Fradkin's method (suitably modified for this non–conservative system) where again L is not conserved and the same restrictions apply regarding the discontinuities and the choice of sign as for the three–dimensional isotropic harmonic oscillator (see §1.7). The analogue of the Jauch–Hill–Fradkin tensor is easily obtained from the cartesian form of (2.17.1) (or alternatively using Fradkin's method suitably modified for this non–conservative system) namely

$$\ddot{x}_i - \frac{1}{2}\alpha\frac{\dot{r}}{r}\dot{x}_i + \mu r^{\alpha}x_i = 0, \quad i = 1,2,3. \tag{2.17.5}$$

Making the combination $(2.17.5)_i\ \dot{x}_j + \dot{x}_i(2.17.5)_j$ gives

$$\ddot{x}_i\dot{x}_j + \dot{x}_i\ddot{x}_j - \alpha\frac{\dot{r}}{r}\dot{x}_i\dot{x}_j + \mu r^{\alpha}(x_i\dot{x}_j + \dot{x}_i x_j) = 0. \tag{2.17.6}$$

Dividing (2.17.6) throughout by r^α gives the conserved tensor

$$A_{ij} = \frac{\dot{x}_i \dot{x}_j}{r^\alpha} + \mu x_i x_j. \tag{2.17.7}$$

The energylike integral is given by

$$\begin{aligned} E &= \frac{1}{2}\operatorname{tr}(A_{ij}) \\ &= \frac{1}{2}\frac{\dot{\boldsymbol{r}}\cdot\dot{\boldsymbol{r}}}{r^\alpha} + \frac{1}{2}\mu r^2, \end{aligned} \tag{2.17.8}$$

or can equivalently be found upon integration of the scalar product of $r^{-\alpha}\dot{\boldsymbol{r}}$ and (2.17.1).

The equation of the velocity hodograph is given by

$$\dot{\boldsymbol{r}}^T(2EI - A)\dot{\boldsymbol{r}} = \mu L^2. \tag{2.17.9}$$

Since $\hat{\boldsymbol{L}}$ is constant, the motion is planar and for convenience we assign x_3 to be the variable in the direction of $\hat{\boldsymbol{L}}$. The eigenvalues of the 2x2 matrix in (2.17.9), which determine the velocity hodograph in the plane, are

$$\lambda = E \mp \left(E^2 - \mu k^2\right)^{\frac{1}{2}} \tag{2.17.10}$$

and, if we rotate the velocity hodograph (2.17.9) so that the cartesian unit vectors $\boldsymbol{i}$ and $\boldsymbol{j}$ become the principal axes,

$$\frac{\dot{x}^2}{\left(E + (E^2 - \mu k^2)^{\frac{1}{2}}\right)/\mu} + \frac{\dot{y}^2}{\left(E - (E^2 - \mu k^2)^{\frac{1}{2}}\right)/\mu} = \frac{\mu L^2}{k^2} \tag{2.17.11}$$

which is more compactly written as

$$\frac{\dot{x}^2}{a^2} + \frac{\dot{y}^2}{b^2} = \frac{\mu L^2}{k^2}. \tag{2.17.12}$$

Equation (2.17.12) describes an ellipse only when L is constant.

The equation of the orbit is then given by

$$\boldsymbol{r}^T[2EI - A]\boldsymbol{r} = k^2. \tag{2.17.13}$$

If we also rotate the orbit (2.17.13) so that the cartesian unit vectors $\boldsymbol{i}$ and $\boldsymbol{j}$ become the principal axes,

$$\frac{x^2}{a^2} + \frac{y^2}{b^2} = 1, \tag{2.17.14}$$

which is of course an ellipse. Expressing (2.17.14) in terms of plane polar coordinates, where the angle between $\boldsymbol{J}$ and $\boldsymbol{i}$ is θ_0 gives

$$r^2 = \frac{k^2}{E - (E^2 - \mu k^2)^{\frac{1}{2}} \cos 2(\theta - \theta_0)}, \tag{2.17.15}$$

which has the same structure as the orbit equation for the three–dimensional isotropic harmonic oscillator (see (1.7.16)) except that L^2 is now replaced by k^2, the generalised angular momentum and λ^2 by μ. The equation for the acceleration hodograph is given by

$$\ddot{\boldsymbol{r}}^T(2EI - A)\ddot{\boldsymbol{r}} = \frac{\mu^2 L^4}{k^2} + \mu \dot{L}^2 \tag{2.17.16}$$

which can be rotated onto principal axes to give

$$\left(\frac{\ddot{x}}{a}\right)^2 + \left(\frac{\ddot{y}}{b}\right)^2 = \frac{\mu^2 L^4}{k^4} + \frac{\mu \dot{L}^2}{k^2} \tag{2.17.17}$$

which is again only an ellipse when L is constant or $\mu^2 L^4/k^4 + \mu \dot{L}^2/k^2$ is constant.

Figure 2.17.1 shows the elliptic oscillator orbit and the construction of the corresponding velocity hodograph for the generalised problem when $\alpha = -6$ and $E > 0$. Note that the elliptical velocity hodograph in the three–dimensional isotropic harmonic oscillator problem ($\alpha = 0$) is now distorted into a cigar–shaped curve. The origin still remains at the geometric centre of the velocity hodograph. Figure 2.17.2 shows the variation in the magnitude of the angular momentum vector along the orbit corresponding with Figure 2.17.1. Note that the angular momentum is largest where r is smallest and *vice versa*. This should be the case since $L = \frac{1}{2} k r^{\frac{\alpha}{2}}$. Figure 2.17.3 geometrically demonstrates the construction of $\boldsymbol{L}$ corresponding with Figures 2.17.1 and 2.17.2. The shaded parallelograms represent the magnitude of $\boldsymbol{L} = \boldsymbol{r} \times \dot{\boldsymbol{r}}$.

Figure 2.17.4 shows both the displacements and corresponding velocities at regular time intervals for the elliptical case $\alpha = -6$ and $E > 0$. Kepler's second law is now invalid as the area enclosed between the orbit and any two vectors drawn from the origin to two consecutive solid round time markers on the orbit is clearly not constant for every pair of solid round time markers over the entire length of the orbit. It should be obvious that the initial phase difference between the displacement and velocity vectors is $\pi/2$ radians as the displacement lies along the $+x-$axis at $t = 0$ while the velocity is purely along the $+\dot{y}-$axis. The phase difference in general between the displacement and velocity vectors is not constant since $\boldsymbol{r} \cdot \dot{\boldsymbol{r}} = r\dot{r}$ which is nonzero except when $\dot{r} = 0$, *i.e.* at the extremities of the motion. This is also evident by comparing the angle between the corresponding displacement and velocity vectors for a range of time intervals using the solid round time markers on the

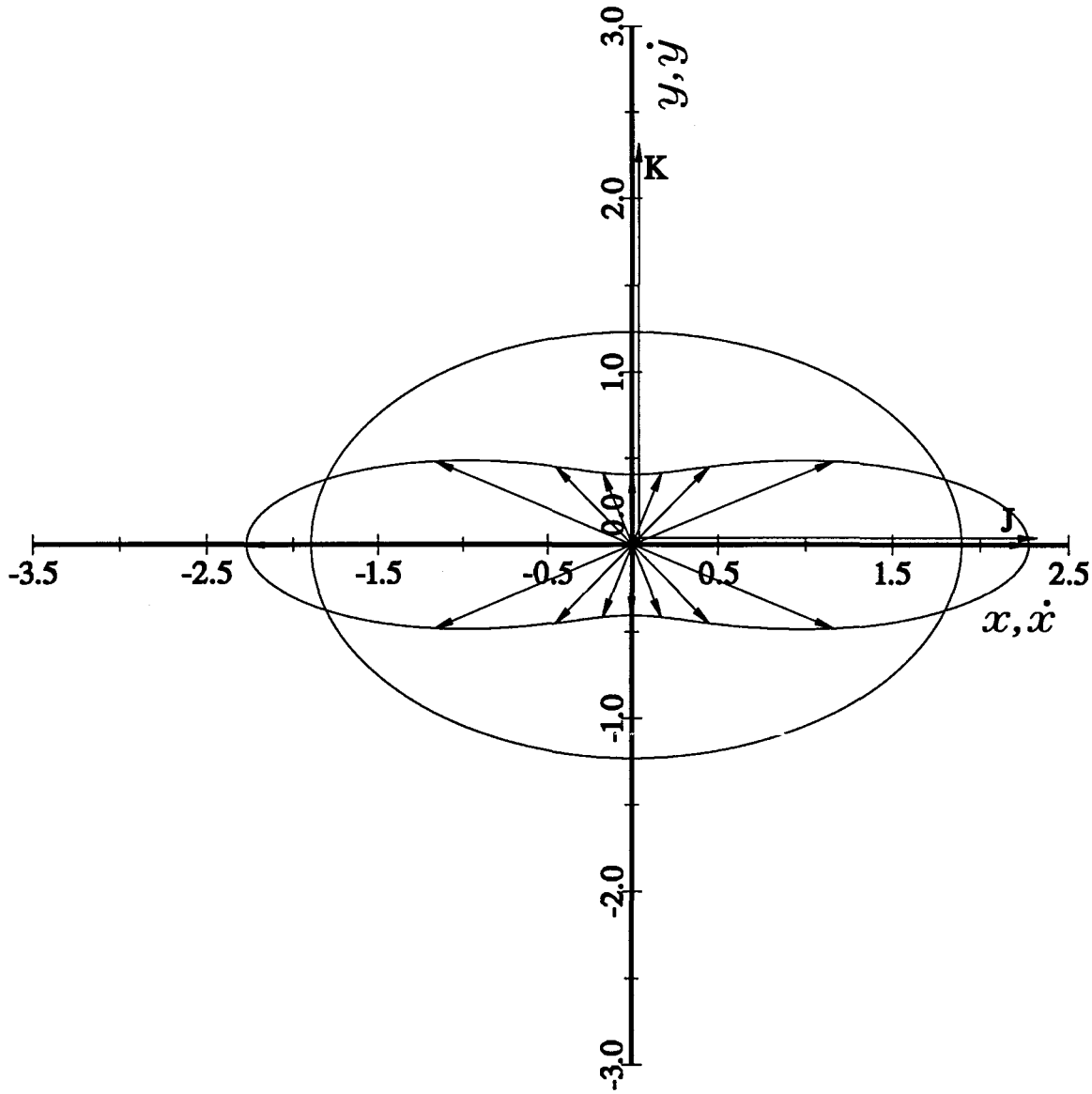


Figure 2.17.1. The elliptical oscillator orbit and the construction of the corresponding velocity hodograph for the generalised oscillator problem with a selection of velocity vectors drawn from the origin on the same set of axes as the displacement. The constants have the values $\alpha = -6$, $\mu = 5$, $a = 1.893\dot{9}$, $b = 1.2309$, $k = 5.2129$ and $K = J = 2.3164$. The origin lies inside the velocity hodograph. The axes have been kept the same as those in the generalised Kepler plots for purposes of comparison. Note that $\boldsymbol{K}$ is discontinuous when $\theta = 0$ or π and $\boldsymbol{J}$ is discontinuous when $\theta = \pi/2$ or $3\pi/2$.

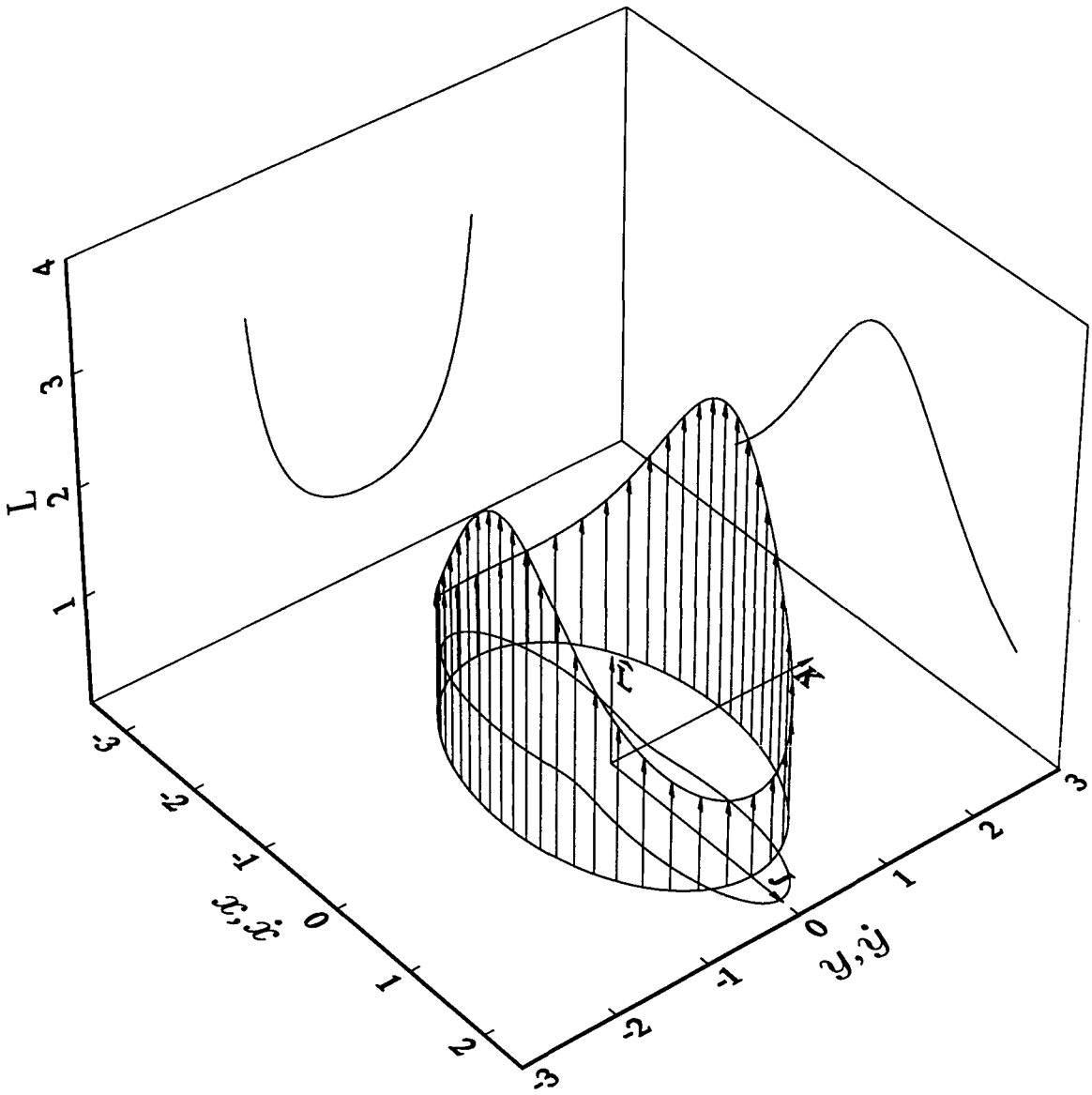


Figure 2.17.2. The variation in the magnitude of the angular momentum vector along the orbit corresponding with Figure 2.17.1. The projections of the angular momentum curve onto planes parallel to the the xy, xL and yL planes are also shown. In this example the angular momentum is constant in direction but not in magnitude.

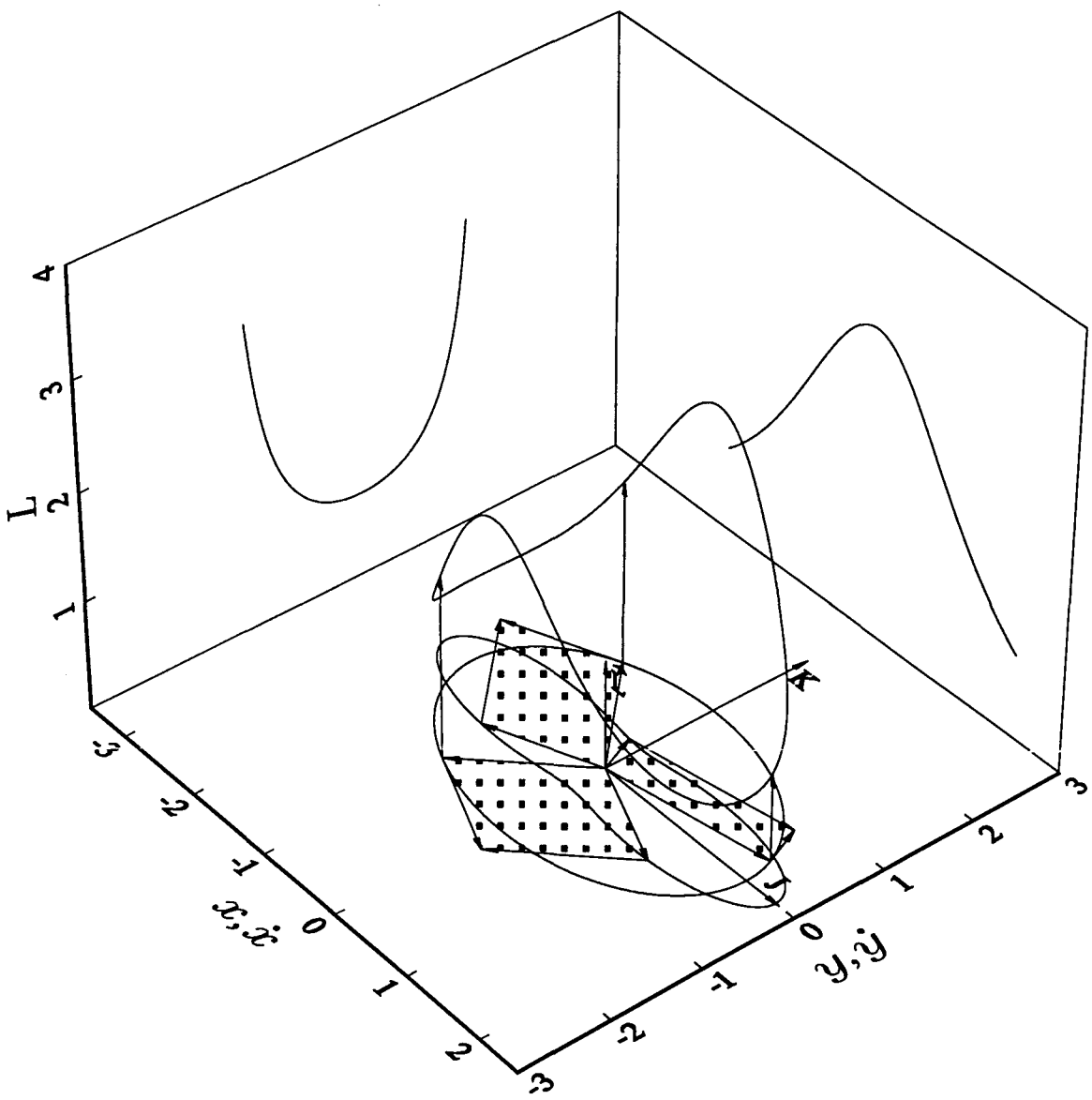


Figure 2.17.3. The elliptical oscillator orbit with its corresponding velocity hodograph associated with Figures 2.17.1 and 2.17.2 demonstrating the construction of $\boldsymbol{L}$. The height of the angular momentum vector placed at the vertex of the shaded parallelogram touching the orbit is equal in magnitude to the shaded area.

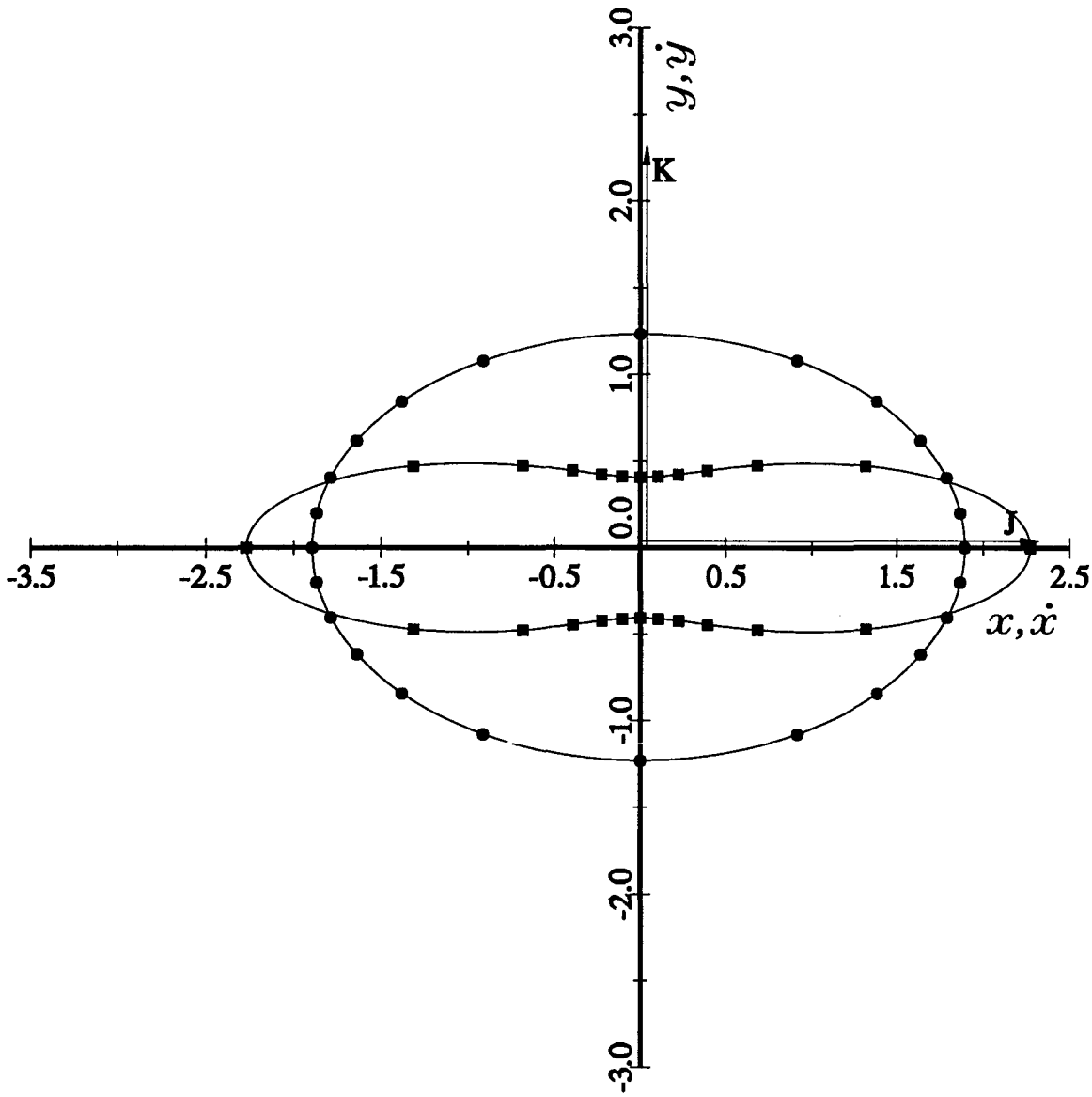


Figure 2.17.4. The elliptical oscillator orbit with its corresponding velocity hodograph. The circles (–●–●–●–) show the displacements of the particle at the time intervals $iT/24$, $i = 0, \ldots, 24$ and the squares (–■–■–■–) give the corresponding velocities. Kepler's second law is now invalid as equal areas are not swept out in equal times. The phase difference between the velocity and displacement vectors is not constant. The constants are chosen as for Figure 2.17.1.

orbit and the corresponding solid square time markers on the velocity hodograph and counting the number of round markers from the rightmost vertex of the ellipse in a counter–clockwise direction to the displacement of interest and then counting off the same number of square markers on the velocity hodograph starting from the square marker at the top of the velocity hodograph (since at $t = 0$ the velocity is purely along the $+\dot{y}-$axis) in a counter–clockwise direction to obtain the corresponding velocity or *vice versa*. Alternatively, if the velocity hodograph plot is rotated clockwise through $\pi/2$ radians about its geometric centre, it is apparent that the corresponding displacements, velocities and the origin are not collinear except at the vertices of the curves. In summary, the phase difference between $\boldsymbol{r}$ and $\dot{\boldsymbol{r}}$ is not constant in the generalised oscillator. Note also that the velocity increases slowly as the particle moves from the aphelion to the perihelion and *vice versa* (the increase is faster than for the three–dimensional isotropic harmonic oscillator problem).

Figure 2.17.5 shows the elliptic oscillator orbit and the construction of the corresponding velocity hodograph for the generalised problem when $\alpha = 3$ and $E > 0$. Note that the elliptical velocity hodograph in the three–dimensional isotropic harmonic oscillator problem ($\alpha = 0$) is now distorted into a dumbbell–shaped curve. The origin still remains at the geometric centre of the velocity hodograph. Figure 2.17.6 shows the variation in the magnitude of the angular momentum vector along the orbit corresponding with Figure 2.17.5. Note that the angular momentum is greatest where r is largest and *vice versa*. This should be the case since $L = \frac{1}{2}kr^{\frac{\alpha}{2}}$. Figure 2.17.7 geometrically demonstrates the construction of $\boldsymbol{L}$ corresponding with Figures 2.17.5 and 2.17.6. The shaded parallelograms represent the magnitude of $\boldsymbol{L} = \boldsymbol{r} \times \dot{\boldsymbol{r}}$.

Figure 2.17.8 shows both the displacements and corresponding velocities at regular time intervals for the elliptical case $\alpha = 3$ and $E > 0$. Kepler's second law is now invalid as the area enclosed between the orbit and any two vectors drawn from the origin to two consecutive solid round time markers on the orbit is clearly not constant for every pair of solid round time markers over the entire length of the orbit. It should be obvious that the initial phase difference between the displacement and velocity vectors is $\pi/2$ radians as the displacement lies along the $+x-$axis at $t = 0$ while the velocity is purely along the $+\dot{y}-$axis. The phase difference in general between the displacement and velocity vectors is not constant since $\boldsymbol{r} \cdot \dot{\boldsymbol{r}} = r\dot{r}$ which is nonzero except when $\dot{r} = 0$, *i.e.* at the extremities of the motion. This is also evident by comparing the angle between the corresponding displacement and velocity vectors for a range of time intervals using the solid round time markers on the

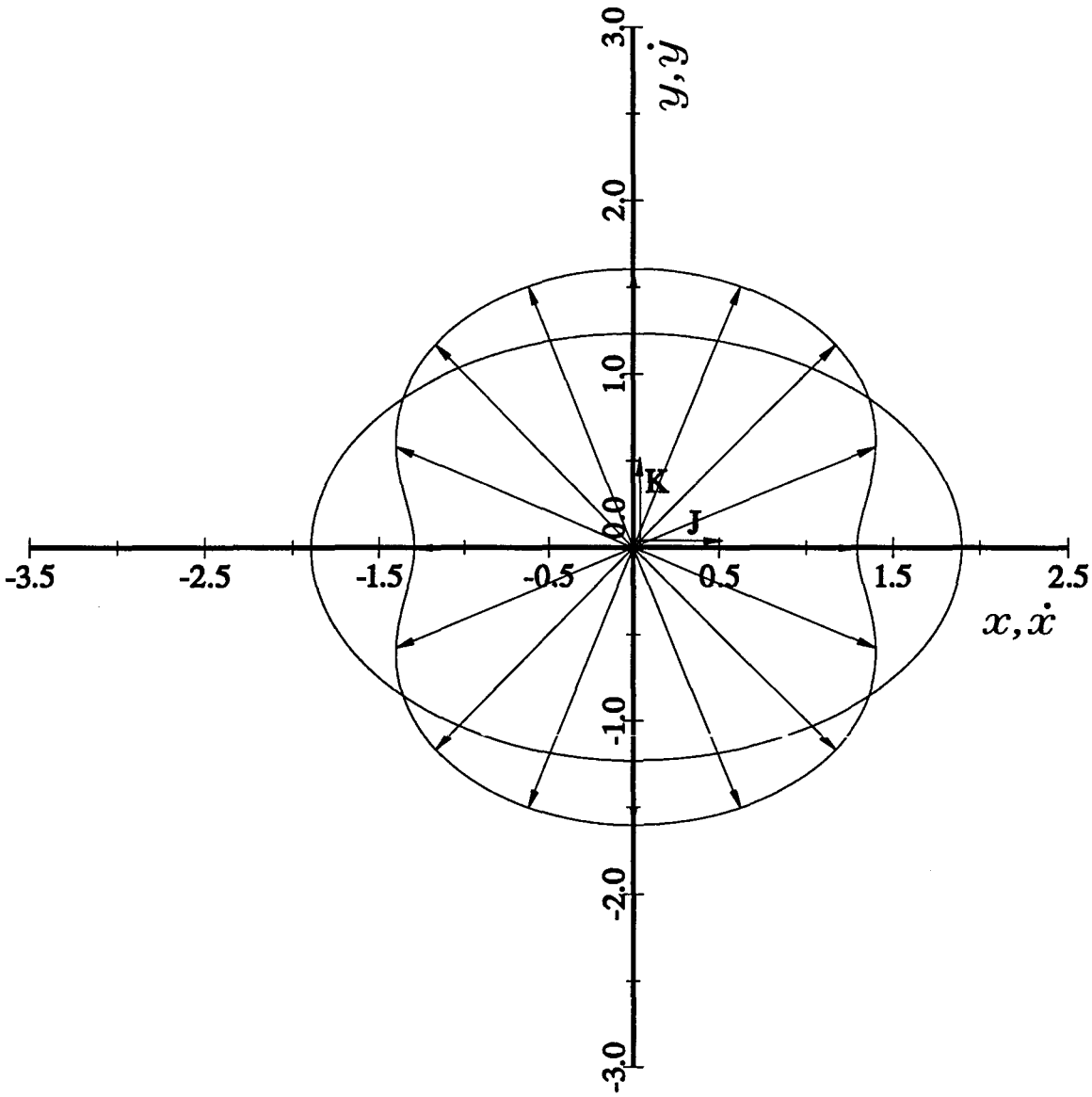


Figure 2.17.5. The elliptical oscillator orbit and the construction of the corresponding velocity hodograph for the generalised oscillator problem with a selection of velocity vectors drawn from the origin on the same set of axes as the displacement. The constants have the values $\alpha = 3$, $\mu = 0.25$, $a = 1.893\dot{9}$, $b = 1.2309$, $k = 1.1656$ and $K = J = 0.5180$. The origin lies inside the velocity hodograph. The axes have been kept the same as those in the generalised Kepler plots for purposes of comparison. Note that $\boldsymbol{K}$ is discontinuous when $\theta = 0$ or π and $\boldsymbol{J}$ is discontinuous when $\theta = \pi/2$ or $3\pi/2$.

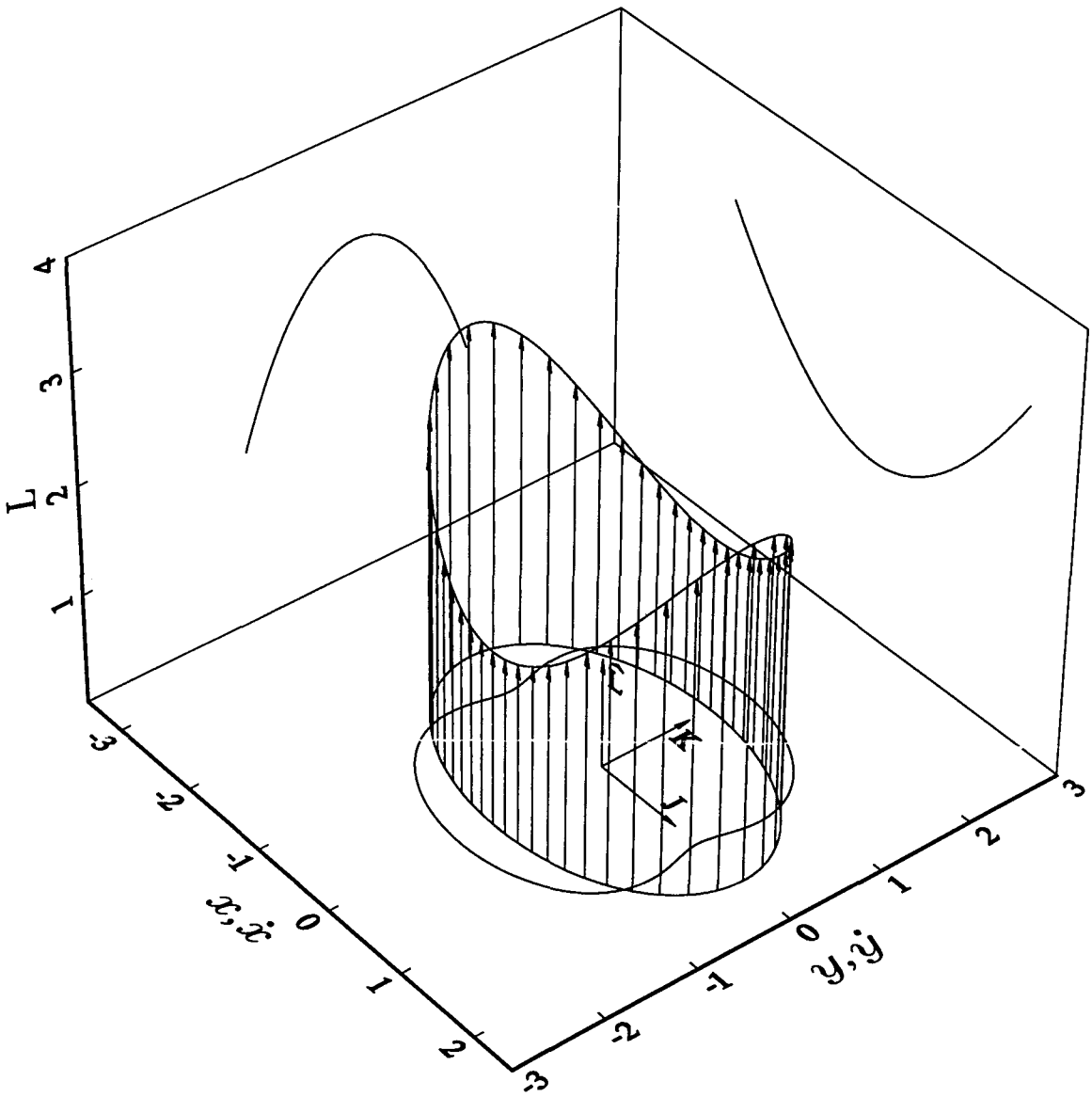


Figure 2.17.6. The variation in the magnitude of the angular momentum vector along the orbit corresponding with Figure 2.17.5. The projections of the angular momentum curve onto planes parallel to the xy, xL and yL planes are also shown. In this example the angular momentum is constant in direction but not in magnitude.

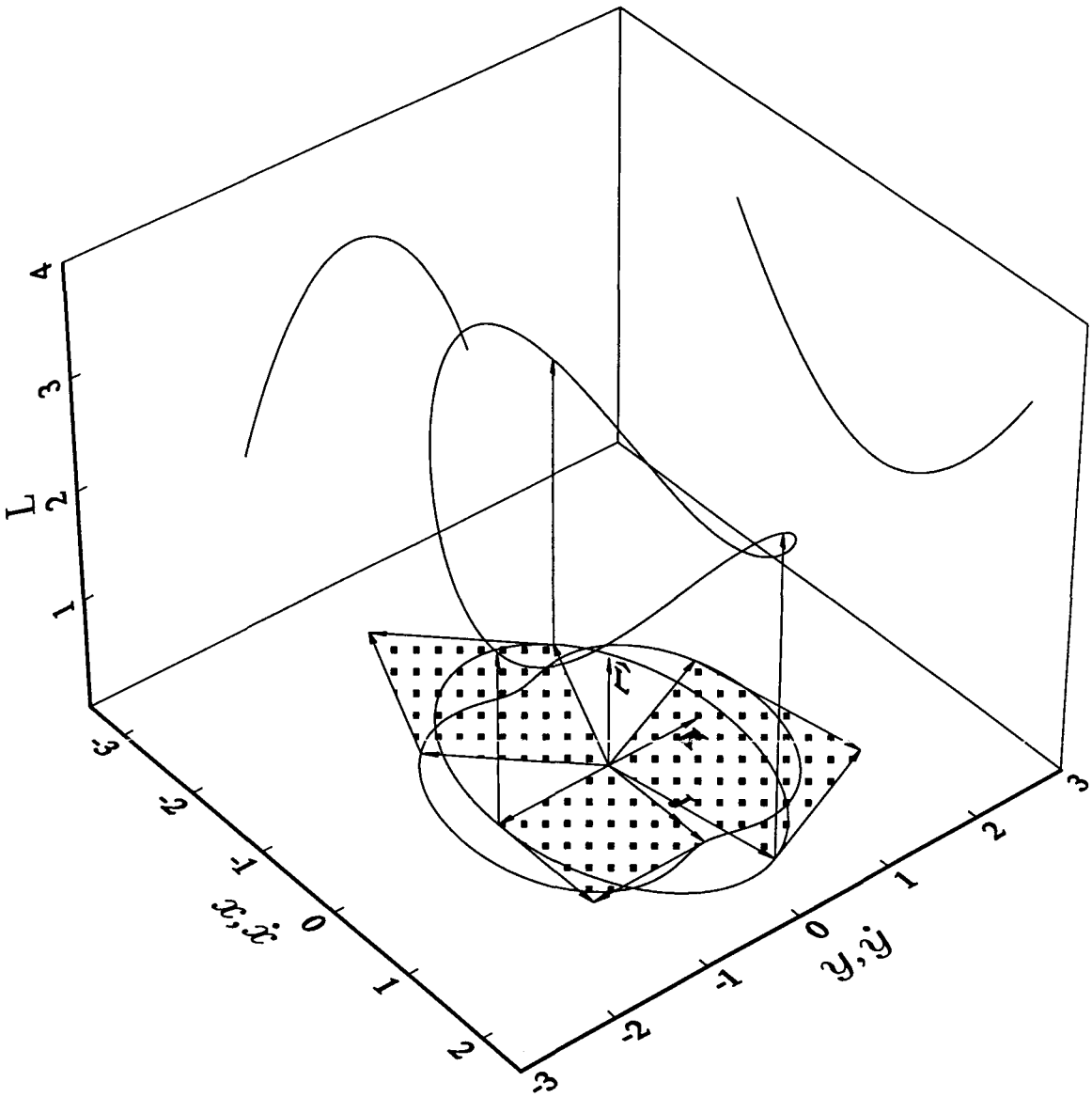


Figure 2.17.7. The elliptical oscillator orbit with its corresponding velocity hodograph associated with Figures 2.17.5 and 2.17.6 demonstrating the construction of $\boldsymbol{L}$. The height of the angular momentum vector placed at the vertex of the shaded parallelogram touching the orbit is equal in magnitude to the shaded area.

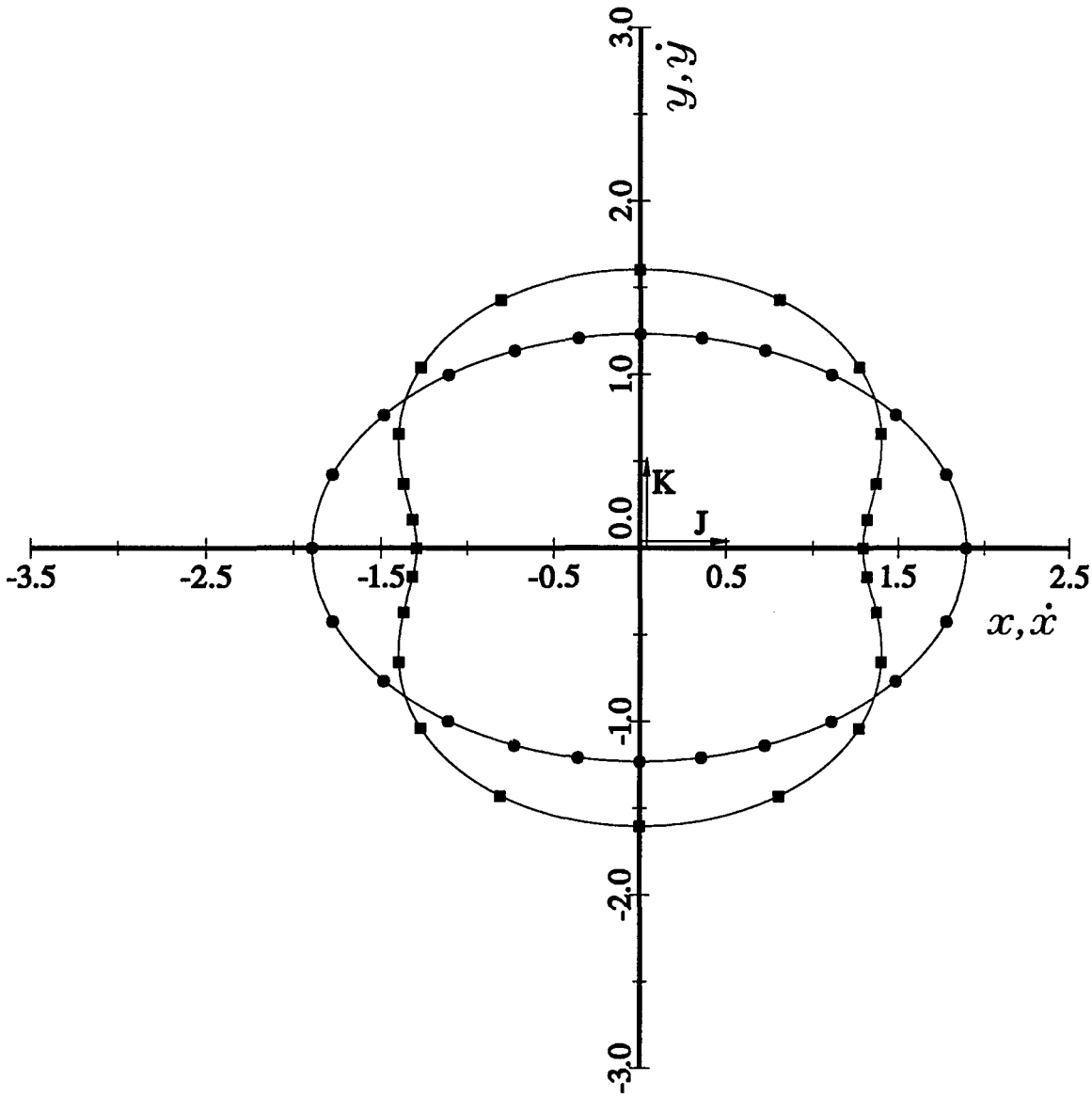


Figure 2.17.8. The elliptical oscillator orbit with its corresponding velocity hodograph. The circles (–•–•–•–) show the displacements of the particle at the time intervals $iT/24$, $i = 0, \ldots, 24$ and the squares (–■–■–■–) give the corresponding velocities. Kepler's second law is now invalid as equal areas are not swept out in equal times. The phase difference between the velocity and displacement vectors is not constant. The constants are chosen as for Figure 2.17.5.

orbit and the corresponding solid square time markers on the velocity hodograph and counting the number of round markers from the rightmost vertex of the ellipse in a counter–clockwise direction to the displacement of interest and then counting off the same number of square markers on the velocity hodograph starting from the square marker at the top of the velocity hodograph (since at $t = 0$ the velocity is purely along the $+\dot{y}-$axis) in a counter–clockwise direction to obtain the corresponding velocity or *vice versa*. Alternatively, if the velocity hodograph plot is rotated clockwise through $\pi/2$ radians about its geometric centre, it is apparent that the corresponding displacements, velocities and the origin are not collinear except at the vertices of the curves. In summary, the phase difference between $\boldsymbol{r}$ and $\dot{\boldsymbol{r}}$ is not constant in the generalised oscillator. Note also that the velocity decreases slowly as the particle moves from the aphelion to the perihelion and *vice versa* (the opposite behaviour to that of the three–dimensional isotropic harmonic oscillator problem).

The period T is found from (2.17.4) and (2.17.15) and is

$$T = \frac{4}{k}\int_0^{\frac{\pi}{2}} \left[\frac{k^2}{E - (E^2 - \mu k^2)^{\frac{1}{2}}\cos 2\theta}\right]^{\frac{4-\alpha}{4}} \mathrm{d}\theta. \tag{2.17.18}$$

Since

$$E - \left(E^2 - \mu k^2\right)^{\frac{1}{2}}\cos 2\theta = \left(\mu k^2\right)^{\frac{1}{2}}\left\{\frac{E}{(\mu k^2)^{\frac{1}{2}}} - \left[\left(\frac{E}{(\mu k^2)^{\frac{1}{2}}}\right)^2 - 1\right]^{\frac{1}{2}}\cos 2\theta\right\} \tag{2.17.19}$$

and using (2.15.13), equation (2.17.18) reduces to

$$T = 2\pi\mu^{\frac{\alpha-4}{8}}k^{-\frac{\alpha}{4}}P_{(\alpha-4)/4}(z), \tag{2.17.20}$$

where

$$z = \frac{E}{(\mu k^2)^{\frac{1}{2}}} \tag{2.17.21}$$

and the limits of the integral in (2.17.18) are changed from $[0, \pi/2]$ to $[0, \pi]$ through the substitution $\eta = 2\theta$. The argument of the Legendre function, z, can be shown to be a function of the eccentricity as follows. From (2.17.11) the semi–major and semi–minor axes are given by

$$a^2 = \left(E + \left(E^2 - \mu k^2\right)^{\frac{1}{2}}\right)/\mu \tag{2.17.22}$$

and

$$b^2 = \left(E - \left(E^2 - \mu k^2\right)^{\frac{1}{2}}\right)/\mu. \tag{2.17.23}$$

Combining (2.17.22) and (2.17.23) gives

$$a^2 + b^2 = \frac{2E}{\mu} \tag{2.17.24}$$

$$a^2 b^2 = \frac{k^2}{\mu}. \tag{2.17.25}$$

Using (2.17.24) and (2.17.25) and the property of an ellipse that $b^2 = a^2(1 - e^2)$, (2.17.21) becomes

$$\begin{aligned} z &= \left[\frac{1}{4}\left(\frac{2E}{\mu}\right)^2 \left(\frac{k^2}{\mu}\right)^{-1}\right]^{\frac{1}{2}} \\ &= \frac{2 - e^2}{2(1 - e^2)^{\frac{1}{2}}}. \end{aligned} \tag{2.17.26}$$

The terms involving μ and k in (2.17.20) can be written as

$$\mu^{-\frac{1}{2}} \left(\frac{k^2}{\mu}\right)^{-\frac{\alpha}{8}} = \mu^{-\frac{1}{2}} a^{-\frac{\alpha}{2}} (1 - e^2)^{-\frac{\alpha}{8}} \tag{2.17.27}$$

and, using (2.17.27), (2.17.20) can be rearranged into an expression for a generalised Kepler's third law as (with R in place of a)

$$TR^{\frac{\alpha}{2}} = \frac{2\pi}{\mu^{\frac{1}{2}}} (1 - e^2)^{-\frac{\alpha}{8}} P_{(\alpha-4)/4}\left[\frac{2 - e^2}{2(1 - e^2)^{\frac{1}{2}}}\right]. \tag{2.17.28}$$

Figures 2.17.9 and 2.17.10 show two families of geometric–centred oscillator ellipses with differing semi–major axis lengths for two different values of the eccentricity. Figure 2.17.11 shows the relationship between the periodic time of the orbit and the semi–major axis lengths for the families of ellipses shown in Figures 2.15.13 and 2.17.9. Figure 2.17.12 shows the relationship between the periodic time of the orbit and the semi–major axis lengths for the families of ellipses shown in Figures 2.15.14 and 2.17.10. Figure 2.17.13 shows the relationship between the periodic time of the orbit and the eccentricity for the elliptical oscillator orbits as given by equation (2.17.28). The Legendre functions were calculated from the first definite integral expression in (2.15.13) for $\nu < -1/2$ and the second expression for $\nu \geq -1/2$ using an adaptive numerical technique. The two different definite integral expressions were used in order to improve the convergence of the integration algorithm although they are both valid for any value of ν. In order to verify the results from the integration, the Legendre functions were also calculated in Maple [90] using $P_\nu(z) = F(-\nu, \nu + 1; 1; (1 - z)/2)$, where F is the hypergeometric function and the results were found to agree up until the tenth decimal place over the interval of

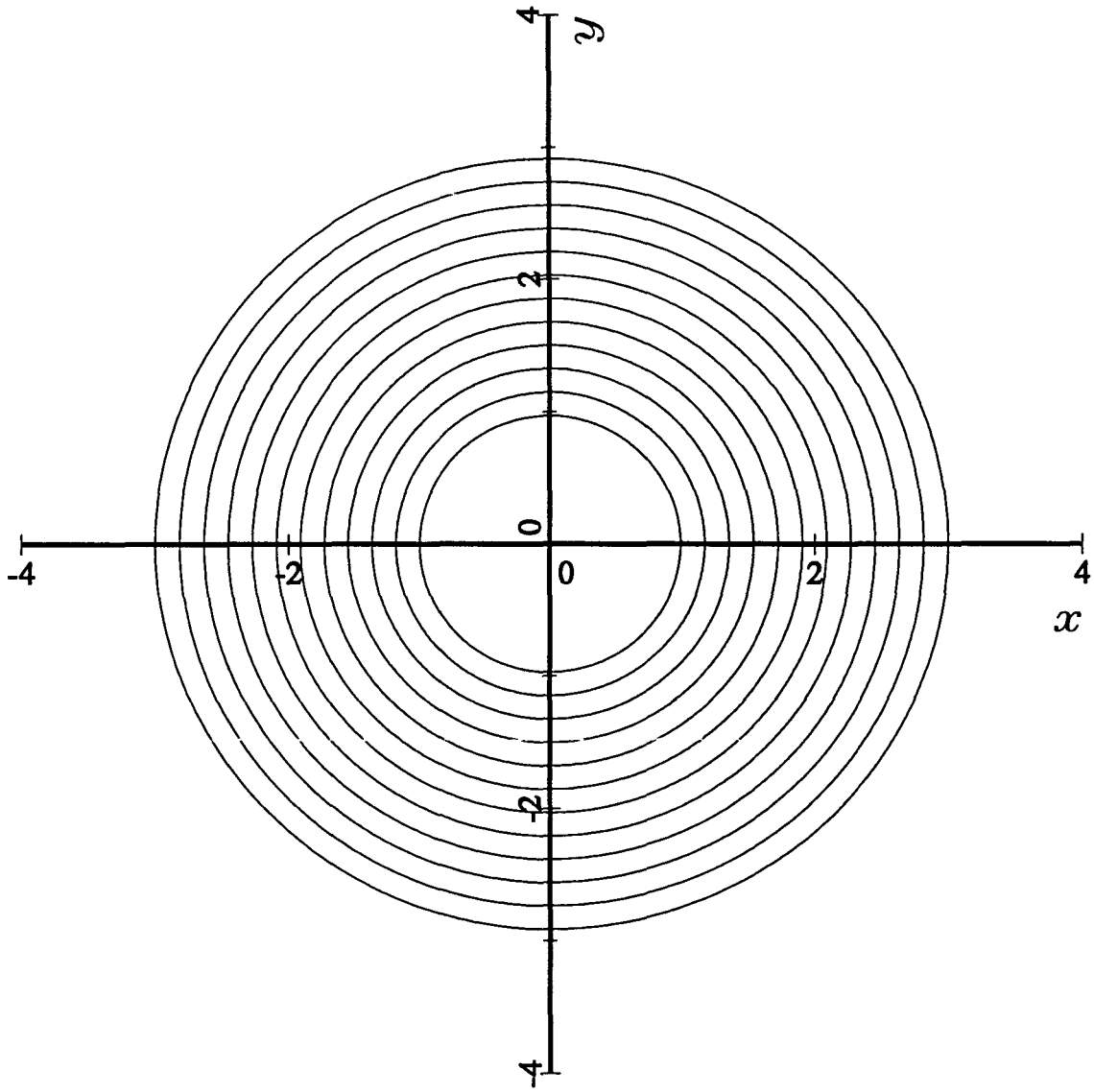


Figure 2.17.9. A family of oscillator orbital ellipses with differing semi–major axis lengths for a fixed value of the eccentricity. The constants have the values $e = 0.24$ and $a = 2i/11 + 1$, $i = 0, \ldots, 11$.

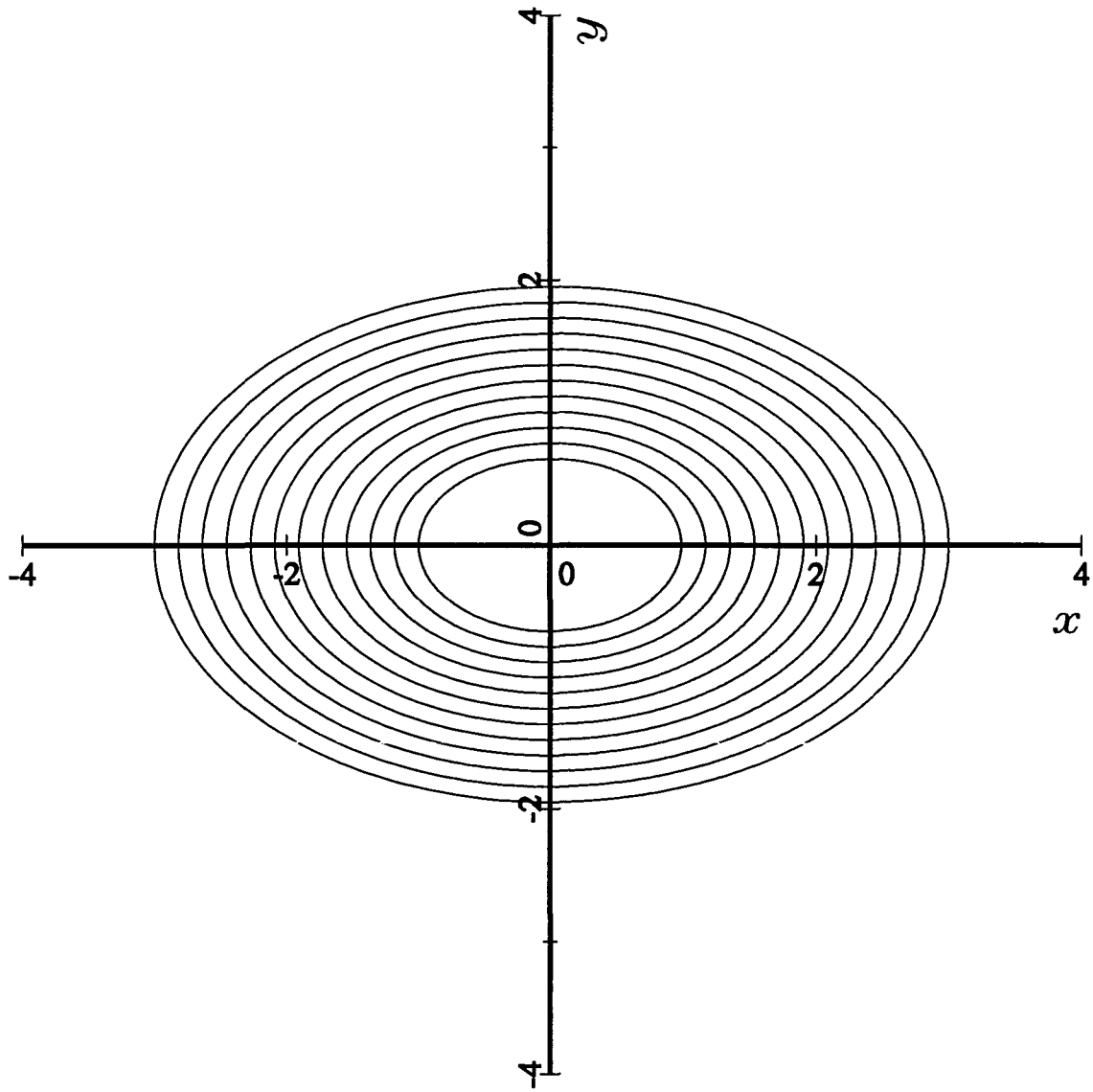


Figure 2.17.10. A family of oscillator orbital ellipses with differing semi–major axis lengths for a fixed value of the eccentricity. The constants have the values $e = 0.76$ and $a = 2i/11 + 1$, $i = 0, \ldots, 11$.

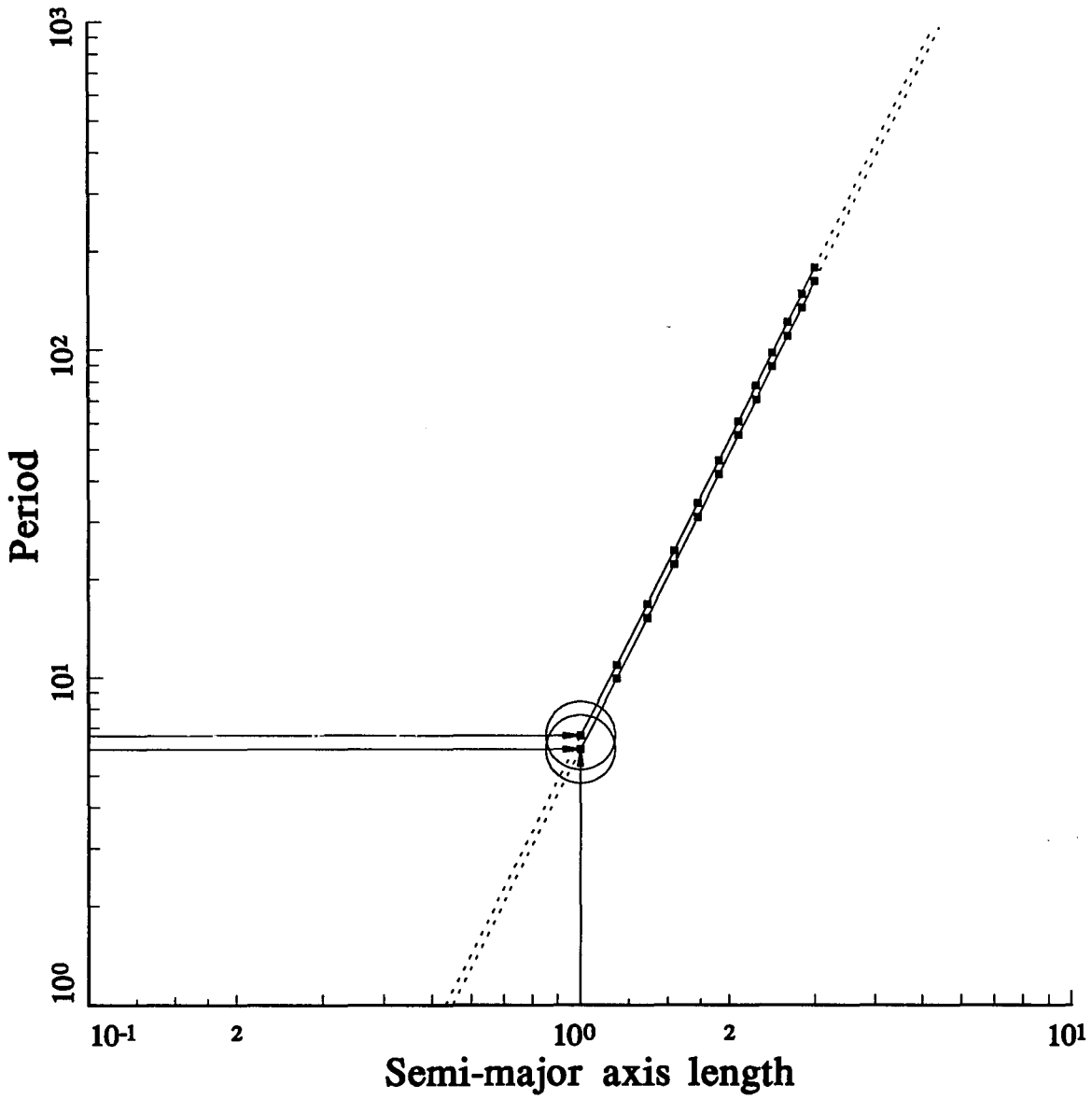


Figure 2.17.11. The periodic time versus the semi–major axis length for the families of orbital ellipses shown in Figures 2.15.13 and 2.17.9. In both cases the constants have the values $\alpha = -6$, $\mu = 1$, $e = 0.24$ and $a = 2i/11 + 1$, $i = 0, \ldots, 11$. The slope of both curves is 3 and the $y-$intercept is 6.6222 for the upper curve (Kepler case) and 6.0147 for the lower curve (oscillator case).

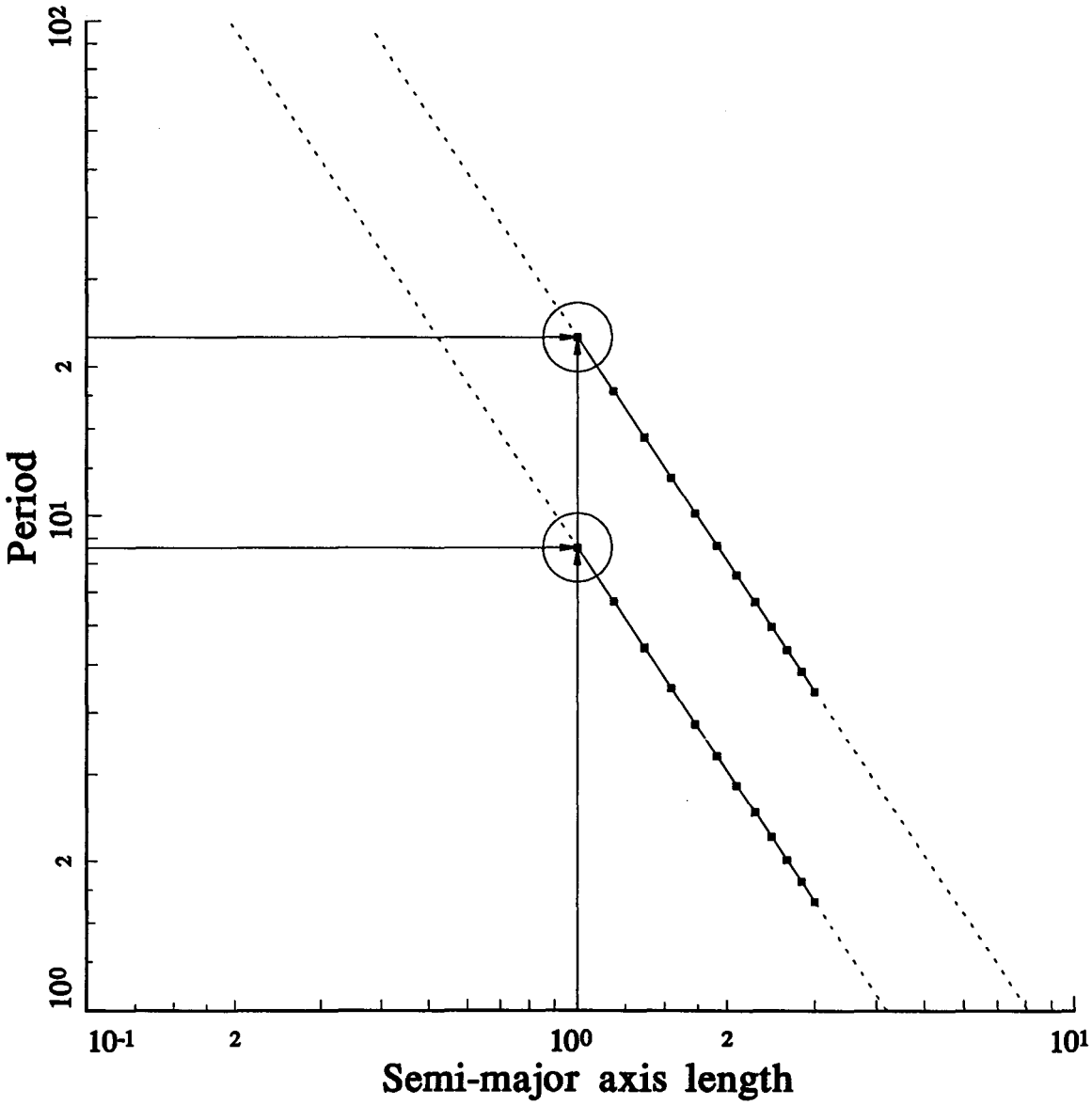


Figure 2.17.12. The periodic time versus the semi-major axis length for the families of orbital ellipses shown in Figures 2.15.14 and 2.17.10. In both cases the constants have the values $\alpha = 3$, $\mu = 1$, $e = 0.76$ and $a = 2i/11 + 1$, $i = 0, \ldots, 11$. The slope of both curves is -1.5 and the $y-$intercept is 22.8873 for the upper curve (Kepler case) and 8.6055 for the lower curve (oscillator case).

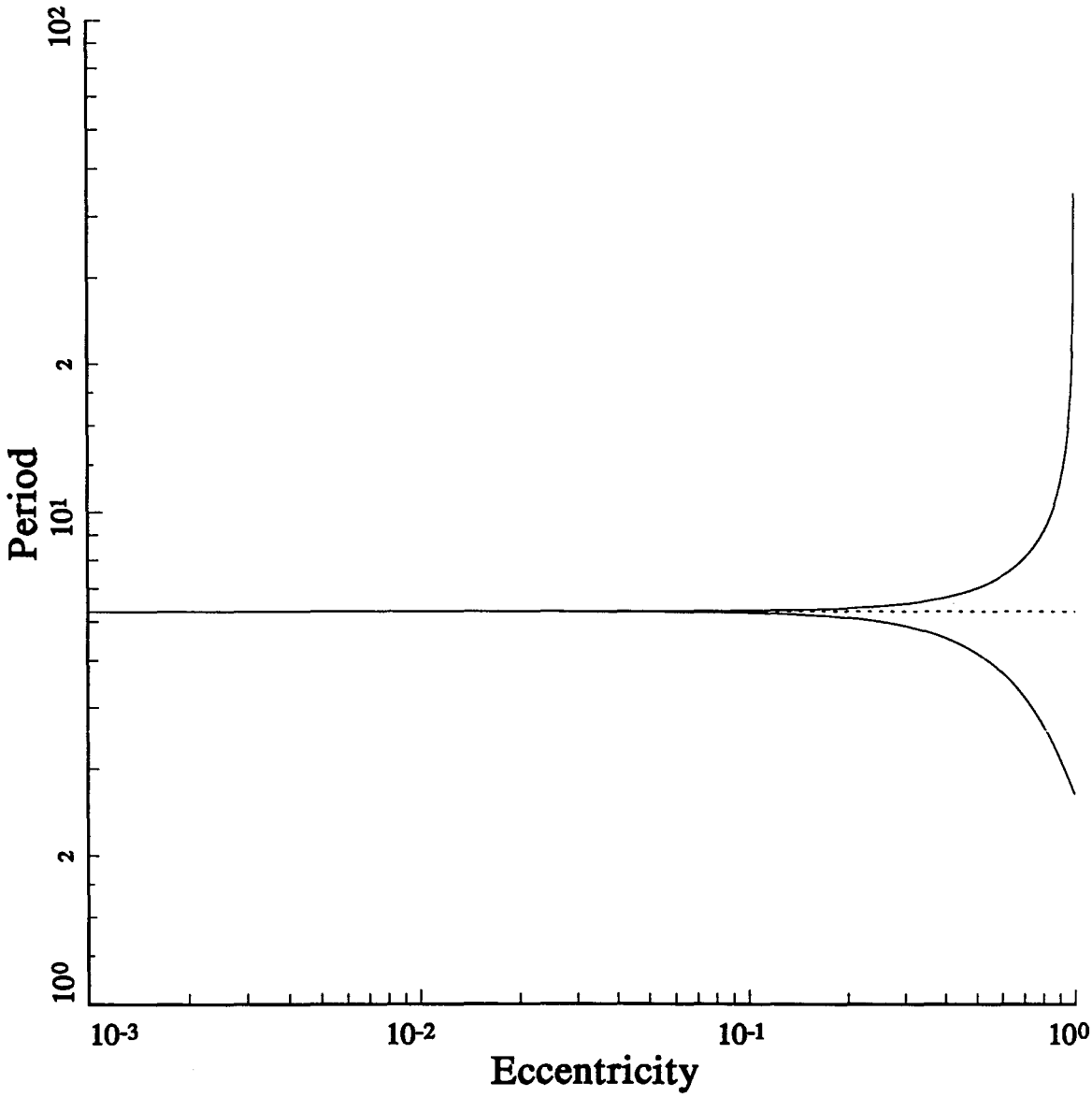


Figure 2.17.13. The periodic time versus the eccentricity for the generalised oscillator problem. The upper curve corresponds to the choice of constants $\alpha = 3$, $\mu = 1$, $a = 1$ whilst the lower curve corresponds to the choice $\alpha = -6$, $\mu = 1$ and $a = 1$. The dotted line indicates a constant period of 2π radians independent of the eccentricity, which is the case when $\alpha = 0$.

convergence of the hypergeometric series, *i.e.* $-1 < (1-z)/2 < 1$ or $-1 < z < 3$. The definite integral expressions (2.15.13) are preferable in this case since they can be used over the whole domain of interest, *i.e.* $z \geq 1$ (see Ince [55, §7·24 pp164*ff*]). For eccentricities equal to zero (which imply circular orbits) the period is given by equation (2.17.28) which reduces to $2\pi R^{-\frac{\alpha}{2}}/\mu^{\frac{1}{2}}$ since $P_\nu(1) = 1$, while for eccentricities equal to unity (which imply parabolic orbits) and $\alpha = 3$ the period tends to infinity while for $\alpha = -6$ the period tends to a limiting value (see Figure 2.17.13). The period was calculated for eccentricities between zero and one.

It is straightforward to show that (2.17.1) is also invariant under the similarity transformation

$$(t, \boldsymbol{r}) \rightarrow \left(\bar{t}, \bar{\boldsymbol{r}} : t = \gamma \bar{t}, \boldsymbol{r} = \gamma^{-\frac{2}{\alpha}} \bar{\boldsymbol{r}}\right) \tag{2.17.29}$$

or, in terms of an infinitesimal generator of a point transformation, (2.17.29) can be written equivalently as

$$G = t\frac{\partial}{\partial t} - \frac{2}{\alpha} r \frac{\partial}{\partial r}. \tag{2.17.30}$$

Using (2.17.29) the energy integral (2.17.8) can be shown to transform according to

$$E = \gamma^{-\frac{4}{\alpha}} \bar{E} \tag{2.17.31}$$

and using (2.17.4)

$$k = \gamma^{-\frac{4}{\alpha}} \bar{k}. \tag{2.17.32}$$

Also, (2.17.22) transforms as

$$a = \gamma^{-\frac{2}{\alpha}} \bar{a} \tag{2.17.33}$$

and, using (2.17.33), it is found that

$$T a^{\frac{\alpha}{2}} = \bar{T} \bar{a}^{\frac{\alpha}{2}} \tag{2.17.34}$$

is also invariant and hence that (2.17.28) is consistent with the transformation (2.17.29) and the symmetry (2.17.30) since (2.17.28) is invariant under the first extension of G, $G^{[1]}$.

Similarly z (2.17.21) is invariant under (2.17.29) and (2.17.30) and hence the eccentricity from (2.17.26). It is also worth noting that the energy for the generalised Kepler problem transforms as $E = \gamma^{\frac{2}{\alpha}} \bar{E}$ (2.15.22) whereas, for the generalised oscillator problem, it transforms as $E = \gamma^{-\frac{4}{\alpha}} \bar{E}$ yet the semi–major and semi–minor axes transform identically.

To summarise, the equation

$$\ddot{\boldsymbol{r}} - \frac{1}{2}\alpha\frac{\dot{r}}{r}\dot{\boldsymbol{r}} + \mu r^{\alpha}\boldsymbol{r} = \boldsymbol{0} \tag{2.17.35}$$

describes motion in the plane having the following properties.

(i) The orbit is an ellipse with the geometric centre at the origin (oscillator–like),

(ii) the areal velocity is $\frac{1}{2}kr^{\frac{\alpha}{2}}$ and

(iii) the period and semi–major axis are related by

$$TR^{\frac{\alpha}{2}} = \frac{2\pi}{\mu^{\frac{1}{2}}}\left(1-e^2\right)^{-\frac{\alpha}{8}} P_{\frac{(\alpha-4)}{4}}\left[\frac{2-e^2}{2(1-e^2)^{\frac{1}{2}}}\right]. \tag{2.17.36}$$

In the case of (2.17.35) with $\alpha = 0$, (2.17.36) gives the usual isochronism of the three–dimensional isotropic harmonic oscillator. The energy integral, E, (2.17.8) corresponding to (2.17.35) must always be positive (as is the case with the three–dimensional isotropic harmonic oscillator). In general the conservation of the areal velocity is lost as a result of the angular momentum not being constant. As with the previous case there exists a generalised angular momentum k which is related to the geometry of the orbit in the same way as the angular momentum was when it was conserved (*i.e.*, in the three–dimensional isotropic harmonic oscillator the k^2 in (2.17.15) is replaced by L^2 and μ by λ^2). Equation (2.17.36) is the generalised form of Kepler's law for the oscillator–type problem. Again the proportionality depends on the eccentricity of the orbit. For $\alpha = 0$ (2.17.30) becomes $r\dfrac{\partial}{\partial r}$, which maps solutions onto solutions of the same eccentricity. This is not reflected in the period semi–major axis relationship which is independent of the eccentricity for $\alpha = 0$. For general α (2.17.30) not only maps solutions onto solutions of the same eccentricity, but the period semi–major axis relationship is only constant for orbits of the same eccentricity. It does not appear that (2.17.36) possesses values of α (apart from zero) for which the constant of proportionality is independent of the eccentricity.

Rewriting the energy equation (2.17.8) in terms of $\dot{r}$ and using the substitution $q = r^2$ give

$$\dot{q} = 2q^{\frac{\alpha}{4}}\left(-\mu q^2 + 2Eq - k^2\right)^{\frac{1}{2}}. \tag{2.17.37}$$

Again referring to G&R [43, 2.26ff] it should be clear that (2.17.37) can be solved and subsequently inverted to give r as a function of time for the two cases $\alpha = 0, 4$. In these instances it is possible to obtain expressions for both θ and the area swept out in the ellipse as functions of time as described in §2.16.

1.) $\alpha = 0$

$$r = \frac{1}{\mu^{\frac{1}{2}}}\left(E + \left(E^2 - \mu k^2\right)^{\frac{1}{2}} \cos 2\mu^{\frac{1}{2}}(t - t_0)\right)^{\frac{1}{2}} \tag{2.17.38}$$

$$\theta = \arctan\left(\frac{k\mu^{\frac{1}{2}} \tan \mu^{\frac{1}{2}}(t - t_0)}{E + (E^2 - \mu k^2)^{\frac{1}{2}}}\right) + \theta_0. \tag{2.17.39}$$

The area swept out by the orbit is given by

$$S = \frac{1}{2}kt. \tag{2.17.40}$$

The above results agree (as they should) with the equivalent results for the three–dimensional isotropic harmonic oscillator (see (1.7.47) and (1.7.50)).

2.) $\alpha = 4$

$$r = \frac{k}{\left(E - (E^2 - \mu k^2)^{\frac{1}{2}} \cos 2k(t - t_0)\right)^{\frac{1}{2}}} \tag{2.17.41}$$

$$\theta = k(t - t_0) + \theta_0. \tag{2.17.42}$$

The area of the orbit is given by G&R [43, 2.554.3 and 2.2553.3 (case $a^2 > b^2$)]

$$S = \frac{k}{2\mu^{\frac{1}{2}}} \arctan\left(\frac{k\mu^{\frac{1}{2}} \tan k(t - t_0)}{E - (E^2 - \mu k^2)^{\frac{1}{2}}}\right). \tag{2.17.43}$$

As with equation (2.15.42) θ increases linearly with time. The function $\rho(t)$ described above in (2.16.14) can be obtained explicitly for these two cases using $\rho(t) = 2S(t)/\bar{L}$ from (2.16.16). Since the orbit is also elliptical in this case and the area swept out in the corresponding three–dimensional isotropic harmonic oscillator is constant, it is not really surprising that the time transformation required to convert (2.16.13) to the three–dimensional isotropic harmonic oscillator involves the area swept out in the original elliptic orbit.

By making the choice

$$\mu_{\text{osc}}{}^{\frac{1}{2}} = \mu_{\text{kep}}{}^{\frac{1}{2}} \left(1-e^2\right)^{-\alpha/8} P_{\frac{(\alpha-4)}{4}}\left[\frac{2-e^2}{2\left(1-e^2\right)^{\frac{1}{2}}}\right] \Big/$$

$$\left[\left(1-e^2\right)^{-(\alpha+1)/4} P_{\frac{(\alpha-1)}{2}}\left[\left(1-e^2\right)^{-\frac{1}{2}}\right]\right] \qquad (2.17.44)$$

and with a suitable set of initial conditions, it is possible to construct elliptic orbits with period semi–major axis relationships identical to those obtained from (2.15.32). The only differences between the resulting ellipses are the location of the origin and the differences in areal velocities.

Figure 2.17.14 shows an elliptical oscillator orbit superimposed over the corresponding Keplerian orbit in the case $\alpha = -6$. The constants are chosen according to equation (2.17.44) so that the orbits are the same size (ignoring the different origins) and have the same period as those in §§1.5 and 1.7. The symbols show the respective displacements at regular time intervals. Note that the angular velocity is greater for the Keplerian orbit at $\theta = 0$ than for the oscillator, however, at $\theta = \pi$ the angular velocity for the oscillator is now larger. Figure 2.17.15 shows an elliptical oscillator orbit superimposed over the corresponding Keplerian orbit in the case $\alpha = 3$. The constants are chosen according to equation (2.17.44) so that the orbits are the same size (ignoring the differences in origin) and have the same period as those in §§1.5 and 1.7. The symbols show the respective displacements at regular time intervals. Note that the angular velocity is greater for the oscillator orbit at $\theta = 0$ than for the Keplerian one. However, at $\theta = \pi$ the angular velocity for the Keplerian orbit is now larger.

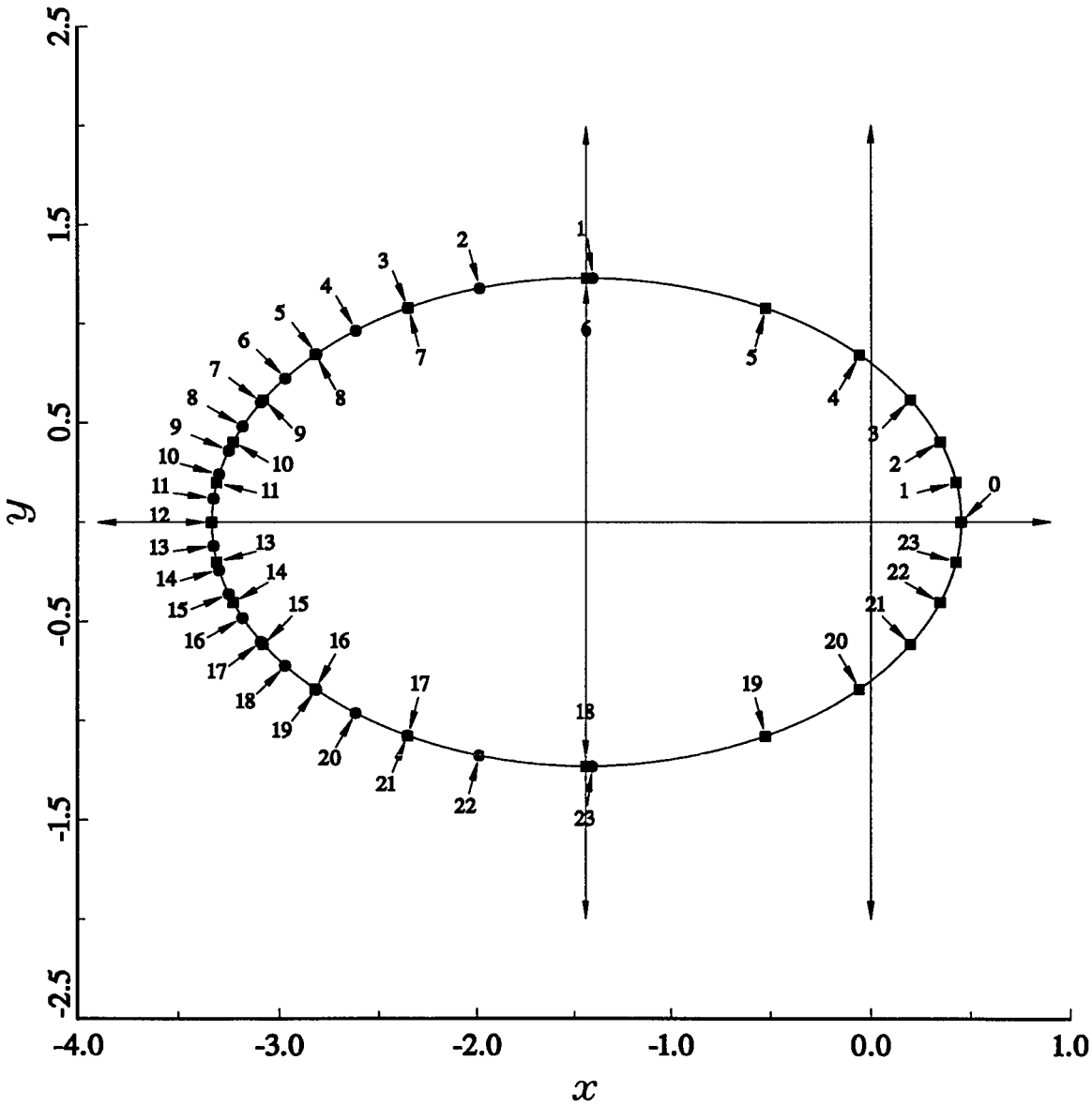


Figure 2.17.14. The elliptical oscillator orbit superimposed over the corresponding Keplerian orbit. The constants for the Keplerian orbits are $\alpha = -6$, $\mu = 20.0420$, $A = 1.25$, $\theta_0 = 0$, $K = J = 0.95$ and for the oscillator $\alpha = -6$, $\mu = 3.2482$, $a = 1.893\dot{9}\dot{9}$, $b = 1.2309$, $k = 4.2016$, $K = J = 1.8670$ and the period T is in both cases 14.6479. The circles (-●-●-●-) show the displacements of the Keplerian particle at the time intervals $iT/24$ (indicated by the numbered arrows) and the squares (-■-■-■-) the equivalent oscillator displacements for the same time intervals. Note that the origins do not coincide.

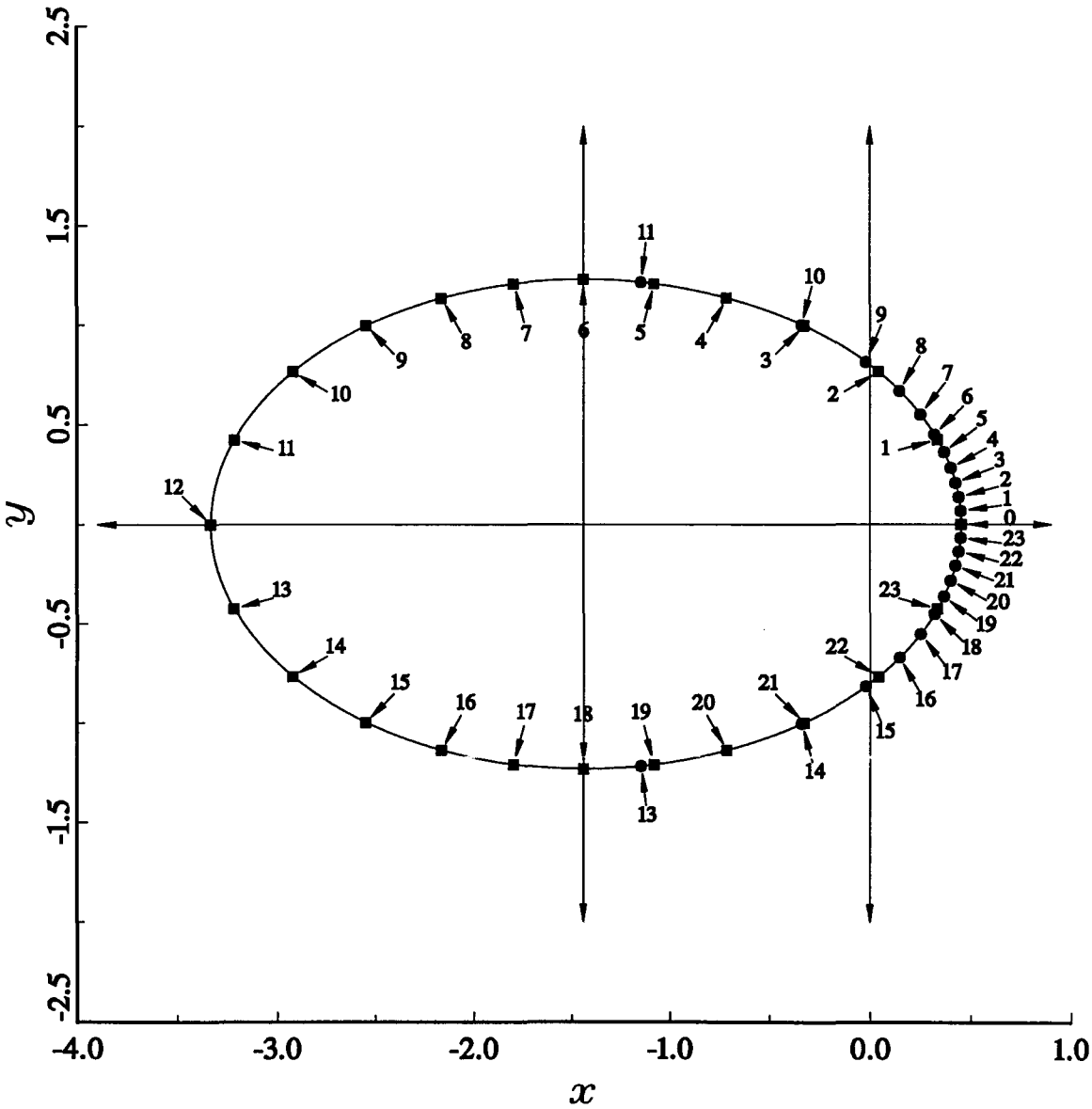


Figure 2.17.15. The elliptical oscillator orbit superimposed over the corresponding Keplerian orbit. The constants for the Keplerian orbits are $\alpha = 3$, $\mu = 0.3594$, $A = 1.25$, $\theta_0 = 0$, $K = J = 0.95$ and for the oscillator $\alpha = 3$, $\mu = 0.0508$, $a = 1.89\dot{3}\dot{9}$, $b = 1.2309$, $k = 0.5255$, $K = J = 0.2335$ and the period T is in both cases 14.6479. The circles (-●-●-●-) show the displacements of the Keplerian particle at the time intervals $iT/24$ (indicated by the numbered arrows) and the squares (-■-■-■-) the equivalent oscillator displacements for the same time intervals. Note that the origins do not coincide.